Study on the Impact of Variation in Design Parameters on the Performance of Solar Photovoltaic System

THESIS SUBMITTED FOR THE DEGREE OF DOCTOR OF PHILOSOPHY (ENGINEERING)

BY

TARAK NATH CHELL

(Ph.D. Reg. No. - D7/ISLM/91/18)

SCHOOL OF ENERGY STUDIES
JADAVPUR UNIVERSITY
KOLKATA –700032
INDIA

2024

JADAVPUR UNIVERSITY
KOLKATA – 700 032, INDIA

INDEX NO. **D-7/ISLM/91/18**

1. **Title of the thesis:**

   Study on the Impact of Variation in Design Parameters on the Performance of Solar Photovoltaic System.

2. **Name, Designation & Institution of Supervisors:**

   Prof. Ratan Mandal, Professor, School of Energy Studies, Jadavpur University, Kolkata, India.

   Prof. Tushar Jash, Professor, School of Energy Studies, Jadavpur University, Kolkata, India.

3. **List of Publications:**

   Peer-Reviewed / UGC approved Journals

   (i) **Techno-Economic and Environmental Performances of Mono- and Poly- Crystalline Silicon Solar Cell Based SPV Power Plants: A Case Study at Saboo, Ladakh in India, Indian J. of Environmental Protection,** Paper No-20230914, 2023 (Accepted on 29th November 2023).

   (ii) **Study on Efficiency Behaviour of Polycrystalline Silicon Solar Photovoltaic Module-An Experimental Approach, Solar RRL**, Manuscript No-solr.202400410 (Under Review)

   (iii) **Development of TiO2-based Acrylic Color-Dye Sensitized Solar Cell: An Emerging Possibilities in Third-Gen Solar Cell Technology, APSE Applied Solar Energy**, Article ID- AppSolEn2460245Mandal (Under Review)

   (iv) **Possibilities of Private Bus Operators Adopting Electric Buses in Passenger Transport: A Case Study in Kolkata, India,** Indian J. of Environmental Protection, Vol. 43, No. 5, 440-451, MAY 2023.

4. **List of Patents:** Nil

5. **List of Presentations in National / International Conferences:**

   (i) **A review of the change in performance of photovoltaic panels due to dust Accumulation-Challenges and their solution, 2020.** International Conference On Sustainable Water Resources Management under Changed Climate, ISBN number: 978-81-941009-3-5,2020,301-309.

CERTIFICATE FROM THE SUPERVISOR

This is to certify that the thesis entitled "**Study on The Impact of Variation in Design Parameters on The Performance of Solar Photovoltaic System**.", submitted by **Mr. Tarak Nath Chell**, who got his name registered on 21.12.2018 for the award of **Ph.D. (Engineering)** degree of **Jadavpur University** is absolutely based upon his own work under the supervision of **Prof. Ratan Mandal**, Professor, School of Energy Studies, Jadavpur University and **Prof. Tushar Jash**, Professor, School of Energy Studies, Jadavpur University, and that neither his thesis nor any part of the thesis has been submitted for any degree / diploma or any other academic award anywhere before.

Ratan Mandal

Prof. Ratan Mandal 22/04/24

Director
School of Energy Studies
Jadavpur University
Kolkata - 700032

Tushar Jash 22-04-2024

Prof. Tushar Jash

STATEMENT OF ORIGINALITY

I, **Tarak Nath Chell**, registered on 21.12.2018, do hereby declare that the thesis entitled "**Study on The Impact of Variation in Design Parameters on The Performance of Solar Photovoltaic System**", contains literature survey and original research work done by the undersigned candidate as part of Doctoral studies.

All information in this thesis have been obtained and presented in accordance with existing rules and ethical conduct. I declare that, as required by these rules and conduct, I have fully cited and referred all materials and results that are not original to this work.

I also declare that I have checked this thesis as per the "Policy on Anti Plagiarism, Jadavpur University, 2019", and the level of similarity as checked by iThenticate software is 7%.

Tarak nath chell

Signature of the Candidate:

Date: 22/04/2024

Certified By

Supervisors:

Ratan Mandal 22/04/2024

1. Prof. Ratan Mandal
   Professor
   School of Energy Studies
   Jadavpur University

Director
School of Energy Studies
Jadavpur University
Kolkata - 700032

Tushar Jash 22-04-2024

2. Prof. Tushar Jash
   Professor
   School of Energy Studies
   Jadavpur University

ACKNOWLEDGEMENT

The present work would not have been possible without the inspiration and kind support from many people whom I know and in whatever way I would acknowledge them for their support, it would fall short of what they actually mean to me.

I would like to express my deepest gratitude to my respected supervisor **Prof. Ratan Mandal** (Professor, School of Energy Studies, Jadavpur University) and **Prof. Tushar Jash** (Professor, School of Energy Studies, Jadavpur University) for his continuous support and judicious guidance during this research. His diligent motivation helped in the successful completion of my work.

I would like to show my heartiest gratitude to my **Parents** and my **Wife** for their constant motivation for completing this research work, without their support this project would not have been a reality.

I would also like to acknowledge **Dr. Deepanjan Majumdar** (Niti Aayog) for showing me the right directions during the difficult times while executing this work.

I am also very much thankful to my respected seniors and fellow scholars **Dr. Atanu Dutta, Dr. Bijoy K. Majhi, Mr. Debanjan Bagui, Mr. Arnab J. Mandal**, and my friends for actively and constantly supporting me during the complete research tenure. I would also like to express my thanks to the non-teaching staffs of School of Energy Studies, Jadavpur University, for the support during this present research.

Date: 22/04/2024
Place: Kolkata

Tarak nath Chell

Tarak Nath Chell

Dedicated to

my Parents,

my Son

&

my Wife

CONTENTS

Nomenclature

Symbol	Meaning	Symbol	Meaning
A	Total area of solar cells, m^2	PM_{10}	Particulate Matter 10 µm or less
E_g	Band gap energy of a semiconductor cell, eV	P_{max}	Maximum power output, W
E_g	Band gap	P_{mpp}	Maximum power point
$E_{g, ref}$	Band gap energy of a semiconductor cell at test condition	Pr	Prandtl number
E_{g0}	Band gap energy of a semiconductor cell at 0°K	PR	Performance Ratio
FF	Fill Factor	p-Si	Polycrystalline
G	Global solar radiation	PV	Photovoltaic
G	Global radiation, W/m^2	P-V	Power-Voltage
G_s	Surface radiation, W/m^2	q	Charge on Electron, (1.602×10-19 C)
I	Current, A	$q_{cond.}$	Conduction heat flux over PV cell , W/m^2
I_0	Reverse saturation current, A	$q_{conv.}$	convection heat flux over PV cell, W/m^2
I_0	Dark saturation current	R^2	Coefficient of determination
$I_{0, max}$	Maximum reverse saturation current	R_d	Diffuse solar radiation ratio
I_d	Diode current, A	Re_x	Reynolds number
I_m	Maximum operating current	R_s	Solar cell series resistance, Ω
I_{max}	Current at maximum power, A	R_{sh}	Solar cell shunt resistance, Ω
I_{pv}	Photo current, A	T_a	Ambient temperature, °C
$I_{pv, ref}$	Photo current at test condition, A	T_a	Ambient temperature
$I_{s, rev}$	Reverse saturation current, A	T_{Back}	Back temperature
I_{sc}	Short circuit current, A	T_c	cell temperature, °C
I_{sh}	Solar cell shunt current, A	T_m	Cell temperature, K
I_t	Total irradiance, W/m^2	$T_{m, ref}$	Test condition temperature, K
J_{sc}	Short-circuited current	T_{ref}	Reference temperature ,°C
K	Material conductivity, W/m K	T_s	Surface temperature, °C
k	Boltzmann constant, (1.3806503×10-23 J/K)	UV	Ultraviolet
K_{ev}	k/q , 8.61×10^{-5} eV/K	V	Voltage, V
L	Length of the solar cell, m	V_d	Diode voltage, V

m-Si	Monocrystalline
n	Diode ideality factor
N_p	Parallel connection
N_s	Series connection
Nu_x	Nusselt number
pH	Potential of Hydrogen
P_{in}	Input power
PLR	Power to Land occupancy Ratio
V_m	Maximum operating voltage
V_{max}	Voltage at maximum power , V
V_{oc}	Open circuit voltage, V
w_m	Weighted of monsoon season
w_{su}	Weighted of summer season
w_w	Weighted of winter season
x	Linear dimension
y	Thickness of the material

Subscripts

a	ambient
p	parallel
oc	open circuit
sc	short circuit
rev	reverse
su	summer
w	winter
m	monsoon
c	cell
ev	electron volt
cond	conduction
conv	convection
sh	shunt
s	series

Greek Symbols

β	Slope
η	Efficiency
β_{Tref}	Temperature coefficient
γ	Surface azimuth angle
δ	Solar declination angle
η	Conversion efficiency
η_{Tref}	Electrical efficiency of panel
ν	Viscosity, m^2/s
ϕ	Latitude
ω	Hour angle
ρ	Glass diffuse reflectivity
θz	Zenith angle

Abbreviations

ANSI	American National Standards Institute
APE	Average Photon Energy
AWG	American Wire Gauge
BIPV	Building Integrated Photovoltaic
CDA	Cumulative Dust Accumulation
MBE	Mean Bias Error
MNRE	Ministry of New and Renewable Energy
MPE	Mean Percentage Error
MPPT	Maximum Power Point Tracking
NDC	Nationally Determined Contributions

CLF	Cleaning Loss Factor	PET	Polyethylene terephthalate
CUF	Capacity Utilisation Factor	PMSY	Pradhan Mantri Suryodaya Yojana
DAT	Dual-Axis Trackers	PO	Polyolefin
EDS	Energy Dispersive Spectrometry	RH	Relative Humidity
EL	Electroluminescence	RMSE	Root Mean Square Error
GCC	Gulf Cooperation Council	RMS	Root Mean Square
GFR	Glass Fiber Reinforced	RO	Reverse Osmosis
GHI	Global Horizontal Irradiance	RRMSE	Relative Root Mean Square Error
GHI	Global Horizontal Irradiance	RTD	Resistance Temperature Detector
GPI	Global Performance Indicator	RTS	Rooftop solar
IEC	International Electrotechnical Commission	SAT	Single-Axis Trackers
I-V	Current-Voltage	SEM	Scanning Electron Microscopy
JNNSM	Jawaharlal Nehru National Solar Mission	STC	Standard Test Conditions
KCL	Kirchhoff's Current Law	TDS	Total Dissolved Solids
KVL	Kirchhoff's Voltage Law	TDS	Total Dissolved Solids
LCOE	Levelized Cost of Electricity	TSS	Total Suspended Solids
LCR	Land Coverage Ratio	VRE	Variable Renewable Energy

List of Figures

List of Tables

Chapter 1

Introduction

1.1 Introduction

Global electricity generation experienced a steady increase of approximately 2.5%, reaching a total of 28,294 terawatt-hours (TWh) in 2022. This growth is indicative of the sustained expansion in global electricity demand driven by a multitude of factors, including increasing demands from industrial, residential, and agricultural sectors, etc. Throughout this period, Renewable electricity generation experienced significant growth, estimated at approximately 8% in 2022, reaching a total of 8,540 TWh (Ember, Global Electricity Review 2023). The collective growth in wind and solar photovoltaic (PV) generation proved substantial, meeting 80% of the upsurge in total global electricity demand for the year. This remarkable growth highlights the accelerating shift towards renewable energy sources. In 2022, renewable energy sources accounted for roughly 30% of the world's total electricity generation, highlighting their increasing importance in the global energy landscape (Ember, Global Electricity Review 2023). Solar PV maintained its position as the fastest-growing electricity source for the 18th consecutive year, with a remarkable surge of 24% in 2022 (Fig.1.1). The proportion of solar energy in the worldwide electricity supply increased by 0.8 percentage points, rising from 3.7% in 2021 to 4.5% in 2022.

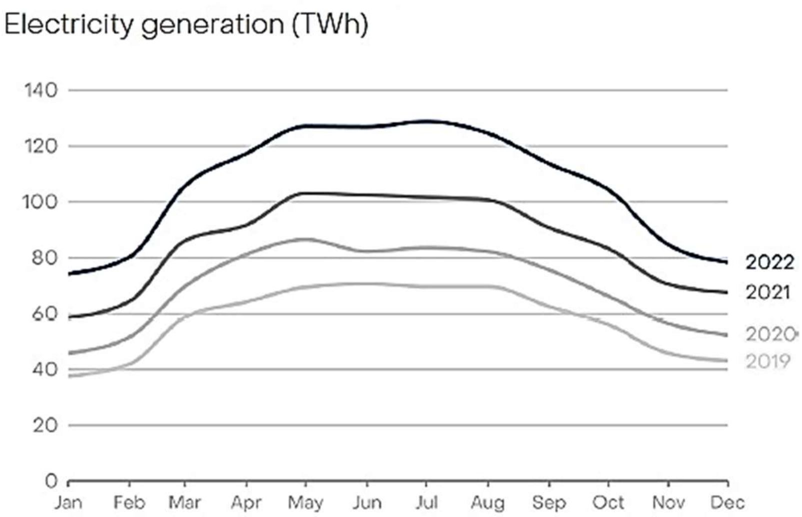

Fig. 1.1 Global solar generation (Ember,2023)

This significant expansion highlights the growing importance and effectiveness of solar PV technology in addressing global energy needs. As solar PV continues to improve and become more cost-effective, it plays an essential role in driving the transition towards renewable energy and reducing dependence on fossil fuels. Additionally, in 2023, India secured the fourth position globally for installed renewable capacity, with an addition of 13.5 GW power throughout the year, and ranked fifth in solar power capacity (MNRE, 2023). According to the updated Nationally

Determined Contributions (NDC) by 2030, India aims to achieve approximately 50% of its cumulative electric power installed capacity from non-fossil fuel-based energy resources (MOEF, 2023). Another assessment, taking into account land availability and solar radiation, has estimated the potential of solar power in India to be approximately 750 GW_p (MNRE, 2023). Fig.1.2 illustrates the scenario of electricity generation from renewable and non-renewable sources in India. Over the past decade, the deployment of solar energy has led to a slight decrease in at present India's power sector emissions intensity to 632 gCO_2/kWh, which is below the level recorded as 648 gCO_2/kWh in 2000 (Ember,2023).

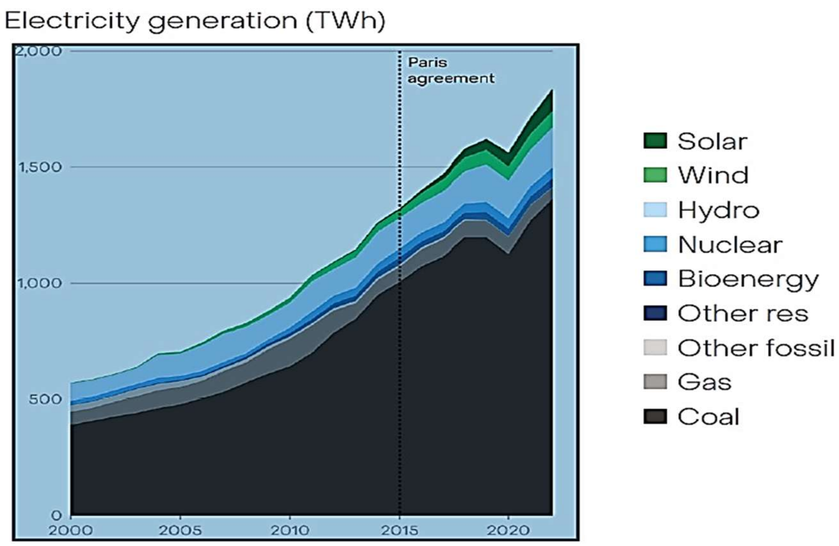

Fig. 1.2 Electricity generation in India from various sources (Ember,2023)

Given the vast potential for solar PV installation in India, we are intensifying the efforts in this domain. The primary advantage of PV systems is indeed their ability to capture solar radiation and convert it directly into electricity. This capability enables PV systems to generate clean, renewable energy without emitting greenhouse gases or other pollutants. PV systems are versatile and can be deployed in various locations, from residential rooftops to large-scale solar farms, making them a key player in the transition towards sustainable energy sources. However, many of these areas, although rich in sunlight, face challenges such as high ambient temperatures and infrequent rainfall, leading to dust accumulation on PV modules. This accumulation of dust, referred to as "Soiling", can significantly hamper the performance of PV systems by obstructing sunlight from reaching the PV cells. Traditionally, the temperature effects on PV modules are considered during system design, but the impact of dust accumulation is often overlooked or arbitrarily accounted for during the design, deployment, and operation of PV systems. Additionally, domestic pollution contributes to soiling, as indicated by the concentration of particulate matter (PM) smaller than 2.5μm and 10μm in the atmosphere. These particles may consist of a combination of different elements, including pollen, fibres, metals, metal oxides, hydrocarbons (unburnt oil) and organic substances. An earlier study has categorized particles found in the atmosphere (Bagnold, 2012), as illustrated in Table 1.1. and classified dust particles into sediment types based on particle size distributions (Blott et al., 2012) as shown in Table 1.2. Particle size, composition, and shape can vary significantly across different geographical regions worldwide. Additionally, deposition mechanisms and rates can vary naturally depending on the location.

Table 1.1 Classification of atmospheric particles from earlier studies

Particles	**Size (mm)**
Pebbles, etc	1mm and above
Sand	0.02 to 1
Dust	0.001 to 0.02
Thin Smoke/Haze	10^{-6} to 10^{-4}
$PM_{2.5}$	0.0025
PM_{10}	0.01

Table 1.2 Segmentation of sediments according to particle size distribution

Sediment Type	**Diameter (µm)**
Clay	0 - 4
Very Fine Silt	4-8
Fine Silt	8-16
Medium Silt	16-31
Coarse Silt	31-63
Very Fine Grained	63-125
Fine-Grained	125-250
Medium Grained	250-500
Coarse-Grained	500-1000

In urban areas like Kolkata, the loss in PV performance can be significantly higher compared to arid regions like Jodhpur, India, due to dust deposition. This difference is primarily attributed to the particle size distribution of the dust prevalent in these locations, with a higher concentration of small particles proving more detrimental to PV performance (Sisodia et al., 2020).

Energy loss due to soiling can be attributed to various factors, broadly categorized into two main groups: PV module and system characteristics, and the influence of environmental factors. Solar PV systems are typically designed to maximize energy production. Consequently, certain characteristics of PV modules and systems remain fixed, and some of these features can exacerbate soiling losses, particularly in the absence of regular cleaning. Roof-top systems, often situated in inaccessible areas, face challenges in maintaining cleanliness. Below are some characteristics that can contribute to soiling losses:

PV panel and system characteristics

- Tilt angle
- Orientation
- Glazing surface characteristics
- PV technology
- PV module cell configuration

Environmental factors

- Height of installation
- Average wind speed
- Occurrence of dew
- Airborne dust concentration
- Presence of liquid particular matter in air
- Location and distance of the source
- Probability of a dust storm
- Distribution of dust particle sizes

Evaluating the performance of PV systems typically revolves around the total energy output over a specified period. Energy yield stands out as a critical metric for comparing various PV technologies, installation techniques, tilt and orientations, as well as a balance of systems. Consequently, dust deposition emerges as a crucial factor influencing the energy yield from PV modules. Given that dust deposition loss varies with the environment, it presents challenges to the deployment of PV systems, underscoring the importance of addressing this issue for the efficient operation of solar power installations.

The decision to implement restorative measures is contingent upon evaluating both the financial implications stemming from reduced energy output and the associated expenses incurred in executing these strategies. Consequently, the significance of energy loss resulting from dust accumulation emerges as a crucial factor, its magnitude varies depending on the geographical context. The accumulation rate of dust on PV modules demonstrates seasonal fluctuations, necessitating the conduct of systematic experiments spanning a minimum period of one year to accurately capture these variations. While such meticulous examinations are instrumental in the planning of PV system installations, they typically necessitate several years to gather a substantial dataset. This thesis seeks to investigate a cost-effective accelerated approach for examining the nature of dust deposition and its relationships with various PV technologies.

1.2 Research Motivation

Over the past decade, there has been a decline in the global weighted average levelized cost of electricity for utility-scale solar photovoltaics (PV), rendering solar PV one of the most economically efficient sources of electricity today. The significant cost reduction is attributed to advancements in PV cells, module technologies, and materials. As a result of these advancements, the installed capacity of solar PV in India has been steadily increasing day by day. Various government schemes have also contributed to the increased installation capacity of solar PV. Jawaharlal Nehru National Solar Mission (JNNSM), Pradhan Mantri Kisan Urja Suraksha evam Utthan Mahabhiyan (PM-KUSUM), Atal Solar Krushi Pump Yojana, Solar Rooftop Subsidy Scheme, Grid-connected Rooftop Solar Scheme, Pradhan Mantri Suryodaya Yojana (PMSY), New Solar Power Scheme (PM JANMAN), play a crucial role in driving the adoption of solar PV technology across India and signifies a commitment to providing rooftop solar (RTS) power systems. Since 2014, the installed capacity of solar power has surged nearly 29 times, rising from 2.82 GW to 81.81 GW (MNRE, 2024). While government much attention is given to boosting solar installation capacity, numerous issues emerge post-installation, including various environmental effects, challenges with tilt angle installation, and degradation of PV cells, which are largely overlooked, thereby contributing to energy loss in solar PV plants. Real-time estimations of dust accumulation on solar PV panels, along with the impact of temperature and other environmental factors, are utilized to determine the optimal tilt angle and cleaning frequency. This process aims to maximize power generation in various locations across India, both before and after the installation of solar photovoltaic panels. Determining the optimal tilt angle, cleaning frequency and proper cleaning process for a particular area will actively serve as a foundational component for this research.

1.3 Aim and Objectives

The rapid advancement of solar photovoltaic (PV) technology has positioned it as a prominent contender in the global pursuit of sustainable energy solutions. Solar energy, harnessed through PV panels, offers a clean and abundant source of electricity, thereby mitigating the environmental impacts associated with traditional fossil fuel-based power generation. However, the performance of PV panels is intricately tied to the prevailing environmental conditions, including sunlight intensity, temperature, and shading effects. Understanding and optimizing the performance of these panels under diverse conditions is paramount for realizing their full potential and widespread adoption. The primary goal of this study is to enhance the understanding and expertise regarding installation of optimized solar PV systems. This objective is achieved through the pursuit of the following specific aims:

a) To study the performance of solar photovoltaic panels under various conditions using a laboratory designed, cost-effective solar simulator.

b) To study the influence of dust accumulation on the power generation of photovoltaic panels with various tilt angles in outdoor environmental conditions for Kolkata.

c) To investigate the optimum system design and operational parameters, based on the techno-economic performance of solar panels under real-time outdoor characteristics for site latitude tilt angle 22.5° of kolkata.

d) To demonstrate a simulation-based solar tree model and compare its performance with respect to the site latitude (22.5°) tilt solar PV installation.

1.4 Thesis Outline

The current study could be organized into three phase-based approaches. The primary focus revolves around comprehensively evaluating the performance of solar PV panels under various environmental conditions. To facilitate this investigation, a low-cost solar simulator has been designed and implemented within a laboratory setting. This simulator replicates key environmental parameters, such as sunlight intensity and spectral distribution, allowing for controlled experimentation and analysis. By subjecting PV panels to simulated conditions representative of real-world scenarios, the study aims to gain valuable insights into panel performance dynamics and uncover strategies for enhancing efficiency and reliability.

The second phase, due to different tilt angles affects the amount of sunlight received by the panels and thus plays a vital role in determining its energy output. By investigating the influence of dust accumulation on PV panel power generation across various tilt angles, valuable insights can be gained into the optimal design and maintenance practices for solar installations in Kolkata This study aims to provide a comprehensive analysis of how dust accumulation affects the performance of PV panels with different tilt angles under real-world outdoor conditions in Kolkata. By measuring and analyzing the changes in power generation over time, an attempt has been made to quantify the impact of dust deposition on energy output and identify strategies to mitigate its adverse effects.

In the third phase, the research sets out to explore this dynamic intersection, focusing on the optimization of solar energy systems with a keen eye on both technical and economic facets. Situated within the context of real-time outdoor conditions and attached by a site latitude angle of 22.5° degrees, this investigation seeks to uncover the optimal system design and operational parameters that maximize the techno-economic performance of solar panels. The choice of the site latitude angle of 22.5° degrees is not arbitrary but rather strategic, reflecting a geographical relevance that resonates with regions sharing similar solar irradiance patterns. By centring around this specific latitude, this study aims to provide insights that are directly applicable to a wide array of locales, facilitating the scalability and adaptability of the findings.

Continue the analysis by focusing on the technical aspects, this study further explores the comparative assessment of the tree model performance, taking into account the impact of dust accumulation and installation area availability on power generation. By scrutinizing these factors in relation to site latitude, this study aims to unravel the complex relationship between environmental variables and solar energy efficiency.

The upcoming chapters outline the strategic advancements of the current study. Chapter 2, delves into a literature review that synthesizes findings from various researchers pertinent to the study's objectives, thereby identifying research gaps. In Chapter 3, the particulars regarding the experiment setup, measurement process, and methodology are described in details. Chapter 4, deals with modelling and analysing the performance of photovoltaic panels under standardized laboratory conditions. chapter 5, conducts an experimental study to examine the impact of dust accumulation on power generation from solar PV modules installed at various tilt angles, across different weather conditions. Chapter 6, explores the operational efficiency of a solar power plant in Kolkata with a 22.5° tilt angle during regular maintenance for dust cleaning, along with calculating associated costs. Chapter 7, examines the design of a novel solar photovoltaic tree model and its power generation pattern in response to the effects of dust. Finally, Chapter 8, outlines the concluding remarks and presents possibilities for future research based on the findings of the present study.

Chapter 2

Literature Review

2.1 Introduction

The rapid expansion of renewable energy drive in the world as well as India is exemplified by the increasing adoption of solar photovoltaic technology for power generation. In recent years, the solar industry has experienced remarkable growth, propelled by substantial cost reductions in photovoltaic modules and a growing energy demand. While over time most of the research work has been dedicated to enhancing the power output of solar photovoltaic systems, the impact of environmental factors on system performance has been largely overlooked. One of the major environmental factors that affect the efficiency of photovoltaic modules is soiling on the modules' surface. The accumulation of dirt on the panel surface, poses a significant threat to the efficiency of photovoltaic systems by obstructing the sun's irradiation from reaching photovoltaic cells, thereby diminishing power generation. Despite the challenges related to addressing the issue of soiling, which involves inefficient water consumption and the potential for panel damage, it is imperative to implement these strategies to uphold system performance and minimize financial losses. A lot of studies have been conducted in this field over the years. Some of these research works have been discussed in the following section. The present study deals with the measurement of dirt accumulation on solar photovoltaic modules in the present environmental conditions of Kolkata, West Bengal. Throughout the process, we try to find out various considerations of technical, economic, and environmental parameters in the entire research work, revealing aspects of the work used in majorly solar photovoltaic installations with Indian different environmental conditions perspective.

2.2 Literature Review

In India, the domestic and industrial energy demand increased rapidly, thereby adding a burden on energy resources. Huge amounts of pollutants were released from the conventional energy-producing sector and it was affecting the environment. Energy generation from solar radiation is one of the most suitable alternatives for mitigating the environmental impact and to addresses future energy crises. In India, 90% of the country's area except for some northern parts of the country receives solar radiation of 3.0–6.5 kWh/m^2 per day during the summer season. Jamil et al. **(Jamil et al., 2016)** used Liu & Jordan isotropic model and explored the accessibility of solar radiation on an inclined flat surface facing due south in India's humid subtropical climate. It reported monthly, annual, and seasonal optimum tilt angle and accessibility of solar radiation at suggested locations of Aligarh and New Delhi. The authors recommended that monthly or seasonal optimum tilt angle better utilized solar radiation in comparison to the annual tilt angle.

Global solar installed capacity has grown day by day and more than half of the installed capacity was distributed in household, commercial, and industrial roofs. The alignment (tilt and azimuth) of solar panels frequently relies on the specific rooftop where PV panels are installed, rather than being specifically configured for optimal performance. Haghdadi et al. **(Haghdadi et al., 2017)** compared two different systems' performance with respect to different tilt angles and validated the same using theoretical simulation results. The authors introduced a novel approach for deriving the geographical coordinates, tilt angle, and azimuth orientation of PV systems from the recorded generation data. The method involves two primary steps. Initially, the longitude of the PV system is approximated by determining the time differential between solar noon (extracted from the recorded PV generation profile) and local noon. Subsequently, the PV generation was represented as a function reliant on latitude, tilt angle, and azimuth orientation, facilitating the inference of any unspecified parameters through the fitting of the observed data to a parametric curve aimed at minimizing errors. The researcher tested three case studies, firstly simulated generation of a theoretical photovoltaic system using weather data, secondly measured generation of photovoltaic systems with validated location and orientation, and finally measured generation from PV systems with self-reported information. The experimental result of the first case study shows the Mean Absolute Deviation of estimating tilt, azimuth, latitude, and longitude to be 6.7°, 10.89°, 0.23°, and 4.89° respectively. In a second case study, the simulated Model calculated the average change in annual generation per degree change in tilt angle to be 0.69%, and per degree change in azimuth to be 0.34% (deviation of ±10° from the optimal tilt angle or ±15° from optimal azimuth angle that results in a reduction of approximately 5% in annual energy generation. Therefore, a deviation of 6.7° and 10.89° would result in an error in estimated annual energy generation of about 4.6% and 3.7%, respectively, while in the more optimal tilt and azimuth range. For case study three, the results show mean absolute deviation values of 4.18° when estimating the tilt angle, 17.63°for the azimuth angle, 3.75°for latitude, and 1.18° for longitude. The authors have presented an automated method for identifying PV system location, tilt, and azimuth. The longitude of a PV system's location was identified by finding the difference between solar noon and local noon. Then data from clear sky time was fit via least squares to the best surface using a model for PV system output with variables tilt, azimuth, and latitude, to identify the parameters simultaneously.

Mono-crystalline solar cell mostly uses silicon because of its high reliability and performance. The overall performance of monocrystalline solar cells depends on different parameters like irradiance, tracking angle and cell temperature. Generally, cell temperature affects the photovoltaic parameters like fill factor, maximum power, open circuit voltage and short circuit current. Chander et al. (**Chander et al., 2015)** studied the influence of temperature on the photovoltaic solar cell with the help of a solar cell simulator. Cell temperature in the simulator was varied between the range of 25°C to 60 °C for radiation ranging between 215–515 W/m^2. In the simulator, a mono-crystalline solar cell was used as a power source and power-voltage and current-voltage characteristics were observed. It was observed that with the increase of cell temperature, short circuit current slightly increased whereas open circuit voltage, fill factor and maximum power point also decreased. The mathematically calculated relative changes in photovoltaic parameters with temperature were determined as the open circuit voltage was observed to change from -0.0022/°C to -0.0025/°C, the maximum output power decreased by 0.002/°C, the fill factor decreased by -0.0013/°C, and the short circuit current increased by 0.002/°C.

The integration of photovoltaic systems directly into building structures, known as Building Integrated Photovoltaic (BIPV), has historically been limited to a niche market. However, there is a significant anticipated surge in demand for BIPV in the foreseeable future. One major hurdle in this integration has been the substantial weight of conventional photovoltaic modules, ranging from 12 to 16 kg/m^2 for glass-back sheet modules to 16 to 20 kg/m^2 for glass-glass modules, which poses challenges, especially for retrofitting old buildings where this extra load wasn't initially factored into the design. Recent research by Martins et al. **(Martins et al., 2018)** has shown promising results in addressing this weight issue. The study demonstrated the feasibility of producing lightweight PV modules, weighing only 5 kg/m^2, by substituting the typical front glass with a thin polymer sheet and the standard back sheet with a composite sandwich structure. These sandwich structures typically consist of two skins bonded to a core using a stiff adhesive. By following appropriate PV lamination guidelines and utilizing ionomer as a sandwich adhesive, **(Martins et al., 2017)** achieved high bending stiffness in the modules. Moreover, these modules successfully passed ageing tests with less than 5% power loss, meeting the requirements of IEC 61215 (IEC, 2016). The researchers have presented a novel lightweight PV module architecture weighing 6 kg/m^2, capable of withstanding stringent IEC ageing tests that can be fully manufactured in a PV laminator in under 30 minutes. The module architecture was based on a composite sandwich back sheet and a polymeric front sheet. To facilitate efficient manufacturing using conventional lamination lines, encapsulated foil was used instead of liquid epoxy for assembling the composite sandwich back sheet. While ionomer was found to be a suitable sandwich adhesive for producing lightweight PV modules due to its favourable mechanical properties under thermal cycling and damp-heat conditions, a specific polyolefin (PO) adhesive was developed to overcome stiffness reduction observed at high temperatures. The PO formulation exhibited high rigidity not only at room temperature but also at temperatures above 80°C, providing the polymer with a higher storage modulus at the module's operating temperature.

Combining this formulation with an aluminium (Al) honeycomb core resulted in a sandwich with a Young's modulus of 17.6 GPa. Modules produced using the PO/Al sandwich showed minimal losses in electrical performance after thermal cycling and damp-heat tests. To demonstrate scalability, medium-area modules composed of sixteen cells were fabricated and endured 1000 hours in damp-heat conditions with only a 3% loss in maximum power. Further reliability testing included evaluating the mechanical resistance of the solution under static mechanical loads to ensure that the measured bending stiffness is sufficient to resist specific loads, and hail tests to assess the front-sheet's resistance to hail, in accordance with IEC standards.

A solar cell requires sturdy materials, with tempered glass being a popular choice due to its strength compared to standard glass, making it capable of withstanding mechanical loads and extreme temperature variations. Typically, sunlight's apparent light transmittance is around 90–92% for commonly used 3.2–4 mm thick solar glasses. Various types of glasses, including coated and patterned ones, are utilized on crystalline Si and thin-film Si cell-based modules. Tints and coatings are applied to manipulate glass properties, enhancing overall performance. Polymer materials, particularly epoxy and glass fiber reinforced (GFR) polymers, are considered viable alternatives to reduce the weight and cost of PV panels. Priyadarshini et al. **(Priyadarshini et al., 2023)** aimed to create a composite plate as an alternative to traditional solar glass. A 4 mm thick plate was fabricated using a hand lay-up technique. Initially, clear epoxy resin (L4AU) was mixed with a hardener at a ratio of 10:3 and poured into a silicone mold measuring 210 × 297 mm. After curing for 24 hours at room temperature, the plate was removed from the mold. The resulting epoxy solar glass exhibited uniform thickness and mechanical properties. Its tensile strength ranged from 2.4 to 2.6 kg/mm^2, and flexural strength ranged from 7.03 to 8.43 kg/mm^2, with an average efficiency of 15.14%. Mechanical properties and efficiency could be enhanced by adjusting material thickness or introducing reinforcements without compromising transparency. Despite the need for improvements in mechanical properties and efficiency, epoxy solar glass offered advantages such as easy fabrication, cost-effectiveness, and availability. It can serve as an alternative to tempered glass in solar panels. Further research can explore enhancing the mechanical properties and efficiency of epoxy solar glass, broadening the scope of solar cell advancements.

Photovoltaic modules are susceptible to weather conditions and are responsive to the accumulation of dust, resulting in noticeable decreases in yield. The impact of dust on PV modules varies depending on their type and technology. Kazem et al. (**Kazem et al., 2022)** organised a practical study in different cities in Oman to measure the rate of dust accumulation and examine the source and properties of dust components. The researcher also conducted an indoor experimental study to investigate the influence of individual dust elements on the performance of two different types (mono-crystalline and poly-crystalline) of solar modules. The study revealed that the most polluting dust, containing a high percentage of ash and volatile building material, led to a degradation rate of 54% for polycrystalline and 47% for monocrystalline modules. The results indicated that contamination levels of 5 g/m^2 on the monocrystalline PV module led to a decrease in the power output by 12%, 6%, 6%, 7%, 3%, 4%, and 4% for ash, calcium carbonate, limestone, cement, sulfur, sawdust, and brown soil, respectively. For the polycrystalline module, under the same contamination level (5 g/m^2), the observed deteriorations were 5%, 4%, 4%, 1%, 2%, and 2% for ash, sand, limestone, sawdust, black silicon carbide, and silica gel, respectively. The researcher also identified the best manual cleaning methods, revealing that water cleaning with cloth and rubber brushes was deemed suitable for low ash components and volatile building materials and that the overall best cleaning method was to clean with sodium solution with rubber brushes. It was suggested based on practical data that periodic cleaning intervals ranging from 10 days for polycrystalline modules and 15 days for monocrystalline modules were better for those particular cities.

The negative effects of soiling solar photovoltaic installations include reduced solar irradiation received by photovoltaic cells and damage to the solar panels. When particles settle on the panel's surface, sunlight is impeded, and incident photons are either absorbed or reflected. With an increase in particle accumulation, less irradiation reaches the cells, leading to a reduction in power output. Pouladian-Kari et al. **(Pouladian-Kari et al., 2022)** proposed a solution known as NightFlip and used it to mitigate the negative effects of soiling on solar photovoltaic installations. The key features of NightFlip included the automated inversion of solar panels at night, utilizing natural condensation to remove dirt without causing damage to the panel surfaces. The experimental results indicated that the combination of panel rotation during the day and inverted panel position overnight helps prevent high dust deposition and discourages the creation of bonds between dust particles and the glass surface. The low accumulated dust on the active surface area of photovoltaic panels can be naturally cleaned off by the effects of gravity with dew formation overnight. To assess the effectiveness of NightFlip, it was compared to other fixed and tracker-based photovoltaic systems. Six parameters were analyzed, including water consumption, CO_2 emissions reduction, total annual revenue, payback period, capacity factor, and levelized cost of electricity (LCOE). The results suggested that single-axis trackers (SAT) and Dual-axis trackers (DAT) with NightFlip consume less water due to their ability to reduce the impact of soiling. In terms of CO_2 emissions reduction, standard SAT and DAT systems showed a 34% and 44% reduction compared to fixed-type systems, respectively, and NightFlip systems further improved this reduction by an additional 1%. Regarding revenue, SAT and DAT with NightFlip led to a 34%

and 44% increase compared to fixed-type systems. In economic terms, the payback period for the standard SAT with the NightFlip system was approximately 5.41 years, as compared to 6.19 years for the Fixed-Type system. The levelized cost of electricity (LCOE) showed a 17% decrease for SAT and DAT systems with NightFlip compared to a 13% decrease for their equivalent systems without NightFlip, with SAT with NightFlip demonstrating the best performance in this criterion. Overall, the NightFlip system appeared to offer promising advantages in terms of water consumption, CO_2 emissions reduction, revenue generation, payback period, and LCOE when compared to other fixed and tracker-based photovoltaic systems.

Solar irradiance, ambient air temperature, and dust represent the key environmental factors crucial for evaluating the performance of PV systems. The accumulation of dust on solar panels negatively affects the PV module's efficiency by obstructing the absorption of incident solar energy. Cleaning PV modules at appropriate intervals can mitigate income loss. The optimal cleaning frequency depends on various factors such as the region's climatology, labour and cleaning material costs, electricity prices, PV technology, and the tilt and azimuth angles of the installation. To achieve their research objectives, authors Yazdani and Yaghoubi **(Yazdani and Yaghoubi, 2022)** installed four identical PV modules at Shiraz University in Iran and analyzed the power loss of solar PV panels due to dust deposition over a period of 6 months, to cover both dry and rainy seasons. The possible variations in power losses due to short-circuit current in solar panels were investigated in outdoor conditions on both clear and cloudy days. The authors observed that short-circuit current loss could serve as a good indicator of dust density on PV modules but actual power loss may differ significantly from the decrease in short-circuit current under low light conditions and high dust density levels. Experimental results revealed that, on average, soiling short-circuit current loss underestimated actual soiling power loss by approximately 9%, with this discrepancy increasing with higher dust density. The observed soiling rate in the initial week of dust deposition was 0.27%/day, decreasing to 0.13%/day in the last week. This observation supported the superiority of the exponential model over linear and power relations in estimating the dust effect on PV systems in the case study. The optimal cleaning period for a solar farm was determined to be 17.50 and 6.39 days for manual and machine-assisted washing methods, respectively. However, the study also highlighted the significant impact of weather conditions on the cleaning schedule optimization for the plant, a ±20% variation in environmental conditions could lead to up to a 29.4% and 33.5% change in the optimal cleaning schedule for machine-assisted and manual cleaning methods, respectively. The investigation also revealed that the optimal cleaning interval was evaluated for a specific year, emphasizing that the economic cleaning frequency is not constant and may decrease in the later years of operation due to the adverse effects of ageing on PV panel performance and a reduction in electricity prices.

Humidity serves as an ambient parameter that alters the trajectory of direct visible solar radiation through refraction, reflection, and diffraction. This dispersion phenomenon impedes the reception of direct solar radiation by water vapour particles present in the atmosphere. The hot climate experiences particularly high levels of humidity in the atmosphere. Gwandu and Creasey **(Gwandu and Creasey, 1995)** investigated the impact of humidity on the absorption of solar radiation and its consequent effect on generated electrical power in this climatic zone. The study utilized a monocrystalline silicon photovoltaic module consisting of 33 cells connected in series. Variations in the module's open-circuit voltage (V_{oc}) and short-circuit current (I_{sc}) with different irradiance levels were established. Additionally, the analysis included an examination of the relationship between solar radiation intensity and humidity. Researchers observed that changes in wind speed influenced relative humidity, with higher wind speeds associated with lower relative humidity levels (observed during 0800 - 1100 hrs), while lower wind speeds led to increased relative humidity (observed during 1430 - 1700 hrs). The effect of relative humidity was found to be non-linear, consistent with the irregular distribution and varying sizes of water vapour particles in the atmosphere. This phenomenon aligns with the non-linear attenuation of electromagnetic radiation in water, as observed in underwater communication systems employing sonar signals. The overall findings suggested that higher wind speeds contribute to lower module temperatures, thereby compensating for the non-linear (small), decrease in irradiance levels with increasing humidity. Furthermore, the acquired data indicate that humidity levels are not sufficiently high to pose a threat to the cost-effective utilization of solar energy conversion systems.

Tripathi et al. **(Tripathi et al., 2021)** also investigated the effects of humidity on PV panel performance. The panel's performance they were examined in a laboratory setting under varying humidity conditions. PV performance parameters were determined by measuring output voltage and current, solar radiation incident on the panel's surface, and surface temperature, while humidity levels were manipulated artificially in the laboratory. Humidity levels within the laboratory were adjusted using a humidifier, a miniature water sprayer, to assess the impact of humidity on PV panel operation. A 20W polycrystalline PV panel was employed for the study, with humidity levels ranging from 65.40% to 98.20% which was measured using a hygrometer. Initially, solar radiation was set at 854 W/m² using artificial light sources. Subsequently, as humidity levels increased, the panel's surface temperature and solar insolation were recorded using an infrared digital pyrometer and solar meter, respectively. Additionally, the panel's output power was calculated at a constant output load of 48 ohms with each rise in relative humidity level, determined by the output current and voltage across the load. The experiment examined that in outdoor environments, solar radiation and surface temperature significantly influence PV panel performance, while humidity also plays a vital role. The study revealed that a 50.15% increase in humidity led to a 24.05% reduction in solar radiation reaching the panel surface and a 36.22% decrease in panel output power. Furthermore, the presence of water droplets in the environment contributed to cooling the panel surface, evidenced by an 11.40% decrease in surface temperature as humidity levels increased from 65.40% to 98.20%. it was concluded that humidity can serve a dual role in the operation of PV panels, affecting both solar radiation intake and panel surface temperature.

The decline in performance of an energy system over its lifespan is an inevitable outcome dictated by natural laws. This phenomenon is particularly pronounced in solar cells operating at elevated temperatures, with the situation exacerbated when modules are left in an open-circuit state. The most significant impact is observed in voltage decreases as temperature rises. Boussaid et al. **(Boussaid et al., 2016)** investigated the influence of open-circuit conditions on the degradation of photovoltaic (PV) modules in desert environments. To illustrate this, a comparative study was conducted involving two identical modules (A1, A2) exposed to sunlight under similar conditions: one in an open circuit and the other connected to a charge. The results of this experiment may be used to inform the simulation phase and predict the average lifespan of both modules. The electrical characteristics of both modules were measured before exposure to sunlight and after 100 and 330 days. Module A1 experienced a degradation rate of maximum power of 7.8% after 100 days and 18.9% after 330 days, while module A2 experienced rates of 11.8% and 22.8% for the same respective periods. Additionally, amorphous silicon (a-Si: H) solar cells operating under open-circuit conditions exhibited greater degradation compared to those under maximum power conditions after 13 days of field exposure. For module A1, there was a degradation of short circuit current (I_{sc}) of 7.7% after 100 days and 17.8% after 330 days, and for module A2, 13% and 20.9% for the same respective periods. Similarly, the degradation of voltage in open circuit (V_{oc}) for module A1 was 0.5% after 100 days and 6% after 330 days, while for module A2 it was 0.9% and 6.5% for the same periods. Conversely, there was a slight increase in the fill factor (FF) for both modules over time, indicating improved energy conversion efficiency. Notably, module A1 exhibited a more significant evolution in fill factor compared to module A2. Over a span of 18 to 24 years, the average annual degradation rate for all connected modules was 0.8%, whereas for modules in open circuits it was 0.6% per year. The performance of C-Si photovoltaic modules was attributed to climatic conditions and operational contexts. Empirical evidence suggested that mono-crystalline silicon PV modules exposed to solar radiation in open circuit conditions within desert environments exhibited visible degradation compared to those connected to a charge, over a three-year period of sun exposure. Thermal cycles experienced by C–Si cells in such natural environments, characterized by wide temperature variations, were considered the primary factor contributing to degradation.

The distribution of the solar spectrum is primarily influenced by two environmental factors: the atmospheric path length and cloud cover. Air mass calculations enable the determination of atmospheric path length, while the estimation of cloud cover is facilitated by the clear sky index, which adjusts for air mass. Building upon this framework, an empirical method was proposed for predicting average photon energy (APE) values, leveraging air mass and clearness index. Additionally, APE contour maps were generated using the clearness index and air mass to assess the spectrum's impact on PV power performance. Peng et al. **(Peng et al., 2019)** introduced a novel approach called the air mass cumulative distribution function method (AMCDF) to depict the relationship between normalized short-circuit current and air mass. The study also documented and verified, for the first time, the influence of the diffuse solar radiation ratio (R_d) on short-circuit current under high air mass conditions. Based on these findings, a new model was developed, combining the air mass cumulative distribution function and the diffuse solar radiation ratio to evaluate the spectrum's effect. Compared to conventional models, this proposed model exhibited higher prediction accuracy. Moreover, it could forecast short-circuit current even under high air mass conditions due to its consideration of the diffuse solar radiation ratio. The experimental findings indicate that when the air mass is below 4.5, the correlation between the normalized short-circuit current and the cumulative distribution function of air mass can be accurately modelled by a fifth-degree polynomial. However, for air masses exceeding 4.5, this correlation becomes erratic. Further examination of the irregular data reveals that the irregularity stems from the influence of the R_d.

The performance of PV cells can be impacted by material and design parameters, as well as several ubiquitous factors, including dust, humidity, and air velocity. Dust deposition is influenced by various environmental and weather conditions, such as pedestrian and vehicular activities, volcanic eruptions, pollution, and wind can contribute to the lifting of dust particles into the atmosphere and their subsequent scattering. The irradiance level of sunlight is influenced by water vapour particles present during humidity. Furthermore, humidity can infiltrate the enclosure of the solar cell. Mekhilef et al. (Mekhilef et al., 2012), examined the simultaneous effects of dust accumulation, humidity level, and air velocity on PV efficiency and subsequently, elucidated how each of these factors influences the others. To summarize, dust settling on PV surfaces can diminish efficiency, while humidity typically leads to degradation in solar cell performance. The irradiance is non-linearly altered by humidity, while irradiance itself causes minimal variations in

V_{oc} in a non-linear manner but significant variations in I_{sc} in a linear fashion. Increased wind speed facilitates heat dissipation from the PV surface, potentially enhancing efficiency by reducing temperature. However, higher wind velocities can also disperse dust, leading to shading and decreased PV performance. It was observed that dust, humidity, and air velocity are interconnected factors influencing PV performance, necessitating a holistic approach to the study to accurately assess cell efficiency.

Accurately determining the back temperature of PV modules is of significant importance for predicting the performance of PV systems, especially in low-power and domestic applications where minor performance fluctuations are frequently accepted. Recognizing the limitations of existing models developed in other geographical regions, Obiwulu et al. **(Obiwulu et al., 2020)** conducted a study specifically tailored to the Nigerian context. The aim was to devise implicit meteorological parameter-based models, considering factors such as relative humidity, global solar radiation, ambient temperature, and extra-terrestrial solar radiation. The models were intended to estimate back temperature under various tilt angles in Lagos, Nigeria, where geographical and climatological variations differ significantly from other regions. Their study involved the development of 48 empirical models and their comparison with existing literature-based models. Parameters such as Mean Bias Error (MBE), Mean Percentage Error (MPE), Root Mean Square Error (RMSE), Relative Root Mean Square Error (RRMSE), coefficient of determination (R^2), and Global Performance Indicator (GPI) were utilized for evaluation. Through meticulous experimentation and statistical analysis, model 44, a hybrid incorporating relative humidity, global solar radiation, and ambient temperature-based parameters for horizontally installed PV modules, emerged as the top performer. In the experimental setup, various modules were subjected to predetermined tilt angles, with measurements taken for output voltage, global solar radiation (G), ambient temperature (T_a), relative humidity (RH), and back temperature(T_{Back}). Calculations were made for daily extra-terrestrial solar radiation, daily declination of the sun, mean daily sunrise hour angle, and maximum possible daily sunshine duration. These data were instrumental in developing and validating the models. The findings from the study underscore the critical role of tilt angle optimization in maximizing energy absorption and utilization in PV systems, alongside the importance of temperature control for achieving peak efficiency. Model 44, identified as the most accurate and reliable among the proposed models, serves as a valuable tool for engineers and researchers in site selection and performance evaluation of PV systems, not only in Lagos, Nigeria but also in similar climatic conditions worldwide.

Qu and Li **(Qu and Li, 2019)** investigated the significant impact of various factors, including the solar spectrum, light intensity, series resistance, parallel resistance, curve factor, and temperature, on the fill factor (FF) of photovoltaic (PV) systems. The primary objective was to analyze the behaviour of key parameters such as short-circuit current (I_{sc}), open-circuit voltage (V_{oc}), maximum operating current (I_m), and maximum operating voltage (V_m) at different temperatures using a custom-built experimental setup capable of precise temperature control. The study assesses the relationship between these parameters under specific temperature conditions, aiming to determine the degree of agreement between experimental results and theoretical formulae. Relative errors within an acceptable range were considered, typically less than 2%, to validate the agreement between definition and theoretical predictions. Additionally, the temperature gradient of FF was calculated when errors met the predefined criteria, enabling an understanding of FF's temperature response for temperatures below 40 °C. The experimental setup comprised four main components: a natural-light-source simulation system, a PV-module power generation system, a PV-module temperature-control system, and a data acquisition system. Analysis of multicrystalline silicon PV modules revealed practically identical dependencies of the I-V characteristics on temperature, with characteristics shifting inward as temperature increased from 6 to 40 °C. Furthermore, V_{oc} and V_m demonstrated a negative correlation with temperature, declining as the temperature rose, while I_{sc} and I_m showed an increase with temperature, albeit with minimal differences between the two. Both experimental and theoretical methods confirmed a decrease in FF with rising temperature, indicating a negative temperature coefficient. The temperature coefficients derived from the two methods were -0.00093 1/°C and -0.0015 1/°C, respectively. These findings emphasized the importance of considering temperature effects when evaluating PV system performance.

Solar cells exhibit superior performance when operating at approximately 298 K compared to other temperature ranges. However, variations in sun insolation, influenced by seasonal and latitudinal changes, can lead to significant fluctuations in temperature, thereby affecting solar cell performance. Exceeding a certain temperature threshold negatively impacts the performance parameters of solar cells due to the temperature-dependent nature of intrinsic carrier concentration, band gap (E_g), and dark saturation current (I_0) in semiconductor materials like silicon. Performance metrics of silicon solar cells, including efficiency (η), short-circuited current (J_{sc}), open-circuited voltage (V_{oc}), and fill factor (FF), are directly or indirectly influenced by temperature variations. Sharma et al. **(Sharma et al., 2023)** thoroughly examined the theoretical effects of temperature changes beyond an optimal range (300 to 400 K) on silicon-based solar cell performance under AM1.5 spectrums. Despite being semiconductor-based electronic devices capable of harnessing clean energy from the sun, the performance parameters of solar cells are highly contingent upon sun insolation. Hence, the author explored the impact of temperature fluctuations on diverse performance metrics of silicon-based solar cells. The short circuit current primarily relies on the cell area and doping concentration. Despite temperature fluctuations, the short circuit current remains insignificantly affected. Moreover, the J_{sc} of a solar cell correlates with the band gap of its material. Consequently, an increase in band gap leads to a decrease in short circuit current J_{sc} due to temperature-induced changes in the band gap. Hence, while short circuit current indirectly correlates with temperature, this effect is minimal and can be disregarded. As the intrinsic carrier concentration of solar cells rises with temperature, the V_{oc} decreases. The following observations were made by the authors, these observations are (i) Shifting the optimal temperature range, i.e., from 20 to 27°C, results in significant alterations in open circuit voltage, fill factor, and efficiency. (ii) With an increase in temperature from 300 to 400 K, all three factors exhibit a downward trend, indicating a decrease with rising temperature. Therefore, mitigating the adverse effects of temperature on solar cell performance becomes imperative, especially if temperatures surpass the optimal range. The researchers suggested the development of new solar cell technologies aimed at reducing temperature-related impacts.

PV monitoring systems typically necessitate a large array of parameters to be logged, including temperatures, irradiances, voltages, currents, and more. These monitoring systems find utility in research settings where comprehensive monitoring of individual cell temperatures within a PV module is necessary, as well as in PV installations requiring multiple monitoring systems to cover an extensive network. Specifically concerning photovoltaic systems, having a thorough understanding of the meteorological conditions at the installation site is beneficial, along with comprehensive monitoring of the PV system performance. There is a broad selection of commercial data loggers designed for climate monitoring, yet they tend to be costly, complex, and challenging to manage. Consequently, there is a need for continued development of data acquisition systems capable of efficiently gathering and processing meteorological data, along with monitoring the operational performance of PV systems. Fuentes et al. **(Fuentes et al. 2014)** developed a low-cost data logger for monitoring photovoltaic systems, emphasizing its affordability, autonomy, ease of use, accuracy, and flexibility for various applications. The cost of the data logger is approximately 60 €, offering advanced features compared to more expensive commercial options. The new low-cost portable data logger meets the accuracy requirements set by the IEC61724 (International Electrotechnical Commission) standard for monitoring photovoltaic systems. The data logger is reliable, capable of monitoring all required parameters accurately, and can withstand harsh environmental conditions. The authors examined a successful outdoor campaign that tested the data logger in different configurations for six months. It emphasizes the device's reliability, precise parameter monitoring capability, and resilience against severe environmental conditions. Its features include 8 analogue inputs of 18 bits, a broad voltage range up to 96 V, 3 analogue inputs for low-cost temperature sensors, and unlimited digital temperature sensors.

Looking at the necessity for a suitable data acquisition device to accurately characterize a solar PV module under genuine operational conditions. Amiry et al. **(Amiry et al., 2018)** proposed a PV module I-V curve tracer, which is based on rapid and automatic load resistance variation. The researchers explored modelling and physically extracting parameters within the realm of photovoltaic energy, utilizing single-diode, traditional double-diode, and alternative double-diode models. It delved into the performance evaluation of a PV polycrystalline module using these extracted physical parameters and I-V curves. Moreover, the study discussed the characterization of PV modules under actual operating conditions employing a cost-effective acquisition device. The researchers investigated the impacts of temperature and solar irradiance on module performance, and the results were compared with existing literature to affirm the reliability of the measurements developed a cost-effective acquisition device for efficient characterization under real operating conditions, and extracted physical parameters using various solar cell models and extraction techniques. The precision of the measurements heavily relied on the accuracy of the current and voltage sensors, as well as the resistances utilized. Consequently, it would be immensely beneficial for the platform to integrate an I-V curve tracer equipped with multiple circuits that could be adjusted based on the V_{oc} and I_{sc} values provided by the PV generator. The study evaluated the performance of the derived physical parameters, which are influenced by operating temperature and solar irradiance, and utilizing both the single diode, conventional, and alternative double diode models. Additionally, the study calculated coefficients for temperature correction in current, voltage, and efficiency.

The performance of photovoltaic (PV) modules varies across different locations due to environmental factors that differ globally. Variables such as solar radiation, wind speed, precipitation, temperature, humidity, and the presence of dust can all impact the performance of PV modules. Myyas et al. **(Myyas et al., 2022)** proposed a mechanism aimed at definitively addressing the cleaning challenges associated with PV modules. The solution offers an alternative to water scarcity issues in arid and desert regions by collecting rainwater for cleaning purposes. This method involves recycling cleaning water through dedicated filters, presenting a viable approach applicable to diverse locations. Additionally, it can be utilized to clean and maintain existing solar cells, even those situated in hard-to-reach areas like tile roofs, traditionally cleaned manually. The researcher also discussed several drawbacks of manual cleaning including risks of employee injuries, damage to panels and inadequate maintenance. The amount of water required for cleaning is influenced by environmental conditions. Large-scale PV power plants, such as MW PV power plants, necessitate more manpower and time for manual cleaning, making it challenging to clean all panels simultaneously. Despite the research into water-based cleaning solutions for PV panels, the universal application of such methods is hindered by water availability issues in certain regions. The study address this challenged and solar panel intelligent system cleaning technology was developed. This automated cleaning device tackles two primary limitations of PV system power generation: high PV temperature and reduced radiation on solar panels due to soiling. Furthermore, it enables rainwater harvesting, making it suitable for use in water-scarce desert environments. This innovative project mitigates many of the shortcomings associated with existing systems, particularly regarding water consumption. It incorporates features such as rainwater harvesting, recycling 80% of cleaning water, automatic cleaning cycles, absence of moving parts or robotic elements, and no requirement for manual labour. Moreover, it ensures continuous cleanliness of PV panels, leading to enhanced efficiency compared to traditional systems. Additionally, its minimal maintenance requirements and cost-effectiveness make it a highly attractive option.

Khlifi et al. **(Khlifi et al., 2023)** discussed the optimization of solar panel efficiency through solar tracking systems, which adjust panel positions according to the sun's orientation for maximum irradiation. The study emphasized the importance of monitoring a solar panel's I-V characteristics, achievable through I-V curve tracers. This real-time monitoring enables the detection of failures and the optimization of panel performance to enhance energy efficiency. The proposed I-V tracer comprises three electronic subsystems: sensors, a load, and a data transmission/storage system. Current and voltage values are obtained using specific sensors and a programmable load connected to a boost converter. Control of the boost converter's MOSFET is managed by a developed algorithm implemented in an ATmega 328P microcontroller. The measured values are collected via a computer interface. The resulting I-V curves provide insights into any deficiencies in PV panels that may reduce the power output. These results ware compared with MATLAB simulation values and promising outcomes are shown in the MATLAB simulation. Experiments demonstrate that the proposed tracer, combined with a MATLAB interface communicating with the Arduino board, enables accurate and real-time plotting of I-V characteristics. Comparison with traditional instrumentation, such as multimeters, highlights several advantages of this solution, including real-time graphical data presentation, cost-effectiveness, and time efficiency. Consequently, the proposed tracer facilitates data recording and report creation, aiding in fault diagnosis and the development of accurate prediction tools for photovoltaic panels.

Ayompe et al. **(Ayompe et al., 2011)** presented findings from a field performance monitoring study of a 1.72 kW roof-mounted PV system in Dublin, Ireland. Data collected between November 2008 and October 2009 was analyzed to assess the viability of PV systems for residential installations in Ireland. Various performance parameters were calculated, including annual energy generation, array yield, final yield, reference yield, PV module and system efficiencies, inverter efficiency, performance ratio, capacity factor, array capture losses, system losses, and cell temperature losses. The results provided insights into system performance, aiding in economic and environmental impact assessments of PV-generated electricity and informing policy decisions to promote PV technology adoption in Ireland. The performance data was also compared with data from other locations across Europe and the Middle East. Evaluation of the 1.72 kWp grid-connected PV system's performance parameters was conducted on monthly, seasonal, and annual basis. The monthly total energy generated varied throughout the year, with the highest in June and the lowest in December. The annual total energy generated was 885.1 kWh/kWp. Final, reference, and array yields varied monthly, with the lowest values in December and the highest in June. The annual averages for these yields were 2.41 kWh/kWp/day, 2.85 kWh/kWp/day, and 2.62 kWh/kWp/day, respectively. Low solar insolation during winter months led to reduced final yield. PV module and system efficiencies ranged from 13.8% to 17.1% and 11.3% to 14.3%, respectively, with higher values in December. Inverter efficiency showed monthly variations, with the highest in June and August. The performance ratio ranged from 72.3% to 91.6%, with an annual average of 81.5%. Capacity factor varied from 5.0% to 15.5% monthly, with an annual average of 10.1%. System losses were lowest in December and January and highest in May. Improvements in capture losses were observed in November, December, and January, while temperature-related losses peaked in June. Comparisons with international studies showed that the PV system's performance in Dublin surpassed that of systems in Germany, Poland, and Northern Ireland but was comparable to some areas of Spain and lower than most of Italy and Spain. Despite Ireland's low insolation levels, high wind speeds, and low ambient temperatures contribute to its suitability for PV installations.

The utilization of solar energy presents its own set of challenges, particularly with regard to soiling, which refers to the accumulation of foreign particles on the surface of solar photovoltaic collectors. This build-up diminishes the amount of light that reaches the solar cells, consequently reducing their efficiency. Soiling is influenced by both natural factors and human activities and varies significantly depending on the location, with areas experiencing high insolation often coinciding with high levels of dust. Chiteka et al. **(Chiteka et al., 2020)** highlighted the variable nature of soiling-related losses, emphasizing that these losses fluctuate based on the energy generated during a given period. In a semi-arid climate, an experimental setup was established to assess solar energy utilization. The solar system operated at full capacity daily, from 8 AM to 4 PM, with an average load of 2.5 kW. To ensure efficient energy management, a 40-kWh battery bank was integrated into the system. This setup aimed to utilize nearly all generated power, with surplus energy stored in the battery bank to serve as a buffer during periods of low solar energy availability. The installation included a Victron data logger with online integration, facilitating the storage of solar generation data. Over a span of 7 months, from May 1, 2019, to November 31, 2019, the system was operational, with the solar panels cleaned once per month. Their study developed a model to optimize the cleaning frequency of solar PV plants, employing a metaheuristic approach due to the complexity of the problem. This approach, which focuses on finding near-optimal solutions, represents a novel approach in the field. By considering varying daily soiling rates, the experiment aimed to minimize the number of days between successive cleaning intervals. An empirical model for soiling loss was devised and optimized to reduce cleaning cycles in a 3.6 kWp power plant. The findings revealed that soiling varied significantly from month to month, with daily fluctuations influenced by factors such as wind speed, direction, and humidity. Consequently, soiling cannot be treated as uniform throughout the year. The study concluded that cleaning intervals should be adjusted accordingly, with a suggested frequency of once every 15 days to minimize losses associated with both excessive and insufficient cleaning.

Examining the effects of dust removal on the power productivity of PV modules or systems is vital, especially considering the necessity to utilize the maximum capacity of the PV generators. Younis and Onsa **(Younis and Onsa ,2022)** summarized the findings as follows: First, it was confirmed that local climate plays a significant role in determining the most suitable cleaning method. Secondly, it was noted that there was a preference for anti-soiling coatings in North Africa, whereas water-based methods were popular in Gulf Cooperation Council countries. Thirdly, it was found that natural cleaning by wind was ineffective in desert regions of Africa and the Middle East. Lastly, the researchers recommended a weekly cleaning frequency for Arabia, with variations across Africa. This summary underscored the influence of weather patterns on the choice of dust mitigation methods. The study revealed that it was important to recognize that each geographic location presents unique advantages and constraints, and not every method mentioned necessarily offers both. The following points highlight key observations, and findings intended to inform designers and suppliers during the planning phase of PV systems or power plants.

- In North Africa, the researchers advocated for Hydrophobic Nano-coating as an effective method for dust mitigation, tailored to the specific climatic conditions. The recommendation is grounded in field experiments and tangible results, suggesting a preference for anti-soiling coatings or passive cleaning technologies in this region of Africa.

- In the Gulf Cooperation Council (GCC) countries, which are part of the Middle East, the researchers focused on water-based cleaning methods such as manual cleaning, rainfall cleaning, and mechanized cleaning. These methods were deemed effective and economically viable based on the researchers' findings.
- In regions where rainfall is scarce, relying solely on passive cleaning techniques such as anti-soiling coatings alongside natural cleaning by rainfall may prove insufficient.
- It is important to clarify that electrostatic cleaning and electrodynamic dust shield cleaning technologies are still in the development phase and undergoing laboratory testing. Therefore, they cannot be relied upon or regarded as low-performance cleaning methods at this stage.
- The studies reviewed in this article indicate that the optimal cleaning frequency for PV systems in operation in Arabia is once a week. However, for Africa, it is suggested that multiple short and long-term studies be conducted in various regions of the continent to determine the most suitable cleaning frequency.
- In desert regions across Africa and the Middle East, scheduling the cleaning of PV arrays based on the soiling threshold is crucial for generating economically viable PV power. However, it's important to note that the costs associated with cleaning depend on the specific technique employed.
- The impact of wind on cleaning the surfaces of PV panels is generally weak and can often be disregarded. In fact, in many cases, wind can exacerbate dust deposition, making it ineffective to rely on wind as a cleaning mechanism, especially in the desert regions of Africa and the Middle East.

Brackish water, seawater, and wastewater are potential options for washing PV modules, albeit requiring prior treatment, which can significantly escalate costs. Investigations into soiling assist in evaluating the economic viability of cleaning PV panels versus leaving them unwashed and facing energy loss. Boeing et al. **(Boeing et al., 2022)** assessed the impacts on photovoltaic system energy output post-washing with lower quality water, examining whether it promoted detrimental substance deposition on panel surfaces and analyzing accumulated dust composition. Researchers explored the impact of different water types on soiling removal and dust chemistry. Over approximately 18 months, five sets of PV panels underwent eight cleanings, while one group remained unwashed. Parameters such as power output, solar insolation, temperature, and rainfall were measured to determine the most efficient cleaning method over time. Dust samples collected pre- and post-washing underwent chemical analysis to characterize composition. Wash water quality was evaluated for total dissolved solids (TDS), total suspended solids (TSS), major ions, and metals. Potential panel compound accumulation was examined via scanning electron microscopy (SEM) coupled with energy dispersive spectrometry (EDS). The findings indicated a 1.88% decrease in energy generation efficiency due to dust accumulation on solar panels. Cleaning with distilled water proved most effective in recovering normalized efficiency, with a mean recovery of around 1.32% over eight cleanings, followed by treated wastewater (0.92%), treated wastewater with surfactant (0.73%), vacuum cleaner (0.27%), and groundwater (0.24%). Cleaning with treated wastewater alone surpassed treated wastewater with surfactant. Post-cleaning, the highest normalized mean efficiency was observed in panels washed with distilled water (11.79%), followed by treated wastewater (11.74%), treated wastewater with surfactant (11.72%), vacuum cleaner (11.67%), groundwater (11.66%), and the control group (11.64%). Examination of dust composition revealed that the dust deposited on the PV panels originated from the ground, a conclusion supported by the organic analysis. Anions found in dust composition included chloride, fluoride, nitrate, sulfate, and phosphate. Pyrolysis-GC/MS identified organic compounds related to local suspended soil and pollen on panel surfaces, with soil being the primary source.

The presence of sea salt in brackish water is influenced by climatic conditions. During the dry season, when sea levels are higher than freshwater levels, sea salt containment increases. Conversely, during monsoon and tidal periods, freshwater levels rise, reducing sea salt containment. This fluctuation in sea salt levels has environmental implications for PV performance, as temperature, soiling, and irradiance directly affect panel efficiency. Soiling, whether from dust or sea salt deposition, reduces PV output by causing partial shading. This shading can lead to overheating in affected cells, potentially resulting in panel failure. Dewi et al. **(Dewi et al.,2021)** explored the climate's impact on sea salt deposition on PV panels and investigated its effects on panel output and efficiency. It built upon previous research conducted during the dry season, extending to the rainy season with data collected from floating panels. The study simulated sea salt soiling on PV panels during the rainy season, observing a 2.09 W difference in power production between normal and sea salt-soiled conditions, with the potential for greater differences as sea salt deposition increases. Additionally, a 29-day experiment floating a PV panel above brackish water demonstrated the detrimental effect of sea salts on panel electrical properties over time, leading to reduced performance. Despite this decline, PV panels remain crucial for providing electricity to remote areas, particularly in sea salt-affected regions like fisherman villages. Floating PV panels can be deployed atop boats, ensuring a reliable power source for fishermen during extended fishing trips far from utility infrastructure.

Dust build up on PV panels, particularly in desert regions, can obstruct solar radiation, significantly diminishing panel efficiency. Moharram et al. **(Moharram et al., 2013)** aimed to devise a method for removing dust from PV panels using minimal water and energy. A cleaning technique was applied incorporating water and a surfactant based on a methodology by Abd-Elhady et al. (2011) at a PV power plant in Cairo, Egypt. It utilized a non-pressurized water system to assess its suitability for dusty environments like Egypt and to develop an efficient cleaning system. An experimental setup was established at the German University in Cairo, Egypt, and similar setups were erected in Stuttgart, Germany, and Southern Europe. Cleaning experiments, with water alone and with a surfactant, were conducted daily for 10 minutes over 45 consecutive days, employing a controlled water flow of 12 Liters/min, starting each day to minimize water evaporation. Over the 45 days, water consumption amounted to approximately 10% of the initial tank volume. Three experiments assessed cleaning's impact on solar cell performance: one without cleaning, one with non-pressurized water cleaning, and one with surfactant-infused water cleaning. Findings indicated that dust accumulation gradually reduces panel efficiency to a significant extent, emphasizing the necessity of cleaning, especially in arid regions like Egypt. Cleaning with non-pressurized water resulted in a daily efficiency decrease of 0.14%, plummeting by 50% after 45 days, indicating its ineffectiveness. However, a blend of anionic and cationic surfactants proved highly effective, regardless of dust particle charge, maintaining panel efficiency consistently. Employing this proposed surfactant-based cleaning system minimizes water and energy requirements for PV panel maintenance.

A comprehensive comprehension of degradation mechanisms in PV modules and operational rates in the field is imperative to foster the expansion of this market. Degradation in PV modules leads to the emergence of various defects across different parts such as the frame, junction box, and front and back sides. Common defects include encapsulant browning, hot spots, milky patterns, delamination, and bubble formation in the encapsulant, as well as cracks in the back sheet polymer, corrosion in junction box connections, bus-bars, front grids, and anti-reflection coatings, along with discolouration and insulation degradation in junction cables. These issues, among other failures in the PV system, ultimately impact energy yield. The extent of PV module degradation is heavily influenced by climate conditions as well as factors like lamination materials, solar module processing, environmental aggressiveness, PV technology, exposure duration, installation method, solar tracking systems, solar radiation concentration mechanisms, and PV system voltage. PV module degradation tends to be more pronounced in hot and dry climates, while corrosion is prevalent in hot and humid regions. Sánchez et al. **(Sánchez et al., 2021)** conducted an analysis on 56 m-Si PV modules exposed outdoors for 22 years in Seville, Spain, identifying significant degradation signs. The findings were compared with conclusions from other studies analyzing degradation in identical PV cells from the same manufacturer after exposure periods ranging from 12 to 17 years. The analysis employed visual inspection, infrared thermography, electroluminescence (EL), and electrical performance evaluation. Results revealed severe damage such as junction box tube degradation, golden brown discolouration, encapsulant delamination with prominent milky patterns, oxidation of front grid metal fingers, bus-bar damage, and AR layer degradation, with lesser instances of back sheet delamination and bubbling. The degradation of PV module power output reached a total of 30.89%, with a mean annual degradation rate of 1.4%, attributed to losses in short circuit current, open circuit voltage, and fill factor. Studies applying exposure periods close to or exceeding 20 years showed significantly higher degradation rates, especially with severe discolouration, milky patterns, and oxidation processes. Electroluminescence tests provided further insights, identifying cracked cells and their impact on the inactive zone. It is noteworthy that the tested modules were manufactured in the 1990s, featuring thicker and smaller cells compared to current PV modules. Despite advancements in manufacturing processes, mechanical or thermal stresses during shipping, transportation, assembly, and exposure can induce micro-cracks, emphasizing the need for electroluminescence inspection at each installation step and adaptation of standards to current manufacturing and installation practices.

In numerous urban locales, rooftop solar systems have been set up, harnessing generated power for self-use and feeding surplus energy back into the grid. Because land constraints often prohibit ground-level solar photovoltaic installations, utilizing rooftop space proves a viable alternative for electricity generation. Such rooftop solar initiatives not only alleviate power shortages but also mitigate the harmful emissions associated with fossil fuel-based energy production. Sharma and Goel **(Sharma and Goel, 2017)** exemplified this approach by installing an 11.2 kW_p PV system comprising forty solar modules covering a total area of 77.6 m^2. Arranged in series and parallel arrays, these modules, unobstructed by shadows, were set at a tilt angle of 21° facing south with an azimuth angle of 0°, mounted on metal frames supported by concrete pillars. Regular cleaning every 15 days minimized soiling losses. The DC to AC conversion, facilitated by a 3-phase transformer-based inverter (Solivia model SOL 11.0-1TR3-E4), with a rated efficiency of 95.6%, seamlessly integrated the generated power into the state grid. The study aimed to evaluate the system's performance in terms of final yield, performance ratio, and efficiency, benchmarking against prior research. Monitored from September 2014 to August 2015, the 11.2 kWp grid-connected PV system at a constituent institute of Siksha ‘O’ Anusandhan University in Bhubaneswar, India, exhibited promising monthly and annual performance metrics. Its yearly average final yield of 3.67 sun-hours per day (h/d) (1339.55 kWh/kW$_p$/year) surpassed that of most studies globally, with notable exceptions such as South Africa and select Indian studies. The system demonstrated an average PV efficiency of 13.42% and an inverter efficiency of 89.83%, both exceeding benchmarks in many regions. Overall system efficiency stood at 12.05%, delivering an annual supply of 14.960 MWh to the grid. The mean performance ratio of 0.78 outperformed comparable studies in Greece, Thailand, Ireland, Spain, South Africa, and India. Moreover, the installation led to an annual reduction of approximately 14.661 tons of CO_2 emissions. This comprehensive assessment underscores the viability of rooftop solar PV systems as a sustainable power solution for eastern India. It also highlights their potential for deployment in off-grid, remote regions of Odisha and beyond.

The efficacy of a solar photovoltaic system (SPV) hinges on various site-specific parameters like latitude, seasonal variations, cloud cover, and air quality. Consequently, conducting an exhaustive analysis of SPV system performance yields invaluable insights for predicting future performance, thereby enhancing power system planning and demand-side management. At the Indian Institute of Science, Bangalore, India, a 20 kWp SPV system was erected atop the library, oriented southward at a 13° inclination matching the location's latitude **(Vasisht et al., 2016)**. The primary aim was to scrutinize solar plant performance across diverse seasons and climatic nuances of Bangalore. The system boasts an annual yield of approximately 28.9 MWh. Performance assessment employs established metrics such as Capacity Utilization Factor (CUF) and Performance Ratio (PR). With a CUF of 16.5%, the SPV system falls within the range of well-performing solar plants in India. Its average PR of around 85% suggests commendable system performance. Temperature moderation (T_{mod}) significantly impacts energy output. The annual average $T_{mod\,(M)}$ registers at 45 °C, albeit η_i, the module efficiency, varies with T_{mod} across seasons. In summer, for T_{mod} > 45 °C, η_i declines by 0.08% per degree rise. In monsoon, a 0.04% decrease per degree rise is observed for T_{mod} > 35 °C. Post-monsoon, η_i decreases by 0.06% per degree rise for T_{mod} > 38 °C. Conversely, winters exhibit a minimal decline in η_i due to intermittent natural cooling, courtesy of cool breezes and low ambient temperatures. The study underscores the inverse relationship between PR_{avg} and T_{mod}. PR_{max} peaks in winter and post-monsoon, owing to lower T_{mod} and T_{amb} in winter, and higher Global Horizontal Irradiance (GHI) post-monsoon. Conversely, PR_{avg} during monsoon and post-monsoon exceeds that of winter and summer due to intermittent rainfall in the former, maintaining module surface temperatures low, and more clear days in the latter. The findings emphasized that module efficiency, primarily influenced by module temperature, significantly impacts SPV system performance. Thus, optimizing module surface temperatures, particularly during summers and analogous weather conditions, is imperative for maximizing the benefits of rooftop SPV installations.

Performance Ratio (PR) serves as a metric to gauge the efficiency of electricity generation in PV power plants, calculated by comparing actual generation to nominal capacity. It enables assessments of efficiency across different weather conditions and technological standards. Environmental variables, such as increased PV module temperature causing generation losses, impact the PR. Nakamoto and Eguchi **(Nakamoto and Eguchi, 2024)** conducted a study to evaluate generation efficiency using PR and Data Envelopment Analysis (DEA) metrics and introduced the weather-corrected PR to address such effects. The researchers compared both indices based on monthly data from utility-scale PV power plants and examined how efficiency values were affected when electricity generation was capped. Additionally, the meta-frontier DEA framework was implemented to measure the influence of seasonality and technical factors on generation efficiency at the monthly level. A notable contribution of the study was the proposal of a model to assess the robust efficiency of Variable Renewable Energy (VRE) power plants, considering uncertainties impact on efficiency values. The study identifies seasonal and technical sources of inefficient power generation at the monthly level and discusses strategies for establishing new PV power plants and managing existing ones. The findings revealed that the average power generation inefficiency during the study period was 0.445, primarily due to seasonal and technical factors. Furthermore, the results indicated a significant disparity between observed and simulated values of power generation efficiency, stemming from variations in weather conditions, power plant site area, and data sources. Increasing the use of PV modules with higher electricity output levels can elevate the DC/AC ratio, thereby enhancing power generation efficiency and stability, and reducing daily and seasonal fluctuations in power generation.

As society progresses, the demand for electricity surges alongside the imperative to combat climate change, driving the quest for renewable energy sources like solar and wind. This need becomes even more pressing with the emergence of Smart Cities, which are voracious consumers of electricity. However, installing renewable energy power plants, particularly solar photovoltaics , faces a major hurdle: the scarcity of open land, especially in urban areas. In response, a sustainable solution emerges: the SPV Tree model, as proposed by Vyas et al. **(Vyas et al., 2022)**. The research focuses on designing technologically and economically viable SPV Tree models compared to traditional ground-mounted SPV plants, aiming to maximize power generation while minimizing land usage. They conducted procedural and simulation studies to design these SPV Trees, which feature PV modules integrated into elegant superstructures for lighting, remote power, and tariff applications. The study compared four distinct SPV Tree designs with conventional ground-mounted SPV plants, analyzing parameters such as specifications, Power-to-Land Occupancy Ratio (PLR), Land Coverage Ratio (LCR), and land cost. Instead of a battery bank, an on-grid inverter was utilized to convert DC power from PV modules to AC power, exporting it to the grid. The proposed SPV Tree Models-Tulip Tree, Sunflower Tree, Marigold Tree, and Daisy Tree-combine renewable energy generation with aesthetically pleasing designs inspired by nature. These models offer a sustainable and green energy solution for urban landscapes, where land availability is scarce and costs are prohibitive. Simulation studies revealed compelling results: the SPV Tree models boasted significantly lower LCR and higher PLR compared to conventional ground-mounted plants, indicating optimal land usage and power generation efficiency. The Daisy Tree model exhibited the lowest LCR and highest PLR among the four models, achieving remarkable land cost savings compared to traditional setups. By minimizing land requirements while maintaining high power generation capacity, SPV Trees emerge as a highly effective solution for renewable energy deployment, particularly in urban settings where space is at a premium. The cost savings from reduced land procurement can be redirected to other aspects of the project, such as panel procurement, construction, and maintenance. Overall, SPV Trees offer a promising pathway towards achieving clean and sustainable electricity generation in a space-efficient manner, facilitating the transition to a greener future.

Despite their smaller ground footprint compared to conventional solar PV installations, solar trees have not yet achieved widespread adoption as scalable renewable energy solutions due to their higher cost, primarily attributed to increased structural expenses. The arrangement of solar panels in solar trees is optimized to minimize shading effects, but inadequate branch and trunk design can lead to instability, higher material costs, and ultimately, a higher levelized cost of energy. Dey and Pesala **(Dey and Pesala, 2020)** aimed to find a balance between energy generation and structural costs to enhance the feasibility of solar tree deployment. The researchers initially optimized the orientations of multiple solar panels within a solar tree to maximize power generation and then positioned them to minimize both shading losses and structural material requirements. Analytical calculations were conducted to estimate annual shading losses based on actual solar insolation data and the sun's movement throughout the year. While the wider spacing between panels reduced shading losses, it also increased the ground footprint area, necessitating longer branches and trunks and thus, more structural material. Through a genetic algorithms-based multi-objective optimization approach, they determined optimal panel positions and selected a design that achieved an optimal balance between shading loss and structural material mass. This design was validated through optical simulations using ZEMAX. To further reduce structural mass while maintaining integrity at high wind speeds, finite element modelling was employed to analyze the von Mises stress on the structure, resulting in individual optimization of trunk and branch dimensions. Despite the significant challenges of high shading losses and increased structural material requirements, the study focused on maximizing power generation while minimizing structural material needs. A 3 kWp solar tree was designed for Chennai, optimizing panel orientation based on actual solar insolation data, and using genetic algorithms for positioning to minimize shading losses and ground footprint area. The resulting optimal balance led to annual shading losses of only 0.17% and a normalized ground footprint area of 1.67. Further optimization of branch dimensions for static loading conditions using von Mises criteria resulted in a 20% reduction in structural material requirement. The study validated shading losses and power generation through ray optic simulations and proposed a design framework applicable to larger solar trees for various locations. Additionally, lightweight materials like Fiber-Reinforced Plastic (FRP) were suggested to minimize overall weight, easing transportation and installation.

The use of organic solar cells presents innovative opportunities beyond conventional applications, offering lightweight, highly flexible, and colourful alternatives. These cells can seamlessly integrate into various fabrics like jackets, handbags, and tents, as well as be utilized in landscaping to create artificial "solar plants" resembling natural greenery. These installations not only maintain aesthetic appeal but also deliver economic and environmental benefits by eliminating the need for water, pesticides, fertilizers, and maintenance associated with real plants and grass, making them particularly attractive in water-scarce regions while minimizing environmental impact. Cao et al. **(Cao et al., 2014)** showcased the feasibility of crafting a "solar palm tree" using organic solar cells on flexible polyethylene terephthalate (PET) substrates. Employing a poly(3-hexylthiophene) (P3HT) and [6,6]-phenyl-C61-butyric acid methyl ester (PCBM) film as the active layers, these flexible devices exhibited a maximum power conversion efficiency (η_P) of 2.7 ± 0.1%. Despite this, the flexible devices demonstrated remarkable flexibility, with only a ~12% efficiency drop after 1000 bending cycles with a bending radius of 1.2 cm. Moreover, they successfully up-scaled the device area to over 6 cm^2 on flexible substrates, crafting "solar palm leaves" by shaping the flexible organic solar cells into palm leaf structures. The fabrication process involved patterning the PET substrates and applying layers of ZnO nanoparticles and P3HT: PCBM. The devices were then shaped using steel rule dies and laminated for encapsulation. The resulting solar palm leaves, with an active area of 6.5 cm^2, were capable of producing power under outdoor sunlight. The prototype yielded a voltage of 1.70 ± 0.05 V, a current of 32.5 ± 0.9 mA, and a maximum output power of 13.8 ± 0.9 mW, suitable for operating a mini-fan. In "LED mode," with devices connected in series, the voltage increased to 5.1 ± 0.3 V, the current decreased to 9.3 ± 0.8 mA, and the maximum power output remained at 12.8 ± 0.8 mW, appropriate for powering LEDs. Additionally, they fabricated large-area leaf-shaped devices with the same structure through lamination, demonstrating good environmental stability despite limited photovoltaic performance due to series resistance effects. These leaf-shaped devices were then integrated to construct a solar palm tree prototype capable of providing sufficient power to operate a mini-fan or LEDs outdoors. Although the colour of these leaf devices, utilizing P3HT: PCBM, does not mimic green, alternative photoactive organic materials can be explored to achieve desired colours, particularly through the application of specially formulated green polymers to replicate natural greenery.

2.3 Architecture of Review

The literature discussed so far widely acknowledges that dust accumulation significantly affects both the power generation and design considerations of solar PV plants. Conversely, the cleaning maintenance schedule for solar panels within such plants assumes a crucial role in restoring their capacity for maximum power extraction.

Oriantiation and angle	• The panels to face south in the Northern Hemisphere and their tilt angle matches the latitude, seasonal adjustments ensure efficient energy capture throughout the year.
Selection of solar PV panels	• Monocrystalline panels: high efficiency, durability, low light performance, power density, lower temperature coefficient.
Environmental effects	• Solar PV panel power generation is affected by various environmental factors such as radiation, temperature, wind direction, wind speed, and humidity.
Dust deposition	• Dust deposition challenges solar PV power generation by reducing light transmission, creating shading effects, and interfering with tracking systems.
Measurement procedure	• Measurement of various parameters of solar PV panels assessing Solar Irradiance, Temp., Voltage. and Current, Power Output, FF, Energy Yield, and Angle of Incidence.
Cleaning operation	• Solar PV panel cleaning depends on cleaning frequency, timing, water quality, cleaning solution, equipment, technique, safety precautions, and inspection.
PV Plants cost analysis	• Analyzing the cost of PV plants involves assessing various factors such as CUF, PR, ROI, payback period, and Operations and Maintenance costs.
PV Tree mode design	• Space saving solar PV tree model involves maximizing energy production with a optimal structure, branch configuration, and attention to aesthetics and landscaping.

Fig. 2.1 Architecture of review process

Conducting an in-depth study on these aspects can provide valuable insights into optimizing cleaning schedules, designing dust mitigation strategies, and improving overall system performance and efficiency. Detailed architecture of the review process is shown in Fig. 2.1.

2.4 Conclusion

Solar photovoltaic (PV) systems emerge as the most favourable alternative for power generation in India. The adoption of solar installations is increasing, both for household rooftop solar systems and for larger-scale projects aimed at transferring power to the grid as an alternative energy source. Extensive examination of the literature has uncovered a lack of exploration regarding the optimal tilt angles for solar PV plants in specific regions or areas, as well as the necessary cleaning frequency throughout the year to achieve maximum energy generation. Dust deposition on solar panels within solar power plants significantly impacts their power generation capacity. While previous studies have primarily focused on the effects of dust deposition at a particular tilt angle, the influence of dust deposition on power generation across multiple tilt angles simultaneously, especially in various regions of India, remains largely unexplored. To evaluate the power generation performance of solar PV panels across varying tilt angles in diverse environmental scenarios, including analysis of dust deposition, comprehensive assessments are necessary. Several studies have suggested the importance of selecting appropriate cleaning methods for removing dust from solar panels. However, determining the most suitable method for a specific region, considering factors such as geographical location, water availability, weather conditions, and dust deposition patterns, remains unresolved. In this study, all significant aspects have been taken into account to encompass the power generation process effectively. This includes variations in PV panel tilt angles, determining the optimal cleaning frequency, and identifying the most suitable cleaning techniques specifically tailored for Kolkata, West Bengal. Moreover, the study incorporates a cost analysis of both energy generation and cleaning processes for both rooftop small installations and large-scale power plants. The interaction between these aspects of solar PV systems is explored in the subsequent chapters.

Chapter 3

Methodology and Experimental Setup

3.1 Introduction

The process of measuring various parameters in solar photovoltaic (PV) systems assesses their characteristics to ensure their efficient operation, effectiveness, and performance. These measurements are vital for system monitoring, maintenance, and optimization. Accurate measurement and monitoring of these parameters ensure the dependable and efficient functioning of a solar photovoltaic system, maximizing energy production and reducing maintenance costs throughout the lifespan of the PV system. Monocrystalline (m-Si) and polycrystalline (p-Si) materials are commonly used in diverse industries, encompassing electronics and solar energy, differing in their atomic structure and physical properties. The selection between these materials depends on specific application requisites. In this study, the m-Si solar photovoltaic module is considered due to its distinct advantages, such as higher solar cell efficiency (Green et al., 2021), lower electrical resistance, superior electrical properties attributed to its single-crystal structure (Kittel 2004), and increased mechanical strength (Dieter 1986). m-Si material also exhibits comparatively better heat tolerance (Green et al., 2014) and efficiency at elevated operating temperatures than some other alternative technologies like thin-film or organic solar cells, which is particularly important in hot climates or during high solar irradiance periods (Skoplaki and Palyvos, 2009). Integration of m-Si silicon solar modules with effective thermal management techniques, such as heat sinks or passive cooling systems, further enhances their heat tolerance (Johnston et al., 2021). These modules are renowned for their durability and prolonged operational life, even in challenging environmental conditions, indicative of their heat-resisting capability (Jankovec et al., 2016).

However, despite of showing exhibit superior heat tolerance of m-Si modules compared to other types, the actual performance in high-temperature conditions can also hinge on factors like material quality, design, and the presence of shading or soiling. Proper system design and maintenance play a pivotal role in optimizing solar module performance during hot climates or heat waves. The higher efficiency of m-Si modules leads to greater power generation from a given area of solar modules compared to other technologies (Eicke et al., 2022).

In the present study, epoxy glass-based solar modules are considered due to their cost- cost-effectiveness, facile manufacturing process, availability, and lighter weight in comparison to tempered glass (Hassan and Osama, 2015). Epoxy solar glass exhibits tensile strength ranging from 2.4 to 2.6 kg/mm^2 and flexural strength between 7.03 and 8.43 kg/mm^2. The average efficiency, standing at 14%, closely aligns with the efficiency range observed in m-Si solar modules, generally between 15% and 17% as indicated by (Tyagi et al., 2013). The enhancement of the mechanical properties and efficiency of epoxy glass-based solar modules can be achieved by adjusting the thickness of the composite material or introducing reinforcements without compromising transparency (Priyadarshini et al., 2023). Epoxy solar glass emerges as a potential alternative material for solar modules instead of tempered glass.

A solar simulator replicates natural sunlight conditions for testing and measuring the performance of solar modules and other photovoltaic devices. These simulators employ diverse light sources to mimic sunlight. Natural sunlight encompasses a full spectrum of colours, including all visible wavelengths, making it ideal for accurate colour temperature representation and providing balanced, natural illumination. The use of tungsten halogen lamps in solar simulators is preferred due to their high light intensity, cost-effectiveness, usability, and spectral interval closely resembling natural light (Roberts et al., 2014, Irwan et al., 2015). Several experiments have shown the potential of tungsten halogen lamps to serve as a cost-effective alternative to expensive test systems for solar simulators (Kongtragool and Somchai, 2008; Landrock et al., 2011).

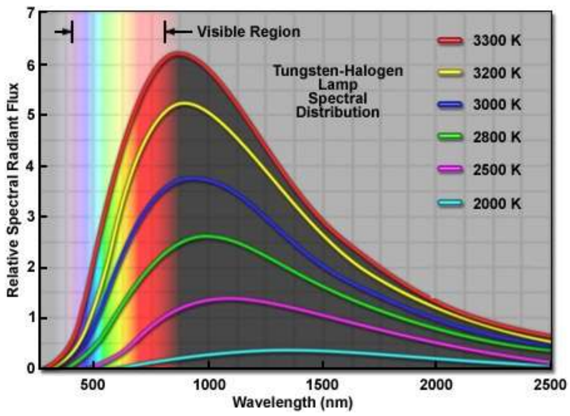

Fig. 3.1 Tungsten halogen lamp spectral distribution

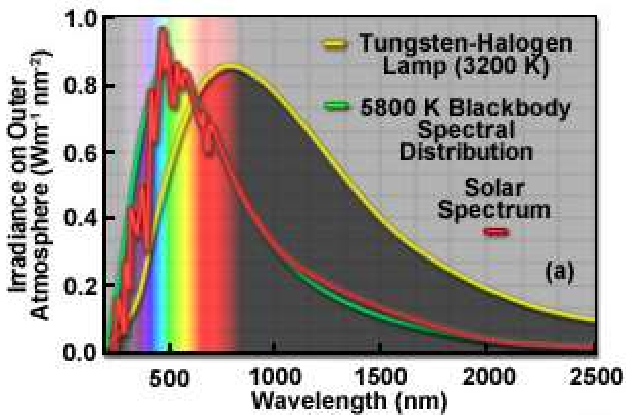

Fig. 3.2 Spectral distribution tungsten halogen lamp and blackbody radiators

Higher colour temperatures produce light that appears whiter and closely resembles natural sunlight, whereas lower colour temperatures introduce yellow and reddish tones into the light. Tungsten, while not a perfect blackbody due to its emitted radiation falling short of the ideal scenario, is a superior emitter that comes close to approximating a genuine blackbody. Across a significant portion of the visible wavelength range, the colour temperature of tungsten surpasses the equivalent true temperature measured in degrees Celsius. Tungsten-halogen lamps, functioning as incandescent sources, emit light covering a continuous spectrum, ranging from ultraviolet through visible to infrared wavelengths (Fig. 3.1). When compared with the spectrum of sunlight and that of a theoretical 5800 K blackbody radiator (Fig. 3.2), tungsten-halogen lamps typically emphasize longer wavelengths. Consequently, as the temperature nears tungsten's melting point, there's a noticeable increase in the proportion of visible light emitted (source: https://zeiss-campus.magnet.fsu.edu/print/light-sources/tungsten-halogen-print.html).

3.2 Theoretical Framework

In PV power generation systems, obtaining accurate current-voltage (I-V) characteristics is imperative for enhancing the efficiency of PV modules. A PV module consists of numerous cells interconnected in series and parallel configurations. The equivalent circuit of a PV cell can be likened to a substantial p-n junction-based photodiode. Fig. 3.3 illustrates a single-diode circuit model of a PV module, which was used to anticipate the performance of the PV module.

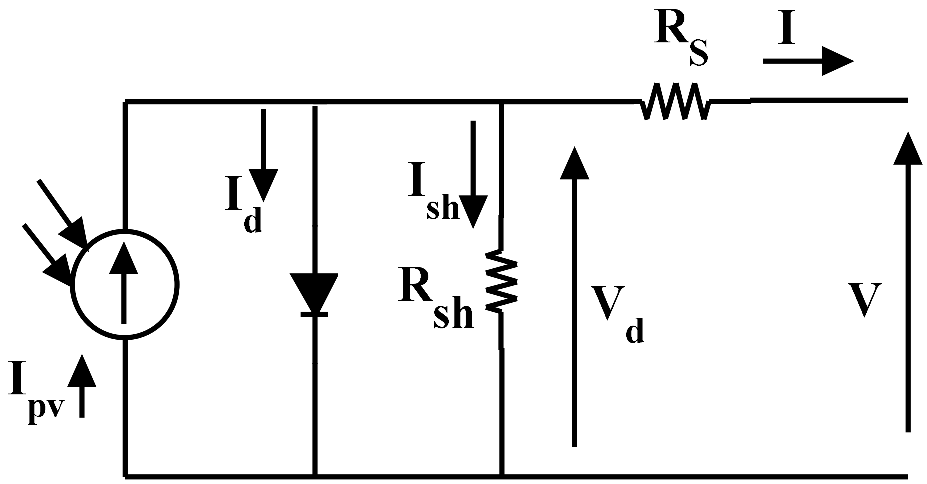

Fig. 3.3 Equivalent circuit of solar PV module

Analysis of above Fig. 3.3, using KVL the equations of solar PV module (Nayan and Ullah, 2015).

$$V = V_d - R_s \times I \tag{1}$$

$$= \frac{n \times k \times T_{pv}}{q} \ln\left(\frac{I_d}{I_0} + 1\right) - R_s \times I \tag{2}$$

Applying KCL on PV module equivalent circuit gives the equation as shown below.

$$I = I_{pv} - I_d - I_{sh} \tag{3}$$

In equation (3), the photo-current is I_{pv} and it was generated from a PV module which depends on solar radiation and temperature.

$$I_{pv} = \frac{V + R_s \times I}{R_{sh}} \tag{4}$$

$$I_{pv} = \frac{G}{1000}\left[I_{pv,ref} + \left(\frac{dI_{pv}}{dT_m}\right)\bigg|_{T_m = T_{m,ref}} (T_m - T_{m,ref})\right] \tag{5}$$

Here standard solar PV module experimental conditions were used G=1000 W/m^2 and $T_{m,\ ref}$ =25°C (Ramkiran, B. et al.,2020) Basic characteristic of a semiconductor diode is a non-linear and it was defined by following the exponential equation. (Ishaque, K. et al., 2011).

$$I_d = I_0\left[e^{\left(\frac{q \times V_d}{n \times k \times T_m}\right)} - 1\right] \tag{6}$$

Here, I_d and V_d are diode current and voltage across the diode.

PV module operates the reverse bias region of the semiconductor diode then reverse saturation current ($I_{s,\,rev}$) is

$$I_{s,rev} = \frac{I_{sc}}{\left[e^{\left(\frac{V_{oc}}{N_s \times V_T}\right)} - 1\right]} \tag{7}$$

Here, the I_{sc} short circuit current of each cell at reference solar radiation and temperature. The number of solar cells connected in the module represents N_s for series connection and N_p for parallel connection.

$$I_0 = I_{s,rev}\left(\frac{T_m}{T_{m,ref}}\right)^3 e^{\left(\frac{1}{K_{ev}}\left(\frac{E_{g,ref}}{T_{m,ref}} - \frac{E_g}{T_m}\right)\right)} \tag{8}$$

When a solar module receives illumination, photons having higher energy than the bandgap energy of the semiconductor material lead to the absorption of photon energy and the creation of electron-hole pairs (Tina and Scrofani, 2008). The Varshni equation delineates the temperature's dependence on the semiconductor's bandgap and can be expressed as follows:

$$E_g = E_{g0} - \frac{7.02 \times 10^{-4} \times T_m^2}{1108 + T_m} \tag{9}$$

Here, used silicon semiconductor material's constant value of α and β is 7.021×10^{-4} eV/K and 1108 K. Above equation, n is detonated as diode ideality factor, $T_{m,\,ref}$ is standard test condition temperature of solar module in K, E_g is band gap energy of a semiconductor cell eV, T_m is cell temperature in K, and E_{g0} is band gap energy of a semiconductor cell at 0°K. The constant value k is Boltzmann constant ($1.3806503 \times 10^{-23}$ J/K), q is a charge on Electron (1.602×10^{-19} C), K_{ev} is k/q and the value is 8.61×10^{-5} eV/K.

The cell temperature is also dependent on open circuit voltage (V_{oc}), following the relation given below (Wen, Cai, et al., 2012).

$$V_{oc} = \frac{E_g}{q} - \frac{n \times k \times T}{q}\left(\ln\frac{I_{0,max}}{I_{sc}}\right) \tag{10}$$

Here, $I_{0,\,max}$ is the maximum reverse saturation current. The equation shows that energy bandgap decreases with cell temperature and also decreases open circuit voltage.

The fill factor (FF) is the ratio of maximum power output (P_{max}) at maximum power point to the product of open circuit voltage (V_{oc}) and short circuit current (I_{sc}) relation given below.

$$FF = \frac{P_{max}}{V_{oc} \times I_{sc}} = \frac{V_{max} \times I_{max}}{V_{oc} \times I_{SC}} \tag{11}$$

The efficiency of solar cells is expressed as

$$\eta = \frac{P_{max}}{P_{in}} = \frac{V_{max} \times I_{max}}{I_t \times A} = \frac{FF \times V_{oc} \times I_{sc}}{I_t \times A} \tag{12}$$

Where I_t is total irradiance and A is the total area of solar cells.

The above equation shows that the fill factor decreases with cell temperature due to a change in open circuit voltage and short circuit current (Chander et al., 2015).

3.2.1 Effect of Wind Velocity on Solar Module Performance

Due to the effect of wind velocity on solar cells, the conversion efficiency of solar photovoltaic cells (Mekhilef et al., 2012) can be formulated in equation (13)

$$\eta = \eta_{T_{ref}}[1 - \beta_{T_{ref}}(T_c - T_{ref}) \quad (13)$$

Where the Electrical efficiency of the solar module at 1000 W/m^2 radiation and T_{ref} temperature is represent $\eta_{T_{ref}}$ and $\beta_{T_{ref}}$ represent photovoltaic material properties at T_{ref} temperature. These two parameter values are specified by the manufacturer. According to law of conservation of energy, the equation is,

$$q_{cond.} = q_{conv.} - G_s \quad (14)$$

Here it was considered that heat transfer is one direction and velocity on photovoltaic cell surface is horizontal and uniform.

$$q_{cond.} = \frac{-2K(T_c - T_s)}{\Delta_y} \quad (15)$$

Where K is material conductivity, y is the thickness of the material, T_c is cell temperature, T_s is surface temperature, T_a is ambient temperature and G_s is the surface radiation.

$$q_{conv.} = h(T_s - T_a) \quad (16)$$

Using the flat plate's external turbulent flow convection correlation (Incropera et al., 1996), the corresponding Nusselt number was calculated, $N_{u_x} = 0.0296\, Re_x^{4/5} Pr^{1/3}$, 0.6 < Pr < 60

Reynolds number is calculated as $Re_x = \frac{velocity \times x}{v}$ (17)

The Pr (Prandtl number) and ν (viscosity) values are read from atmospheric air tables in an average of surface and ambient temperature.

$$h = \frac{Nu.k}{L} \quad (18)$$

L is the length of the solar cell in meters.

Finally, according to the energy conservation principle, the following equation was implemented

$$\frac{-2K(T_c - T_s)}{\Delta_y} = h(T_s - T_a) \quad (19)$$

From the above equations and discussions, it can be concluded that the wind speed and temperature are inversely proportional to each other, resulting in increased cell module efficiency. In an experimental study conducted by Ahmed et al. (Ahmed et al., 2023), it was observed that as the wind velocity increased to 5 m/s, the efficiency of the cells rise from 14.8% to 16.5%. Moreover, at a wind velocity of 7.20 m/s under 800-820 W/m^2 solar radiation, the module temperature dropped from 57.50 °C to 33 °C.

3.2.2 Humidity's Impact on Solar Module Performance

During the analysis of the humidity effect, two scenarios are typically considered: one involves the impact of water vapour particles on solar radiation levels, while the other concerns the infiltration of water vapour into the enclosure of the solar module. When solar radiation interacts with water vapour droplets, it can either be reflected or diffracted by direct components of radiation, potentially diminishing the amount of radiation that reaches the solar module. Consequently, this reduction can lower the overall effectiveness of solar modules. Humidity has the propensity to cause dust and dirt particles to adhere to the surface of solar modules, forming a layer that diminishes the amount of radiation absorbed by the solar cells. This reduction in absorption subsequently leads to decreased efficacy. Empirical data from Rahaman et al. (Rahaman et al., 2015) demonstrated that the output power decreases as relative humidity and solar cell temperature increase.

3.2.3 Dust and Dirt Impact on Solar Module Performance

The decline in solar PV module efficiency is predominantly linked to the accumulation of dust on the module surface. Numerous global studies have investigated the impact of dust on solar PV modules across varying conditions, environments, and durations. In one such inquiry, researchers noted a substantial degradation in performance in desert regions, where dust accumulation on PV module surfaces resulted in an approximate 40% reduction in solar efficiency (Kumar, S. and P. B. L Chaurasia., 2014). The presence of air pollution significantly diminishes the energy output of PV modules (Maghami, M. R., 2016), showcasing a reduction in solar energy production of about 17-25% across affected regions. This decline is attributed to both ambient particulate matter (PM) and its deposition on photovoltaic surfaces, with each contributing roughly equally to the overall efficiency decrease (Bergin, M. H. et al., 2017). The adherence of particles to PV modules disrupts the received solar radiation by absorbing and scattering incident radiation (Qasem, H. et al., 2014). In practical usage, when PV modules are exposed to dust, the heat balance shifts. The dust obstructs certain cells, impeding their functionality and leading to reduced electric current generation by these shaded cells (Chen, Y. et al., 2019).

Overall, various equations and scenarios demonstrate the sensitivity of photovoltaic cell performance to cell temperature under diverse environmental parameters. When installed in open environments, solar module performance is notably affected by two crucial factors: solar radiation and the surface temperature of the solar module.

3.3 Experimental Installation Study Area and Climate

The experimental setup was established at the School of Energy Studies, Jadavpur University, located in Kolkata, India, at a latitude of 22.57°N and a longitude of 88.37°E. Kolkata recognized as the 'city of joy,' serves as the capital city of West Bengal and lies within the Gangetic Delta, close to the eastern coast of India. Kolkata is situated in a tropical climatic region and features a warm and humid climate during summer and relatively mild winters (ECBC, 2017). The city experiences three primary seasons: summer, monsoon, and winter. Summer temperatures hover around 30°C, occasionally soaring above 40°C, particularly in dry periods, mainly in April-May. The monsoon season, commencing in the first week of June and extending until the first week of October, brings rainfall from the Bay of Bengal branch of the Southwest monsoon. Kolkata receives approximately 1248 mm of rain during the monsoon, contributing to the annual total of 1640 mm (Regional Meteorological Centre, Kolkata, www.imdkolkata.gov.in). During October and November, the post-monsoon season witnesses cyclonic storms originating from the Bay of Bengal, resulting in heavy rainfall in Kolkata. Winter lasts approximately two and a half months, with temperatures dropping to about 12°C between December and January. The annual average solar radiation in Kolkata measures 5.19 kWh/m^2/day. Solar radiation levels vary throughout the year, ranging from 4.42-6.40 kWh/m^2/day in summer, 4.42-5.40 kWh/m^2/day during the monsoon, and 4.10-5.61 kWh/m^2/day in winter (Kumar, N. M., et al., 2017). All meteorological data was collected from a nearby weather station situated near the experimental setup and the Central Pollution Control Board, India, at the Jadavpur station (WBPCB, Kolkata).

3.4 Experimental Solar Simulator Setup

The solar simulator was established within the Solar Energy Laboratory at the School of Energy Studies, Jadavpur University, operating under standard indoor atmospheric conditions, as shown in Fig. 3.4.

Throughout the experiment, maintain a constant relative humidity level of 55% RH and ensure that no wind flows around the experimental setup. Laboratory-based practical tests are performed to regulate weather conditions, so the influence of relative humidity and wind speed overlaps with the effects of solar radiation and solar PV module temperature. A light source is utilized to provide an intensity of light reaching up to W/m^2, with the capability to adjust the lighting intensity based on specific requirements. Various instruments were engaged for measuring the different parameters like radiation levels, solar module temperature, solar radiation control unit, resistance change unit, as well as data logging and collection unit.

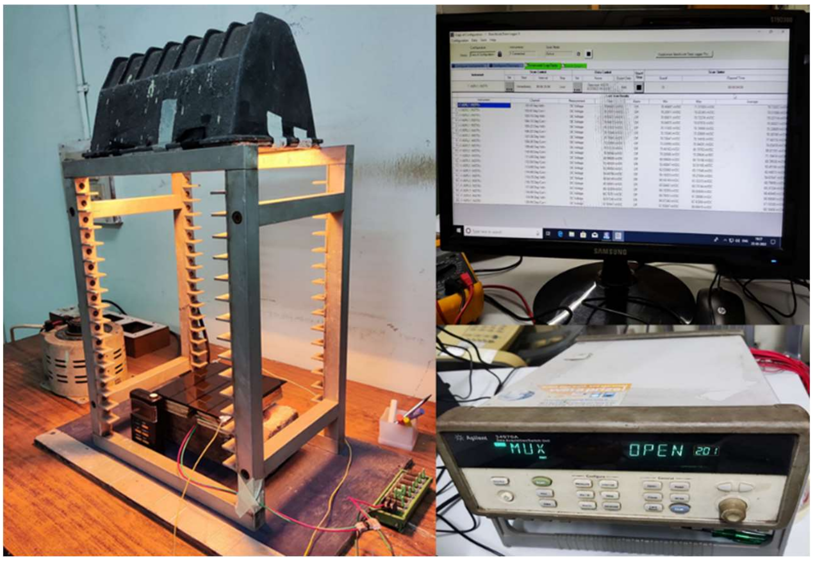

Fig. 3.4 Experimental setup of solar simulator

A schematic diagram illustrating the solar simulator experiment is presented in Fig. 3.5. For this experiment, a 1000 W tungsten halogen lamp (Fig. 3.5b) served as the light source, with available radiation intensity ranging from 10 to 1100 W/m^2 . A voltage variac used (Fig. 3.5a) to change the solar radiation intensity level. For the present study, a m-Si PV module (Fig. 3.5e) was positioned horizontally under uniform solar radiation provided by the tungsten halogen lamp.

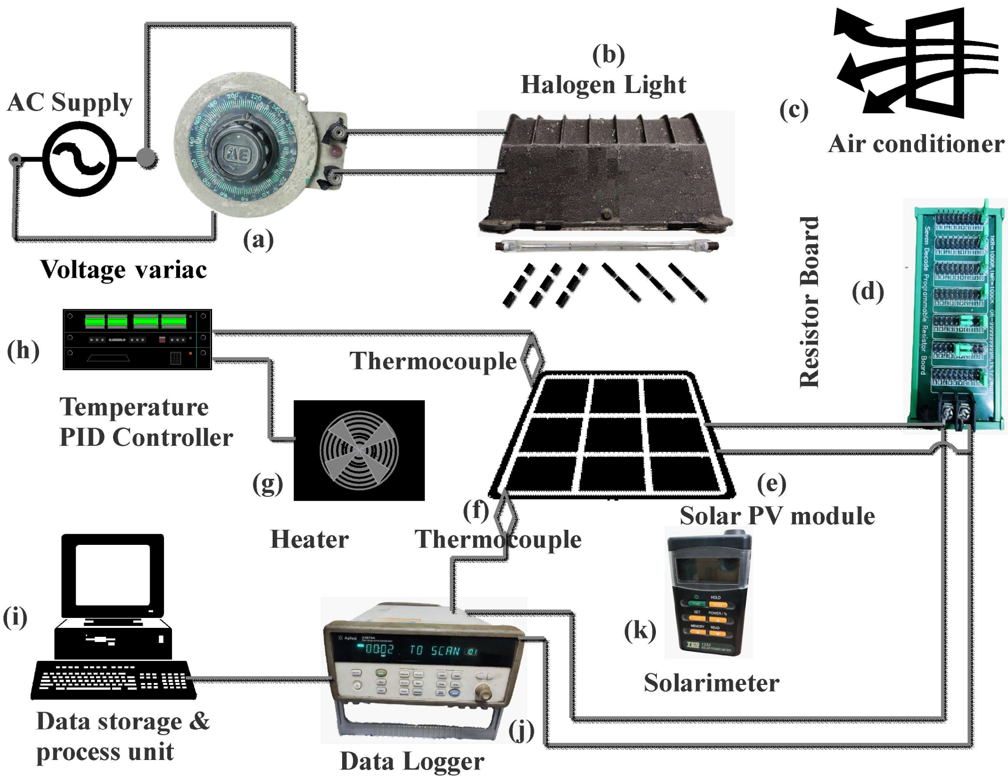

Fig. 3.5 Schematic diagram of PV systems used in laboratory experiment

Specific details and specifications of the solar PV module used in the experiment, as provided by the manufacturer, are detailed in Table 3.1. Additionally, a solarimeter (Fig. 3.5k) was used at the level of the solar module plane to precisely measure the radiation received by the solar module surface. To measure the temperature of the solar PV module, a K-type thermocouple was affixed to the centre of the module's rear side. All K-type thermocouples underwent calibration using a standard temperature sensor for accuracy assurance. A circuit board with an embedded resistor (Fig. 3.5d) was employed to alter resistance while measuring the voltage and current of the solar PV module during the experiment. Due to the variation in radiation, temperature, and resistance, the output voltage, current, and module temperature data were measured and captured using the Agilent 34970A data logger (Fig. 3. 5j) for a duration of five seconds. All recorded data from the data logger was stored in a data storage and processing unit (Fig. 3. 5i) and was further utilized for various ongoing analytical computations. An additional heat source (Fig. 3.5g) was incorporated into the experiment when necessary to elevate the solar module temperature under different hypothetical scenarios, and its operation was controlled by a PID-based temperature control unit (Fig. 3.5h). To reduce the module temperature as required during the experiment, an ice pad was used. Additionally, no additional light sources were introduced into the experimental area during the experiment.

3.5 PV Modules

For all indoor and outdoor experiments, high-efficiency m-Si base photovoltaic modules CNC 165×165-6 used. Fig 3.6(a) shows the m-Si solar PV module, while Fig 3.6(b) illustrates its dimensions. Additionally, the technical specifications of the m-Si solar PV module can be found in Table 3.1.

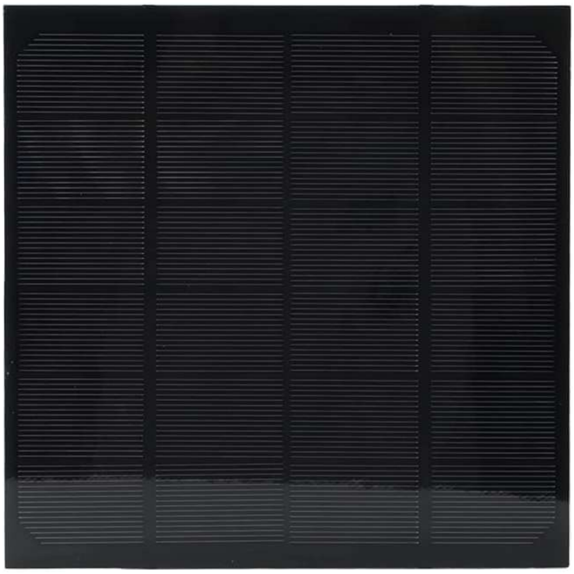

Fig. 3.6(a) Photovoltaic module

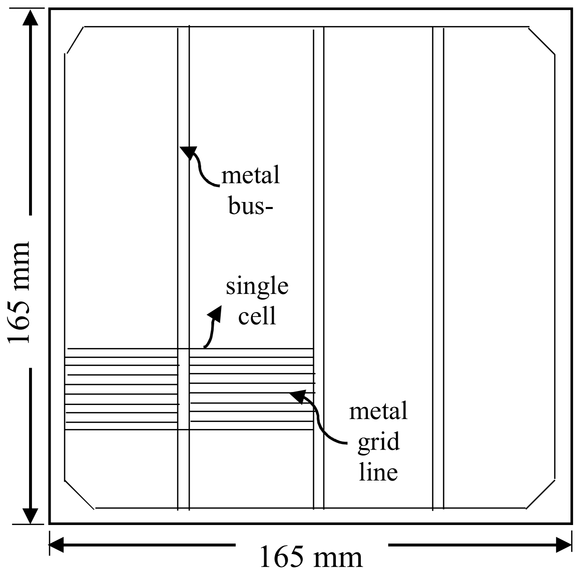

Fig. 3.6(b) Dimensions of photovoltaic modules

Table 3.1. Technical specifications mono-crystalline solar photovoltaic module details

Model No.		CNC 165×165-6
Cell technology		Monocrystalline silicon solar cell
Cell brand		A grade
Maximum power, (Pmpp)	[W_P]	4.5
Power tolerance	[%]	±3
Optimum operating voltage, (Vmpp)	[V]	6
Optimum operating current, (Impp)	[A]	0.75
Open circuit voltage, (V_{OC})	[V]	7.2
Short circuit current, (I_{SC})	[A]	0.83
Temperature coefficient of (I_{SC}, α)	[%/°C]	+0.06±0.01
Temperature coefficient of (V_{OC}, β)	[mV/°C]	-155±10
Temperature coefficient of (Pmpp, γ)	[%/°C]	-0.5±0.05
Cell efficiency, (ηcell)	[%]	19.0
Cell shape	Square	
No. of cell	[series]	12
Cell dimension	[mm]	78×26
Length	[mm]	165
Width	[mm]	165
Weight	[Kg]	0.18
Surface material		Epoxy resin

*Performance at 1000 W/m^2 (Standard test conditions: AM 1.5, cell temperature 25°C)

The electrical characteristics curve of a photovoltaic module from a manufacturer depicts the relationship between its output voltage and current under varying conditions like sunlight intensity and temperature. It typically includes the open circuit voltage (Voc), short circuit current (Isc), maximum power point voltage (Vmpp), and current (Impp). This curve is essential for assessing the module's performance and determining its suitability for specific applications within solar energy systems.The electrical characteristics of the photovoltaic module are described in the following Fig 3.6 (c) and Fig 3.6 (d).

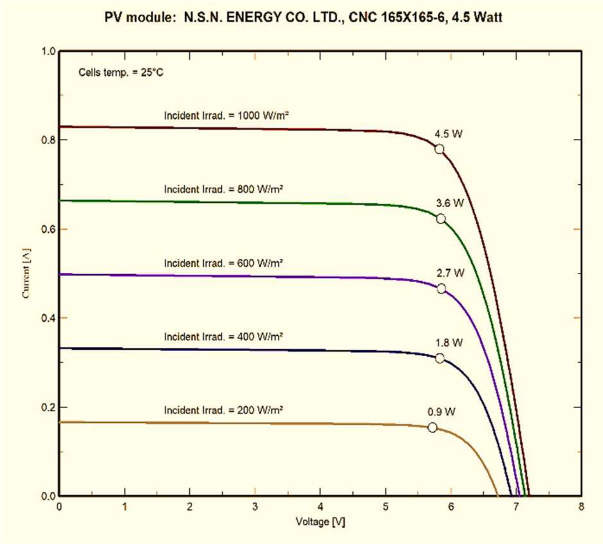

Fig. 3.6(c) Current-Voltage characteristics at different radiation

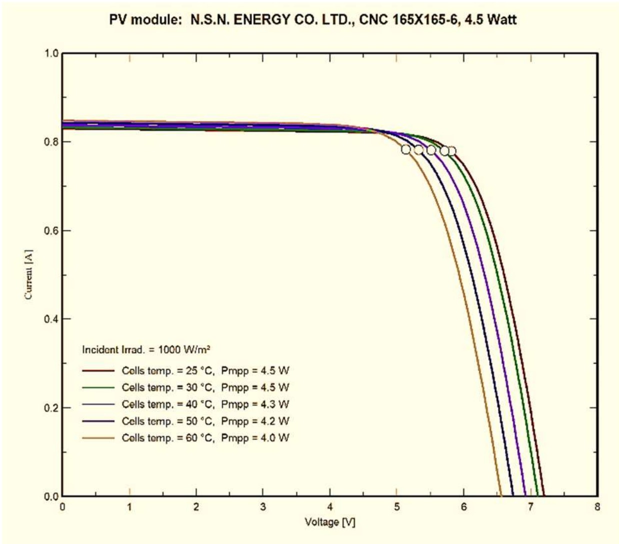

Fig. 3.6(d) Current-Voltage characteristics at different temperature

3.6 Resistor Board

A resistor board, also known as a resistor array or network, is an electronic component that consolidates numerous resistors into a singular unit. The embedded resistor circuit board (Fig.3.7a) in the range of 0 Ω to 1MΩ with an accuracy level of ±1% and a power rating is 0.5 Watts used to vary the voltage and current of the PV module.

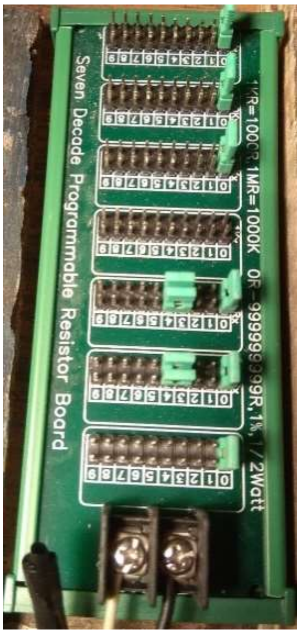

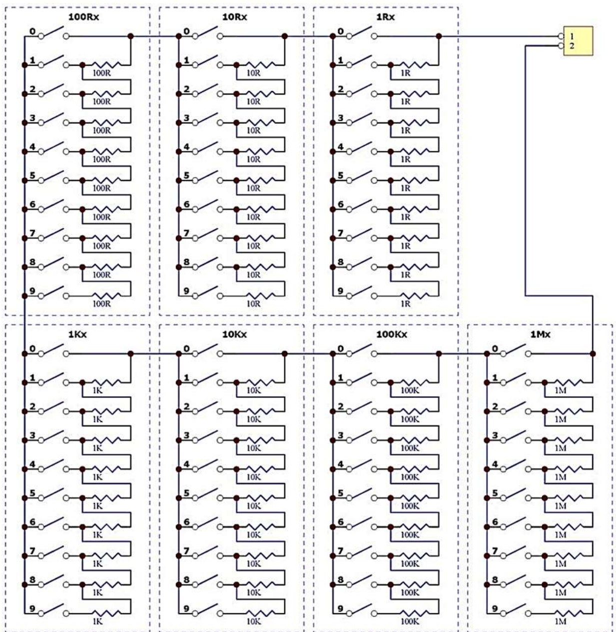

Fig. 3.7(a) Resistor board

Fig. 3.7(b) Circuit diagram of resistor

The circuit board incorporates varying numbers of resistors in columns, which are employed to fine-tune the jumpers to attain the required resistance for the experiment. Figure 3.7(b) illustrates the internal circuitry of the semiconductor-based resistor embedded in the resistor board.

3.7 Voltage Variac

A voltage variac is a type of electrical device used to vary the voltage supplied to an electric load. The primary function of a voltage variac is to provide a continuously adjustable output voltage to the load during experimentation.

Fig. 3.8(a) Experimental used voltage variac

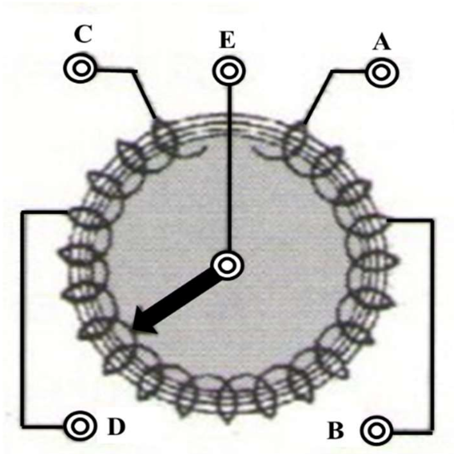

Fig. 3.8(b) Circuit diagram of voltage variac

In the present study, an AE DIMMERSTAT voltage regulator within our indoor solar simulator facility with a measurement accuracy of 1% was utilized. The technical specifications can be found in Table 3.2. By using the rotating knob, a variable voltage output from a consistent AC voltage source can be obtained (Fig. 8.a).

Table 3.2. Technical details of voltage variac

Type	Serial No.	Max. load (A)	Max. kVA	Input	Output
8 D-1P	102/D80764450	8	2.16	240V, 50/60Hz	0-240 V [E&C] 0-270 V [E&C] when input AC or BC

The smooth and precise voltage output from variac is used to control the solar radiation intensity in the solar simulator. The internal coil configuration of the variac is shown in Fig. 3.8b.

3.8 Thermocouple

A thermocouple serves as a temperature-measuring instrument composed of two distinct metal wires connected at one end. The presence of a temperature variation across the thermocouple generates a proportional low voltage, a phenomenon referred to as the Seebeck effect. For the indoor and outdoor experiments, a K-type thermocouple was used for measuring module temperature. K-type thermocouples are constructed from two distinct alloy wires: one wire is Chromel (comprised of Nickel and Chromium), identified as the positive or red wire, while the other wire is Alumel (comprised of Nickel and Aluminum), designated as the negative or yellow wire. The temperature range of this thermocouple spans from -200 °C to 1100°C. Detailed technical specifications of the utilized thermocouple are provided in Table 3.3.

Table 3.3. Technical speciation of thermocouples

ANSI color code	AWG gage	Diameter (mm)	Insulation	Time constant (s)	Accuracy
Red = -, Yellow = +	24	0.51	PVC vinyl insulation	0.2	±0.5◦C

The thermocouple wire in the experimental setup is affixed to the rear side of the solar photovoltaic module to measure the module temperature.

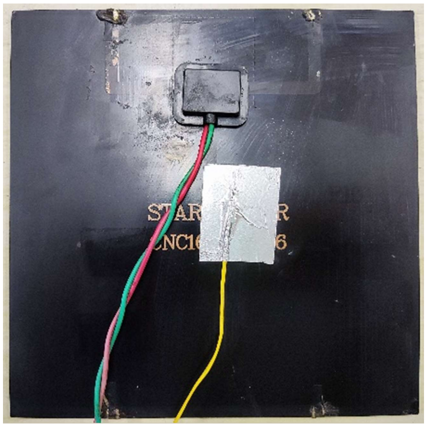

Fig. 3.9(a) Thermocouple attachment back side of solar photovoltaic module

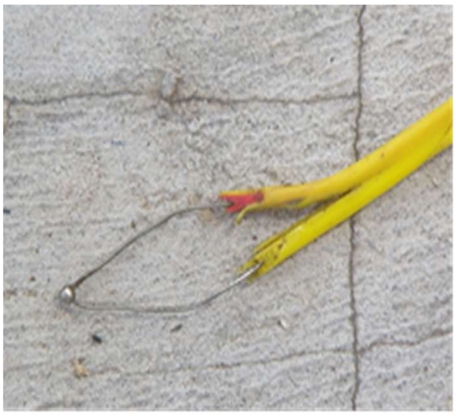

Fig. 3.9(b) Thermocouple junction formation

Prior to utilization, the thermocouples underwent calibration using a standard PT100 RTD temperature sensor in conjunction with a constant temperature oil bath instrument. During the calibration process, the thermocouples were placed within the oil bath at specific temperatures covering the required calibration range. Additionally, precise control of the reference or cold junction of the thermocouple was maintained at 0°C throughout the calibration process.

Fig. 3.10 Constant temperature oil bath instrument

The experimental output data of each thermocouple in terms of millivolt (mV) and respected temperature are also recorded for further use in finding calibration constant. All experimentally used thermocouples calibration constants are shown in Table 3.4.

Table 3.4 K-type thermocouple calibration details

Thermocouple Serial No.	Temperature range (°C)	m (Gradient coefficient)/Gain	C (Intercept Coefficient)/Offset
TC-1(CH2/0°)	0-100	0.96065±0.00377	1.89632
TC-2(CH3/10°)	0-100	0.95872±0.00527	2.29829
TC-3(CH4/22.5°)	0-100	0.96528±0.00259	1.70703
TC-4(CH5/30°)	0-100	0.96407±0.00347	2.13633
TC-5(CH6/40°)	0-100	0.97456±0.00496	1.58603
TC-6(CH7/50°)	0-100	0.97845±0.00577	0.92086
TC-7(CH8/60°)	0-100	0.96411±0.00277	1.92453
TC-8(CH9/70°)	0-100	0.98544±0.00367	0.87404
TC-9(CH10/80°)	0-100	0.96289±0.00387	1.80061
TC-10(CH15/90°)	0-100	0.97484±0.00372	1.21977
TC-11(simulator)	0-100	1.01589±0.0345	1.24655

Integrating above calibration data into the data logger ensures precise measurements during data collection. This enables the data logger to adjust incoming measurements, enhancing the reliability and accuracy of the collected data.

3.9 Solarimeter for Radiation Measurement Sensor

A solarimeter is used to measure solar radiation intensity. It furnishes measurable information concerning the quantity of solar energy or radiant energy received from the sun at a specific place.

Fig. 3.11(a) TES 1333 solarimeter

Fig. 3.11(b) TES 1333 solarimeter solar sensor

The TES 1333 solar power meter seen in (Fig. 3.11a) was used to measure the solar radiation on the horizontal surface of the module. This instrument has a measurement range of irradiation up to 2000 W/m^2, with a spectral response spanning 400-1100 nm with an accuracy of ±0.5% and a measurement resolution of 0.1 W/m^2. The white circular solar sensor as shown in Fig. 3.11(b) was positioned either at the tilt of the solar photovoltaic module or on the horizontal surface, in accordance with the position of the module, solar irradiation values were captured and recorded in W/m^2.

3.10 Ambient Temperature and Humidity Measurement Device

An ambient temperature and humidity measurement device, often referred to as a hygrometer or a thermo-hygrometer, is a tool used to measure and monitor the temperature and relative humidity levels in the surrounding environment. The HTC Easy Log (Fig. 3.12) instrument was used for ambient air temperature and relative humidity measurement with an accuracy level of ± 1 ◦C (range -40◦C to 70◦C) and ± 0.3 % RH (range 0 to 100 % RH) respectively. The resolution of the instrument was 0.1 ◦C for temperature and 0.1% for humidity. Devices are used during experiments to monitor the relative humidity (RH) and temperature conditions in the surrounding environment of experimental area.

Fig. 3.12 Ambient temperature and humidity measurement device

3.11 Data Loggers

The Agilent 34970A data acquisition system (Fig. 3.13a) was utilized for the continuous monitoring and recording of photovoltaic module output data under various conditions. This data logger integrates precision measurement capabilities with adaptable signal connections, serving the production and development of test systems. The switch comprises a three-slot mainframe with an integrated 6 ½ digit digital multimeter (Fig. 3.13b) with an accuracy of ± 0.004%. It allows customizing each channel independently to measure any of 11 distinct functions, all without incurring additional expenses or dealing with signal conditioning accessories. The on-module screw-terminal connections eliminate the necessity for terminal blocks, while a unique relay maintenance feature tracks every closure on every switch, ensuring effortless and predictable relay upkeep. One of the most favoured features of this data logger is its inclusion of a built-in thermocouple reference and 20 two-wire channels.

Fig. 3.13(a) Agilent 34970A data logger

Fig. 3.13(b) Agilent 34970A data logger card

The HP Bench Link Data Logger Pro is a Windows-based application created specifically to simplify the utilization of the Agilent 34970A alongside a PC for the collection and analysis of measurements. This software facilitates test setup, acquisition, and archiving of measurement data, along with real-time display and analysis of incoming measurements. For the current study, the data logger was configured to log data at five-second intervals and store it accordingly.

3.12 Light Source

The experiment utilized a Philips 1000W halogen lamp, adjusted by a voltage variac, to generate consistent radiation intensities ranging from 10 to 1200 W/m^2.

3.13 Temperature Controller

The TZN4S Autonics PID controller, in conjunction with an extra heater, was used for temperature regulation. The supplementary heat became necessary under conditions of low irradiation and high temperatures. Throughout the indoor experiment, an air conditioner was utilized to maintain constant room humidity and module temperature. To achieve temperatures below 20°C for the module when required, an additional ice pad was used.

3.14 Uncertainty Analysis of the Experiment

Following calibration, Experimentally utilized all measuring instruments to assess their uncertainties through calculation. The overall uncertainty of the experiments was determined using Kline and McClintock's equation (Mohtar et al., 2012).

$$\boldsymbol{e_R} = \sqrt{\left(\frac{\partial R}{\partial V_1} e_1\right)^2 + \left(\frac{\partial R}{\partial V_2} e_2\right)^2 + \cdots + \left(\frac{\partial R}{\partial V_n} e_n\right)^2} \quad (20)$$

Where

$\boldsymbol{e_R}$ is a total uncertainty of experiments.

R is a function of an independent variable of V_1, V_2… V_n.

e_i is the uncertainty of nth variable, (i =1,2,…..n)

The comprehensive uncertainty of the experimental arrangement has been presented in Table 3.5, derived from equation (20). As overall experiment's reliability is notably high due to its overall uncertainty being under 2%.

$$\boldsymbol{e_R} = \sqrt{(1)^2 + (1)^2 + (0.5)^2 + (0.3)^2 + (0.5)^2 + (0.004)^2}$$

$$\boldsymbol{e_R} = \mathbf{1.61}$$

Table.3.5 Total Uncertainty of the Experimental Setup

Apparatus	Accuracy (%)
Resistance Board	± 1
Voltage Variac	± 1
Thermocouple	± 0.5
Humidity Measurement Device	± 0.3
Solarimeter	± 0.5
Data Logger	± 0.004
Total Uncertainty of the System ($\boldsymbol{e_R}$)	±1.61

The multimeter is employed to cross-verify the validity of data collected by the data logger system, hence it has been excluded from the uncertainty calculation.

3.15 Multimeter

METRAVI (METRAsafe-19) professional true RMS industrial digital multimeter was used to preciously measure the experimental data. (Table 3.6)

Table 3.6 Professional digital multimeter technical details

Model no.	Components	Accuracy	Resolution	Certifications
Metrasafe-19	DC Voltage	±0.06%	0.01mV to 0.1V	CAT III 1000V, CAT IV 600V, CSA 61010-1, EN-61010-1, IEC-61010-1, Pollution Grade 2, UL 61010B-2-031, UL-61010-1
	AC Voltage	±1.0%	0.1mV to 1V	
	DC Current	±1%	0.01µA to 0.001A	
	Resistance	±0.3%	0.01Ω to 0.001MΩ	
	Temperature	±1.0%	1˚C	

Before commencing the experiment, all indoor and outdoor experimental data are meticulously cross-checked using a professional digital multimeter. Both the output data from the multimeter and the data logger values undergo thorough verification.

3.16 Pyranometer

The pyranometer is used to measure the amount of solar radiation received on the horizontal surface of an object. Exposure to radiation causes the temperature of the blackened horizontal surface to increase. Heat dissipates from this surface through conduction, convection, and radiation. The attained equilibrium temperature serves as a gauge of the radiation level. A thermocouple array is employed to measure this temperature. As the pyranometer sensor outputs data in millivolts, a conversion factor is necessary to convert millivolt readings into Watts per square meter.

$$\text{Watts/meter}^2 = \frac{\text{Displayed Value (in mV)}}{\text{Constant (mentioned on certificate)}} \times 1000$$

Here two pyranometers were utilized, with one employed for measuring direct or beam radiation and the other for measuring diffuse radiation. Both pyranometers were positioned horizontally in the vicinity of the outdoor experimental setup. The detailed technical specifications of the pyranometers are presented in Table 3.7.

Table 3.7 Technical data of pyranometer details

Model No. & Serial No.	Sensor	Spectral range	Sensitivity	Time constant	Maximum intensity
DWR 8101 187025	90 element thermopile	0.3 to 3 μmeter	4 mV/kW/m²	< 22 seconds	>200 mW/cm
DWR 8102 187012	90 element thermopile	0.3 to 3 μmeter	4 mV/kW/m²	< 22 seconds	>200 mW/cm

All pyranometers undergo calibration using a secondary standard Eppley precision spectral pyranometer (model PSP sr. no. 36208F3) in adherence to international standards. As indicated on the certificate, the pyranometer calibration constant for DWR 8101(Sl. No.-187025) is 19.37 $\mu V/W/m^2$, while for DWR 8101(Sl. No.-187012), it stands at 19.47 $\mu V/W/m^2$.

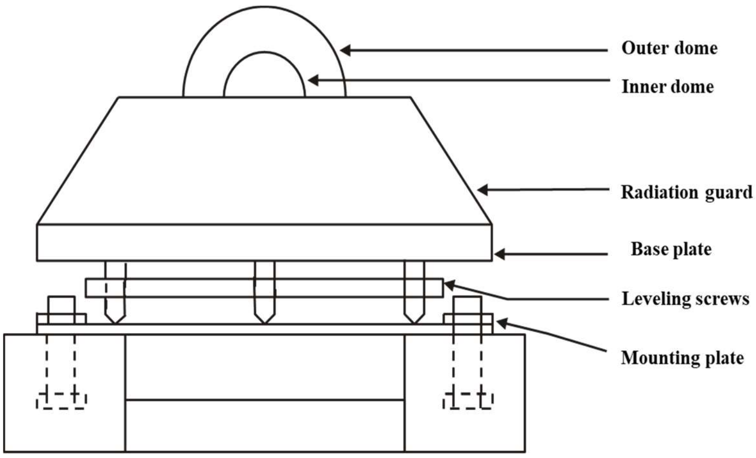

Fig. 3.14 (a) Solar radiation sensor mounting diagram

Fig. 3.14(b) Direct radiation measurement setup

During the experiment, direct radiation was measured using pyranometers mounted on a horizontal surface (Fig. 3.14b). The output data from the pyranometers was automatically recorded by the data logger every five seconds in the laboratory. At the time of installation of the pyranometers on the horizontal mounting plate, level adjustment was performed using three levelling screws, as shown in Fig. 3.14a.

3.17 Diffuse Solar Radiation Measurement

Diffuse radiation was measured by a pyranometer using a shading ring, which involves mounting the pyranometer at the centre of the semicircular shading ring. The shading ring is positioned so that its plane aligns parallel to the path of the daily movement of the sun, ensuring continuous shading of the thermopile element and the glass dome of the pyranometer from direct solar radiation. As a result, only the diffuse radiation received from the sun is measured by the pyranometer.

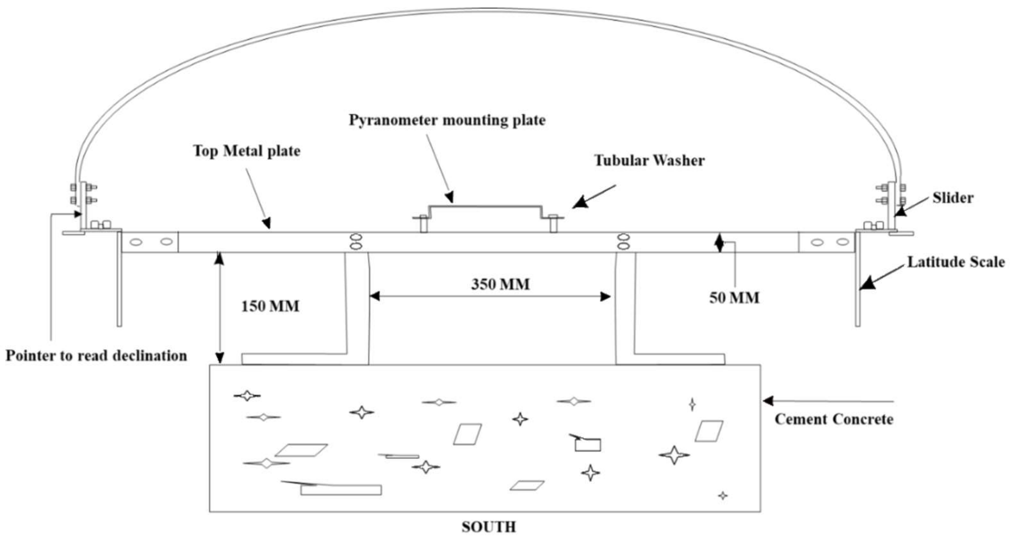

Fig. 3.15 Shading ring installation diagram

The horizontal rectangular frame measures approximately 350×800 mm, with its longer sides oriented in an east-west direction. Two sides of the frame were connected to two angle iron arms (each 700 mm long) with slots along their length, accommodating sliders that hold the semicircular shading ring (Fig. 3.15, 3.17). These arms pivot around a horizontal axis passing through the centre of the rectangular frame and can be adjusted to an angle equal to the site or station's latitude. The movement of the ring along the arms enables adaptations for changes in the sun's declination. Following the installation of the shading ring, a solar radiation sensor was placed on a circular plate. Throughout the experiment duration, the angle of the shading ring was adjusted every 15 days based on the solar declination angle (δ) over the year, as depicted in Fig. 3.16. Additionally, the mounting plane of the pyranometer was adjusted according to the latitude of the installation location.

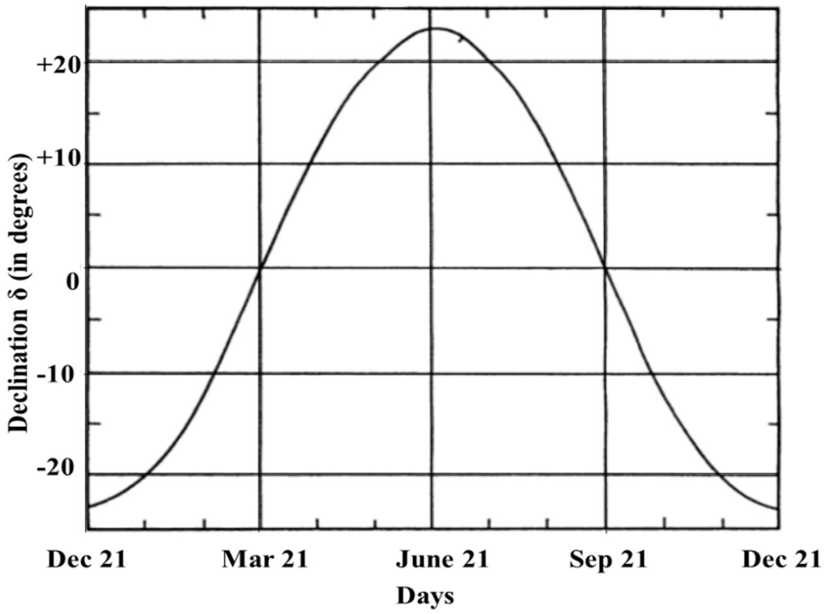

Fig. 3.16 Variation of declination over the year (Sukhatme, S. P. and J. K. Nayak, 2017)

Fig.3.17 Diffuse radiation measurement setup

3.17.1 Calculation Process of Solar Radiation on a Different Tilted Angle

At any point on the Earth, the amount of solar beam radiation energy falling on a surface with any orientation is transformed from the incoming solar radiation to an adjusted value perpendicular to that surface. The relationship between the angle (θ) formed by the incoming beam and the surface's normal, and various factors such as slope (β), latitude (ϕ), declination (δ), surface azimuth angle (γ), and hour angle (ω) is described by a general equation. By employing these parameters, the amount of radiation received by a specific plane can be determined.

3.17.2 Calculation of Solar Irradiation on the Tilted Surface

For, location Kolkata (ϕ= 22.5726° N), date 08th April 2022, global radiation is(I_g) 758.48 W/m^2 and diffuse radiation (I_d) is 286.65 W/m^2.

On this day (N) =98

Declination in degrees (δ)=$23.45\ sin\left[\frac{360}{365}(284+N)\right]$ (21)

$$(\delta)=23.45\ sin\left[\frac{360}{365}(284+98)\right]$$

$$(\delta)= -5.2088°$$

The slope β is the angle made by the plane surface with the horizontal. Solar incidence angle (θ) is the angle between the normal of the module and the sun's rays. The general formula for this angle is

$$cos\theta = sin\phi\ (sin\delta\ cos\beta + cos\delta\ cos\gamma\ cos\omega\ sin\beta) + cos\phi\ (cos\delta\ cos\omega\ cos\beta - sin\delta\ cos\gamma\ sin\beta) + cos\delta\ sin\gamma\ sin\omega\ sin\beta \quad (22)$$

The measurement of time relies on the perceived angular movement of the sun as it travels across the sky, with solar noon marking the moment the sun passes directly over the observer's meridian (Fig. 3.18). Solar time, also known as local apparent time, serves as the reference for all calculations involving the sun's position in the sky. However, it differs from the time displayed by local clocks.

Local apparent time =Standard time ± 4 (Standard time longitude-longitude of location) + (Equation of time correction) (23)

Equation of time correction = $229.18 \times (0.000075 + 0.001868 \times \cos(B) - 0.03207 \times \sin(B) - 0.014615 \times \cos(2B) - 0.04089 \times \sin(2 \times B))$ (24)

Where $\quad B = (N - 81)\frac{360}{364}$ (25)

Hour angle (ω)= ±0.25 (number of minutes from local solar noon)

The hour angle at local solar noon is zero, with each $\frac{360°}{24} = 15°$ of longitude equivalent to 1 h. Where the plus sign applies to afternoon hours and the minus sign to morning hours.

Tilted surface facing south (γ=0)

$$\cos\theta = \sin\delta \times \sin(\phi - \beta) + \cos\delta \times \cos\omega \times \cos(\phi - \beta) \quad (26)$$

Horizontal surface

$$\cos\theta_z = \sin\theta \times \sin\delta + \cos\phi \times \cos\delta \times \cos\omega \quad (27)$$

$$\text{Tilt factor beam radiation } (r_b) = \frac{\cos\theta}{\cos\theta_z} = \frac{\sin\ \times\sin(\phi-\beta)+\cos\delta\times\cos\omega\times\cos(\phi-\beta)}{\sin\theta\times\sin\delta+\cos\phi\times\cos\delta\times\cos} \quad (28)$$

$$\text{Tilt factor of diffuse radiation } (r_d) = \frac{1+cos}{2} \quad (29)$$

$$\text{Tilt factor of reflected radiation } (r_r) = \rho \times \frac{1-cos\beta}{2} \quad (30)$$

Concrete or glass diffuse reflectivity (ρ) = 0.35 value used [Duffie, J. A. and William A, 2013].

Global irradiance (I_g) is the total solar power received by the surface of the solar PV module. (I_g) is the sum of direct, diffuse, and reflection irradiation from the nearby surfaces

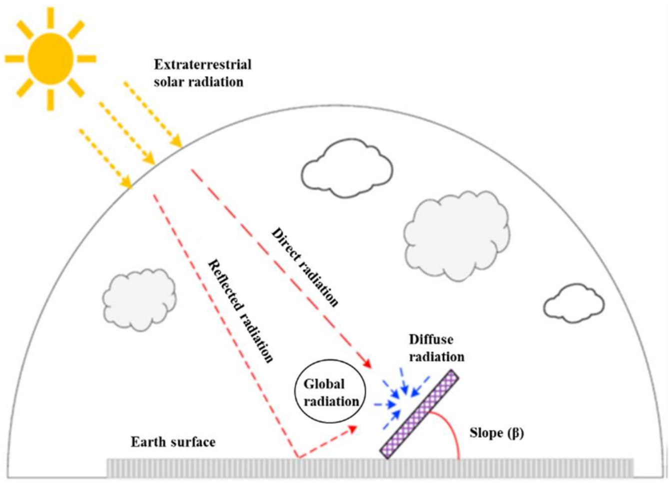

Fig.3.18 Schematic representing of the sky and different constituents of solar irradiation over a PV tilted angle

$$I_{Tilt} = I_{Beam} + I_{Diffuse} + I_{Reflected} \tag{31}$$

$$I_{Tilt} = I_{Horizontal} \times r_b + I_{Diffuse} \times r_d + ((I_{Horizontal} + I_{Diffuse}) \times r_r) \tag{32}$$

Table:3.8 Final sample calculation of solar radiation in different slope

β	0°	10°	22.5°	30°	40°	50°	60°	70°	80°	90°
I_{Tilt}	758.49	774.17	772.48	760.11	730.80	687.68	632.04	565.59	490.34	408.58

Table 3.8 shows the sample calculation of solar radiation in different slopes.

3.18 Air Mass

The concept of "air mass" is commonly defined as a standardized spectral reference employed in calculations concerning solar energy and the efficiency evaluations of photovoltaic systems. This reference characterizes the spectral spread of solar radiation under typical conditions at the Earth's surface. Essentially, air mass quantifies the distance that light travels through the Earth's atmosphere, standardized to the most direct path. It serves as a metric for measuring the extent to which the intensity of solar radiation weakens during its journey through the atmosphere due to absorption by air particles and dust.

$$Air\ mass(m) = \frac{1}{\cos(\theta_z)} \tag{33}$$

where θ_z is the zenith angle. Hence, radiation with an air mass value of m=0 is typically employed for capturing sunlight in outer space, where atmospheric interference is not a factor. Thus at sea level m = 1 when the sun is at the zenith and m = 2 for a zenith angle θ_z of 60°. Air mass 1.5 corresponds to the condition where the sun is at an angle of 48.2 degrees above the horizon. In other words, the sunlight has to pass through 1.5 times the thickness of the Earth's atmosphere to reach the Earth's surface.

The air mass 1.5 spectrum serves as a benchmark for assessing the effectiveness and productivity of solar cells and modules at STC. It is applied in computations to predict the anticipated energy yield of a PV system and to evaluate the performance of an indoor solar simulation configuration.

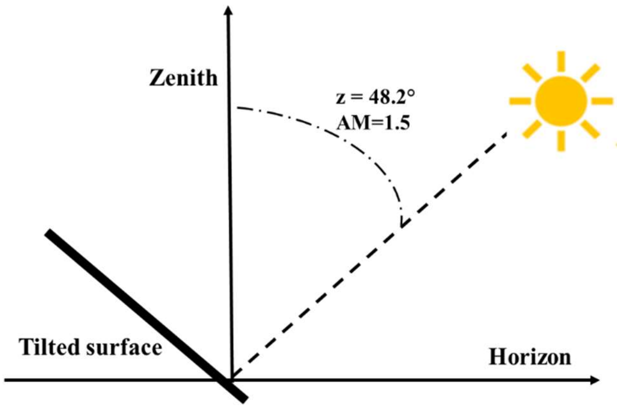

Fig. 3.19 (a) AM 1.5 measurement details

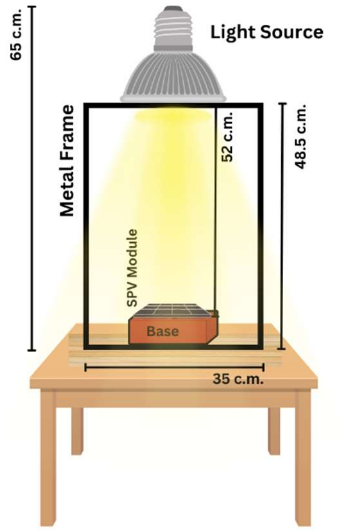

Fig. 3.19 (b) Measurement details of simulating setup

The determination of specific calculations related to air mass 1.5 will be influenced by the context and purpose. In this scenario, it is being employed to compute the power output of a solar module under these conditions (Fig. 3.19(a)). The standardized air mass 1.5 spectrum data encompasses the dispersion of sunlight energy across different wavelengths. This data, when combined with the solar cell's spectral response, is used to estimate the solar cell's efficiency and power output. The output power is then compared with the experimental solar simulator uniform light spectral response data of solar cells, and the most suitable distance of 52 cm (3.19b) from the light source to the horizontal base of the solar cell is determined.

3.19 Outdoor Solar Photovoltaic Experimental Installation

Now for experimental purposes, the ten identical solar modules as stated earlier phase in this chapter, which were previously tested using a laboratory-based solar simulator, were positioned at different tilt angles facing due south in outdoor conditions on the rooftop of the department building of School of Energy Studies, Jadavpur University. Solar modules were installed at tilt angles of ∠0°, ∠10°, ∠22.5°, ∠30°, ∠40°, ∠50°, ∠60°, ∠70°, ∠80°, and ∠90° on a flat rooftop surface, without encountering any shading obstacles. This setup is illustrated in Fig. 3.20, providing a visual representation of how the solar panels are positioned on the rooftop at different tilt angles. Experiment aims to investigate the performance of the solar modules varies with different tilt angles under real outdoor conditions.

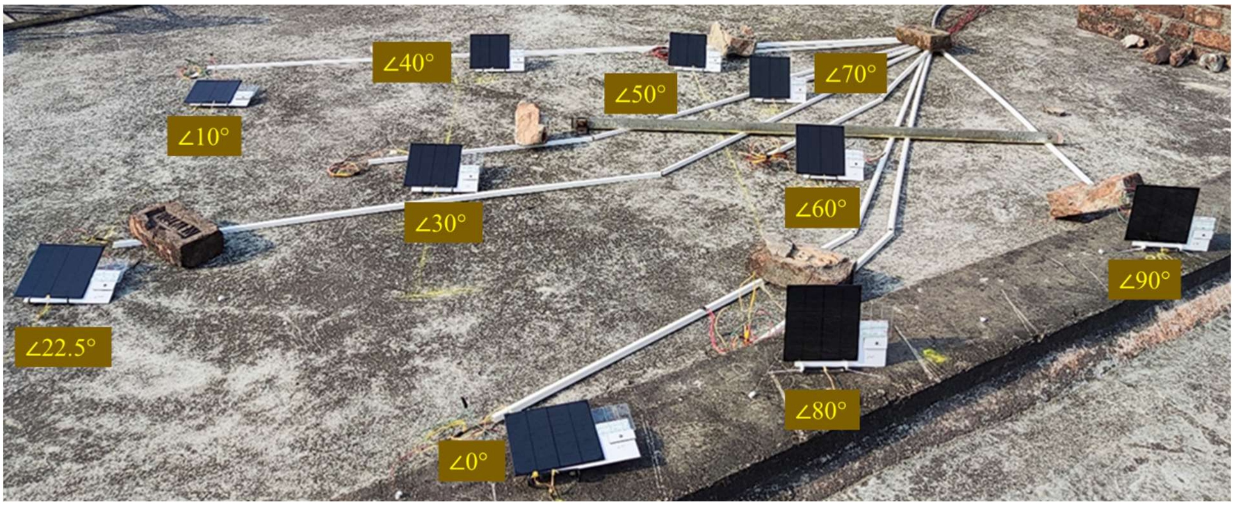

Fig. 3.20 Rooftop solar installation in different angle with due south orientation

A k-type thermocouple was affixed to the midpoint of the rear side of each photovoltaic module to measure the module's temperature. All these thermocouples were linked to a data logger for the purpose of recording data.

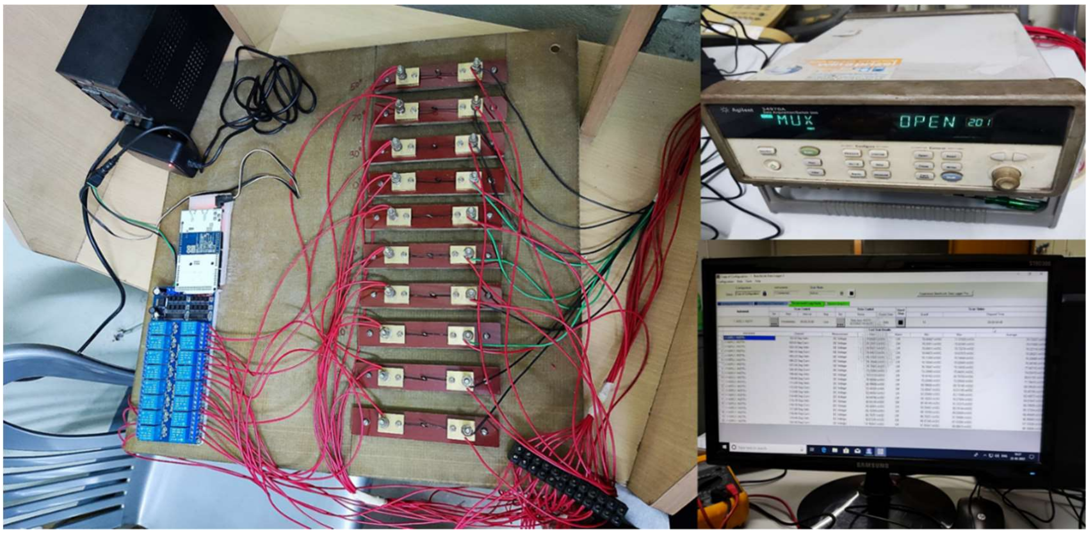

Fig. 3.21 Rooftop solar indoor experimental setup and data acquisition system.

A sixteen-channel relay module was employed to automatically measure voltage and current at specified time intervals from each solar module. For current measurement during the experiment, a high-precision shunt mechanism was installed across each photovoltaic module. Transparent glass slides were utilized at the same incline angle to assess dust accumulation over the experimental period. Data on dust deposition was collected from these glass slides at different intervals. The data measurement setup was established in the solar energy laboratory, depicted in Fig. 3.21.

In this setup, an Arduino Due microcontroller was utilized to oversee the voltage and current measurement process. Voltage was measured for two minutes, while current was measured for thirty seconds, within a logging duration of five seconds. Simultaneously, output data from each photovoltaic module was recorded by the data logger. The experiment was automatically conducted for eleven hours daily according to the experimental schedule, controlled by Arduino-based programming, detailed in Annexure-I.

Furthermore, a schematic diagram illustrating outdoor installations and measurement processes is presented in Fig. 3.22 and Table 3.9 shows the Relay & Arduino Due Configuration.

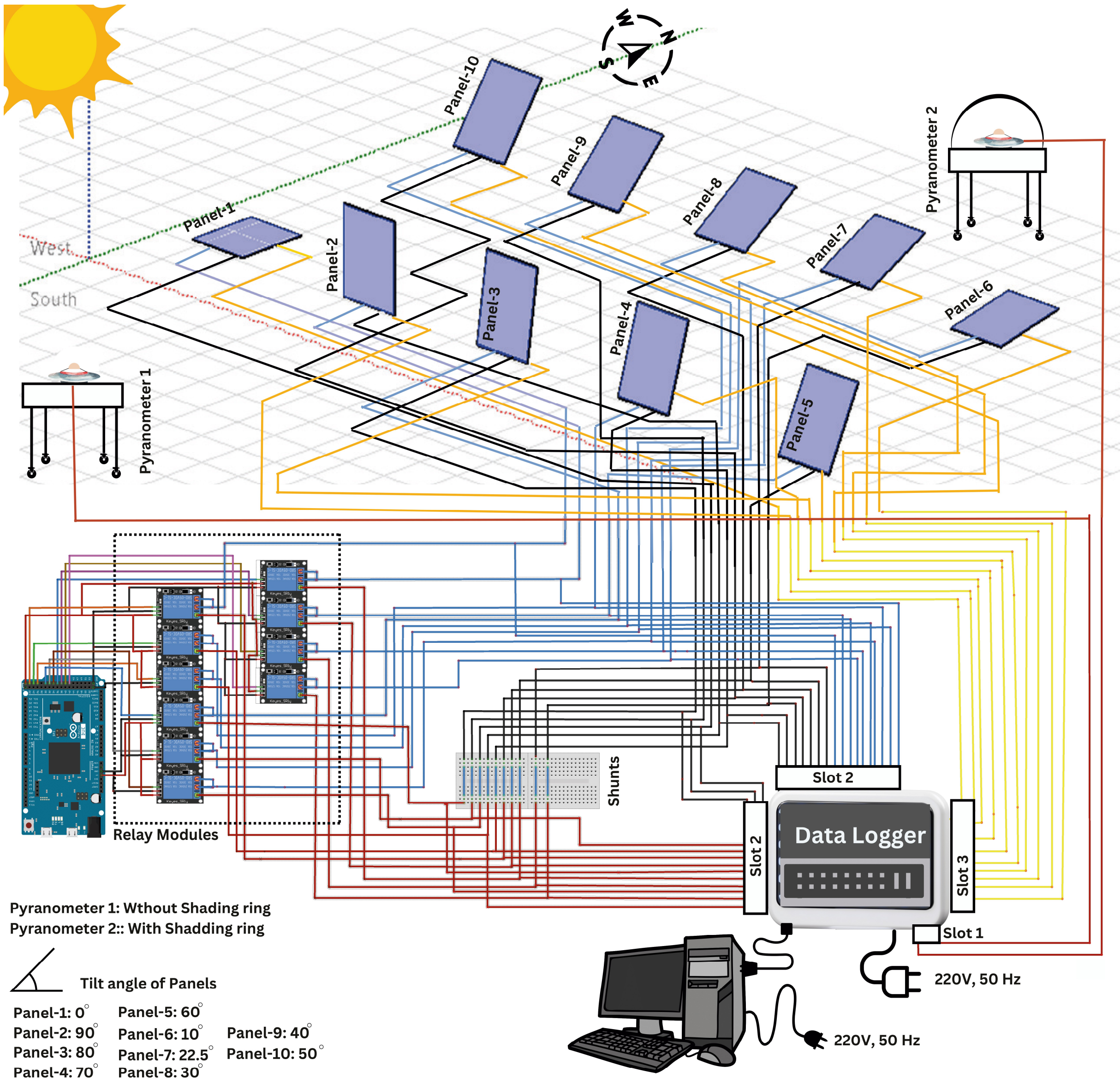

Fig. 3.22 Schematic diagram of outdoor testing facility

The 16-channel relay and Arduino are consistently supplied with 5 volts throughout the experiment. The specific pin configurations are outlined in the Table.3.9 below.

Table.3.9 Arduino Due and 16- channel Relay connected pin configuration

Arduino Due pin No.	16-channel Relay pin No.
22,23	GND
24,25	15,16
26,27	13,14
28,29	11,12
30,31	9,10
32,33	7,8
34,35	5,6
36,37	3,4
38,39	1,2
40,41	+5 V

The output data from all modules was logged in a data logger and saved in a data storage system to be used for further calculations. Beginning with this data, the total daily energy generation from each solar photovoltaic module was calculated.

3.20 Dust Collection and Measurement Process

Transparent glass slides were utilized for the collection of naturally accumulated dirt over a specified period. A glass holder base, equipped with a soiling test bed capable of accommodating multiple glass slides simultaneously, was prepared, ensuring precise alignment with the installation angle of the photovoltaic modules illustrated in Fig. 3.23. To replicate the natural soiling conditions experienced by a photovoltaic module, eight glass samples measuring 75 mm × 25 cm × 1.4 mm were installed to match the equivalent incline angle of the solar photovoltaic modules. These glass samples were positioned to collect dust accumulation throughout the experimental period. Before the initiation of the experiment, the glass slides underwent a thorough cleaning using an acetone solution to remove any pre-existing dust deposited on the surface. Subsequently, they were dried using tissue paper. Hence, the weight of each glass slide was measured using the A & D Company Limited HR-250AZ SHS microbalance system, possessing a precision of 0.001 g.

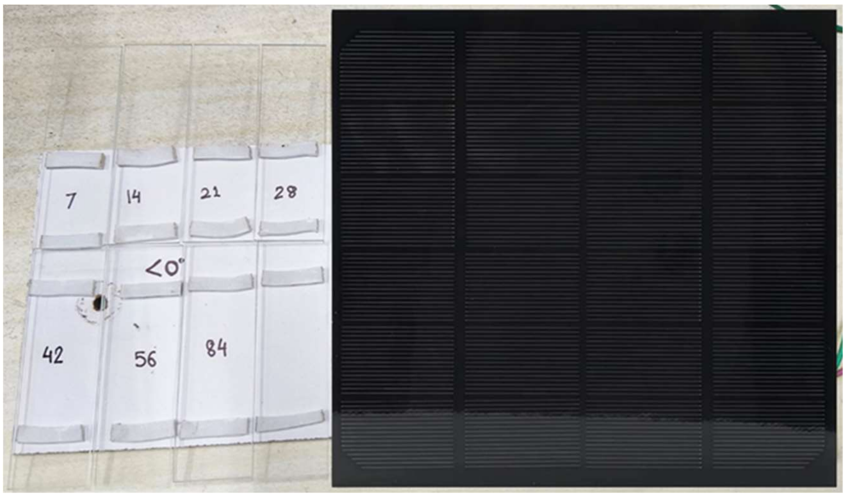

Fig. 3.23 Soiling test bed with glass slide alignment with solar photovoltaic

Subsequently, on various days throughout the experiment, a soiled glass slide was collected, and its weight was measured using a weight machine (refer to Fig. 3.24a).

Fig. 3.24(a) High precision weight balance

Fig. 3.24(b) Glass slide after soling deposition

Initially, the weight of the dusty glass slide was recorded. To ensure a comprehensive error-free experiment, the rear side of the glass slide was meticulously cleaned to eliminate any potential measurement discrepancies caused by dust accumulation or adhesive obstacles (Fig. 3.24b). After cleaning, the weight was measured again. The variance between the weight of the glass slide after the deposition of dirt and its initial weight yielded the mass of the deposited dust. The daily dust deposition density was calculated by dividing the dust mass by the surface area of the slide, measured in grams per square meter (g/m²).

3.21 Current Measurement through Shunt

The measurement of electric current involves directing it through a shunt resistor. A shunt resistor, which is a low-value resistor, is connected in parallel with the load or circuit under measurement. As the current passes through the shunt resistor, a voltage drop occurs across it, enabling the measurement and subsequent calculation of the current passing through it using Ohm's law. This method facilitates precise current measurement without disrupting the operation of the main circuit.

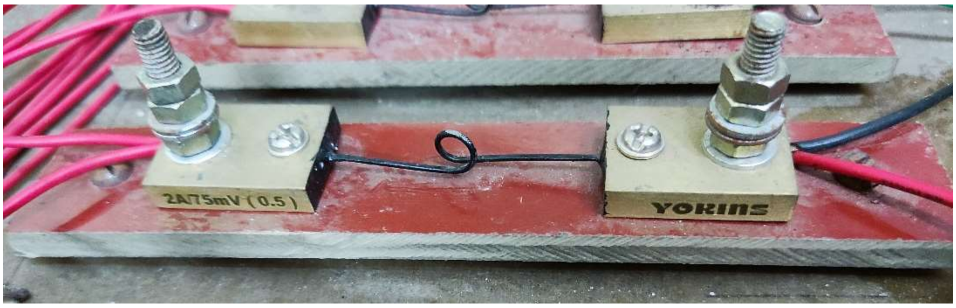

Fig. 3.25 Yokins class 0.5 accuracy level 2A/75 mV shunt

Here in the experimental measurement setup, 10 shunts were used (Fig. 3.25) to measure the current from 10 different incline-angle photovoltaic modules. The experimental used shunt accuracy level 0.5 class.

Sample calculation

Shunt output voltage 32 mV

Current = $\frac{2\,A}{75\,mV} \times 32\,mV = 0.8533\,A$

3.22 Microcontroller

The Arduino Due is an open-source microcontroller board that relies on the Atmel SAM3X8E ARM Cortex-M3 CPU.

Fig. 3.26 Arduino Due microcontroller

Its operation is powered by the Atmel SAM3X8E, which operates as a 32-bit ARM Cortex-M3 CPU running at 84 MHz. This renders it notably more potent compared to the 8-bit microcontrollers featured in other Arduino boards. With 54 digital input/output pins, 12 analog inputs, 2 analog outputs, and various communication interfaces like UART, SPI, I2C, and CAN, the Arduino Due offers extensive functionality. Because of its 32-bit architecture and increased clock speed, it possesses the ability to handle more computationally demanding tasks in contrast to other Arduino boards. This characteristic renders it well-suited for applications that demand higher processing capabilities. To program it, we need to utilize the Arduino Software (IDE), but it's essential to select the "Arduino Due (Programming Port)" as the designated board. The Due programming port employs a native USB interface for both programming and communication. The Arduino Due offers 512KB of flash memory for storing code and 96KB of SRAM for data storage. Refer to Figure 3.26 for an illustration of the Arduino Due microcontroller.

3.23 Relay Module

In Fig. 3.27, there is an electronic module featuring 16 distinct relays. Relays are electronic switches that utilize electromechanical mechanisms to control the flow of electricity within a circuit. In this case, the module is designed to function with a 5V power supply, indicating its compatibility with low-voltage systems. Each of the 16 channels within the module has the capability to independently manage an electrical circuit or device by toggling a switch between an open and closed state.

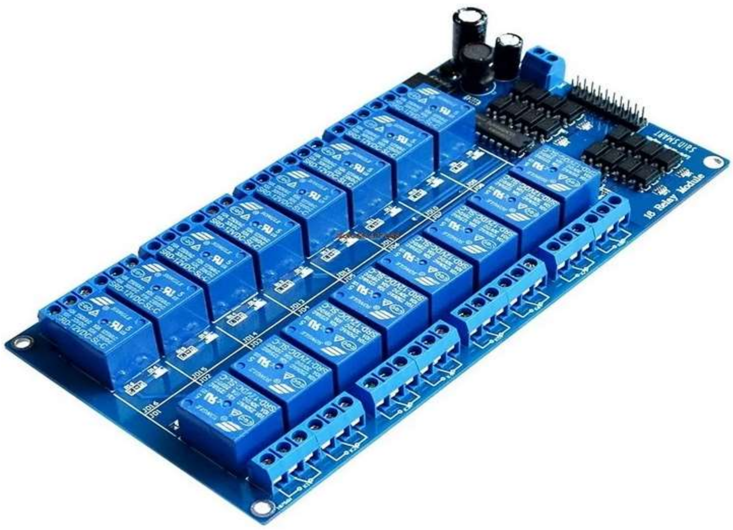

Fig. 3.27 Sixteen channel relay module

Within the experimental setup, control was exercised over 10 relays through the Arduino Due microcontroller. These relays were set in a normally closed condition, employed during the measurement of PV module voltage, and the timing to energize the relays was determined for measuring the current.

3.24 Manual Dust Cleaning Process

As previously mentioned, the accumulation of dust is considered a significant issue affecting the power production of PV modules, demanding constant cleaning and maintenance to address it. The cleaning process can involve either automatic/robotic methods or manual intervention. However, an automatic process would demand an additional energy source and entail higher costs. Therefore, for the current study, a cost-effective and less energy-intensive approach, namely the manual dust cleaning process, was employed.

Fig. 3.28 Solar photovoltaic module used for cleaning purpose

Fig. 3.29(a) Water sprayer

Fig. 3.29(b) Manual dust cleaning process

To illustrate the cleaning mechanism, three pre-existing 110 Wp m-Si solar modules were used, each measuring 67cm×100 cm (Fig.3.28). For this cleaning process, a water sprayer (Fig. 3.29(a)) with a total capacity of 16 L, featuring a plastic BCN type with 8 holes and operating at a working pressure range of 0.3-0.4 MPA, was utilized. Initially, the sprayer was filled with water, and the PV modules underwent cleaning at specific intervals of 1 day, 1 week, 2 weeks, 3 weeks, 8 weeks, and 12 weeks, by maintaining a consistent pressure of 0.4 MPA manually (Fig. 3.29(b)).

Afterwards, the excess water was wiped from the PV modules. Now, by determining the rate of water flow through the nozzle per minute and recording the time required to completely clean the PV module in each scenario, the required water for cleaning purposes can be determined.

3.25 Water Quality Measurement Process for Cleaning

Ensuring the appropriate water quality for cleaning PV modules is crucial to maintaining their efficiency and longevity. The primary water quality parameters for cleaning PV modules include pH level, conductivity, total dissolved solids (TDS) and the absence of microbiological contaminants. Low TDS levels are preferred to avoid mineral buildup on models, while a neutral pH helps to prevent corrosion or residue formation. Additionally, water with low conductivity is desired to minimize the risk of electrical conduction on the modules. Regular testing and monitoring of water quality, including visual inspection for impurities, are essential steps. Using purified water or adhering to specified quality standards helps prevent damage to the modules and ensures optimal performance of the PV system over time.

Fig. 3.30 Water quality measuring instrument & process

The situation mentioned above was addressed in the present study by utilizing six different types of water i.e. Rainwater, RO water, Purified water, Treated water, Tap water and Ground water. For each type of water, the TDS, pH level, and electroconductivity were measured using the pH meter

(Fig. 3.30) by containing them in separate beakers and pouring the pH meter sensor inside the water.

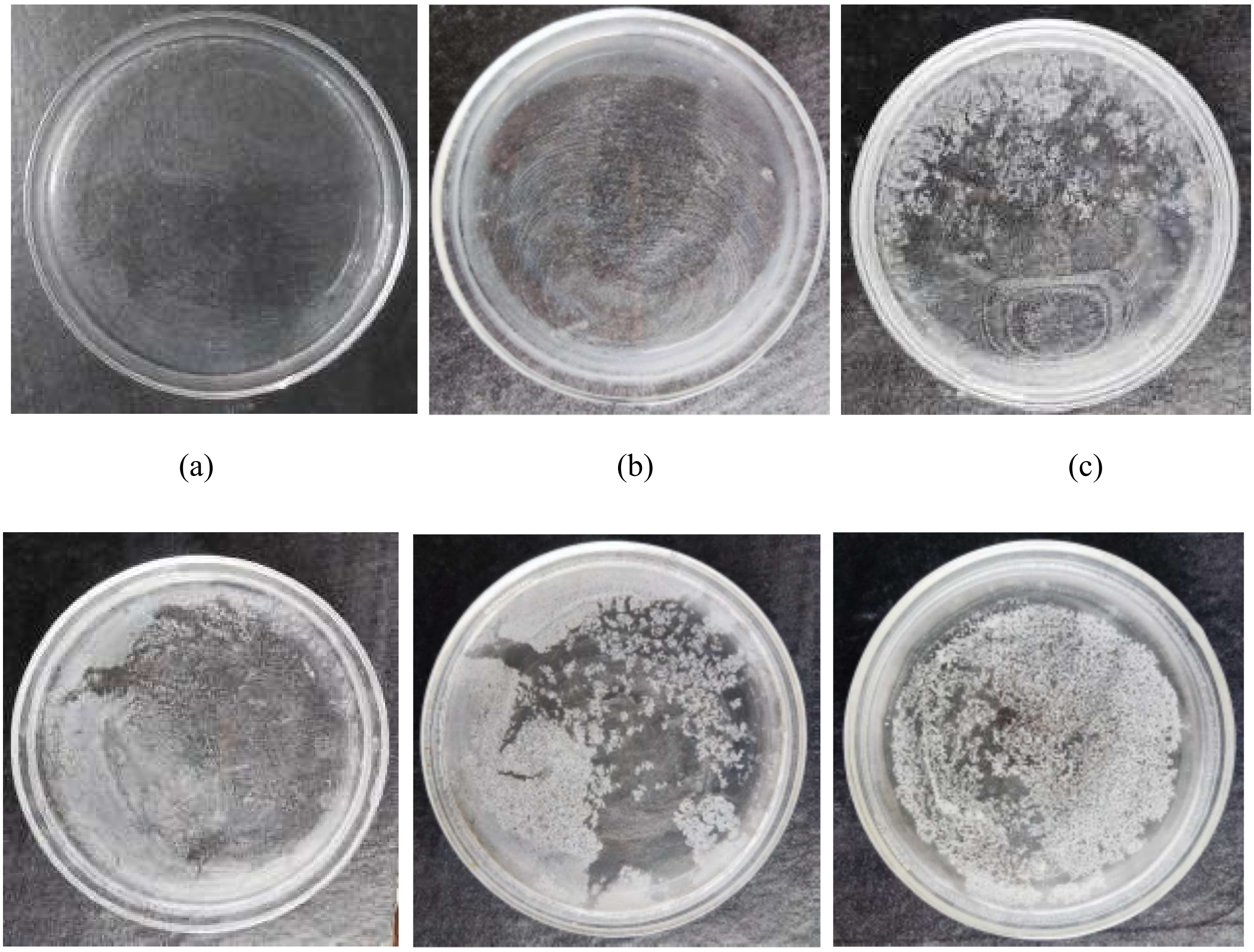

(a) (b) (c)

(d) (e) (f)

Fig. 3.31 Water pollution samples after vaporization process

(a) Rain water (b) RO water (c) Purified water (d) Treated water (e) Tap water (f) Ground water

Furthermore, the pollutant levels of water samples were also determined by showing the precipitation. In this study. Initially, six distinct types of water samples (50 ml) as mentioned above were placed in separate Petri dishes, followed by their vaporization in an air oven at 100°C for 45 minutes. After the vaporization process, the precipitate of dirt and pollutants in the water samples is illustrated in Fig. 3.31 (a)-(f).

3.26 PVsyst Software

PVsyst is a widely used software tool in the field of photovoltaics (PV) for simulating, designing, and analyzing solar photovoltaic systems. In this study PVsyst 7.4 version of solar PV modeling software was used for simulation purposes. Features of the PVsyst solar simulation software have been discussed below.

- Simulation: PVsyst allows users to simulate the performance of PV systems under various conditions, such as different locations, orientations, tilt angles, and system configurations. It takes into account parameters like solar irradiance, temperature, shading, and module specifications to predict the energy production of the system accurately.
- Design: Users can design PV systems using PVsyst by inputting parameters like the geographical location, system size, type of modules and inverters, mounting structures, and shading objects. The software helps optimize the design for maximum energy production and economic feasibility.
- Shading Analysis: PVsyst includes tools for shading analysis, which are crucial for determining the impact of shading from nearby objects like buildings, trees, or terrain. This analysis helps in optimizing the layout of PV arrays to minimize shading losses.
- Financial Analysis: The software provides tools for financial analysis, including the calculation of project costs, energy yields, and financial metrics such as payback period, net present value , and internal rate of return . This helps users evaluate the economic viability of PV projects.
- Database: PVsyst includes a comprehensive database of PV modules, inverters, and meteorological data for various locations worldwide. Users can select components from the database or add custom data to tailor simulations to specific project requirements.
- Performance Evaluation: PVsyst enables users to analyze the performance of existing PV systems by comparing simulated results with actual measured data. This allows for the identification of potential issues and optimization opportunities to improve system performance.
- CO_2 Calculation: Based on the simulated energy production and the CO_2 intensity of the electricity grid, PVsyst calculates the CO_2 emissions avoided by using solar energy instead of conventional grid electricity.
- Report Generation: The software generates detailed reports summarizing the simulation results, design parameters, financial analysis, and other relevant information. These reports are useful for communicating project proposals, findings, and results to stakeholders.

Overall, PVsyst is a powerful tool for engineers, researchers, and professionals involved in the design, optimization, and analysis of solar PV systems, helping them make informed decisions and maximize the performance and profitability of their projects.

3.27 Minitab Statistical Software

Minitab Statistical Software is a powerful tool used for data analysis and statistical visualization. It provides a user-friendly interface for conducting statistical analysis, generating graphs, and interpreting results. In this study, statistical analysis was conducted using Minitab Statistical Software (2021). The features of the Minitab Statistical Software have been discussed herein.

- Data Analysis: Minitab provides a comprehensive suite of tools for data analysis, including descriptive statistics, hypothesis testing, regression analysis, ANOVA (Analysis of Variance), time series analysis, and non-parametric tests.
- Experimental Design: Minitab supports experimental design methodologies for optimizing processes and products. It offers tools for designing experiments, analyzing results, and identifying factors that significantly impact the outcome.
- Predictive Analytics : Minitab Statistical Software offers a comprehensive suite of features tailored for predictive analytics and automated machine learning. From forecasting future outcomes based on historical data to simplifying the machine learning process through automated model selection and hyperparameter tuning, Minitab empowers users to build accurate predictive models with ease. With Minitab, users can perform advanced predictive analytics tasks efficiently, making informed data-driven decisions and forecasts with confidence.
- Simulations and Distributions: Minitab Statistical Software offers powerful tools for simulating and analyzing distributions, enabling users to effectively understand and analyze probabilistic phenomena. With its random number generator and comprehensive suite of probability density, cumulative distribution, and inverse cumulative distribution functions, users can simulate various scenarios and explore the behavior of random variables with precision. Additionally, Minitab facilitates random sampling, bootstrapping, and randomization tests, enabling users to draw insights from data through resampling techniques while ensuring statistical validity. Whether performing Monte Carlo simulations or conducting hypothesis tests, Minitab equips users with the tools needed to make informed decisions and gain deeper insights into the uncertainty inherent in their data.

Overall, its features support various research objectives, from hypothesis testing to predictive modeling, making it a valuable asset for researchers across disciplines seeking to derive insights and make evidence-based decisions.

3.28 Conclusion

In conclusion, this chapter has detailed the comprehensive methodology employed to address the research objectives of this study. The combined methodology and experimental setup detailed in these chapters represent a meticulous and purposeful approach towards understanding the multifaceted dynamics of solar panel's performance parameters concerning dust accumulation at diverse tilt angles and the characterization of collected particles using glass slides. The chapter meticulously delineates the systematic approach adopted for solar data collection, leveraging advanced instrumentation such as sensors, data loggers etc. This approach has been strategically designed to capture precise and comprehensive solar irradiance, temperature, and humidity data, forming the cornerstone for subsequent analysis. Simultaneously, this chapter also outlines a systematic design for the investigation of dust accumulation at various tilt angles. The structured alteration of tilt angles alongside designated dust collection techniques, facilitated by glass slides, aims to discern the nuanced impacts of dust deposition on solar modules. This methodological approach provides valuable insights into the specific types of dust and their properties, crucial for devising effective cleaning and maintenance strategies. Overall, this chapter establishes a solid foundation for the subsequent empirical investigation and analysis. The methodological framework developed herein sets the stage for the exploration and interpretation of data, aiming to provide nuanced insights into the interplay between solar module performance parameters, dust accumulation, and cleaning strategies. The forthcoming chapters will delve deeper into the empirical findings, facilitating a more comprehensive understanding of the relationships observed through this methodological approach.

Chapter 4

Modelling and Analysis of the Performance of Photovoltaic Panels - Simulation and Standard Laboratory Conditions

4.1 Introduction

Photovoltaic panel (PV) power generation prediction under varying levels of irradiance and temperatures is highly beneficial during both the planning and operational phases of a photovoltaic system. There exists a substantial body of literature focused on estimating the current voltage (I-V) characteristics of PV panels. Many studies use formulas derived from an equivalent circuit of the PV panel to describe its I-V characteristics, including diode current represents the flow of electrons across the p-n junction of the solar cell, contributing to the overall current output of the PV panel. The I-V characteristics of PV panels exhibit variations in response to changes in temperature and irradiance. The literature proposes dependencies of equivalent circuit parameters on temperature and irradiance to capture these changes effectively. The equivalent-circuit model of a PV cell is an electrical framework employed for analyzing the behaviour of the PV panel. Such a model provides the I-V and power-voltage (P-V) characteristics, which vary with external factors such as irradiance and temperature (Chaibi et al., 2018). Another study demonstrates based on a single diode model that PV cell parameters such as shunt-resistance (R_{sh}), series-resistance (R_s), diode ideality factor (n), and reverse saturation current (I_0) exhibit a nonlinear relationship with irradiance (Khan et al. 2010), whereas the Siddiqui et al., (Siddiqui et al., 2013) proposed that the diode ideality factor exhibits a linear temperature dependence, while the value of R_{sh} shows a reciprocal dependency on irradiance. Additionally, the parameter I_0 is suggested to vary with temperature, and R_s remains independent of both temperature and irradiance. Therefore, there is a need to analyze the performance of solar PV panels comprehensively using the PVsyst simulation model (PVsyst 7.4, 2023), utilizing the manufacturer data across an extended range of irradiance and temperature values. Despite being based on manufacturer data, PVsyst models are either tailored for specific conditions or purely theoretical analyses, resulting in limited practical applicability and yielding ideal analyses. Consequently, they fail to meet the actual performance of solar PV in real environmental conditions. To overcome this difficulty, it is essential to meticulously analyze the complexities determined by real-world performance and subsequently address them through an experimental model. For this reason, in the present study, it was essential to devise a solar simulator to accurately estimate the performance of solar panels. Categorizing and measuring the various output values of solar PV panels across varying irradiation levels and PV panel temperatures was undertaken. Utilizing these experimental findings, FF factor model and a maximum power model were constructed, adjusting them to incorporate various parameters. These models aim to accurately reflect the performance of solar PV panels in real-world outdoor settings.

4.2 PVsyst Simulation Analysis of Solar PV Panel

Extra-terrestrial solar radiation denotes the solar energy reaching the Earth from the Sun beyond the confines of the Earth's atmosphere. On average, the extra-terrestrial solar radiation flux is around 1361 W/m². However terrestrial solar radiation levels vary widely depending on factors such as time of day, weather conditions, geographical location, and atmospheric phenomena. A range of solar radiation of 0-1600 W/m² allows research to simulate a wide variety of conditions, ranging from low-light situations such as cloudy days or twilight to high-intensity sunlight on clear, sunny days. By covering a broad range of radiation levels in research, it can examine the performance of solar panels, devices, or systems under different solar conditions. This flexibility is crucial for assessing the reliability, efficiency, and robustness of solar technologies across a spectrum of real-world scenarios. Solar radiation levels above 1600 W/m² are relatively rare in most terrestrial environments and typically occur only under extremely bright sunlight conditions, such as in desert regions at high altitudes (Cordero et al., 2016). Many standardized testing protocols for solar energy technologies, such as those developed by organizations like the International Electrotechnical Commission (IEC) or the International Organization for Standardization (ISO), specify a maximum radiation level of 1000 W/m² for standard test conditions (STC). However, experiments may extend beyond this level to assess performance under non-standard conditions or extreme scenarios. Therefore, it is crucial to integrate experimental data with site-specific meteorological data when using simulation models to calculate the energy production of various PV systems. Accurate input parameters are essential for these simulations to yield reliable results regarding PV generator productivity and to aid in selecting the most suitable panel type for a particular application at a specific location, thereby enhancing the economic viability of PV power systems (Durisch et al., 1996). However, initial approach involved designing a PVsyst software based model utilizing data provided by the manufacturer for mono-crystalline solar panels. PVsyst (PVsyst 7.4, 2023) is a software package used for the analysis and simulation of PV system. It's widely used in the solar energy industry for designing, optimizing, and assessing the performance of solar power installations, whether they're small scale residential installations or large scale utility projects. PVsyst allows users to model the behaviour of PV arrays under different environmental conditions, simulate energy production, and evaluate the financial viability of solar project. Chapter 3 comprehensively covers all data provided by solar PV panel manufacturers. Subsequently, the model performance was assessed under various radiation and temperature conditions, simulating standard conditions for analysis. Thus, the performance of solar PV panels across a wide range of solar irradiance, from 200 W/m² to 1600 W/m², within a specific temperature range of 20°C to 60°C were analyzed. The resulting graphs are depicted in Fig. 4.1 to Fig. 4.8. Additional simulation performance results and model equations can be found in Annexure 2. Simulation results depict the actual performance under ideal environmental conditions. The results reveal that the maximum power point (P_{mpp}) increases with rising solar radiation levels, while it decreases with an increase in panel temperature.

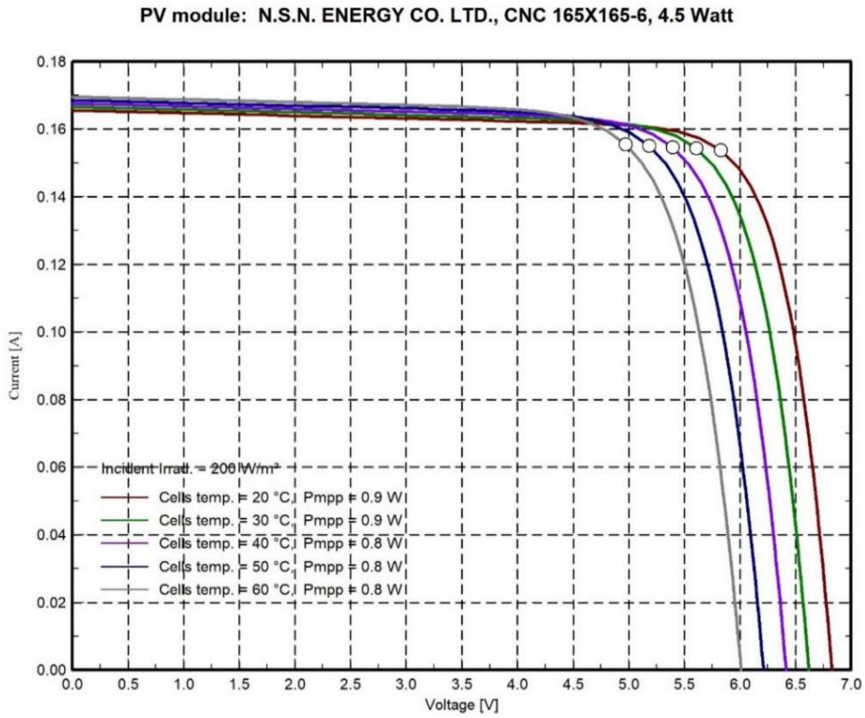

Fig. 4.1 I-V characteristics of mono crystalline solar panel PVsyst simulation model with panel at 200 W/m^2 radiation level

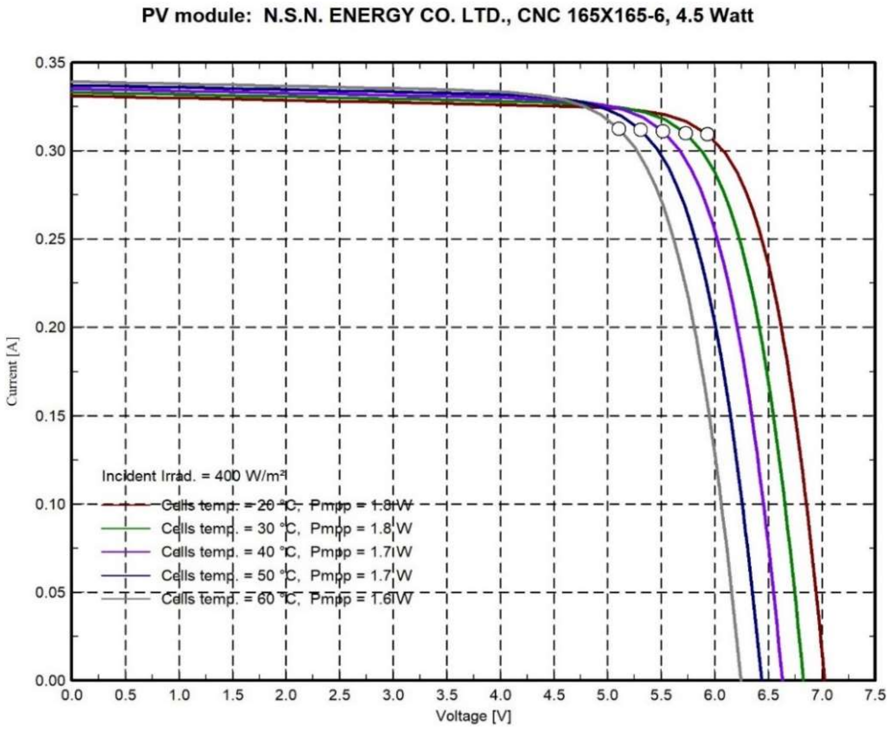

Fig. 4.2 I-V characteristics of mono crystalline solar panel PVsyst simulation model with panel at 400 W/m^2 radiation level

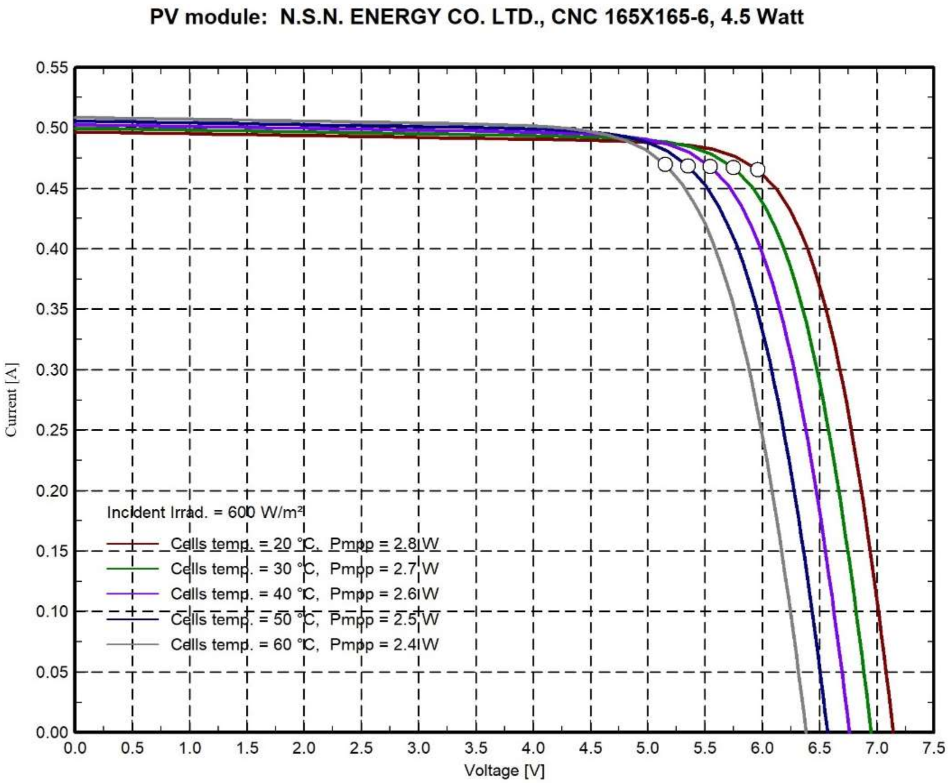

Fig. 4.3 I-V characteristics of mono crystalline solar panel PVsyst simulation model with panel at 600 W/m^2 radiation level

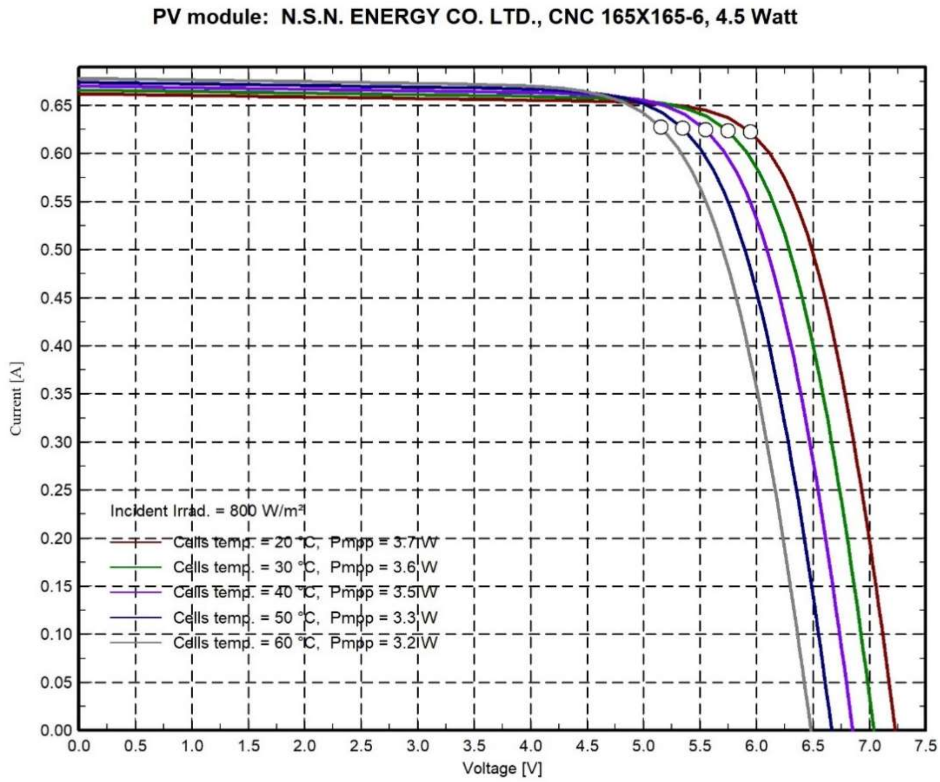

Fig. 4.4 I-V characteristics of mono crystalline solar panel PVsyst simulation model with panel at 800 W/m^2 radiation level

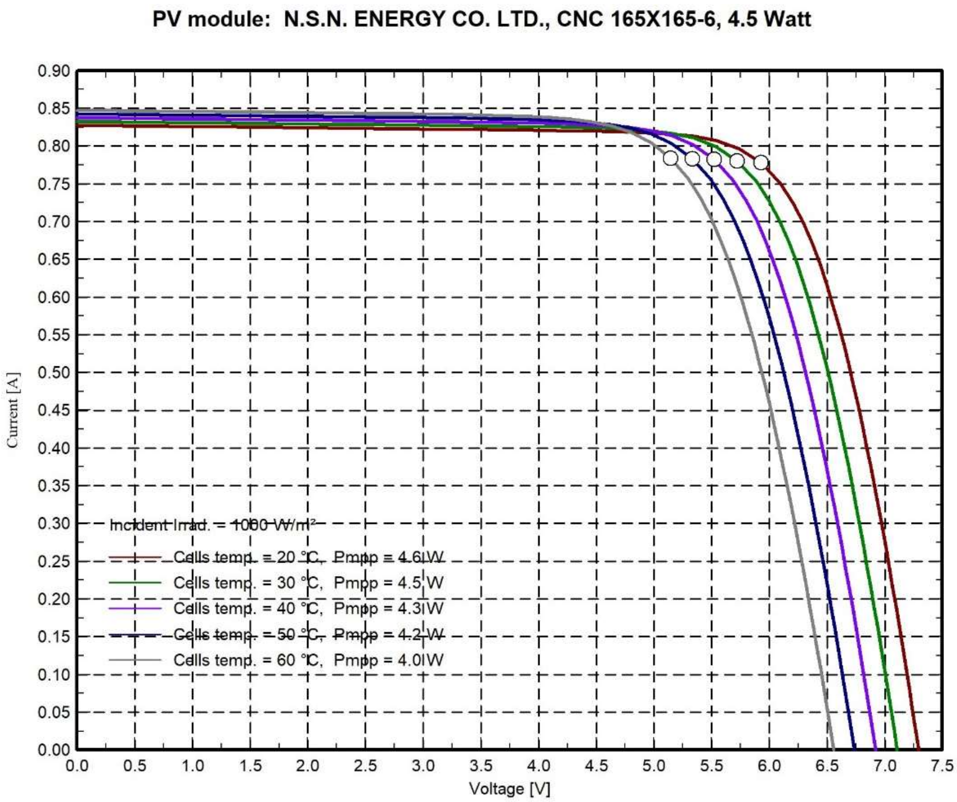

Fig. 4.5 I-V characteristics of mono crystalline solar panel PVsyst simulation model with panel at 1000 W/m^2 radiation level

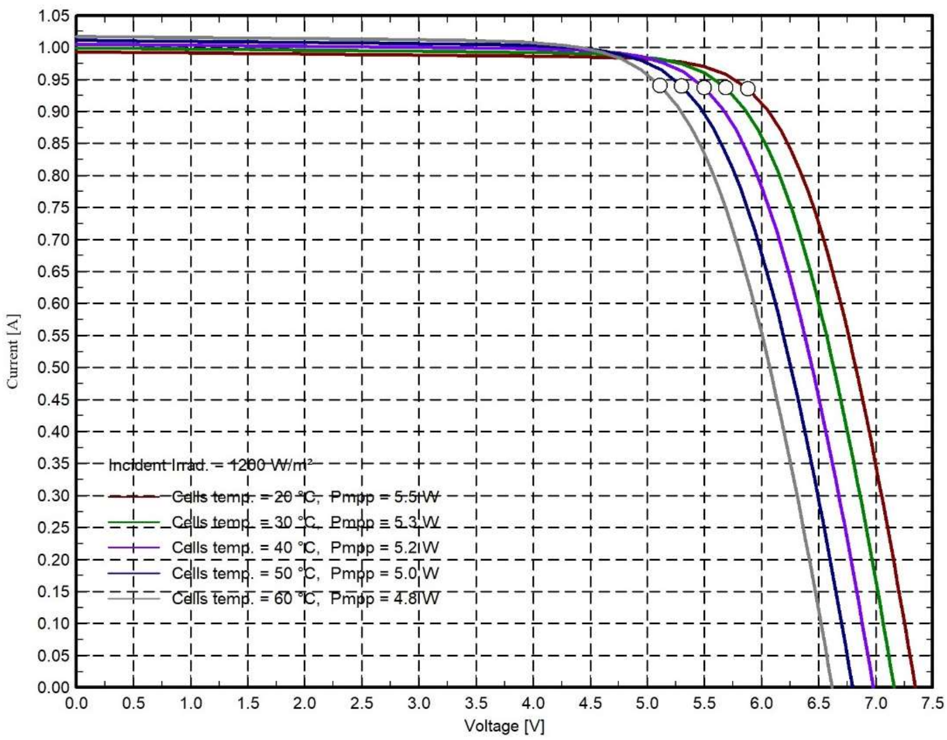

Fig. 4.6 I-V characteristics of mono crystalline solar panel PVsyst simulation model with panel at 1200 W/m^2 radiation level

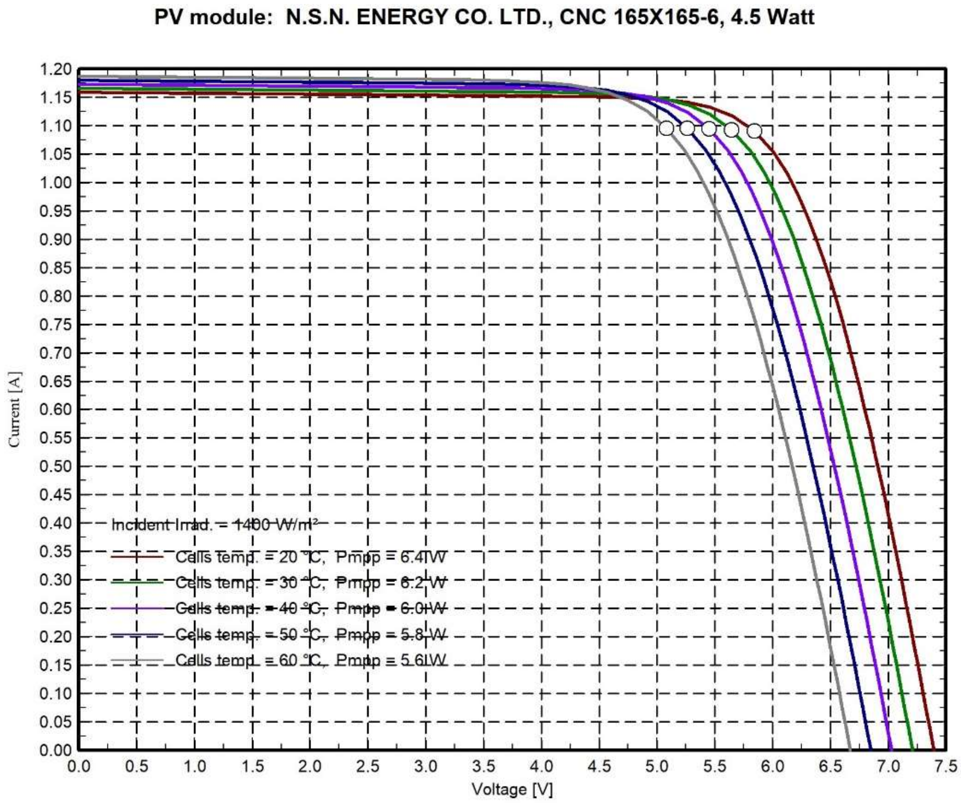

Fig. 4.7 I-V characteristics of mono crystalline solar panel PVsyst simulation model with panel at1400 W/m^2 radiation level

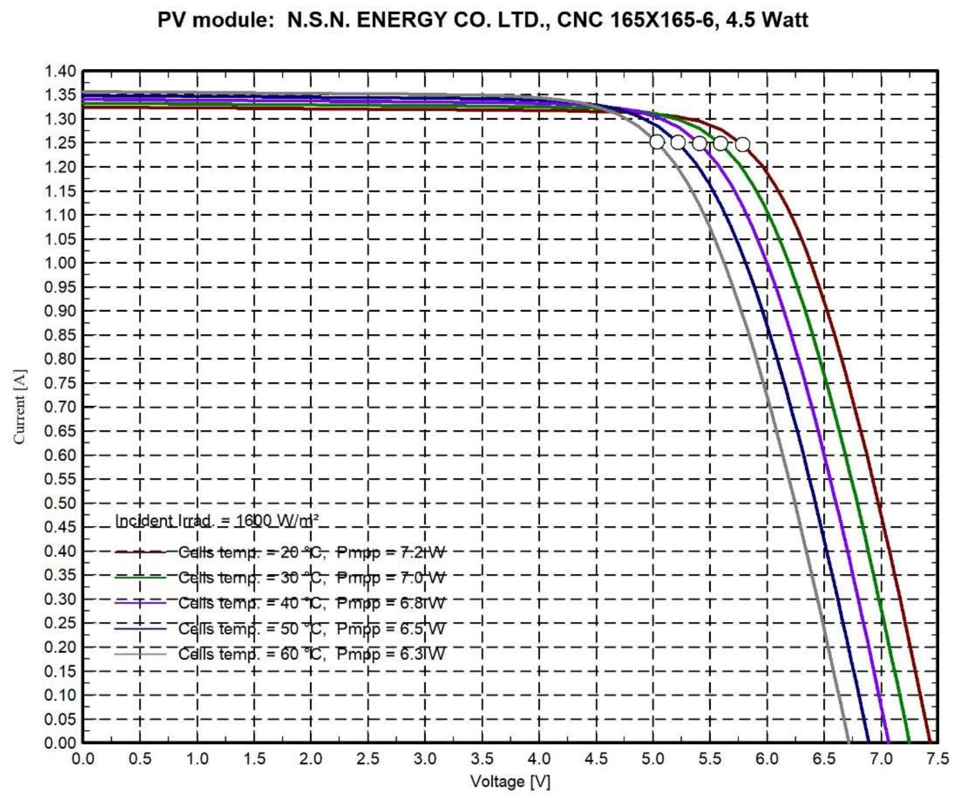

Fig. 4.8 I-V characteristics of mono crystalline solar panel PVsyst simulation model with panel at 1600 W/m^2 radiation level

Siefer and Bett (Siefer and Bett, 2014) have established a connection between temperature and irradiance increases and their impact on electrical properties through experiments conducted in controlled environmental settings using a solar simulator and software-based simulation model. In such controlled experiments, certain parameters can be maintained at a constant level, unlike in natural environments where numerous micro-climatic factors, along with temperature and irradiance, significantly influence panel performance. Soulayman and Hababa (Soulayman and Hababa, 2017) studies have indicated that simulations based solely on Standard Test Conditions (STC) data can result in an overestimation of power production by up to 40%. Nasrin, R. et al. (2018) conducted a simulation-based experimental study revealing that for radiations ranging above 1000 W/m^2 , increase in irradiation leads to a decrease in the electrical efficiency of the panel. The study observed a decrease in electrical efficiency from 13% to 11.2% in the PV cell as irradiation levels increased from 1000 to 3000 W/m^2. Additionally, the temperature of the solar cell rose by 77% within the PV panel system as irradiation levels varied from 1000 to 3000 W/m^2. Specifically, the mean temperature of the solar cell was recorded at 48°C under an irradiation level of 1000 W/m^2, increasing to approximately 85°C at the highest irradiation level of 3000 W/m^2. According to manufacturing standards, a temperature of 25°C marks the peak of the optimal temperature ranges for photovoltaic solar panels. Manufacturers design most solar panels to withstand higher temperatures, and their performance typically remains stable until temperatures surpass 45°C. However, beyond this threshold, the efficiency declines. In a simulation model, it is feasible to specify hypothetical environmental conditions, such as 20°C and 1600 W/m^2 radiation. However, conditions depicted under a simulated environment do not replicate the real-world behaviour of panels. Therefore, a solar testing facility was designed to evaluate the performance of solar panels under actual environmental conditions.

4.3 Experimental Data Analysis of Solar PV Panel

A monocrystalline silicon solar panel with an area of (165×165) mm^2 was utilized for the experiment, employing a solar cell characteristics measurement experimental setup. The experiment was conducted with cell temperatures ranging from 20-60°C under radiation of 200–1000 W/m^2 using Halogen lamps. Chapter 3 describes all the measurement procedures in detail. The I-V and P-V characteristics of the monocrystalline silicon solar cell were documented, leading to the calculation of solar PV panel parameters. Moreover, the relative changes in these photovoltaic parameters with cell temperature were analyzed.

The Fig. 4.9 to Fig. 4.13 illustrate the characteristics of a monocrystalline silicon solar cell in terms of I-V and P-V, under constant radiation conditions, while varying cell temperatures at 20°C, 30°C, 40°C, 50°C and 60°C. The measurements were conducted under radiation intensities of 200, 400, 600, 800 and 1000 W/m^2. The Fig. 4.9 - Fig. 4.13 demonstrate that both the I-V and P-V characteristics are influenced by the cell temperature. Regarding the I-V characteristics, it is evident that the current reaches its maximum and remains relatively constant within the lower voltage range, showing variations with cell temperature within the ranges of 0.15-0.18 A, 0.26-0.30 A, 0.39-0.43A, 0.49-0.53 A and 0.59-0.64 A current under radiation of 200 W/m^2, 400 W/m^2, 600W/m^2, 800 W/m^2 and 1000 W/m^2 respectively. These characteristics follow a pattern wherein the initial current of a solar PV panel is greater at high temperatures of the panel compared to lower temperatures. However, this trend reverses in voltage at around 6 -7 V, 6.2-7.1 V, 6.3-7.2 V, 6.4-7.3 V and 6.5-7.4 V for intensities of 200 W/m^2, 400 W/m^2, 600W/m^2, 800 W/m^2 and 1000 W/m^2 respectively. Subsequently, the current decreases rapidly, reaching a minimum in the range of 0.25-0.52 A with voltages between 3.8-5.4 V. Furthermore, the characteristics corresponding to successively lower cell temperatures persist beyond the higher ones. Similarly, the estimation of P-V characteristics follows a similar pattern to that of the I-V characteristics. Notably, it shows a nearly linear increase with cell temperature in the low voltage range, reaching a maximum within the range of 0.67-3.4 W for all varying radiation. However, beyond this point, it rapidly decreases in the higher voltage range due to the increasing rate of photon generation with cell temperature, resulting in a rapid increment in the reverse saturation current. The P-V characteristics distinctly reveal a peak power point, where the voltage is lower than the V_{oc}. Similarly, at this point, the current is also lower than the I_{sc}. The fluctuations in both current and voltage are almost identical at this juncture for different cell temperatures. The impact of temperature dependence on photovoltaic parameters such as maximum power (P_{max}), short-circuit current (I_{sc}), open-circuit voltage (V_{oc}), fill factor (FF), and efficiency (η) and across the range of 20–60°C at light intensities of 200, 400, 600, 800 and 1000 W/m^2 is shown in Fig.4.14 to Fig.4.18.

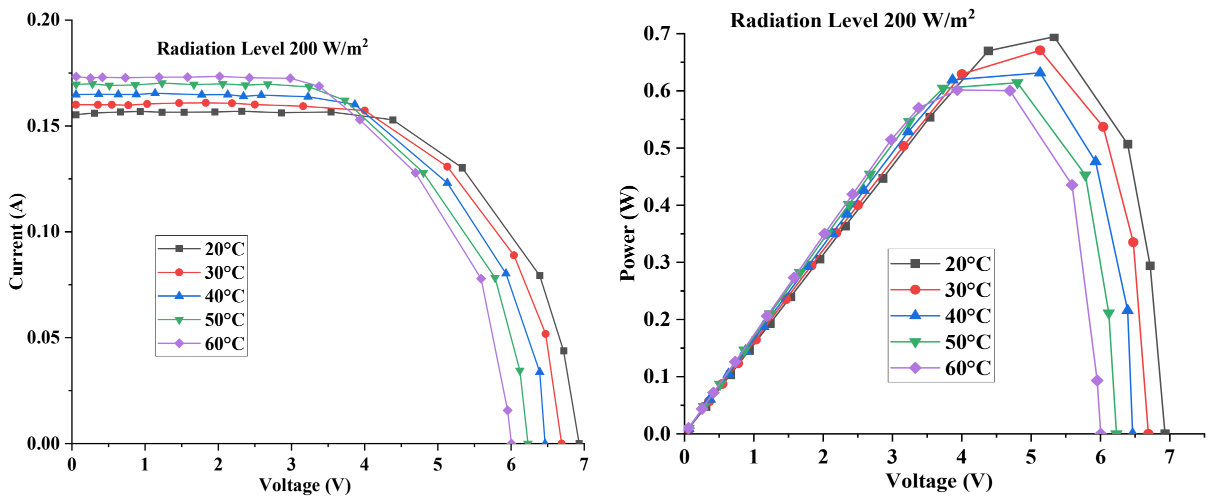

Fig. 4.9 I-V and P-V characteristics of mono crystalline solar panel with panel at 200 W/m^2 radiation level

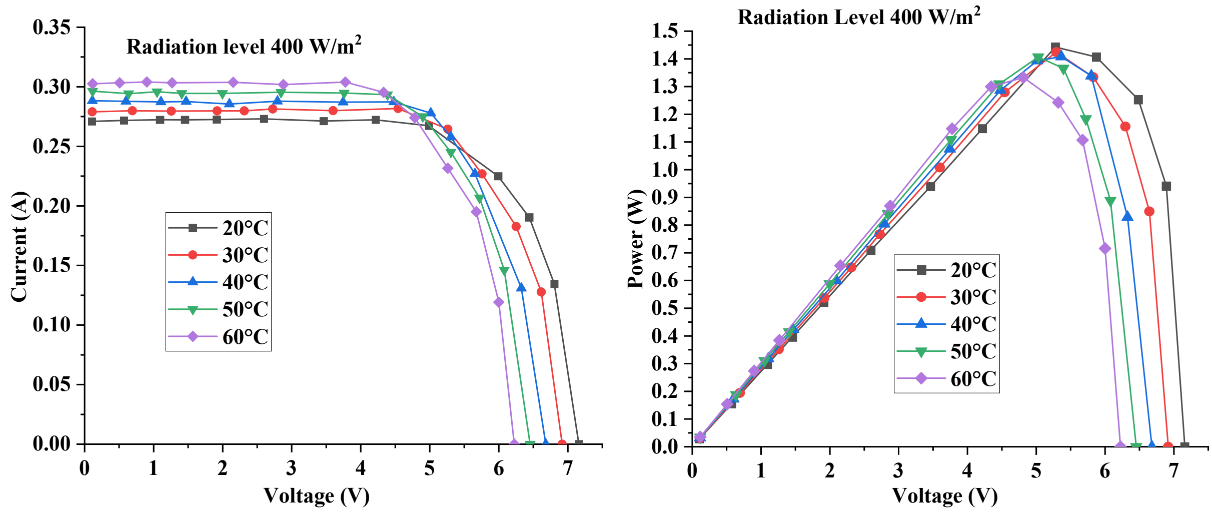

Fig. 4.10 I-V and P-V characteristics of mono crystalline solar panel with panel at 400 W/m^2 radiation level

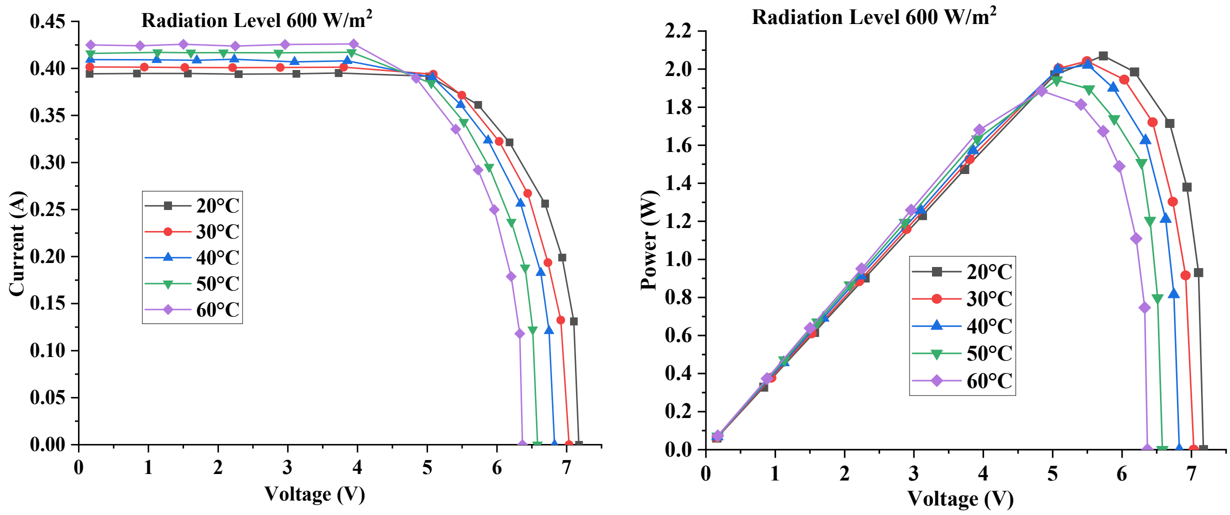

Fig. 4.11 I-V and P-V characteristics of mono crystalline solar panel with panel at 600 W/m^2 radiation level

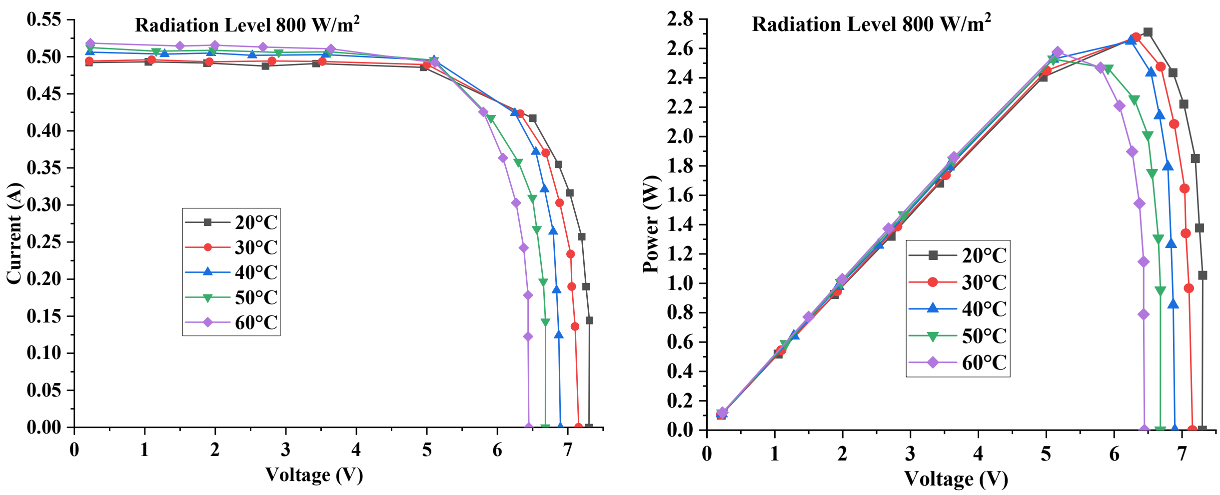

Fig. 4.12 I-V and P-V characteristics of mono crystalline solar panel with panel at 800 W/m^2 radiation level

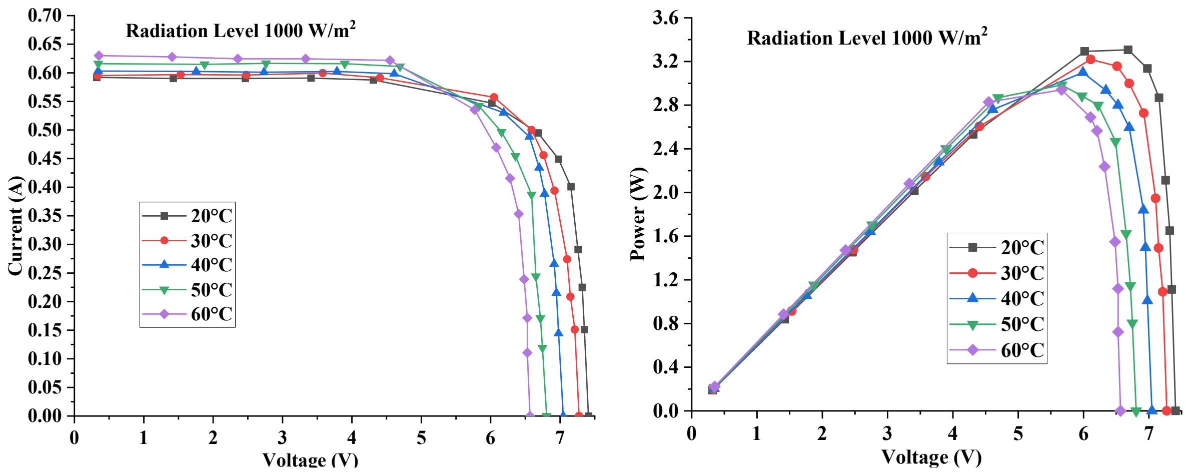

Fig. 4.13 I-V and P-V characteristics of mono crystalline solar panel with panel at 1000 W/m^2 radiation level

4.3.1 Influence of Rising Cell Temperature on Maximum Power Output

An increase in cell temperature typically leads to a decrease in the V_{oc} of the solar cell. Since the maximum power point (MPP) occurs at the intersection of the panel's I-V curve where the product of current and voltage is maximized, a decrease in V_{oc} or I_{sc} results in a lower maximum power point. With increasing temperature, the reverse saturation current of the solar cell tends to rise. This increase in current flowing through the diode junction contributes to higher losses and reduces the overall efficiency of the solar cell, resulting in a decrease in maximum power output. Overall, the combined impact of these factors results in a decrease in maximum power output as the temperature of the solar photovoltaic cell rises. Fig. 4.14 illustrates the experimental finding that maximum power output decreases with increasing cell temperature. The maximum power exhibits variation across the range of cell temperatures, with values ranging from 0.66 W to 3.39 W for all constant light intensities.

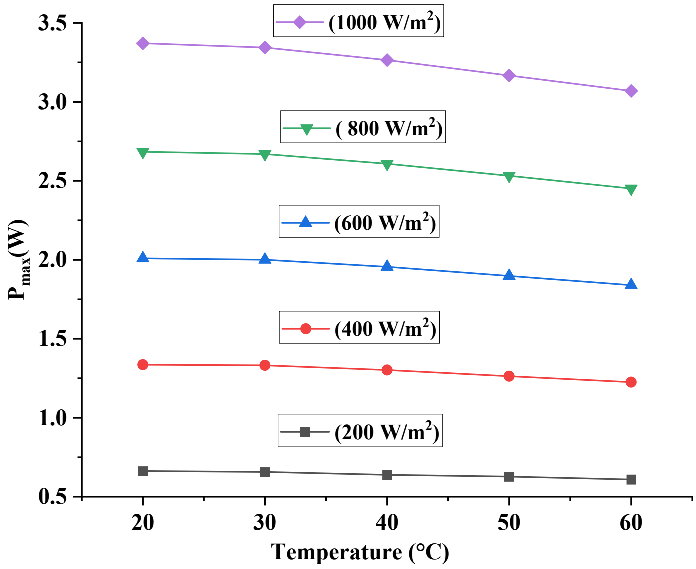

Fig. 4.14 Variation of maximum output power with panel temperature in a range of 20-60 °C at different radiation

As temperature rises, the mobility of charge carriers, electrons and holes within the semiconductor material of the solar cell increases. This increased mobility facilitates the movement of charge carriers towards the contacts, resulting in a higher short-circuit current. Semiconductor materials generally exhibit a reduction in their bandgap energy with an increase in the cell temperature. This temperature-dependent behaviour is accounted for in the Varshni equation, which is linked to the electrical model (Maka and O'Donovan, 2019) as a means to anticipate the impact of increasing cell temperature on the energy band gap. The Varshni empirical relation in equation 4.1 provides insight into the temperature dependence of semiconductor energy band gaps (Maka and O'Donovan , 2022).

$$E_{g,i(T)} = E_{g,i(0)} - \frac{\alpha_i . T_c^2}{T_c + \beta_i} \quad (4.1)$$

$E_{g(0)}$ denotes the band gap at 0°K, i stands for a sub-cell within each layer, T_c represents the cell temperature, while α and β denote material constants. This reduction enables more photons to generate electron-hole pairs by excitation, leading to a higher short-circuit current. Therefore, as temperature increases, the band gap linearly decreases as more solar spectrum photon components are absorbed. Subsequently, a small increase in short circuit current. Experimental findings from this particular stydy also indicate a slight increase in short-circuit current as temperature rises across all radiation levels, as depicted in Fig 4.15. The short-circuit current exhibits variation across the range of cell temperatures, with values ranging from 0.16 to 0.59 A for all constant light intensities.

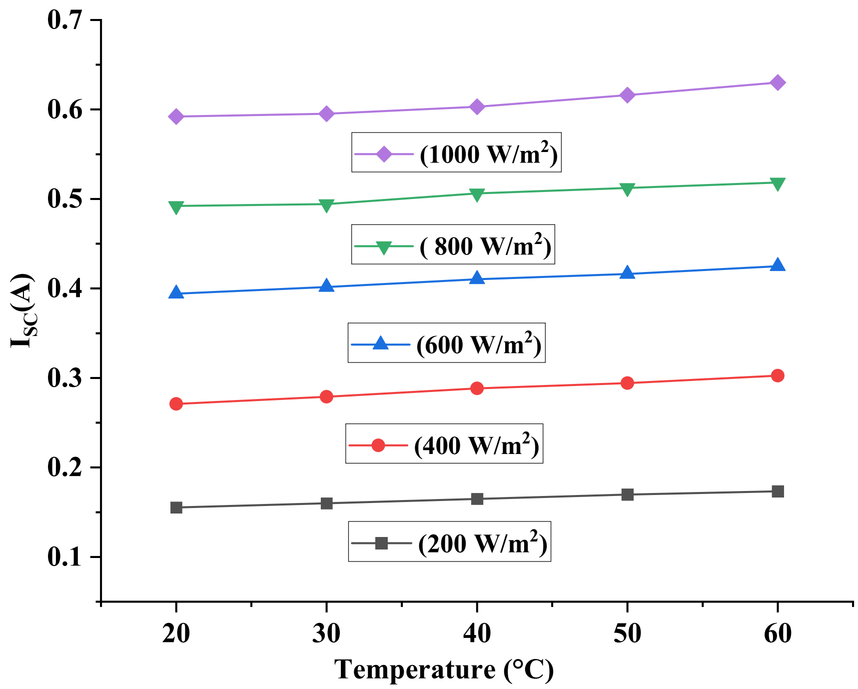

Fig. 4.15 Variation of short circuit current with panel temperature in a range of 20-60 °C at different radiation

4.3.2 Impact of Increasing Cell Temperature on Open Circuit Voltage

As temperature rises, the intrinsic carrier concentration within the semiconductor material increases. This increase in carrier concentration leads to a greater number of thermally generated electron-hole pairs within the cell, resulting in increased recombination rates. This enhanced recombination reduces the number of charge carriers available to contribute to the open-circuit voltage, thus causing a decrease in voltage. The reverse saturation current experiences an impact from the reduction in the energy band gap, leading to a decrease in the open-circuit voltage at a specified temperature. Conversely, as the cell temperature decreases, the energy band gap tends to expand, increasing the open-circuit voltage, thereby enhancing efficiency. The current generated in each cell is contingent upon the incident spectrum, with specific selections tailored for optimal energy band gaps. The variation in energy band gap with temperature is described by equation 4.2 (Kinsey and Edmondson , 2009).

$$\frac{\delta E_g}{\delta T} = \frac{2\alpha}{T+\beta} + \frac{\alpha T^2}{(T+\beta)^2} \tag{4.2}$$

The open-circuit voltage of a solar cell is determined by the built-in voltage, which is related to the energy bandgap of the semiconductor material. With rising temperature, the bandgap of the semiconductor decreases, leading to a reduction in the built-in voltage. Consequently, the open-circuit voltage decreases. Experimental results of particular stydy was demonstrated that the open-circuit voltage decreases with increasing temperature across all radiation levels, as illustrated in Fig. 4.16. The open-circuit voltage exhibits variation across the range of cell temperatures, with values ranging from 6 to 7.05 V for all constant light intensities.

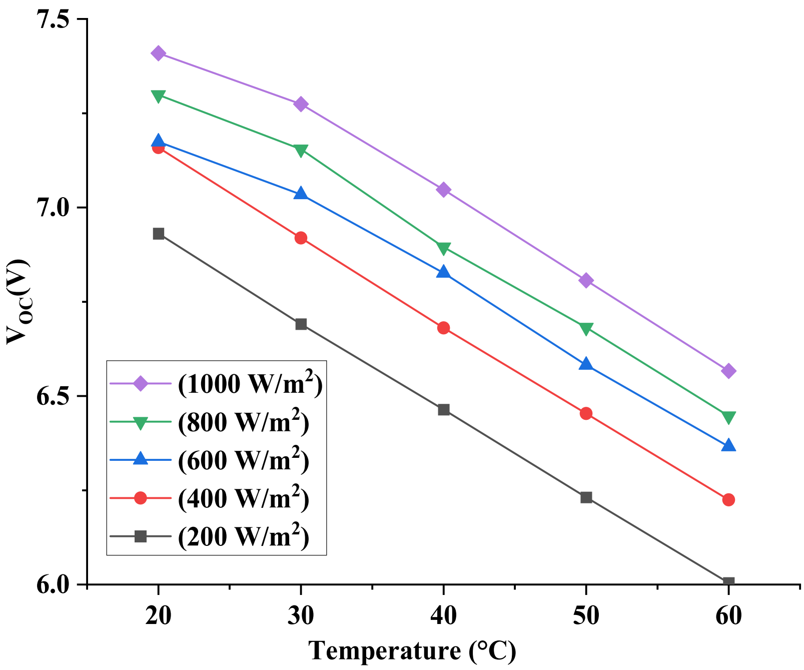

Fig. 4.16 Variation of open circuit voltage with panel temperature in a range of 20-60 °C at different radiation

4.3.3 Influence of Temperature Variations on The Fill Factor of Solar Panels

As the temperature of the solar panel increases, the series resistance within the panel tends to rise. This increase in series resistance leads to higher voltage losses across the internal components of the panel, resulting in a decrease in the fill factor. Additionally, with rising temperatures, the open-circuit voltage of the solar panel typically decreases. Since the fill factor is defined as the ratio of the maximum power point voltage to the open-circuit voltage, a decrease in the open-circuit voltage leads to a reduction in the fill factor. Elevated temperatures can result in higher rates of carrier recombination within the semiconductor material of the solar panel. Increased recombination rates lead to a decrease in the effective charge carrier lifetime, which can affect the fill factor. Experimental results was indicated that the fill factor of solar panels tends to be lower under lower radiation conditions. A decrease in fill factor was observed with increasing temperature; however, at 20°C, the fill factor is slightly lower compared to 30°C under higher radiation. The experimental output for the fill factor is depicted graphically in Fig. 4.17. A visual representation of the experimental findings is provided by the graph, which demonstrates, the fill factor is influenced by different temperatures and radiation conditions.The fill factor exhibits variation across the range of cell temperatures, with values ranging from 0.59 to 0.77 under all constant light intensities.

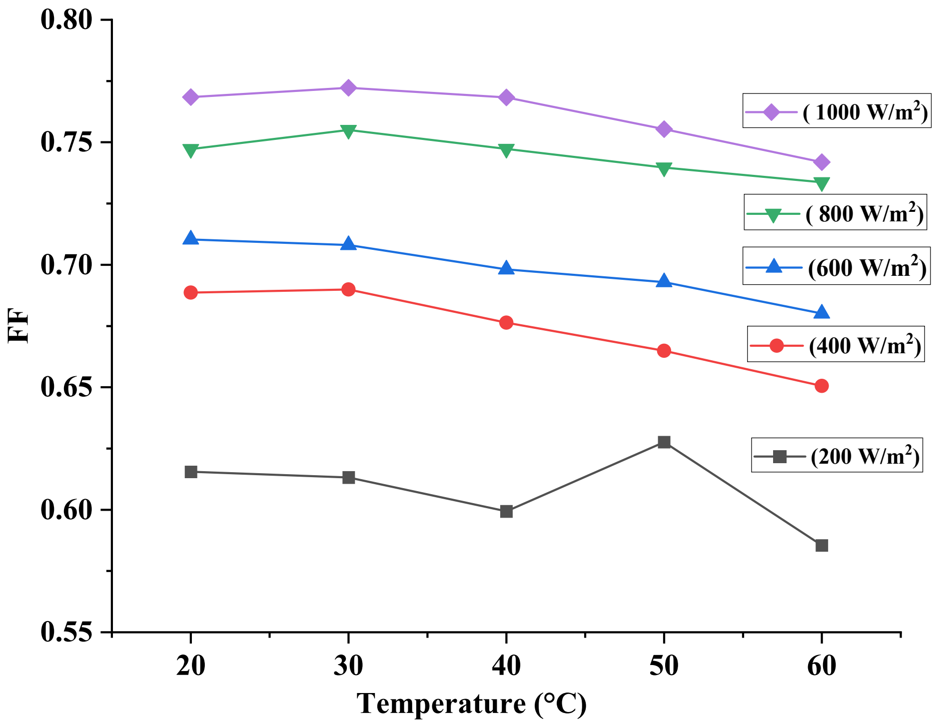

Fig. 4.17 Variation of fill factor with panel temperature in a range of 20-60 °C at different radiation

4.3.4 Impact of Panel Temperature on The Efficiency of Solar PV Panels

As the temperature of the solar panel rises, its efficiency typically decreases. This reduction occurs due to various factors such as decreased open-circuit voltage, increased series resistance, and higher rates of carrier recombination, all of which contribute to lower overall power conversion efficiency.

Elevated temperatures lead to a decrease in the open-circuit voltage of the solar panel. Since the open-circuit voltage is a crucial parameter affecting efficiency, its reduction negatively impacts the overall efficiency of the panel. With rising temperatures, the series resistance within the solar panel tends to increase. This increase results in higher losses within the panel's internal components, leading to a reduction in efficiency. Overall, while solar photovoltaic panels are designed to operate efficiently across a range of temperatures, elevated temperatures can still lead to a decrease in their efficiency. Understanding and managing the impact of temperature on panel efficiency is essential for maximizing the performance and output of solar energy systems. Experimental study was demonstrated that the efficiency of solar photovoltaic panels decreases as the panel temperature increases. The graph illustrating the changes in efficiency with temperature is depicted in Fig. 4.18(a). The efficiency percentage of solar PV panels varies with the surface temperature of PV panel relative to the standard test condition (STC) temperature of 25°C, as illustrated in Fig. 4.18 (b). The efficiency of solar panels exhibits variation across the range of cell temperatures, with values ranging from 11.97 to 13.25 for all constant light intensities.

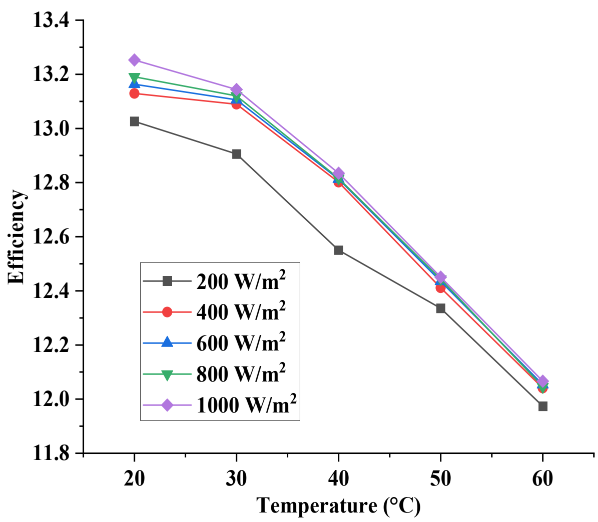

Fig. 4.18(a) Variation of efficiency with panel temperature in a range of 20-60 °C at different radiation

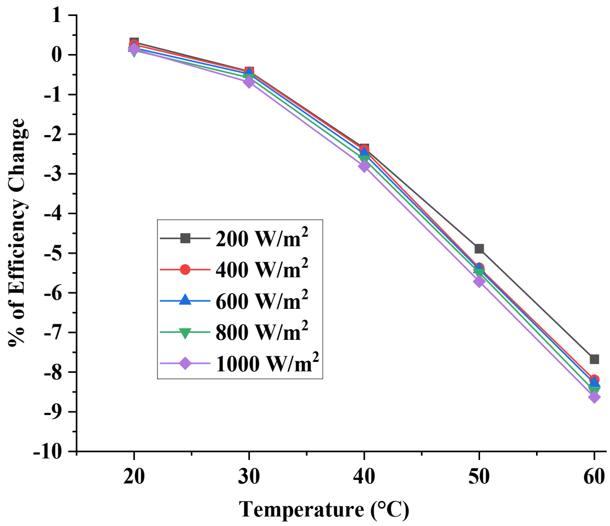

Fig. 4.18(b) Variation of % of efficiency change with panel temperature at different radiation

Based on experimental data, the variation in the maximum power (P_{max}), short-circuit current (I_{sc}), open-circuit voltage (V_{oc}), fill factor (FF) and efficiency (η) with cell temperature at different radiation was descreibed in Table 4.1. Percentage change per degree celcius of the respective parameters were ploted and the slope of the curves thus obtained gave the values for the respective temperature coefficient.

Table 4.1 Experimental temperature coefficient of different parameter of solar PV panel

Radiation W/m^2	P_{max} %/°C	I_{sc} %/°C	V_{oc} %/°C	FF %/°C	Efficiency %/°C
200	-0.20189	0.28870	-0.33412	-0.12199	-0.20189
400	-0.20725	0.28214	-0.32630	-0.11757	-0.20725
600	-0.21078	0.19462	-0.29036	-0.10647	-0.21078
800	-0.21701	0.17833	-0.28742	-0.09084	-0.21701
1000	-0.22383	0.16014	-0.28441	-0.08626	-0.22383
temperature coefficient	-0.19606	0.32907	-0.34601	-0.13408	-0.19606

As previously established within the equation (details discussed in Chapter 3), cell temperature increases, and the energy bandgap decreases, leading to a decrease in the open circuit voltage. The short-circuit current (I_{sc}) is directly proportional to the number of generated charge carriers and their mobility. It is heavily influenced by the generation rate of charge carriers and the diffusion length. With an increase in cell temperature, the rate of generation of charge carriers rises, resulting in an increase in the short-circuit current. The fill factor drops with cell temperature, primarily due to alterations in the corresponding open-circuit voltage and short-circuit current. These variations directly impact the maximum output power. The maximum output power shows a decrease with cell temperature across all constant light intensities, as depicted in Table 4.2, indicating a decline in voltage with cell temperature. This trend is evident from Table 4.2, where the efficiency is observed to decrease with cell temperature across all constant light intensities, attributed to the reduction in corresponding open-circuit voltage and fill factor. The cell temperature-dependent efficiency is reported by Dubey et al. (Dubey et al., 2013) as follows:

$$\eta_c = \eta_{T_{ref}[1-\beta_o(T_c-T_{ref})]} \tag{4.3}$$

In this equation, η_c and η_{Tref} represent the efficiencies of the solar cell at cell temperature and room temperature, respectively. β_o denotes the efficiency temperature coefficient (0.004 K^{-1}), while T_c and T_{ref} stand for the cell temperature and reference temperature of the solar cell, respectively. As the quantity $(T_c - T_{ref})$ rises with cell temperature, the efficiency consequently decreases.

Table 4.2 Experimental output data of different parameter of solar PV panel

Radiation (W/m^2)	Temperature (°C)	V_{OC} (V)	I_{SC} (A)	P_{max} (W)	FF	Efficiency (%)
200	20	6.93077	0.15535	0.66270	0.61550	13.02581
	30	6.69047	0.16005	0.65660	0.61318	12.90582
	40	6.46391	0.16480	0.63851	0.59940	12.55033
	50	6.23120	0.16967	0.62758	0.59360	12.33551
	60	6.00449	0.17329	0.60918	0.58546	11.97390
400	20	7.15912	0.27097	1.33593	0.68865	13.12923
	30	6.91894	0.27901	1.33187	0.68993	13.08937
	40	6.68041	0.28829	1.30258	0.67635	12.80147
	50	6.45358	0.29432	1.26284	0.66486	12.41101
	60	6.22472	0.30255	1.22518	0.65055	12.04080
600	20	7.17411	0.39423	2.00907	0.71036	13.16316
	30	7.03451	0.40161	2.00027	0.70803	13.10552
	40	6.82616	0.41038	1.95562	0.69811	12.81300
	50	6.58224	0.41612	1.89796	0.69294	12.43518
	60	6.36588	0.42492	1.83968	0.68011	12.05334
800	20	7.29876	0.4922	2.68442	0.74724	13.19099
	30	7.15453	0.49426	2.67004	0.75506	13.12031
	40	6.89489	0.50618	2.60801	0.74727	12.81550
	50	6.68174	0.51237	2.53228	0.73967	12.44340
	60	6.44665	0.51831	2.45140	0.73365	12.04596
1000	20	7.40921	0.59213	3.37125	0.76843	13.25281
	30	7.27427	0.59522	3.34353	0.77222	13.14384
	40	7.04704	0.60301	3.26484	0.76830	12.83450
	50	6.80648	0.61601	3.16723	0.75539	12.45078
	60	6.56631	0.63006	3.06941	0.74191	12.06624

4.4 FF Model in Relation to Radiation and Temperature

Based on the experimental data, i have designed a fill factor (FF) model that correlates with radiation and temperature, represented by equation 4.4. The coefficients of this model equation are detailed in Table 4.3. These values delineate the coefficients within the model equation, encapsulating the relationship between the independent variables, such as temperature and radiation, and the dependent variable FF. The R-square value is a statistical measure that represents the proportion of the variance in the dependent variable that is predictable from the independent variables in a regression model. It is often used to assess the goodness of fit of a regression model. The adjusted R-square takes into account the number of predictors (independent variables) in the regression model. For the FF model incorporating radiation and temperature, the R-square (COD) value stands at 0.98065, with an adjusted R-square value of 0.97556. A higher R-square (COD) and adjusted R-square value indicate a better fit of the model to the data, with values closer to 1 indicating a stronger relationship between the predictors and the dependent variable.

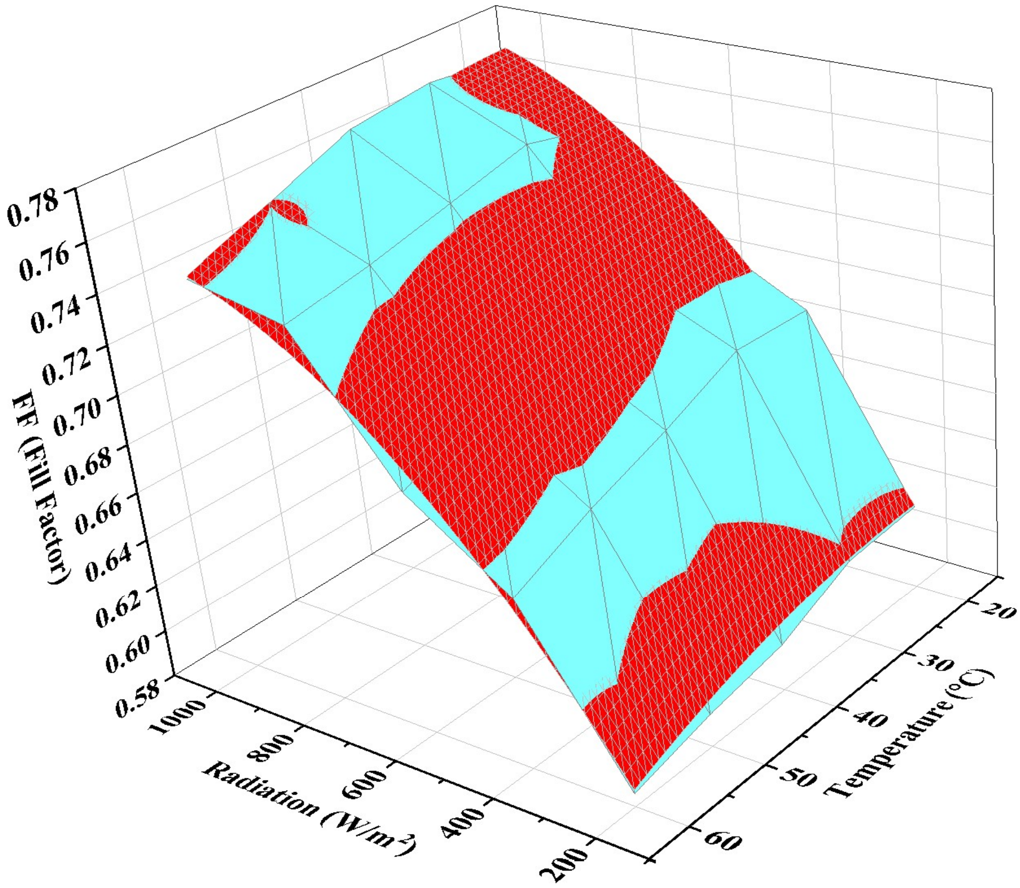

Fig.4.19 FF model in relation to radiation and temperature

$$Z = z0 + A \times exp^{\left(\left(-0.5\times\left(\frac{(x-xc)}{w1}\right)^2\right)-\left(0.5\times\left(\frac{(y-yc)}{w2}\right)^2\right)\right)} \quad (4.4)$$

Table 4.3 Parameter value of nonlinear surface fit regression for FF model

Parameter	z0	A	xc	w1	yc	w2
Value	-423.34594	424.12567	1212.81758	36498.37368	-5.89967	3516.86744

The equation mentioned above was utilized to predict the fill factor value for specific radiation and temperature conditions.

4.5 FF Model with Respect to Open Circuit Voltage and Short Circuit Current

An additional FF model based on the open-circuit voltage (Voc) and short-circuit current (Isc) has been developed , as expressed by Equation 4.5. The coefficients of the model equation are provided in Table 4.3. The designed model exhibited an R-square (COD) value of 0.97679, with an adjusted R-square value of 0.97068.

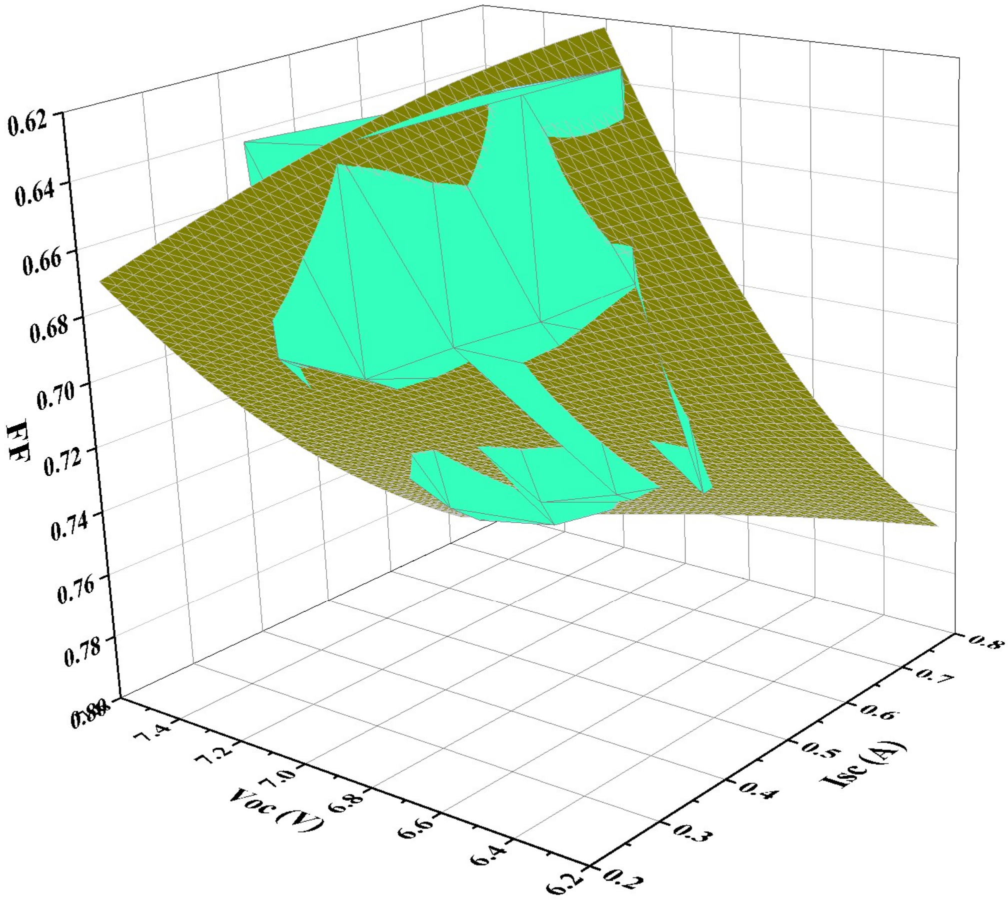

Fig.4.20 FF model in relation to open circuit voltage (V_{oc}) and short circuit current(I_{sc})

$$Z = z0 + A \times exp^{\left(\left(-0.5\times\left(\frac{(x-xc)}{w1}\right)^2\right)-\left(0.5\times\left(\frac{(y-yc)}{w2}\right)^2\right)\right)} \quad (4.5)$$

Table 4.4 Parameter value of nonlinear surface fit regression for FF model in relation to V_{oc} and I_{sc}

Parameter	z0	A	xc	w1	yc	w2
Value	0.86002	-68.71388	5.10776	2.48257	-5.89967	1.83902

Above this equation, it was employed to forecast the fill factor value corresponding to specific open-circuit voltage (V_{oc}) and short-circuit current (I_{sc}) values. This model was employed in recent outdoor experiment to ascertain the true fill factor impacted by the presence of dust. It was specifically used to analyze the fill factor value for calculating the power generation based on the particular open circuit voltage and short circuit current of dusty panels.

4.6 Maximum Power (P_{max}) Model in Relation to Radiation and Temperature

To determine the real performance of power generation from the experimental photovoltaic panels, unaffected by dust and other environmental factors, a maximum power (P_{max}) model was developed . Using nonlinear surface fit regression analysis, I have obtained an R-Square (COD) value of 0.99287 and an Adj. R-Square value of 0.99099.

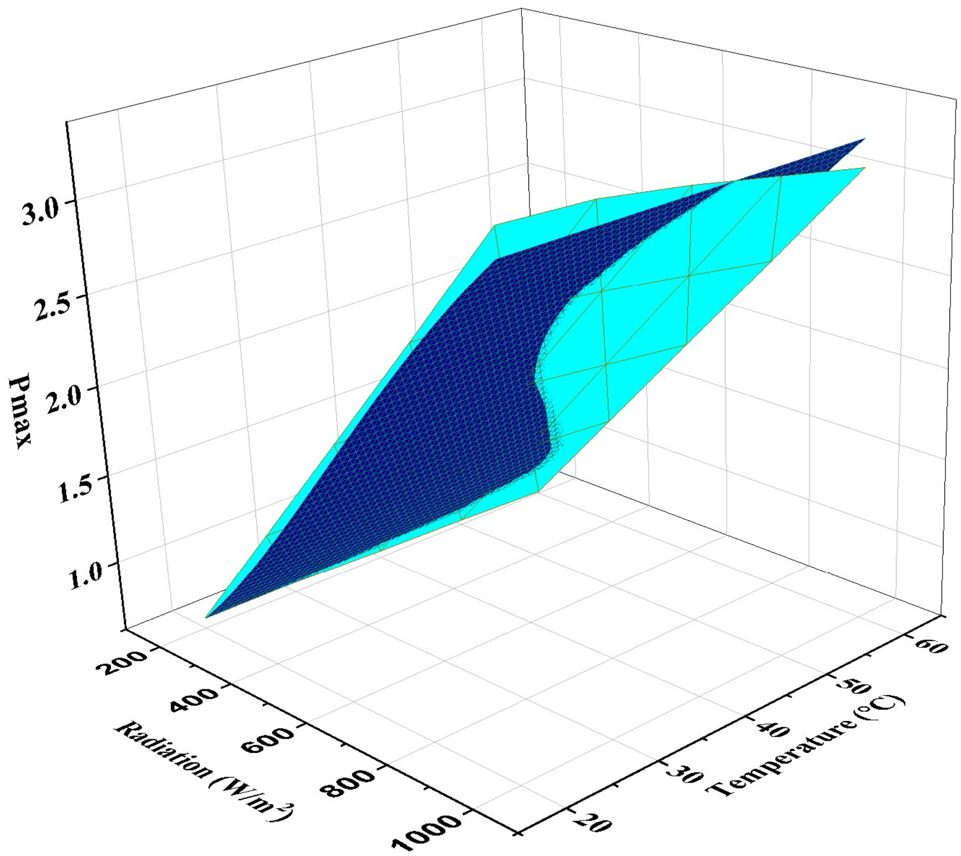

Fig. 4.20 Maximum power (P_{max}) model in relation to radiation and temperature

$$Z = z0 + A \times exp^{\left(\left(-0.5\times\left(\frac{(x-xc)}{w1}\right)^2\right)-\left(0.5\times\left(\frac{(y-yc)}{w2}\right)^2\right)\right)} \quad (4.6)$$

Table 4.5 Parameter value of nonlinear surface fit regression for P_{max} model

Parameter	z0	A	xc	w1	yc	w2
Value	4.46559	-4.30966	-169.5821	742.76853	8.18332E147	5.35927E150

I utilized the results generated by this model to conduct an analysis aimed at computing the power losses of solar photovoltaic panels, thereby determining the precise impact of dust and other environmental factors on power generation from solar PV panels.

4.7 Conclusion

Accurate prediction of photovoltaic (PV) panel power generation across varying levels of irradiance and temperatures is crucial for both the planning and operational phases of PV systems. Numerous studies have focused on estimating the current-voltage (I-V) curve of PV panels, often incorporating expressions based on an equivalent circuit model. The approach in this particular study involves utilizing manufacturer data to design a PVsyst-based model, and validating the same under various irradiance and temperature conditions. While PVsyst simulation models offer valuable insights, they often lack practical applicability due to idealized analyses. Therefore, it's essential to implement the experimental model to accurately assess real-world performance. Controlled experiments highlight actual performance, emphasizing the need for comprehensive testing under real environmental conditions. Hence, three distinct experimental models were developed based on the collected data. Firstly, utilizing the fill factor model, the fill factor was projected for specific radiation and temperature conditions. This predicted fill factor was then employed in calculating the efficiency of solar photovoltaic panels. Secondly, another fill factor model was utilized to forecast the fill factor for particular V_{oc} and I_{sc} values, considering the impact of dust accumulation on solar panel performance. Thirdly, the P_{max} model was employed to estimate the actual maximum power generation of solar panels under specific radiation and temperature conditions, excluding the influence of various environmental factors. This data was subsequently utilized for further analysis, particularly in assessing losses attributed to dust accumulation. Future efforts should combine experimental data with site-specific outdoor experiments, aiming to calculate the energy production for solar photovoltaic panels.

Chapter 5

Experimental Study on Effects of Dust Accumulation on Power Generation from Solar Photovoltaic Panels Installed at Different Tilt Angles under All Weather Conditions

5.1 Introduction

In the previous chapter, the influence of various factors, such as solar radiation and the temperature of photovoltaic (PV) panels on the generation of power from solar PV panels was investigated. Besides, another environmental factor significantly impacting solar cell performance is dust accumulation. Quantity of dust settling on solar panels depends on their mounting tilt angle. Typically, increasing the tilt angle of solar panel installations reduces the density of dust settling on surfaces, owing to the gravitational force (Gholami et al., 2017). The accumulation of dust, particularly over extended periods, is observed to exert a notable influence on the anticipated power output of any solar PV power plant. Over time, air pollution deposition can lead to a decrease in energy production from solar modules by more than 60% (Asl-Soleimani et al.,2001). The impact of dust particles on solar panels varies depending on the specific geographical location of installations and local factors. These local factors are human activities, environmental conditions, and weather patterns. Additionally, the performance of PV modules can be affected by light rainfall, as it helps to clean the accumulated dirt and other debris that may have settled on the surface. Various literature sources have acknowledged that dust accumulation on solar PV panels significantly impacts PV power generation. Over time, the continued accumulation of dust particles on PV panels in dusty regions can lead to a reduction in efficiency of up to 30%, with a potential decrease of up to 17% within just a day (Wakim, 1981, Paudyal and Shakya, 2016). Dust particles primarily affect the solar panel's absorption and reflection capabilities from sunlight (Al-Hasan et al., 2005). Therefore, the study further focused on identifying the dust accumulation patterns across different seasons at the specific experimental area. An outdoor experiment was conducted to evaluate the real time impact of dust accumulation on power generation characteristics of PV panels. Throughout this outdoor experiment, data was accumulated based on various parameters, including panel temperature, radiation levels, dust accumulation rates at different intervals, wind speed and direction, humidity, ambient temperature, and rainfall. The above-mentioned parameters data gathered from the weather stations installed in the experimental area, regarding the specified parameters, is employed in subsequent experimental analyses to derive results.

5.2 Dust Accumulation Patterns Across Seasons at Different Tilt Angles

An outdoor experimental study was conducted on the rooftop of School of Energy Studies building at Jadavpur University, Kolkata, West Bengal, to measure the dust accumulated on solar panels throughout the year across different seasons. To facilitate this examination, ten identical solar PV panels were installed at various tilt angles, specifically 0°, 10°, 30°, 40°, 50°, 60°, 70°, 80°, 90°, in addition to incorporating the latitude angle of 22.5°, corresponding to Kolkata's location. It was ensured that panels were unaffected by shading effects. All solar PV were positioned to face due south to maximize exposure to sunlight throughout the day. To analyze the power generation of solar PV panels in the dust accumulation scenario, open circuit voltage (V_{oc}) and short circuit current (I_{sc}) output of all panels were measured and data were recorded using the data acquisition system at five-second intervals as detailed in Chapter 3. Concurrently, K-type thermocouples were employed to track the temperature of each panel. The dust accumulation on different tilt angles installed solar PV panels was measured by placing glass slides across the panel tilts with a consistent alignment base. As per the Indian Meteorological Department (IMD Annual Report 2022), the seasons in West Bengal, particularly in Kolkata, are generally classified into three main segments throughout the year. Specifically, the summer season is observed to span from March to June, followed by the monsoon season extending from July to October. However, in the experimental year of 2022-23, the Southwest Monsoon arrived in mid-June. Winter typically observed from the month of December to February. The data collection process was commenced from March to May 2022, specifically targeting the summer season. Each month, a systematic series of experiments was conducted to collect dust data at intervals of 7, 14, 21, and 28 days (Konyu et al, 2020). According to the data obtained from the weather station, the April month ambient temperature exhibited notably higher values compared to the other months, with no rainfall recorded during this period. Consequently, it was determined that the data spanning from April 8th to May 4th, 2022, would best represent the entirety of the summer season for subsequent calculations. Concurrently, all other data was routinely collected, with scanning taking place at five-second intervals throughout each day. Fig. 5.1 presents the cumulative dust accumulation (CDA) pattern observed across various tilt angles of solar panel installations during the summer season. The graph illustrates that panel with a tilt angle of 0° demonstrate the highest dust accumulation consistently across all time durations in comparison to other tilt angles. Subsequently, there is a decrease in dust accumulation as the panel tilt angle increases. Tilt angles of 30°, 40°, and 50° exhibit negligible differences in the pattern of dust accumulation, whereas angles of 70°, 80°, and 90° show similarly minimal variations. It is also observable that CDA significantly varies with time. Data obtained from glass slide at 0° tilt shows a CDA of 7.42 gm/m^2 at the end of first 7 days, where the came at the end of 28 days has increased to 11.51 gm/m^2, depicting a CDA of 4.09 gm/m^2 during the next three weeks. This may be explained by gradual decrease in available glass surface resulting in diminishing adhesive property due to already accumulative dust (Isaifan et al., 2019).

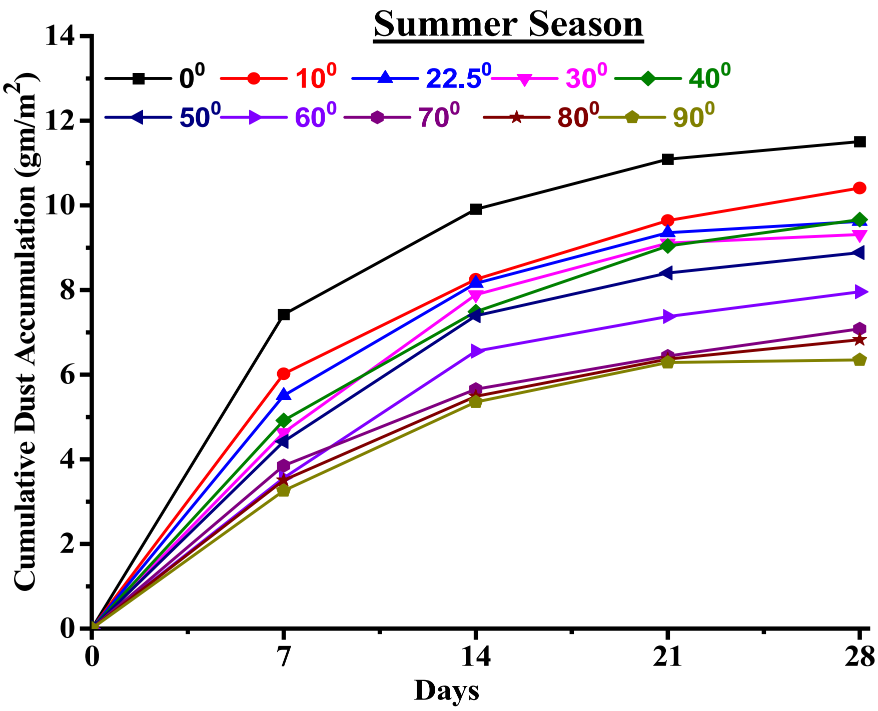

Fig. 5.1 Cumulative dust accumulation pattern in summer season in different tilt angle of solar PV installation

Thus rate of dust accumulation fluctuates over the time periods. The rates of CDA for different tilt angles at various time intervals during the summer season are provided in Table 5.1. Previous literature shows that during the summer and winter seasons in the mining areas of East Singhbhum districts of Jharkhand state, India, average atmospheric dust fall rates were recorded ranging from 7.51 to 28.58 gm/m^2/month and 7.40 to 26.37 gm/m^2/month respectively. The difference in dust fall rates in summer and winter seasons can be attributed to variations in meteorological conditions (Mahato and Singh, 2020). Under real-world conditions characterized by high ambient temperatures, intense solar radiation, dust samples were collected during two regional dust storm events that occurred in Middle Eastern country (Iraq), on May 13 and May 23, 2022. The dust amounts measured were 9.2 g/m^2 and 18 g/m^2, respectively (Almukhtar et al.,2023).

Table 5.1 Cumulative dust accumulation rate (gm/m^2) in different tilt angle at different time intervals during Summer

	∠0°	**∠10°**	**∠22.5°**	**∠30°**	**∠40°**	**∠50°**	**∠60°**	**∠70°**	**∠80°**	**∠90°**
Day-7	7.42	6.02	5.51	4.63	4.92	4.42	3.56	3.85	3.51	3.26
Day-14	9.91	8.25	8.16	7.89	7.49	7.39	6.56	5.66	5.49	5.35
Day-21	11.09	9.64	9.35	9.11	9.04	8.40	7.37	6.44	6.37	6.29
Day-28	11.51	10.41	9.62	9.31	9.67	8.88	7.96	7.08	6.83	6.35

During the monsoon season, data collection commenced in the middle of June and continued through October. Every set of data was collected over a duration of 28-day and for every season, three such data sets were obtained. Data accumulated by the weather station throughout the entire season was verified and finally data gathered during the duration of June 14th to July 11th, 2022 was considered as the representative data set for that particular season. Within this timeframe, the maximum number of rainy days recorded was 16 and the average rainfall for the session was 8.21 mm, closely aligning with the daily area-weighted average rainfall of East and North-East India, which ranges from 4 to 8 mm according to the (IMD Annual Report 2022). Additionally, data from the Regional Meteorological Centre indicated average rainfall for July-August, August-September, and September-October to be 7.9 mm, 7.5 mm, and 7.3 mm respectively (Regional Meteorological Centre, Kolkata WWR report, 2022). Based on the above-mentioned justification, the first dataset was provided to ensure the optimal representation of the monsoon season, with the weightage value of this dataset serving as a representation of the monsoon season. Fig. 5.2 illustrates the dust accumulation at various tilt angles during the monsoon season. Dust accumulation data was collected on a daily basis and at intervals of 7, 14, 21, and 28 days during the monsoon season. In the Fig. 5.2, the daily dust accumulation data was utilized to accurately represent the relationship between dust accumulation and rainfall.

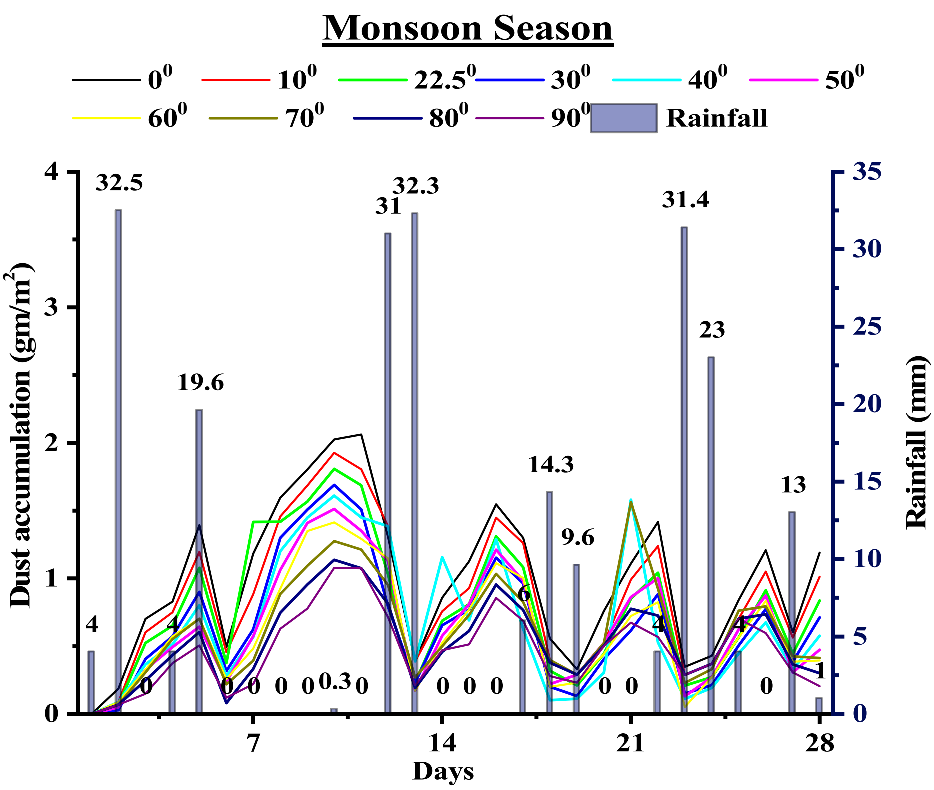

Fig. 5.2 Cumulative dust accumulation pattern in monsoon season in different tilt angle of solar PV installation

The graph illustrates that the weight of dust accumulation varies with rainfall; as the quantity and frequency of rainfall increase, the dust accumulation decreases. Table 5.2 presents the rates of CDA at different tilt angles throughout the monsoon season.

Table 5.2 Cumulative dust accumulation rate (gm/m^2) in different tilt angle at different time intervals during Monsoon

	∠0°	∠10°	∠22.5°	∠30°	∠40°	∠50°	∠60°	∠70°	∠80°	∠90°
Day-7	2.07	2.06	1.97	1.93	1.57	1.47	1.37	1.22	0.99	0.86
Day-14	1.10	1.08	1.02	0.93	0.96	0.83	0.72	0.76	0.66	0.47
Day-21	1.70	1.63	1.58	1.42	1.12	1.13	1.14	1.18	0.83	0.77
Day-28	0.96	0.93	0.92	0.86	0.64	0.55	0.53	0.59	0.46	0.38

During the winter season, data collection commenced from November to February. Cumulative dust accumulation data were gathered continuously from November 18th to January 21st, 2022, spanning a total of 65 rain-free days. The initial 28 days' data were utilized for the winter season's representation, with their weighted values employed for subsequent analysis of PV power generation during winter. Fig. 5.3 demonstrates that the rate of dust accumulation experiences an initial day increase during the onset of the winter season, followed by a gradual decline over time. The graph illustrates that the dust accumulation during the winter season is slightly high with respect to all other seasons.

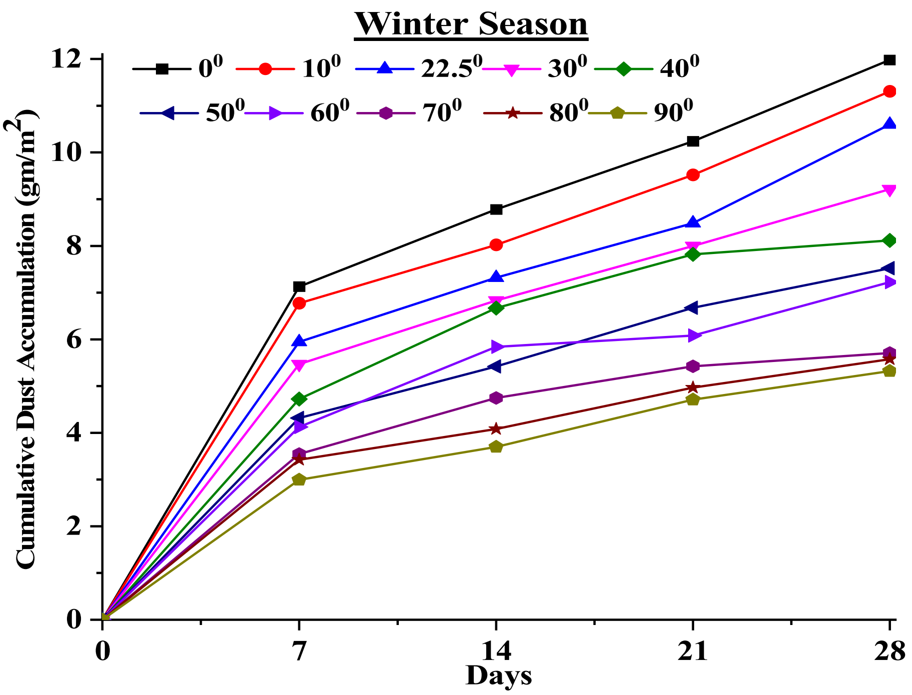

Fig. 5.3 Cumulative dust accumulation pattern in winter season in different tilt angle of solar PV installation

The dust accumulation patterns for the entire 65-day period are visually represented in Fig. 5.4. Here, it is illustrated that over the long term, the rate of dust accumulation is initially observed to increase with time, after which decrease in the rate of dust accumulation on solar PV panels is compared to that of previous weeks. While Table 5.3 provides a structured presentation of the rates of dust accumulation throughout the winter season.

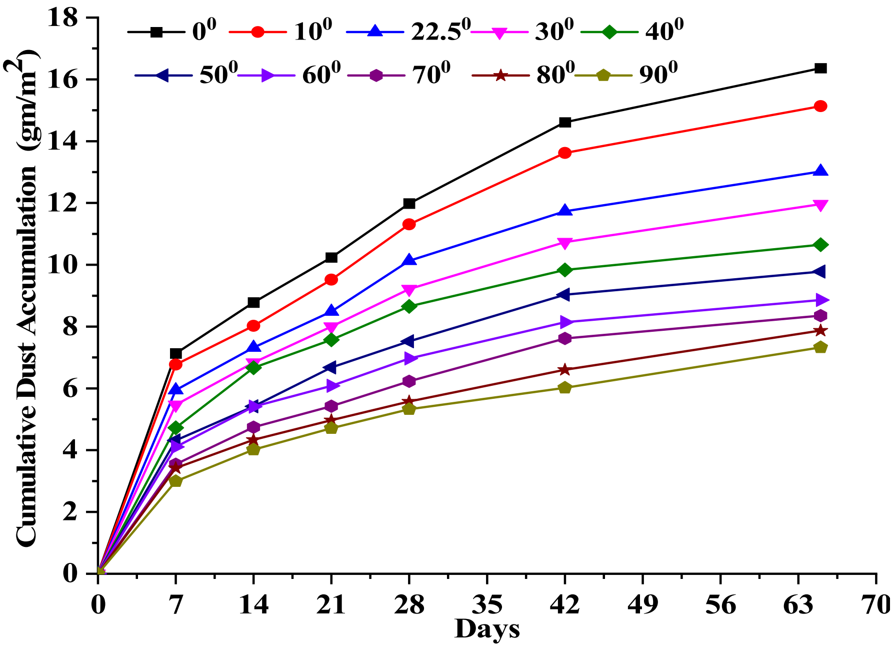

Fig. 5.4 Cumulative dust accumulation pattern in winter season in different tilt angle of solar PV installation

Table 5.3 Cumulative dust accumulation rate (gm/m^2) in different tilt angle at different time intervals during Winter

	∠0°	∠10°	∠22.5°	∠30°	∠40°	∠50°	∠60°	∠70°	∠80°	∠90°
Day-7	7.13	6.77	5.94	5.47	4.72	4.31	4.11	3.55	3.42	3.00
Day-14	8.78	8.02	7.32	6.83	6.67	5.42	5.41	4.75	4.34	4.02
Day-21	10.24	9.52	8.49	8.00	7.57	6.68	6.08	5.42	4.97	4.71
Day-28	11.98	11.31	10.13	9.21	8.65	7.52	6.97	6.23	5.58	5.32
Day-42	14.61	13.62	11.73	10.73	9.83	9.03	8.14	7.62	6.60	6.02
Day-65	16.36	15.14	13.02	11.96	10.65	9.78	8.86	8.35	7.87	7.33

Considering latitude angle (22.5°) for the site of experiment as reference, a comparative analysis can be drawn regarding the extant of dust accumulation or soiling, for other tilt angles (Fig. 5.5-5.7). It is evident that the dust accumulation rate increases as the tilt angle decreases, while it decreases as the tilt angle increases. During the summer season, there is a notable increase of

+20.64% in dust accumulation at a 0° tilt angle and a decrease of -34.04% at a 90° tilt angle compared to the 22.5° tilt angle.

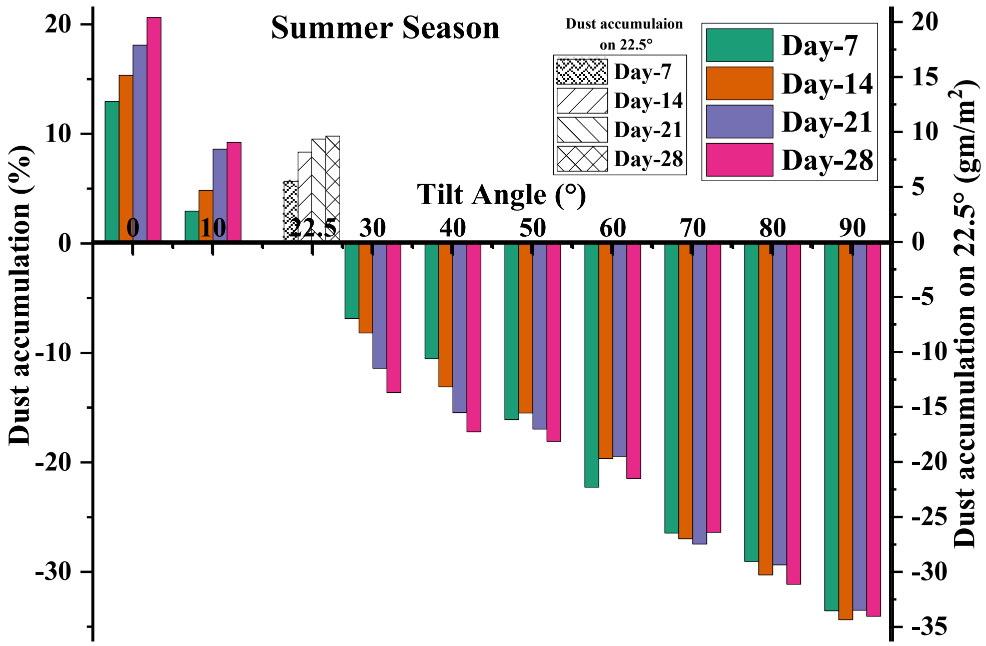

Fig. 5.5 Representation of dust accumulation percentage in summer season relative to the latitude of the site (22.5°) in various tilt angles and durations of solar PV installation

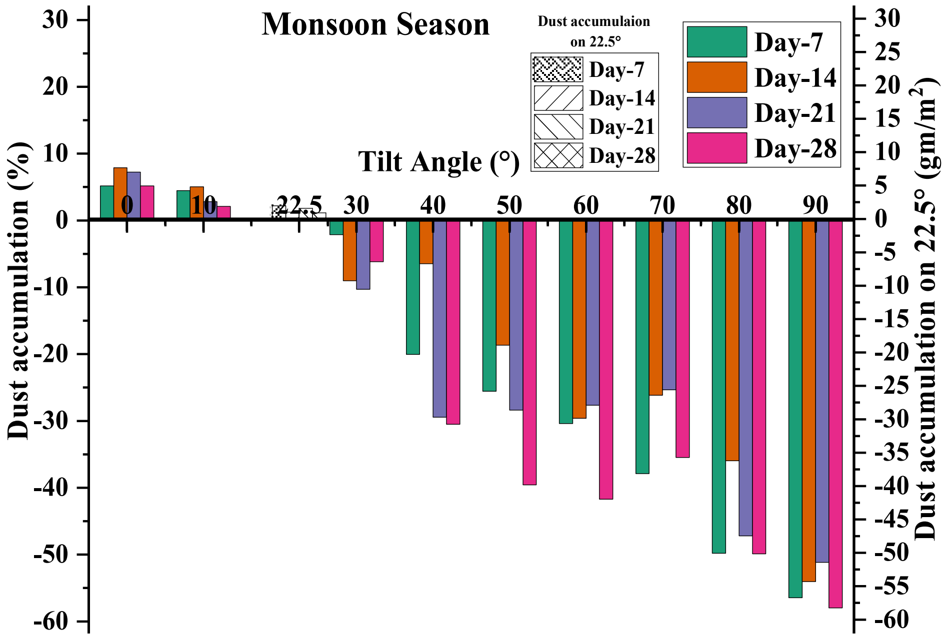

Fig. 5.6 Representation of dust accumulation percentage in monsoon season relative to the latitude of the site (22.5°) in various tilt angles and durations of solar PV installation

During the monsoon season, dust accumulation varied with rainfall, and the accumulation of dust on solar PV panels was relatively small compared to other seasons. Therefore, Fig. 5.6 clearly illustrates that dust accumulation differed across various tilt angles and time durations.

Specifically, there was an increase of +7.89% in accumulation percentage at a 0° tilt angle for a duration of 14 days, while there was a decrease of -57.97% at a 90° tilt angle for a duration of 28 days, relative to the 22.5° tilt angle.

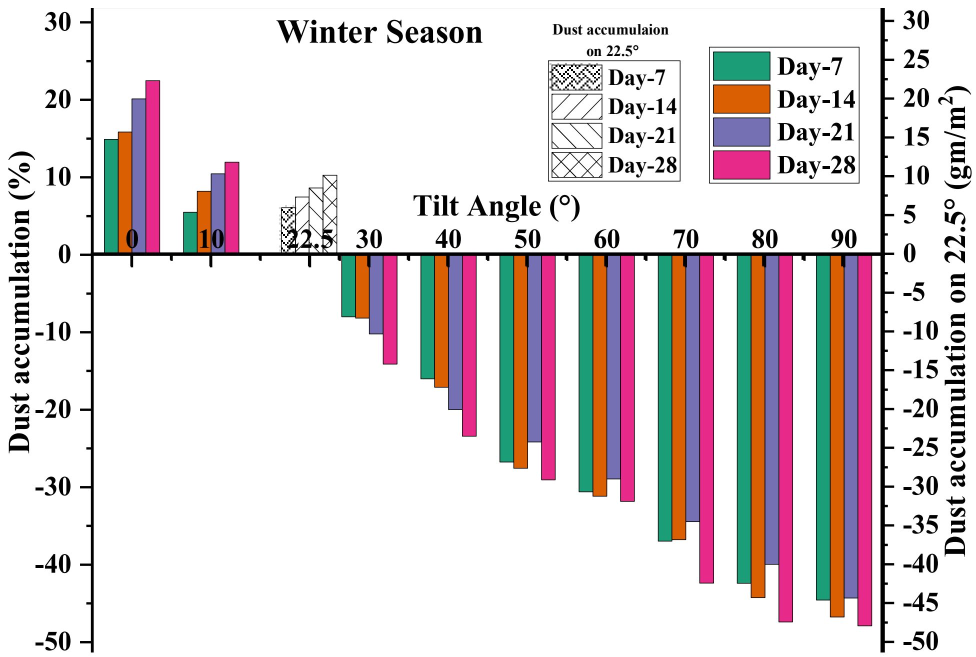

Fig. 5.7 Representation of dust accumulation percentage in winter season relative to the latitude of the site (22.5°) in various tilt angles and durations of solar PV installation

Similarly, in the winter season, Fig. 5.7 depicts an increase of +22.47% in dust accumulation percentage at a 0° tilt angle and a decrease of -47.90% at a 90° tilt angle for the maximum time duration, relative to the 22.5° tilt angle.

5.3 Influence of dust accumulation on energy production at constant Radiation and Temperature

To assess the impact of dust accumulation on solar photovoltaic (PV) power generation, an experiment was conducted to measure the actual power output under consistent radiation and temperature conditions, comparing it with the expected outdoor power generation. This experiment was conducted at a site with a latitude similar to Kolkata during the summer season. According to the literature, the annual average solar radiation in Kolkata is recorded at 5.19 kWh/m^2/day. Solar radiation levels vary throughout the year, with summer ranging from 4.42 to 6.40 kWh/m^2/day, monsoon from 4.42 to 5.40 kWh/m^2/day, and winter from 4.10 to 5.61 kWh/m^2/day (Kumar et al., 2020). Hence, the analysis was carried out based on outdoors experiment during the summer season, at a tilt angle equivalent to site's latitude (22.5°). Data were collected under nearly constant temperature conditions at radiation levels of 400 W/m^2 and 600 W/m^2.

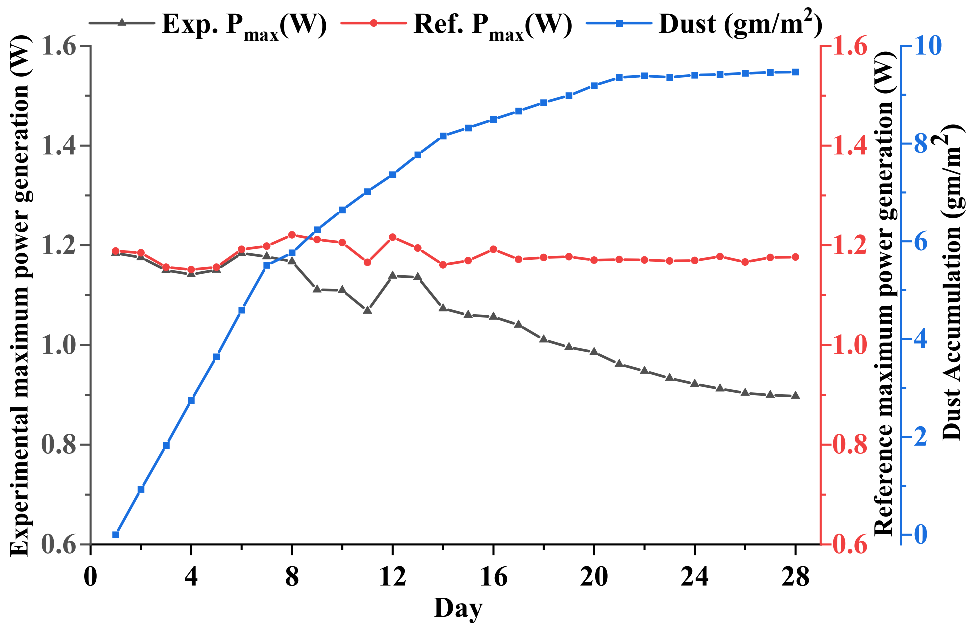

Fig. 5.8 Maximum power variation observed with and without dust accumulation under constant temperature and 400 W/m^2 radiation at 22.5° tilt

In this study, indoor laboratory solar simulator output data was utilized as a reference for maximum power generation (Ref. P_{max}), which was unaffected by dust. The outdoor experimental data served as experimental maximum power generation (Exp. P_{max}). Fig. 5.8 illustrates a decrease in maximum power due to dust accumulation under constant temperature conditions at 400 W/m² radiation, while Fig. 5.9 demonstrates a similar decrease under constant temperature conditions at 600 W/m² radiation.

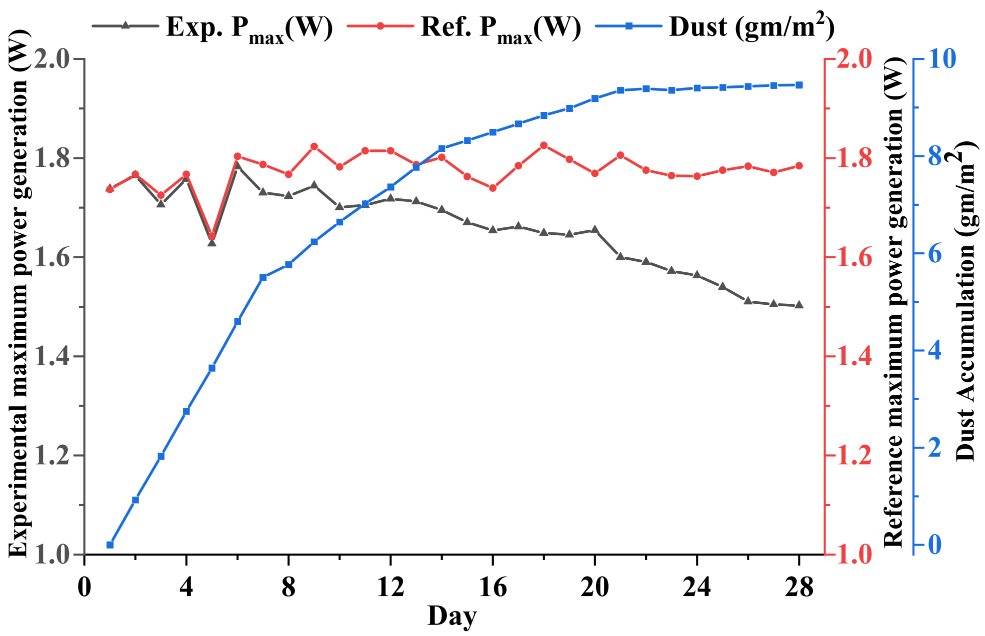

Fig. 5.9 Maximum power variation observed with and without dust accumulation under constant temperature and 600 W/m^2 radiation at 22.5° tilt

Table 5.4 reveals the weekly maximum power reduction resulting from dust accumulation under constant radiation levels. The data indicates an increase in power reduction from 0.35% to 23.72% at 400 W/m², as well as from 0.37% to 15.81% at 600 W/m². Notably, the reduction in power is more pronounced at 400 W/m² compared to 600 W/m². The impact of dust accumulation on sunlight transmission is indeed more significant in lower radiation conditions.

Table 5.4 Weekly maximum power reduction due to dust accumulation in constant radiation level

Duration	Dust (gm/m^2)	Radiation (W/m^2)	Panel Temp. (°C)	Ref. P_{max} (W)	Exp. P_{max} (W)	Maximum power reduction (%)
1st Day	0	400±5	44±0.5	1.1885	1.1844	0.35
		600±5	44±0.5	1.7447	1.7382	0.37
1st week (7 days)	5.5079	400±5	44±0.5	1.1981	1.1773	1.74
		600±5	44±0.5	1.7870	1.7303	3.17
2nd week (14 days)	8.1575	400±5	44±0.5	1.1608	1.0730	7.56
		600±5	44±0.5	1.8016	1.6953	5.90
3rd week (21 days)	9.3543	400±5	44±0.5	1.1715	0.9615	17.92
		600±5	44±0.5	1.8056	1.6002	11.37
4th week (28 days)	9.4667	400±5	44±0.5	1.1765	0.8974	23.72
		600±5	44±0.5	1.7844	1.5024	15.81

When the radiation levels are lower, such as at 400 W/m² compared to 600 W/m², the same amount of dust has a comparatively greater impact on blocking sunlight. This is because lower radiation levels mean there is less overall sunlight available, so any obstruction, such as dust, has a proportionally larger effect on reducing the amount of sunlight reaching the solar panels. As a result, the power reduction due to dust accumulation is often more pronounced in situations with lower radiation levels (Mazumder et al., 2013).

5.4 Maximum Power Point Consideration in PV Power Generation

A solar power plant utilizing MPPT (Maximum Power Point Tracking) technology is designed to optimize the efficiency of energy conversion from solar panels. MPPT is a technique used in solar inverters to ensure that the solar panels operate at their maximum power point, regardless of environmental conditions such as temperature and shading. The MPPT algorithm constantly adjusts the electrical operating point of the solar panels to ensure they are operating at the point where they produce the maximum power output. This is crucial because the output of solar panels varies depending on factors like sunlight intensity and temperature. This is particularly important for large-scale solar installations, where even small improvements in efficiency can translate into significant increases in energy production. Therefore, in this study, maximum power point measurement data is considered for PV generation calculations.

5.5 Normalization of PV power Generation Based on Radiation Values

The relation between solar photovoltaic (PV) power generation, radiation, and cell temperature is crucial in understanding the performance of solar panels. As solar panels absorb radiation, the cell temperature rise beyond the ambient temperature. Higher temperatures reduce the efficiency of solar cells, affecting the power output. Therefore, the overall power generation of solar panels is influenced by a balance between radiation levels (which increase power generation) and cell temperature (which can decrease efficiency). The most suitable method for normalizing energy generation was determined by primarily selecting two random days from each season and analyzing global radiation data, alongside ambient temperature and panel temperature at different tilt angles, to identify the parameters that affected power generation of solar PV panels most. This comprehensive examination provides an understanding the impact of changes in global radiation, and panel temperature in various tilt angles and the influence on energy generation across different seasons. The radiation levels, ambient temperature, and panel temperature data for each season and tilt angle, the results have been illustrated in Fig. 5.10 to 5.15. The complete data set of the analysis have been tabulated in Tables 5.4 to 5.7.

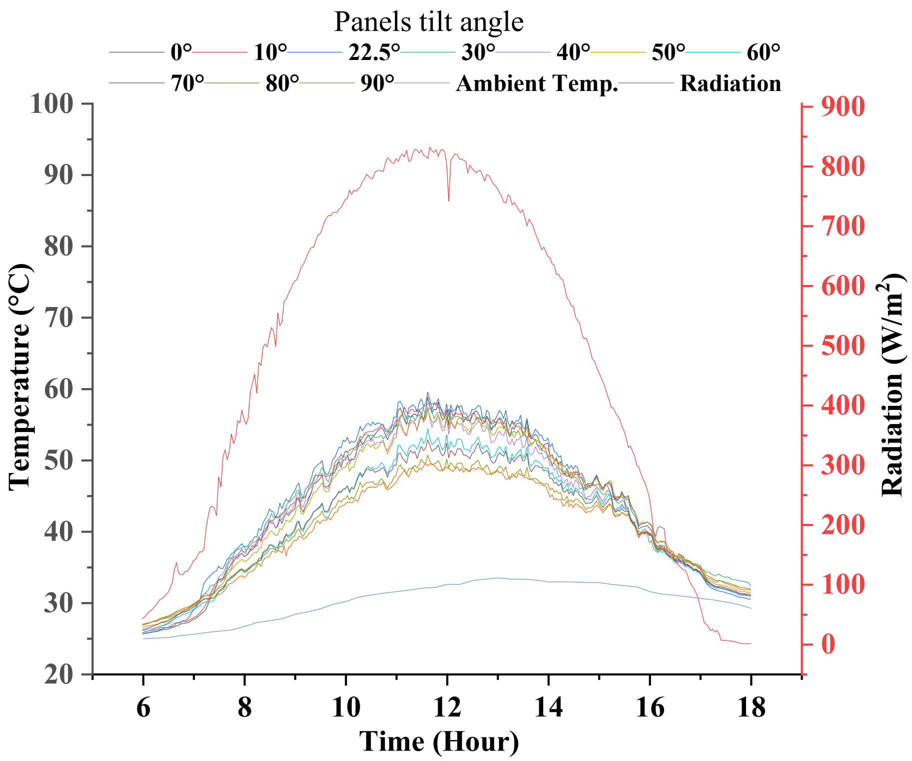

Fig. 5.10 Temperature, ambient temperature and global radiation data in different tilt panels during summer season (Day-1, date- 08-04-22)

Visual representations in corresponding figures can often provide a clearer understanding of the trends and relationships within the data.

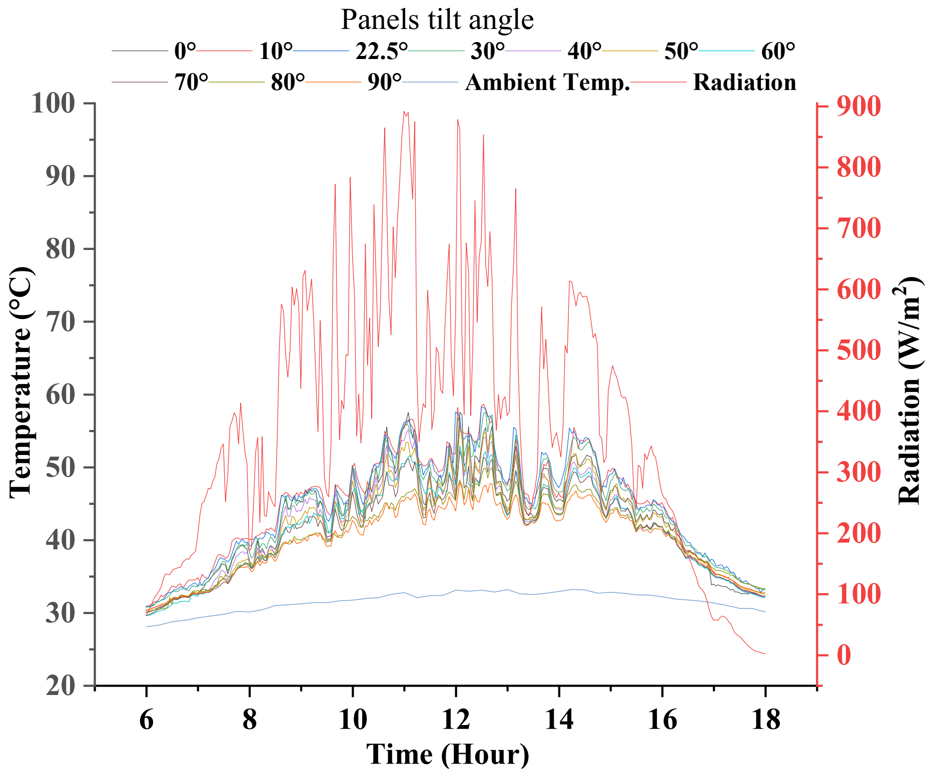

Fig. 5.11 Temperature, ambient temperature and global radiation data in different tilt panels during summer season (Day-13, date- 20-04-22)

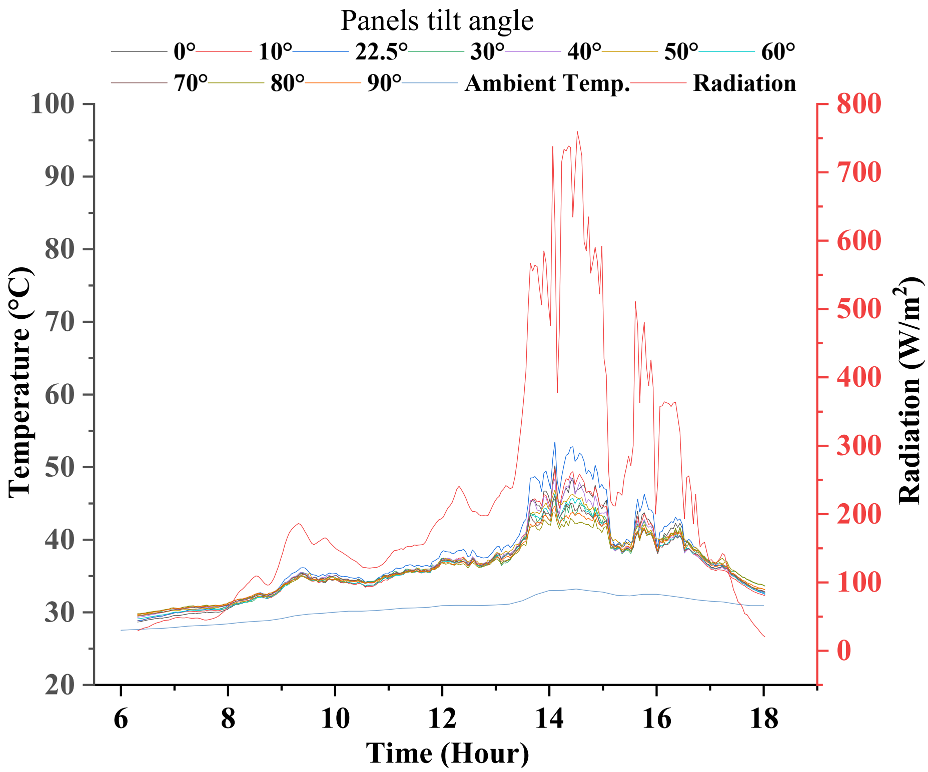

Fig. 5.12 Temperature, ambient temperature and global radiation data in different tilt panels during monsoon season (Day-2, date-15-06-22)

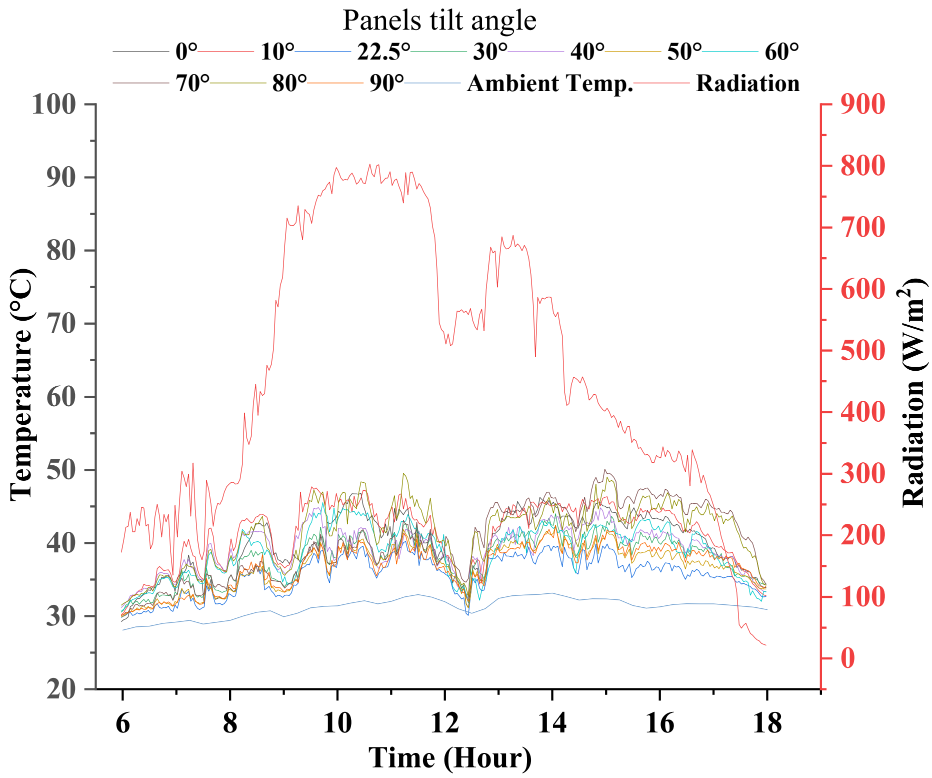

Fig. 5.13 Temperature, ambient temperature and global radiation data in different tilt panels during monsoon season (Day-24, date- 07-07-22)

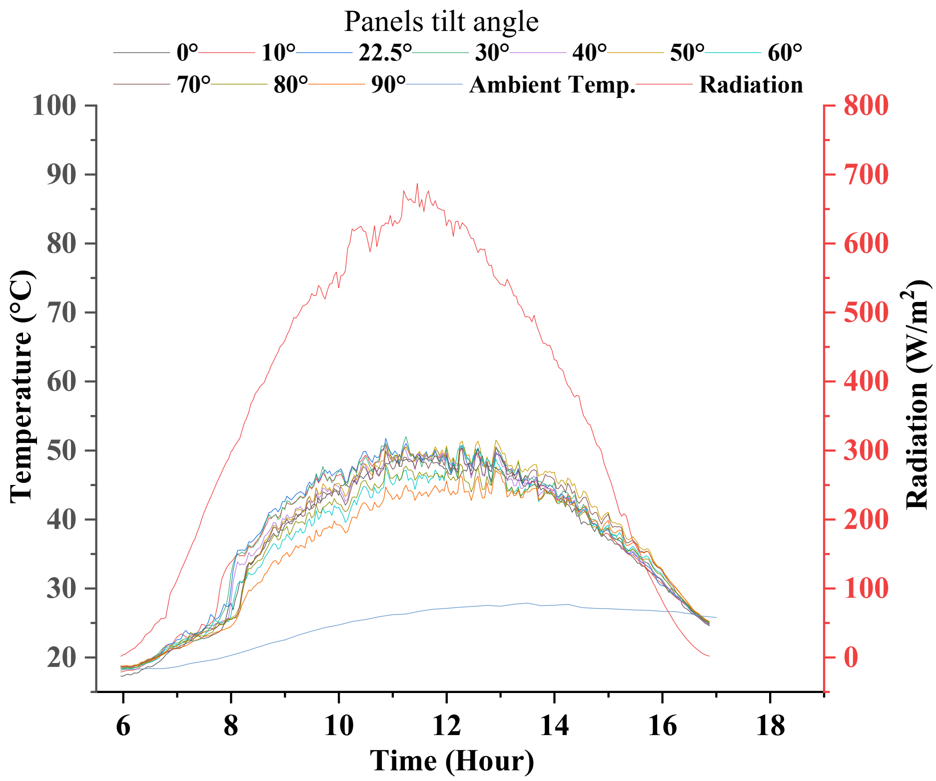

Fig. 5.14 Temperature, ambient temperature and global radiation data in different tilt panels during winter season (Day-7, date- 24-11-22)

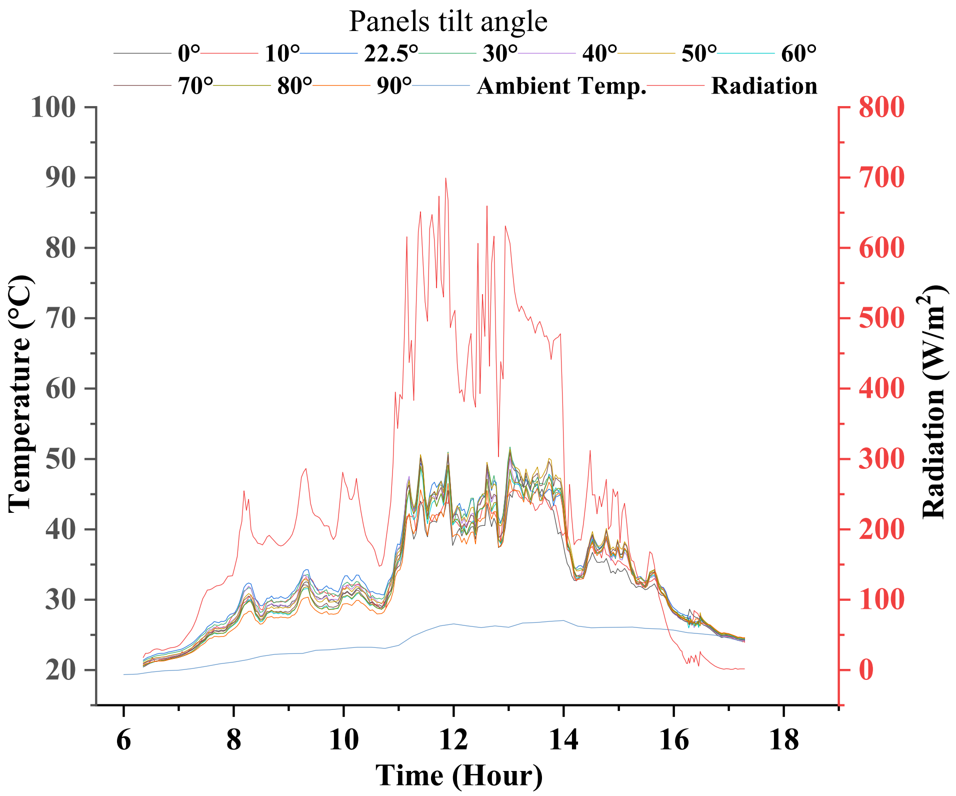

Fig. 5.15 Temperature, ambient temperature and global radiation data in different tilt panels during winter season (Day-23, date- 10-12-22)

During the summer season, the variation in panels temperature was shown, as indicated in Table 5.5 and Fig. 5.10 and 5.11. On specific days, the average ambient temperature was recorded as 30.28°C and 31.57°C, while the average panel temperatures exceeded the average ambient temperature by up to 14.37°C and 13.09°C. When comparing the maximum panel temperatures to the ambient temperature, the difference was even higher, reaching 29.29°C and 27.12°C. Furthermore, comparing the panel temperatures with the panel at site's latitude (i.e. 22.5°), variations ranged from 0.79 to 4.47°C and 0.73 to 4.61°C during day-1 and day-13 of experiment observation respectively. Considering the temperature coefficient value of maximum power described in Chapter 4, it justifies that these small temperature changes do not significantly affect power generation compared to solar radiation. Additionally, the temperature coefficient varies with radiation levels, further emphasizing the dominant influence of solar radiation on power generation compared to temperature variations. This observation suggests that while panel temperature remains relatively stable throughout the summer season, radiation levels fluctuate considerably, potentially impacting the performance of solar panels. Understanding these variations is essential for optimizing the efficiency and output of solar PV systems, particularly during periods of high radiation variability.

Table 5.5 Panels temperature variation different tilt panels during Summer season

Tilt Angle / Day	0°	10°	22.5°	30°	40°	50°	60°	70°	80°	90°
Summer Day-1 08-04-22	Average ambient temperature = 30.28 °C									
	Average temperature difference of solar panels from average ambient temperature									
	13.59	13.64	14.37	13.76	12.99	13.21	11.24	11.05	10.38	9.90
	Temperature difference of maximum temperature of solar panels from average ambient temperature									
	28.58	27.83	29.29	27.17	27.20	26.86	24.15	22.56	20.48	19.27
	Average temperature difference of other tilt angles panels with respect to the 22.5° tilt installed panel									
	-0.79	-0.74	0.00	-0.62	-1.38	-1.16	-3.13	-3.33	-3.99	-4.47
Summer Day-13 20-04-22	Average ambient temperature = 31.57 °C									
	Average temperature difference of solar panels from average ambient temperature									
	11.47	13.05	13.09	12.36	10.62	10.66	9.92	9.61	9.14	8.49
	Temperature difference of maximum temperature of solar panels from average ambient temperature									
	26.01	27.12	26.71	26.02	24.47	23.99	21.37	20.70	18.38	16.36
	Average temperature difference of other tilt angles panels with respect to the 22.5° tilt installed panel									
	-1.62	-0.05	0.00	-0.73	-2.47	-2.44	-3.17	-3.48	-3.95	-4.61

As depicted in Table 5.6 and Fig. 5.12 and 5.13, during the monsoon season, the fluctuation in panel temperature over time is nominal. On specific days, the average ambient temperature was recorded at 30.52°C and 31.17°C, while the average panel temperatures exceeded the ambient temperature by up to 6.78°C and 10.11°C, respectively. When comparing the maximum panel temperatures to the ambient temperature, the disparities were even more pronounced, reaching 22.93°C and 18.91°C. Moreover, when examining panel temperatures with respect to 22.5° tilt, variations ranged from 0.94 to 1.38°C and -0.22 to 1.90°C. Rain fall on solar panels can lower their temperature by dissipating heat through evaporation, especially if the panels were previously exposed to direct sunlight and have absorbed a significant amount of heat. This cooling effect can potentially affect their performance and output.

Table 5.6 Panels temperature variation different tilt panels during monsoon season

Tilt Angle / Day	0°	10°	22.5°	30°	40°	50°	60°	70°	80°	90°
Monsoon Day-2 15-06-22	Average Ambient Temperature= 30.52 °C									
	Average temperature difference of solar panels from average ambient temperature									
	5.82	5.77	6.78	5.67	5.84	5.83	5.40	5.54	5.42	5.50
	Temperature difference of maximum temperature of solar panels from average ambient temperature									
	19.68	19.25	22.93	15.05	18.10	16.32	15.79	15.55	13.18	14.09
	Average temperature difference of other tilt angles panels with respect to the 22.5° tilt installed panel									
	-0.96	-1.01	0.00	-1.12	-0.94	-0.96	-1.38	-1.25	-1.36	-1.28
Monsoon Day-24 07-07-22	Average ambient temperature = 31.17 °C									
	Average temperature difference of solar panels from average ambient temperature									
	8.67	10.11	7.48	6.75	7.94	5.58	7.71	9.05	10.24	5.69
	Temperature difference of maximum temperature of solar panels from average ambient temperature									
	15.63	16.51	12.05	12.84	13.70	11.26	14.35	18.91	18.35	11.18
	Average temperature difference of other tilt angles panels with respect to the 22.5° tilt installed panel									
	1.18	2.62	0.00	-0.73	0.46	-1.90	0.22	1.56	2.75	-1.79

As depicted in Table 5.7 and Fig. 5.14 and 5.15, throughout the winter season, the fluctuation in panel temperatures over time remains minimal. On specific days, the average ambient temperature was recorded at 24.54°C and 23.92°C, while the average panel temperatures exceeded the ambient temperature by up to 15.23°C and 9.74°C, respectively. Comparing these maximum panel temperatures to the ambient temperature reveals even greater differences, reaching 27.20°C and 27.78°C, respectively. Furthermore, when analyzing panel temperatures at different tilt angles in comparison with respect to 22.5° tilt, variations ranged from -0.11 to 2.84°C and 0.21 to 1.96°C. While temperature changes can affect the efficiency of solar panels to some extent, their influence is often secondary to variations in radiation levels. Thus the PV panel output have been normalized based on radiation, approach has been discussed in the next section, which involves the impact of dust on the PV panel.

Table 5.7 Panels temperature variation different tilt panels during winter season

<table>
<tr><th>Tilt Angle
Day</th><th>0°</th><th>10°</th><th>22.5°</th><th>30°</th><th>40°</th><th>50°</th><th>60°</th><th>70°</th><th>80°</th><th>90°</th></tr>
<tr><td rowspan="7">Monsoon
Day- 7
24-11-22</td><td colspan="10">Average Ambient Temperature = 24.54 °C</td></tr>
<tr><td colspan="10">Average temperature difference of solar panels from average ambient temperature</td></tr>
<tr><td>13.74</td><td>15.09</td><td>15.23</td><td>15.22</td><td>14.48</td><td>15.34</td><td>13.49</td><td>14.67</td><td>13.37</td><td>12.40</td></tr>
<tr><td colspan="10">Temperature difference of maximum temperature of solar panels from average ambient temperature</td></tr>
<tr><td>24.90</td><td>26.39</td><td>27.20</td><td>27.47</td><td>26.46</td><td>26.99</td><td>26.23</td><td>25.97</td><td>23.54</td><td>22.55</td></tr>
<tr><td colspan="10">Average temperature difference of other tilt angles panels with respect to the 22.5° tilt installed panel</td></tr>
<tr><td>-1.50</td><td>-0.14</td><td>0.00</td><td>-0.01</td><td>-0.75</td><td>0.11</td><td>-1.74</td><td>-0.56</td><td>-1.86</td><td>-2.84</td></tr>
<tr><td rowspan="7">Monsoon
Day-23
10-12-22</td><td colspan="10">Average Ambient Temperature = 23.92 °C</td></tr>
<tr><td colspan="10">Average temperature difference of solar panels from average ambient temperature</td></tr>
<tr><td>8.14</td><td>8.74</td><td>9.95</td><td>9.74</td><td>9.21</td><td>9.63</td><td>8.56</td><td>9.13</td><td>8.72</td><td>7.99</td></tr>
<tr><td colspan="10">Temperature difference of maximum temperature of solar panels from average ambient temperature</td></tr>
<tr><td>23.81</td><td>22.53</td><td>27.49</td><td>27.78</td><td>26.87</td><td>27.47</td><td>24.91</td><td>26.98</td><td>25.22</td><td>23.18</td></tr>
<tr><td colspan="10">Average temperature difference of other tilt angles panels with respect to the 22.5° tilt installed panel</td></tr>
<tr><td>-1.82</td><td>-1.21</td><td>0.00</td><td>-0.21</td><td>-0.75</td><td>-0.32</td><td>-1.39</td><td>-0.82</td><td>-1.23</td><td>-1.96</td></tr>
</table>

5.6 Comparison of Normalized Generation for Dust Across Varying Tilt Angles and Seasons

Identifying power loss specifically due to dust accumulation proves challenging due to the variation in radiation characteristics. Therefore, the normalization approach has been adopted to assess the impact of dust accumulation on power loss. Without considering the effect of dust accumulation, the normalization method involves equation 5.1, which takes into account the solar simulator power generation data.

$$\text{Normalized Generation without dust} = \frac{\text{Total power generation (solar simulator) in particular day}}{\text{Mean radiation on a particular day}} \quad (5.1)$$

This involves equation 5.2, which considers the outdoor power generation data affected by dust accumulation.

$$\text{Normalized Generation with dust} = \frac{\text{Total power generation(outdoor)on a particular day}}{\text{Mean radiation on a particular day}} \tag{5.2}$$

Equation 5.3, denotes the error percentage in the normalized generation between scenarios with and without dust accumulation, providing insight into the impact of dust on the performance of solar panels.

$$\text{Error (\%)} = \left(\frac{\text{Normalized Generation without dust} - \text{Normalized Generation with dust}}{\text{Normalized Generation without dust}} \times 100\right) \tag{5.3}$$

Fig. 5.16(a) through 5.16(j) distinctly illustrate that the percentage of error increases over time due to dust accumulation during the summer season. As a result, this indicates a decline in the actual power generation under real environmental circumstances. As depicted Fig 5.16(a), it can distinctly have identified that with the increase in dust accumulation, the normalized generation experienced steady dip with time. At the end of 28th day of observation, there was a generation loss of around 36% when the panel tilt angle was set at 0°. However, the impact of tilt angle of solar PV plays as major role showing a balanced influence on power generation. Due to difference in tilt angles, the loss in generation varies after distinct tilt angle. The lowest impact can be visible case of solar PV at 90° tilt due to minimal dust accumulation at its shown in Fig. 16(j). Fig. 5.16(b) through 5.16(i), the generation losses associated with installations of solar PV panels at tilt angles of 10°, 22.5°, 30°, 40°, 50°, 60°, and 70° were depicted. After 28 days, it was observed that the dust accumulation on panels installed at 0° tilt was 11.61 gm/m², whereas those installed at 90° tilt exhibited a dust accumulation rate of 6.35 gm/m². It was observed that the generation losses and dust accumulation decrease with increase in the tilt angle of the solar PV modules.

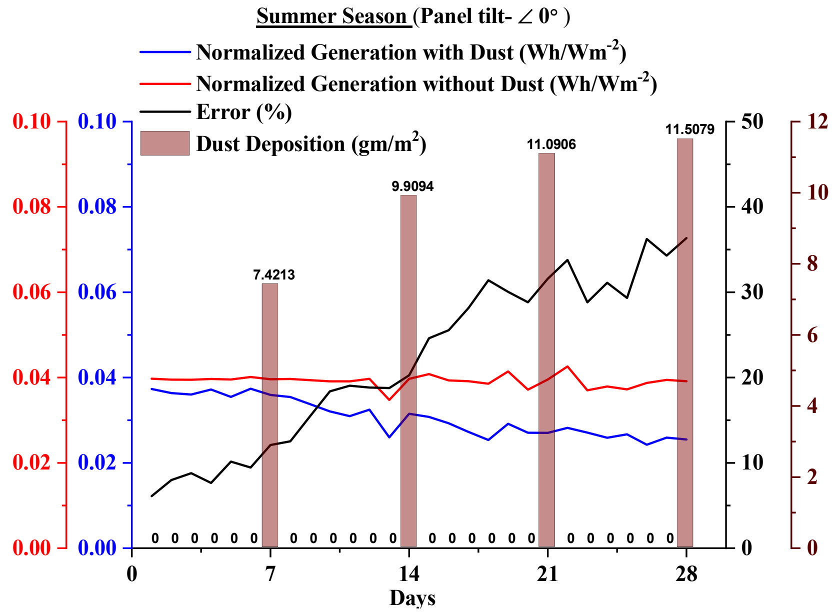

Fig. 5.16 (a) Normalized power generation with and without dust, and % of error at ∠0° tilt

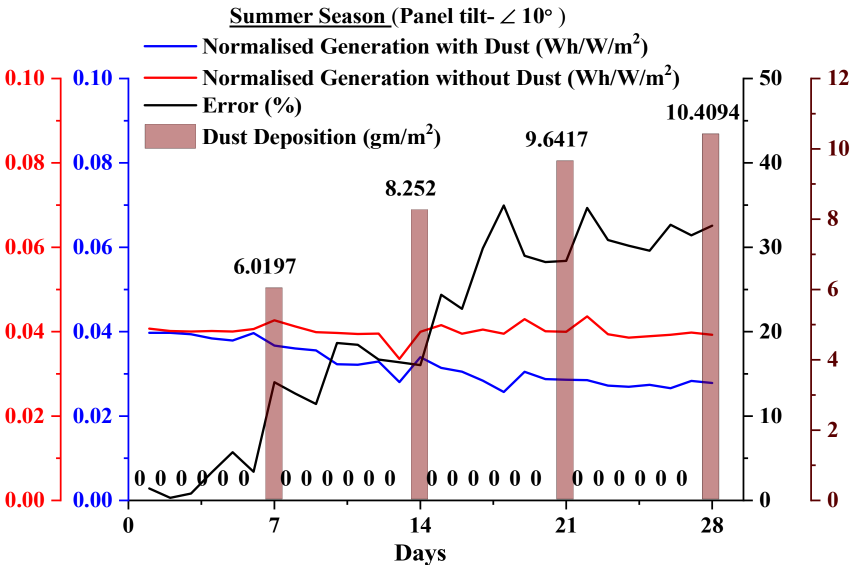

Fig. 5.16 (b) Normalized power generation with and without dust, and % of error at ∠10° tilt

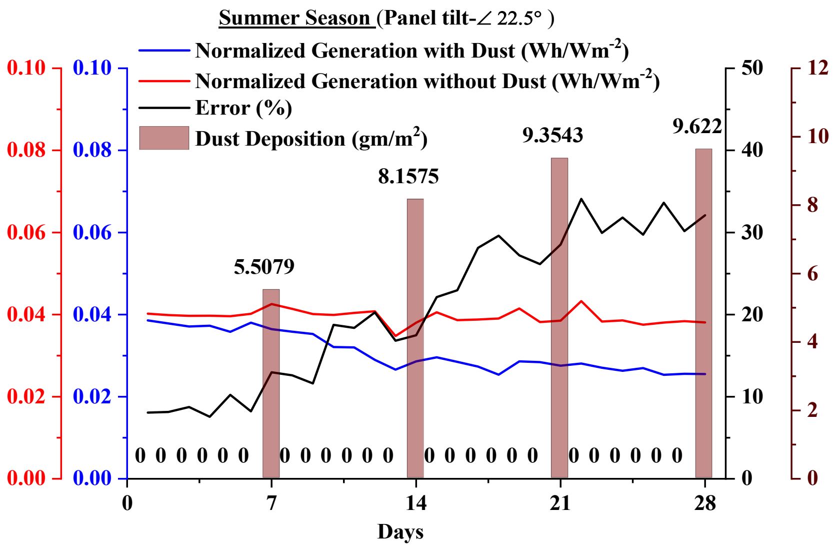

Fig. 5.16 (c) Normalized power generation with and without dust, and % of error at ∠22.5° tilt

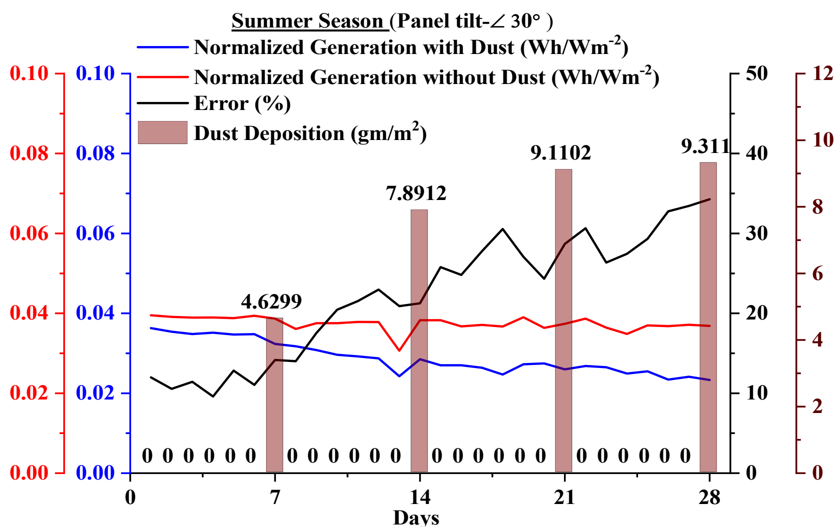

Fig. 5.16 (d) Normalized power generation with and without dust, and % of error at ∠30° tilt

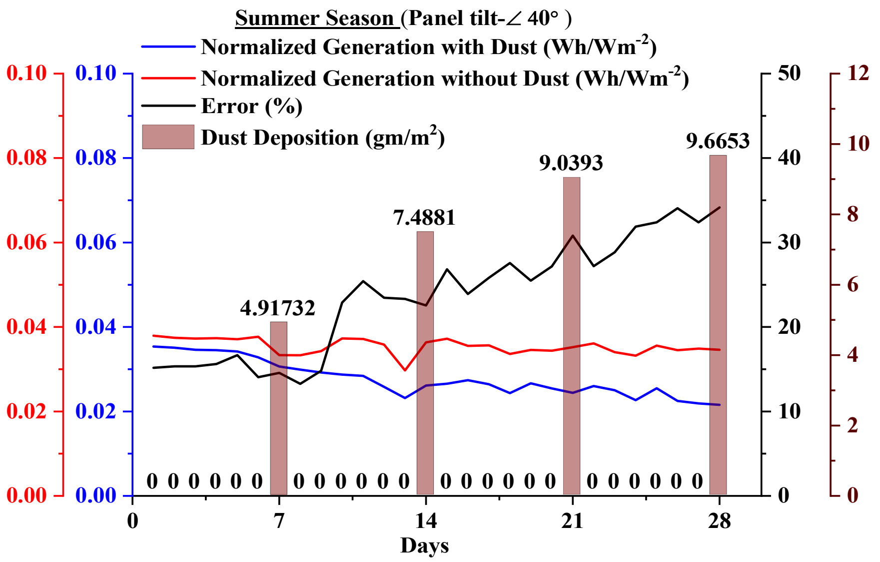

Fig. 5.16 (e) Normalized power generation with and without dust, and % of error at ∠40° tilt

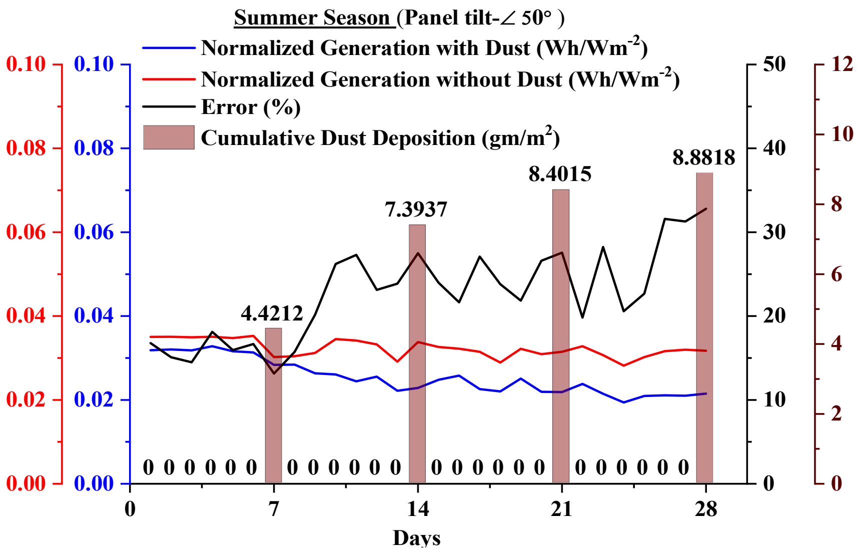

Fig. 5.16 (f) Normalized power generation with and without dust, and % of error at ∠50° tilt

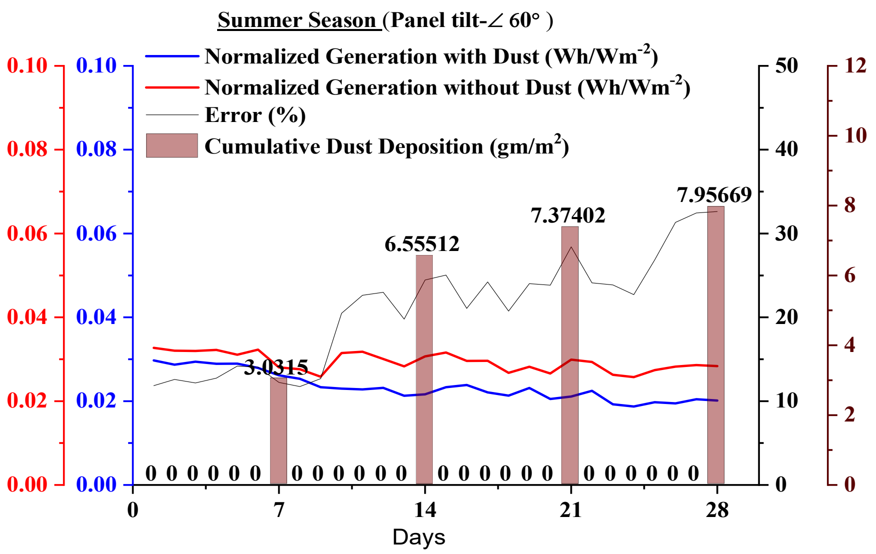

Fig. 5.16 (g) Normalized power generation with and without dust, and % of error at ∠60° tilt

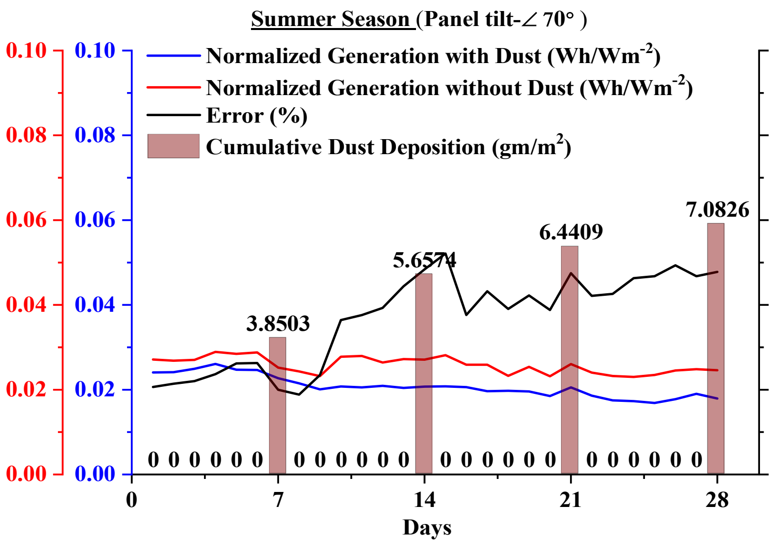

Fig. 5.16 (h) Normalized power generation with and without dust, and % of error at ∠70° tilt

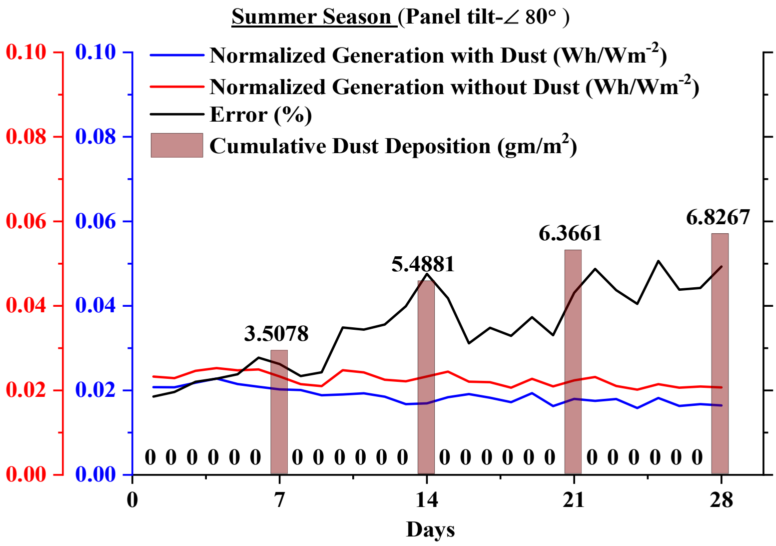

Fig. 5.16 (i) Normalized power generation with and without dust, and % of error at ∠80° tilt

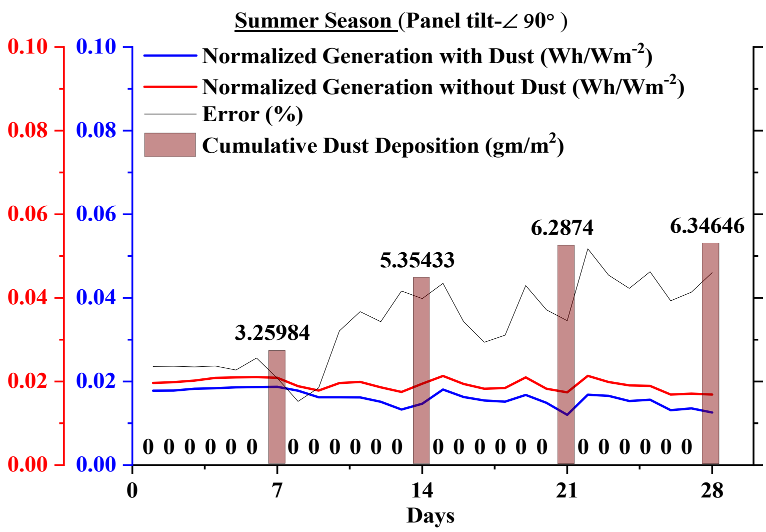

Fig. 5.16 (j) Normalized power generation with and without dust, and % of error at ∠90° tilt

During the monsoon season, the accumulation of dust undergoes changes over time due to rainfall, which cleanses the dust. Consequently, during this season, the loss of power generation due to dust accumulation lacks consistency over time. So, Fig. 5.17 illustrates only the normalized power generation with dust accumulation at all tilt angles during the monsoon season. It's evident that tilt angles of 0° and 10° yielded the highest normalized generation. During the monsoon session experiment, it was observed that dust deposition on modules tilted at 0° was comparatively higher than other angles. However, the effectiveness of rain in dust removal was hindered due to the flat module surface, leading to some dust or dirt remaining adhering with water. Conversely, at 90° tilt angle, the normalized generation was the lowest during the monsoon season. This reduced generation wasn't solely attributed to dust deposition but also to the decreased radiation received at this angle. Additionally, the steep vertical angle of this tilt facilitated effective dust removal by rainwater.

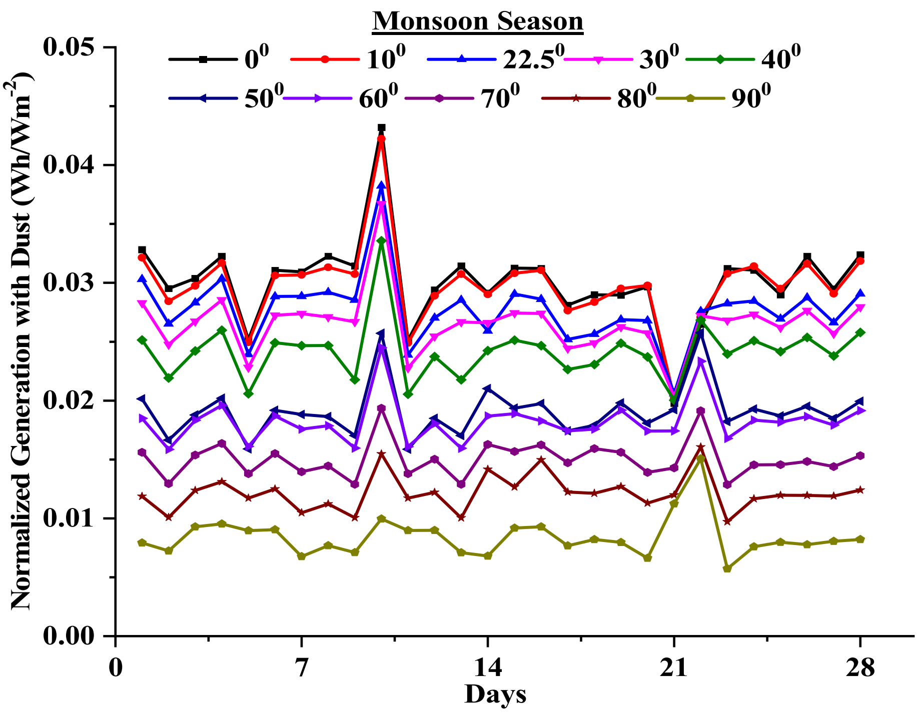

Fig. 5.17 Normalized power generation with dust at all tilt angle during monsoon season

The Fig. from 5.18(a) to 5.18(j) illustrate that through the winter period normalized power generation decreased under outdoor environments due to dust accumulation, resulting in a corresponding increase in error percentage. This indicates a decline in power generation resulting from the impact of environmental dust. As illustrated in Fig. 5.18(a), it is evident that with an increase in dust accumulation, the normalized generation experiences a steady decline over time. By the end of the 28^{th} day of observation, there was a generation loss of approximately 33% when the panel tilt angle was set at 0°. However, the tilt angle of solar PV panels plays a significant role, exerting a balanced influence on power generation. Notably, due to variations in tilt angles, the impact on generation loss varies accordingly. The least impact is observed in the case of solar PV panels set at a tilt angle of 90°, attributed to minimal dust accumulation, as depicted in Fig. 5.18(j). Fig. 5.16(b) through 5.16(i) illustrate the generation losses associated with the installation of solar PV panels at tilt angles of 10°, 22.5°, 30°, 40°, 50°, 60°, and 70°.Following a 28-day observation period, it was noted that dust accumulation on panels at 0° tilt was 11.98 gm/m², whereas installed at 90° tilt exhibited a lower dust accumulation rate of 5.32 gm/m². It was observed that both generation losses and dust accumulation decrease with an increase in the tilt angle of solar PV.

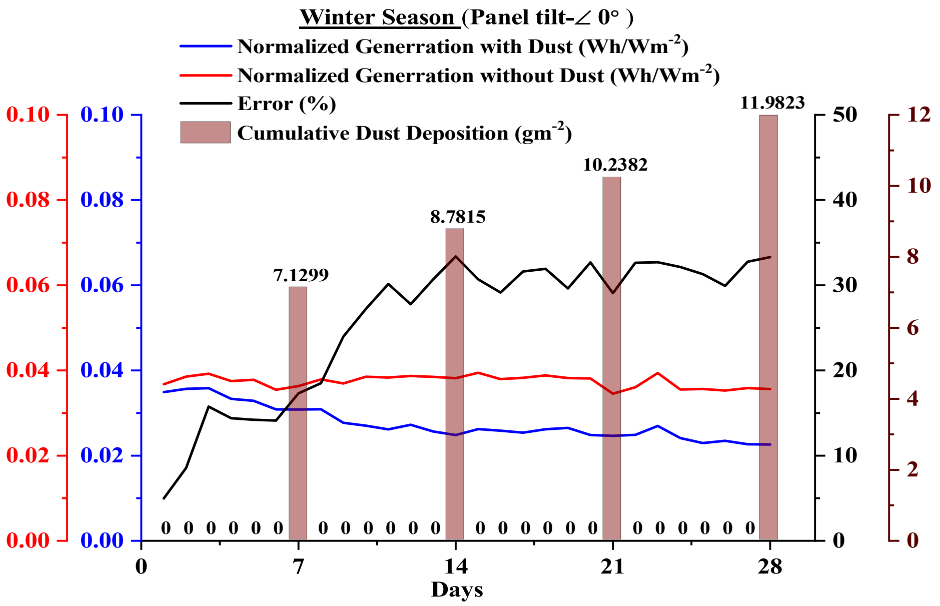

Fig. 5.18 (a) Normalized power generation with and without dust and % of error at ∠0° tilt

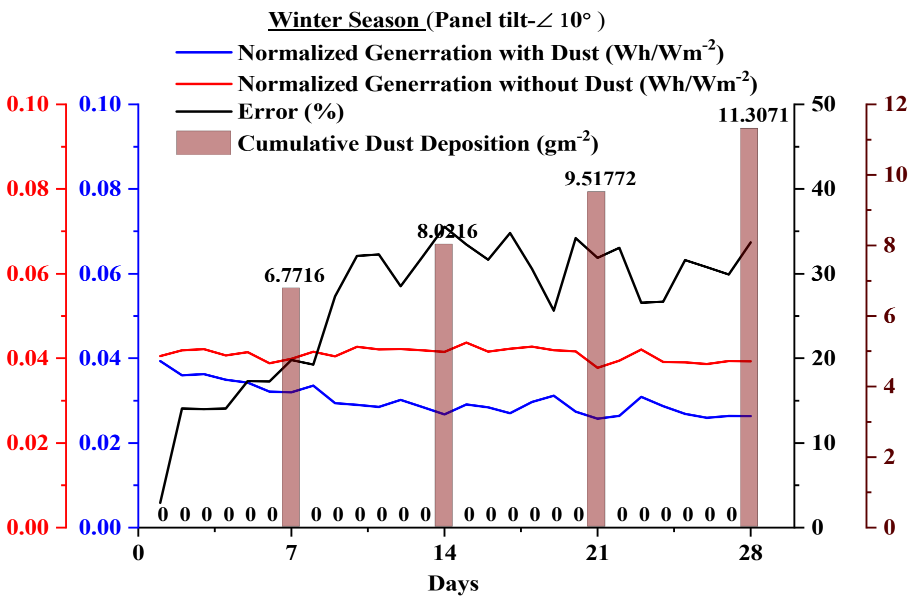

Fig. 5.18 (b) Normalized power generation with and without dust and % of error at ∠10° tilt

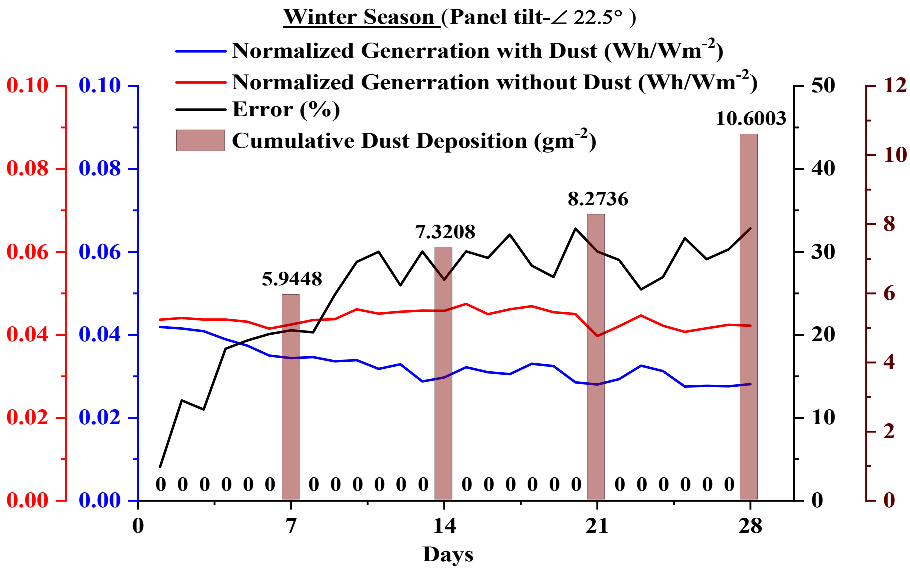

Fig. 5.18 (c) Normalized power generation with and without dust and % of error at ∠22.5° tilt

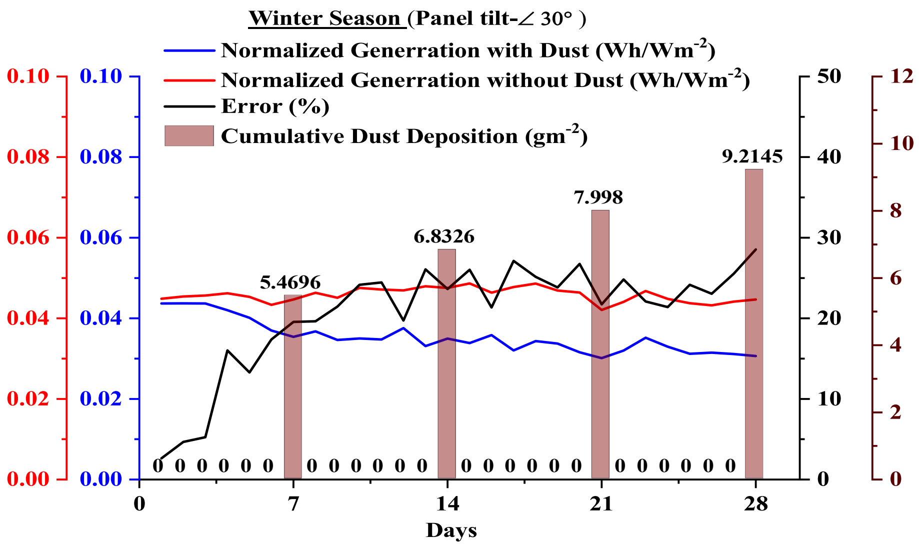

Fig. 5.18 (d) Normalized power generation with and without dust and % of error at ∠30° tilt

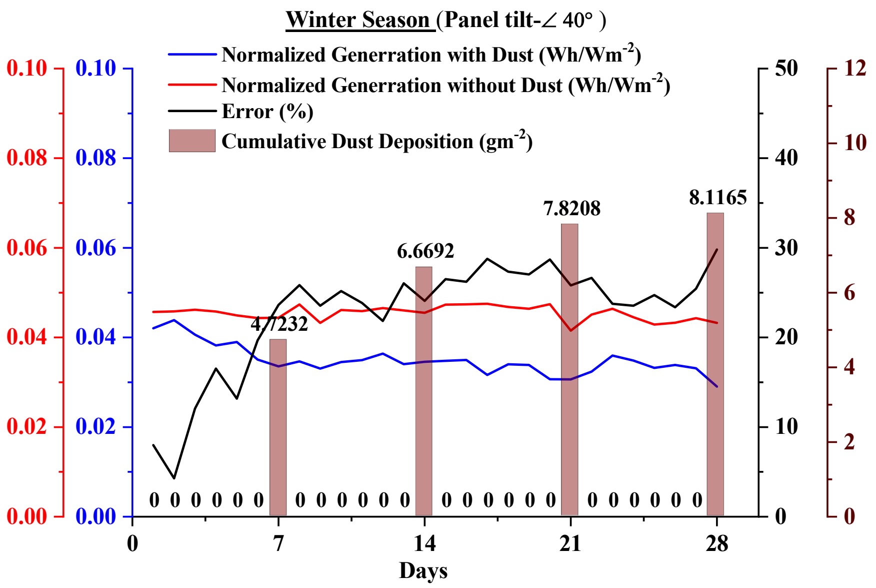

Fig. 5.18 (e) Normalized power generation with and without dust and % of error at ∠40° tilt

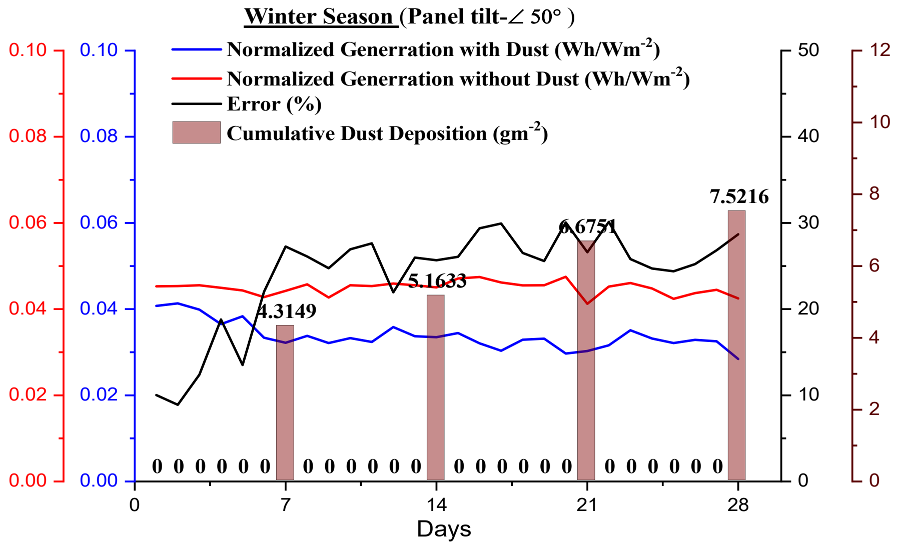

Fig. 5.18 (f) Normalized power generation with and without dust and % of error at ∠50° tilt

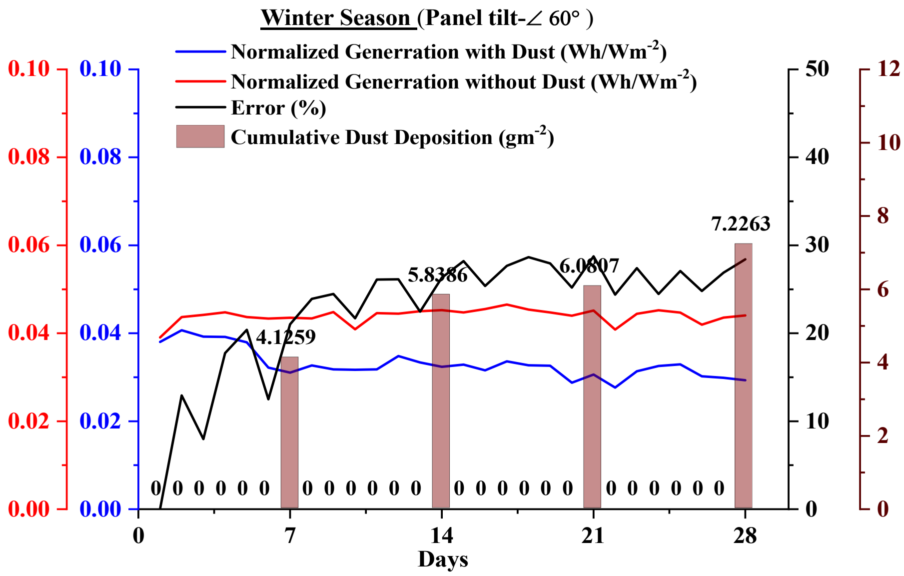

Fig. 5.18 (g) Normalized power generation with and without dust and % of error at ∠60° tilt

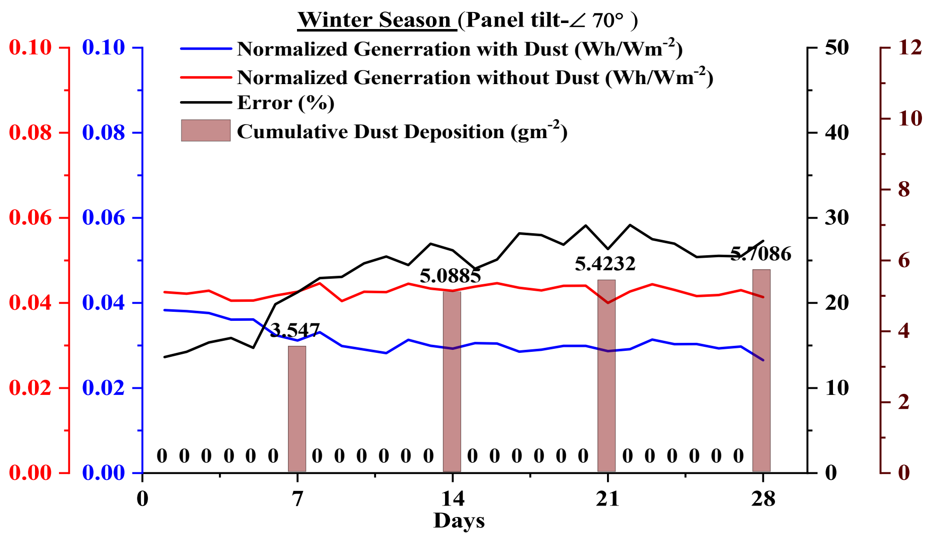

Fig. 5.18 (h) Normalized power generation with and without dust and % of error at ∠70° tilt

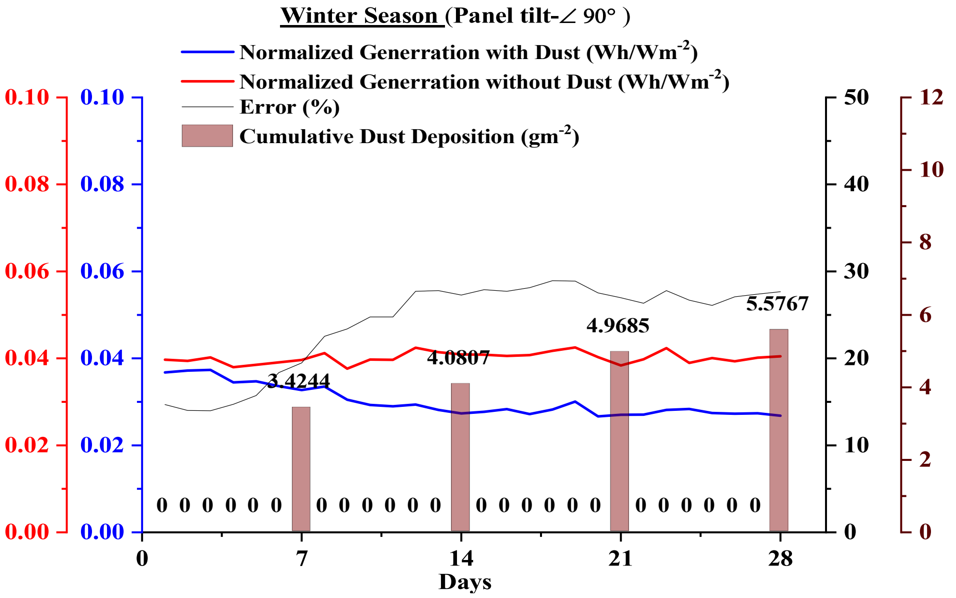

Fig. 5.18 (i) Normalized power generation with and without dust and % of error at ∠80° tilt

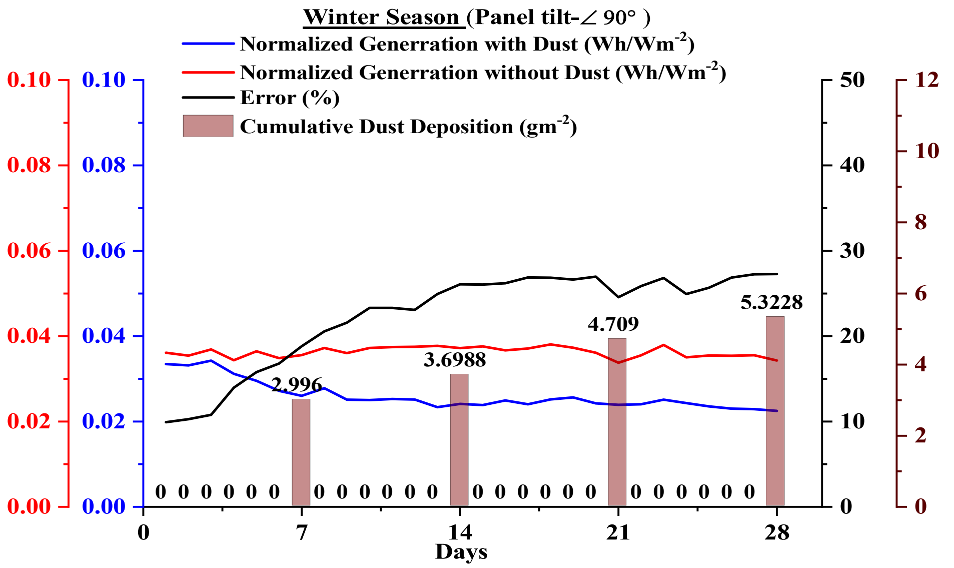

Fig. 5.18 (j) Normalized power generation with and without dust and % of error at ∠90° tilt

5.7 Seasonal Variation of PV Panel Efficiency Due to Dust Accumulation

Dust and dirt accumulating on the surface of solar panels can reduce the amount of radiation reaching the photovoltaic (PV) cells, reducing the overall efficiency of the solar panels. In Fig. 5.19, the efficiency variation throughout the summer season demonstrates a clear decrease over time, indicating the impact of dust accumulation on the declining efficiency. In summer, the maximum power generation of solar PV panel occurs with a tilt angle of 10°. Additionally, power generation is generally higher compared to other seasons due to higher solar radiation in summer. However, generation is slightly suppressed during this season due to higher panel temperatures compared to other seasons.

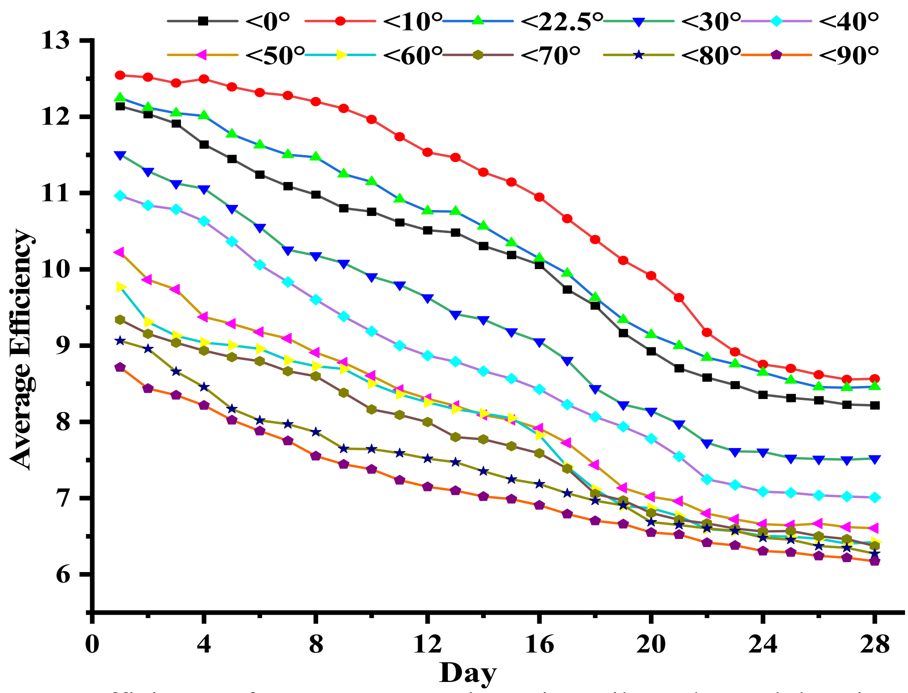

Fig. 5.19 Average efficiency of summer season in various tilt angles and durations of solar PV panels

The graph in Fig. 5.20 demonstrates the fluctuating average efficiency during the monsoon season, indicating daily changes corresponding to variations in input radiation. The presence of rainwater during this season cleans the module, leading to increased efficiency.

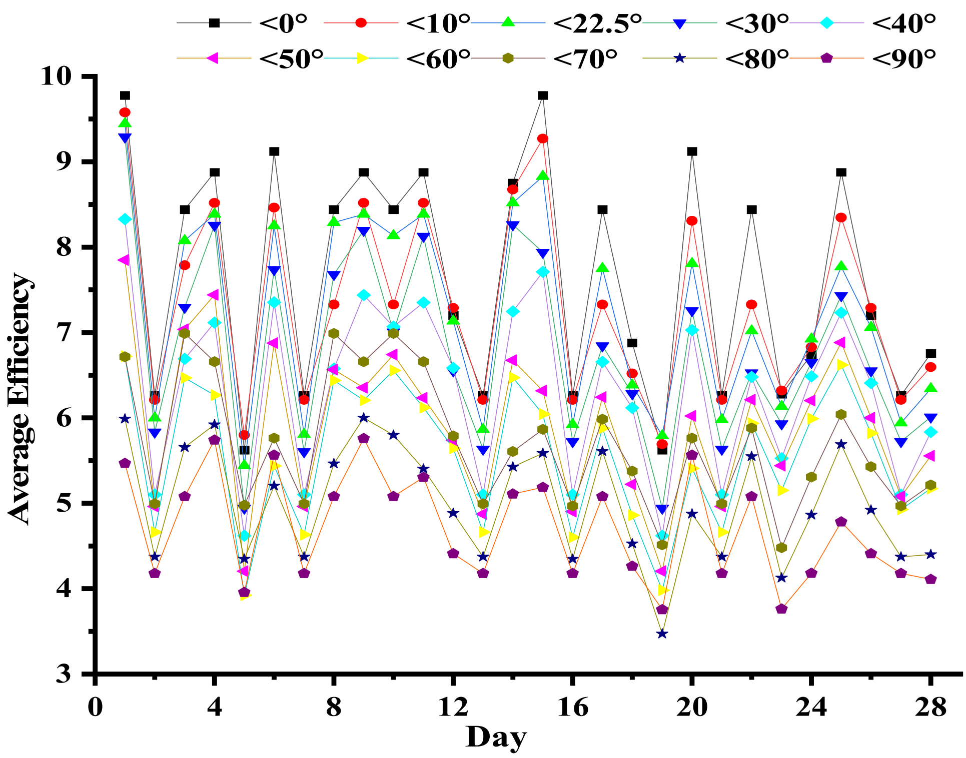

Fig. 5.20 Average efficiency of monsoon season in various tilt angles and durations of solar PV panels

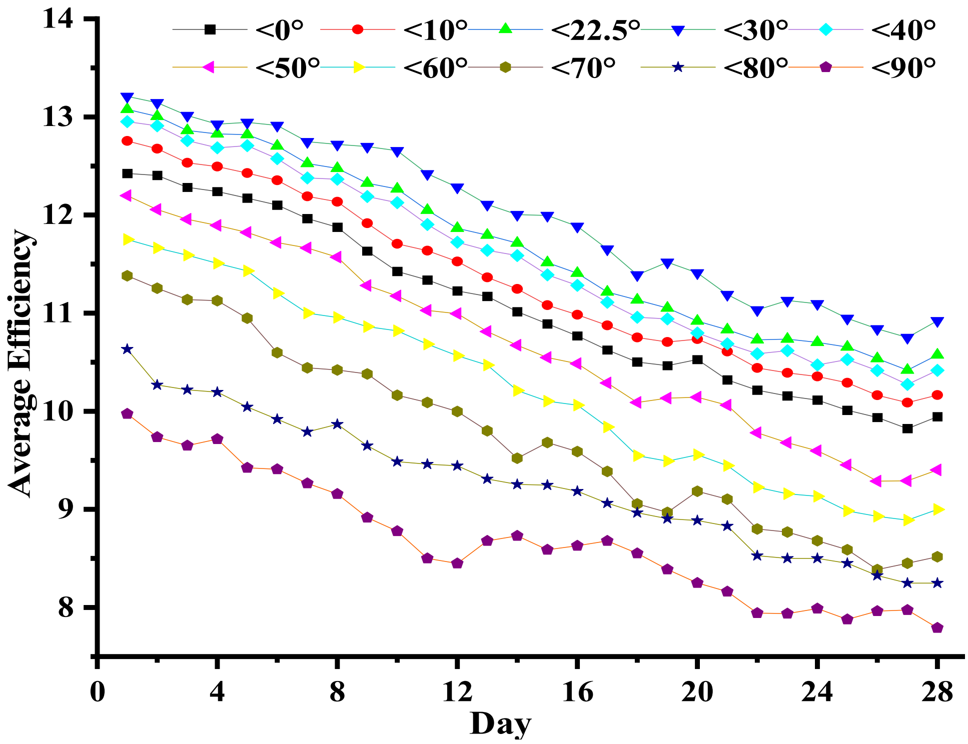

Fig. 5.21 Average efficiency of winter season in various tilt angles and durations of solar PV panels

Fig. 5.21 illustrates the average efficiency during the winter season, where the maximum power is obtained with a panel tilt angle of 30°. Although relatively lower radiation levels fall on the solar panel during this period the efficiency is enhanced by the lower ambient temperature, resulting in decreased solar PV panel temperatures. Consequently, the panels perform more efficiently, despite higher dust accumulation compared to other seasons. Therefore, the decrease in efficiency is slightly less compared to summer.

5.7 Conclusion

Dust accumulation stands out as a significant environmental factor for reaching solar power plant design. The dust accumulation strongly influences the generation of solar PV panels, and over time, it can significantly compromise the health of these panels, potentially leading to damage. Hence, this chapter investigates and explaining the power generation losses attributable to dust accumulation. Herein, the rates of dust accumulation across various tilt angles and at different seasons are explored. The analysis of dust accumulation during the summer season reveals a primarily increasing rate, followed by a slight decrease. During the monsoon season, dust accumulation on solar panels was erratic over time due to intermittent cleansing of the panel surface by rainfall. In Winter, dust accumulation was slightly higher compared to other seasons, yet during this period, lower ambient temperatures and radiation levels helped compensate for the generation loss. The energy production under constant radiation and temperature, influenced by dust accumulation, also demonstrates that during periods of low radiation levels the loss in generation increases compared to periods of high radiation levels. Here, energy generation was normalized with radiation levels, comparing generation with and without dust accumulation, and observed the percentage of error relative to cumulative dust accumulation (CDA). The results indicate that the percentage of error increases over time across all tilt angles and weather conditions. This suggests that dust accumulation significantly affects the power generation of solar panels. The efficiency of the solar panel decreased over time at various tilt angles during both the summer and winter seasons due to dust accumulation. Notably, during the summer, solar PV panel at the 10° tilt angle and while in the winter season; solar PV at the 30° tilt angle panel achieved the highest efficiencies. However, during the monsoon season, the efficiency of the solar panel fluctuated in response to varying intensities of rainfall. Finally, in this chapter, it was concluded that the pattern of dust accumulation throughout the year significantly affects energy generation and leads to efficiency reduction in solar PV installed at various tilt angles.

Chapter 6

To Study the Operational Performance of a Solar Photovoltaic Power Plant in Kolkata (Latitude 22.5°) under Routine Maintenance for Dust Cleaning and Cost Calculation

6.1 Introduction

Solar photovoltaic energy systems have emerged as highly preferable renewable energy sources due to their increased efficiency and the steady decline in both installation and maintenance expenses. In India the top 10 states and West Bengal in terms of solar installed capacity collectively represent 92.66% of the total installed capacity, as depicted in table 6.1, based on data as of March 31, 2023 (MNRE, 2023). States like Rajasthan, Gujarat, and Karnataka have historically been at the forefront of solar energy adoption in India.

Table 6.1 State-wise installed capacity over the last five years for leading states and West Bengal

State/UT	Cumulative Solar Capacity year wise (MW)				
	2018-19*	2019-20*	2020-21*	2021-22*	2022-23*
West Bengal	88.50	127.24	162.65	166.00	179.97
Karnataka	6120.76	7306.18	7383.88	7590.81	8241.40
Rajasthan	3364.03	5275.27	5925.60	12564.87	17055.70
Tamil Nadu	2618.71	3961.56	4527.47	5067.18	6736.43
Gujarat	2478.32	2986.77	4469.87	7180.03	9254.56
Andhra Pradesh	3173.87	3698.32	4291.34	4386.76	4534.19
Telangana	3600.38	3629.10	3961.54	4520.48	4666.03
Madhya Pradesh	1890.93	2309.29	2544.71	2717.95	2802.14
Maharashtra	1648.46	1835.62	2323.79	2631.02	4722.90
Uttar Pradesh	1047.43	1208.52	1836.27	2244.43	2515.22
Punjab	918.73	961.71	982.30	1100.07	1167.26

*As on 31-03-24 Source- https://mnre.gov.in/year-wise-achievement/

However, compared to some other states in India, West Bengal's installed capacity might not be as high due to factors such as land availability, geographical constraints, and industrial priorities. Recently, West Bengal has been gradually increasing its attention to solar energy. The continuous growth of PV systems necessitates proper periodic efficient maintenance to ensure their optimal plant operation. Post-installation, several key challenges arise, including shading and the accumulation of dust and other debris, resulting in a notable reduction in the energy yield from these systems. Therefore, optimal output obtained from a solar photovoltaic power plant depends on various factors, and one of these factors is the regular cleaning of solar panels. Numerous studies have demonstrated the crucial role of periodically removing dust accumulation from PV panels in enhancing the efficiency of power generation from PV modules (Khalid et al., 2023 and

Olorunfemi et al., 2022). Currently, various methods are utilized for cleaning PV panels, encompassing natural cleaning, manual intervention, mechanical techniques, self-cleaning coatings, and intelligent cleaning approaches. Natural cleaning refers to environmental factors such as rainfall and wind to cleanse PV panels, its effectiveness heavily depends upon weather conditions (Al Garni, 2022). Rainfall is known as a natural cleanser for PV panels, efficiently washing down surface dust and consequently uplifting their performance. Nevertheless, inadequate rainfall not only proves ineffective in cleansing the panels but also leads to an accumulation of dust particles and compromising panel efficacy (Jaszczur et al., 2020). High wind velocities also act as an effective natural cleansing method, substantially increasing the resuspension rate and thereby eliminating the accumulated dust from the panel surface (Dagher and Kandil, 2023). Low wind speeds expedite the transfer and diffusion of dust particles in the air, leading to their re-deposition onto the panels. This ongoing cycle of resuspension and re-deposition ultimately leads to the degradation of panel performance (Said et al., 2018). The manual cleaning approach entails utilizing cleaning tools such as nylon, cloth, and silicone rubber foam brushes to remove accumulated dust and dirt from PV panels (Al Shehri et al., 2017). Nevertheless, manual cleaning requires skilled labour and significant water consumption (Alshareef, 2023). Mechanical methods predominantly employ water washing, blowing, vibration, and ultrasonic technology. While water washing demands water, pumps, controllers, and associated equipment, thus consuming significant energy. Additionally, the utilization of high-pressure water pumps consumes a portion of the generated PV power, while the wet panel surface may also attract more dust particles, thereby negatively impacting panel efficiency. Moreover, using low-temperature water for cleaning when the panel surface temperature is elevated can induce thermal shock, posing potential damage to the panels (Al Garni, 2022). Utilizing forced airflow for cleaning is another prevalent mechanical method. This approach involves the utilization of a compressed air apparatus consisting of a compressor, an airflow regulation valve, an air storage tank, and a nozzle and it efficiently eliminates the accumulation of dust on the surfaces of the PV modules (Assi et al., 2012). However, it's crucial to acknowledge that operating the compressor requires a fraction of the electricity generated by the PV panels, which could potentially impact the efficiency of the PV modules. Vibratory cleaning techniques utilize piezoelectric technology to generate vibrations that efficiently cleanse the surface of solar modules. These methods involve mechanical vibrators affixed to the panel, which generate harmonic excitation forces to reduce adhesion between dust particles and the panel surface (Eisa et al, 2023). Ultrasonic cleaning technology relies on ultrasonic cavitation in liquids to remove contaminants, such as dirt and grease, that are submerged in aqueous environments (Zhao et al., 2021). Vibration and ultrasonic dust removal necessitate specialized power sources and also incur significant energy consumption. Self-cleaning coatings, super hydrophobic coatings and Super hydrophilic coating (Quan et al., 2022), along with electrodynamic screens, all of which operate autonomously, efficiently eliminating dust particles (He et al., 2023). Moreover, superhydrophobic coatings exhibit a restricted lifespan and are vulnerable to degradation when exposed to elevated levels of UV radiation (Lisco et al.,2020). The self-cleaning action of super hydrophilic surfaces during photocatalysis is governed by the band gap energy of materials. However, a significant drawback of photocatalysis is its limited effectiveness in dark or shaded areas. (Syafiq et al., 2018). Additionally, hydrophilic surfaces are inclined to accumulate more dust as the coating deteriorates over time from prolonged exposure to UV light. In arid conditions, this approach may become insufficient, requiring manual cleaning (Deb et al., 2018). The electrodynamic screen (EDS) primarily serves the purpose of automatic dust removal through electrostatic force. Nonetheless, its efficacy diminishes when dealing with wet or minuscule dust particles (Sayyah et al., 2016). Moreover, the electric field produced by EDS requires a high-voltage power supply, resulting in a 15% reduction in power generation efficiency (Deb et al., 2018). Advancements in artificial intelligence have led some researchers to integrate traditional mechanical cleaning methods with emerging intelligent algorithms, resulting in the development of smart cleaning robots and drones (Nguyen et al, 2021). However, it is crucial to recognize that the initial and ongoing expenses linked with implementing automated cleaning technologies are comparatively high, requiring sophisticated mechanical and control designs (Quan et al., 2022).

Previous chapter revealed that without regular cleaning soiling of solar photovoltaic panels drastically reduces power generation and adversely affecting the overall economics of solar power plants. Water cleaning of PV panels stands out as one of the most commonly adopted methods for solar PV plants in India. However, it's important to note that a considerable number of PV plants require substantial amounts of fresh water for cleaning purposes. However, solar power plants consume significantly less water compared to thermal power plants. (Jin et al. 2019, Jia et al.2021). In light of this, a state-wise analysis of water scenario of India, has been conducted. The primary focus of the present chapter lies in considering more suitable techniques applicable specifically for Kolkata, West Bengal. It also encompasses an assessment of the cost implications for power plant operations based on dust removal techniques and cleaning duration. Furthermore, it examines the difficulties of technique implementation, cost of cleaning and determines the optimal angle for both new and existing power plant installations.

6.2 State-wise Water Scenario of India

The primary sources of fresh water in India consist of river and groundwater reserve. However, groundwater levels are also influenced in part by rainfall. Groundwater contributes approximately 62% to irrigation, 50% to urban water supply, and 85% to rural water supply in India (CGWB, 2023). Based on water availability and usage, Indian states are categorized into different zones. Baseline water stress is determined by considering water availability and usage patterns. This ratio categorizes Indian states into various zones, reflecting the pressure on water resources. This metric serves as a valuable tool for evaluating water management strategies and prioritizing conservation efforts in different areas. Fig. 6.1 illustrates the baseline water stress levels across various regions of India (IWT 4.0, 2023).

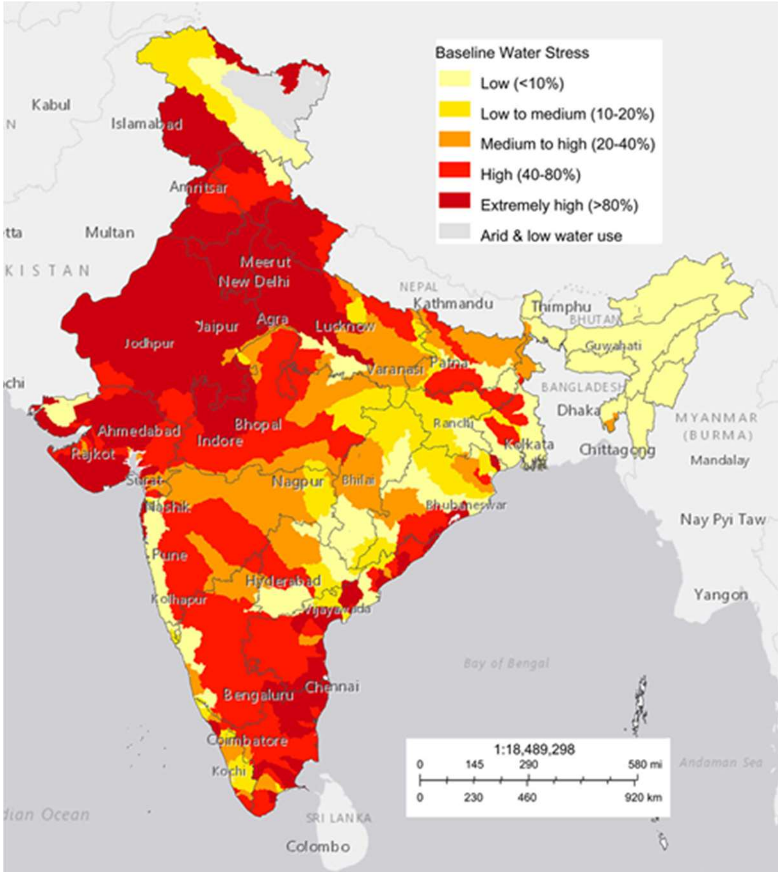

Fig. 6.1 Baseline water stress level of different part of India

Based on the installed solar PV capacity data, there has been a significant increase over the last five years, rising from 29,097.18 MW to 66,780.34 MW in India. Consequently, the usage of water for cleaning purposes has also escalated (BRIDGE TO INDIA, 2018). Fig. 6.2 presents a state-wise overview of the above-mentioned parameters, including Solar PV installations, water consumption, and water stress levels across India.

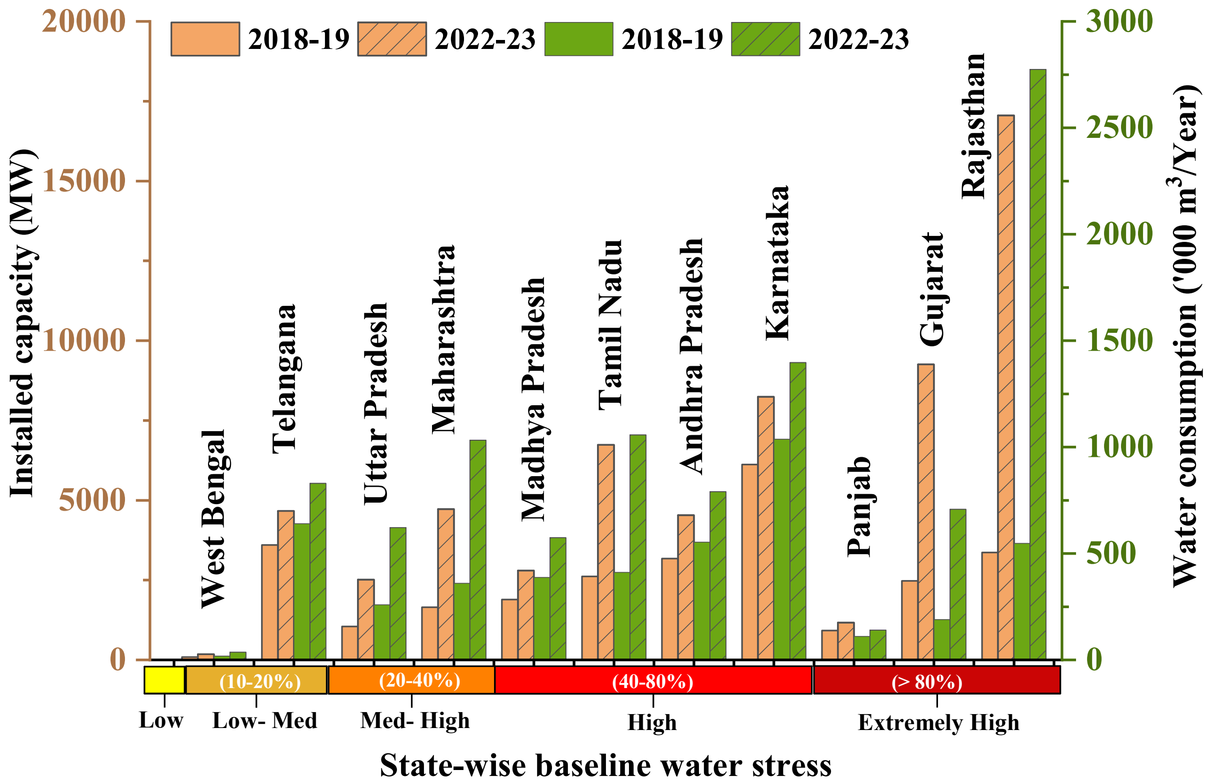

Fig. 6.2 Solar PV installation across, water consumption, and water stress level different states in India

The graph illustrates that 41.15% of the total installed capacity is situated in dry zones, primarily in the western part of India, classified as extremely high water stress zones. Additionally, 36.29% of the installed capacity in the central and southern regions of India falls within high-water stress zones. Another 10.84% of the installed capacity in India is located in areas categorized as medium to high water stress, while the remaining areas are classified as low to medium water stress zones. In view of the current water stress levels across various regions of India, policymakers and project developers must arrange the adoption of suitable techniques for photovoltaic panel cleaning. In the case of West Bengal, it falls within the low to medium water stress level zone. Therefore, the use of water for cleaning purposes in photovoltaic plants does not impose additional strain on water resources in the area or does not create additional economic burdens in the cost analysis of solar PV plants. Furthermore, data from meteorological rainfall records spanning from 1951 to 2022 (as shown in Fig. 6.3) indicate that actual rainfall has been higher compared to the area-weighted normal rainfall over the past four years. Consequently, the groundwater levels have also increased after post monsoon in West Bengal, as well as in some other parts of India (WRIS, 2023).

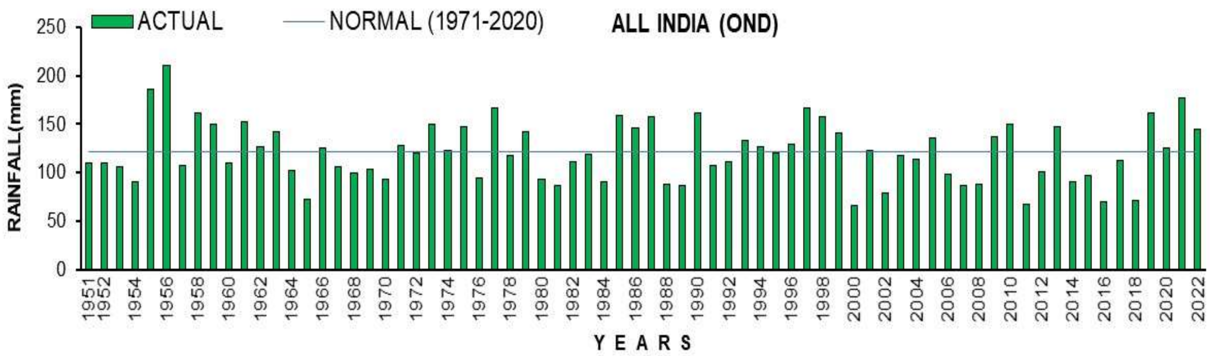

Fig. 6.3 Area weighted rainfall over the country as a whole (1951 - 2022)

Based on the described circumstances, a water-based solar photovoltaic cleaning process is being implemented that consume less water and is more efficient.

6.3 Implemented Dust Cleaning Procedure

The efficiency and power generation of photovoltaic (PV) panels play a crucial role in the operation of solar PV plants. Insufficient cleaning and inadequate exposure to sunlight can lead to significant decreases in the efficiency of PV systems. Therefore, employing specific cleaning methods is essential to maintain optimal performance and restore efficiency levels within the PV plant's operation. One commonly utilized method for effectively cleaning solar panels is the water-based cleaning process. Various literature highlights the use of water for solar PV panel cleaning, such as employing sprinkler systems that spray water across panels in an automated mechanical process (Myyas et al., 2022). Some approaches involve directing water through pipelines to spray over the panel surfaces (Sugiartha et al., 2020), while others may use wet clothes for cleaning (Jaiganesh et al., 2022). However, it's noted that in all cases, there are instances where panels aren't thoroughly cleaned, excessive water is utilized during the cleaning process and in some cases additional power is required for cleaning operation.

In a separate experimental study, distinct cleaning processes were carried out using only water and wet cloth individually, and the results are depicted in Fig. 6.4(a) and (b). These figures clearly demonstrate that after the water wash, a fine layer of dust remained on the solar panels and during the wet cloth washing, dirt spots were noticeable across all panels. The presence of a light slick layer is ascribed to atmospheric fine dust particles and pollutants from vehicles due to the experimental area's proximity to a high-traffic roadside (Dong et al., 2009). Further details regarding the experimental procedure are outlined in Chapter 3.

Fig. 6.4(a) Fine layer of dust particles

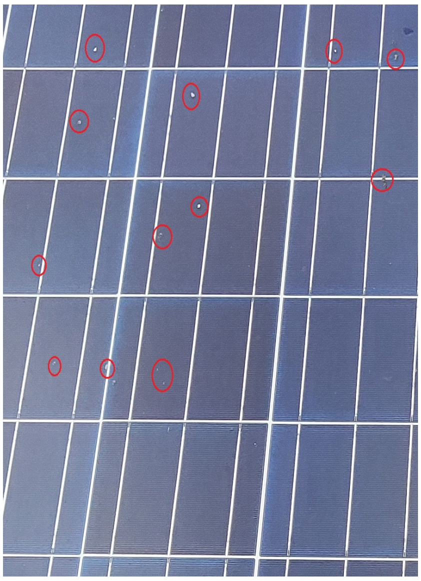

Fig. 6.4(b) Dirt spots across the panel

Fig. 6.4(c) Clean PV panel

Some literature describes a method wherein a combination of pressurized air and water is employed for cleaning PV Panels. This mixture is directed into a nozzle, where it is carefully proportioned before being sprayed onto the dusty solar panel. A specially designed nozzle is utilized to produce a flat-fan spray pattern, ensuring effective cleaning. Both air and water are maintained at a pressure of 3 bars to achieve the desired spray for cleaning the solar panel (Najeeb et al., 2018).

In our proposed cleaning method, there are no moving parts, no requirement for battery replacement, no need for coatings or guard rails, less water consumption, and utilization of a manually operated, pressurized water system with a wiper cleaning mechanism deployment in solar power plants for dust cleaning. In Fig. 6.5 (a) and (b), the initial stage depicts manual cleaning using a pressure water sprayer followed by cleaning with a glass wiper. The sprayer maintains a pressure of 0.3-0.4 MPa and is equipped with 8 nozzles for effective cleaning. Fig. 6.4 (c) illustrates the PV panel post-completion of the cleaning process.

Fig. 6.5 (a) Manual cleaning by water sprayer

Fig. 6.5 (b) Manual cleaning by glass wiper

6.4 Water Consumption Estimate for Cleaning a Single 110 W_p Solar Panel

To measure water usage for cleaning purposes, three 67×100 cm solar panels were utilized. The main focus of this experiment was to assess varying water consumption across different cleaning frequencies. Detailed measurement procedures are outlined in Chapter 3. The resulting data on water consumption are presented in Table 6.2. This water consumption data is also utilized in the analysis of cleaning costs for solar photovoltaic systems.

Table 6.2 Water consumption for Solar PV cleaning for different cleaning interval

Duration	Per Day	1 Week	2 Week	3 Week	4 Week	8 Week	12 Week
Panel-1	180 ml	240 ml	240 ml	390 ml	400 ml	510 ml	730 ml
Panel-2	165 ml	210 ml	210 ml	360 ml	420 ml	540 ml	760 ml
Panel-3	175 ml	230 ml	240 ml	380 ml	430 ml	550 ml	750 ml
Average	173 ml	227 ml	230 ml	377 ml	417 ml	534 ml	747 ml

6.5 Analysis of Water Utilized for Cleaning Solar PV panels

Several studies indicate that water-based cleaning for solar PV panels is one of the most reliable cleaning methods in the solar PV industry (First Solar, 2017). Additionally, the quality of water has a notable impact on solar power generation (Boeing et al., 2022). Brackish water, seawater, and wastewater are potential options for washing modules, but they necessitate pre-treatment, significantly elevating costs (Saidan et al., 2016). Assessing the costs and benefits of cleaning versus leaving PV panels dirty, thereby incurring energy loss, involves tentative soil accumulation. Many large-scale PV solar power plants are situated worldwide, including India, with a preference for arid or semi-arid regions with dusty conditions due to high solar irradiance. However, these areas often lack access to high-quality water resources. Here, experiment was conducted to study varying water qualities commonly used on photovoltaic systems and further investigate whether the use of lower-quality water may potentially lead to mineral deposition or scaling on panel surfaces. Six different types of water have been used for examination purposes. The water samples were gathered from various sources of water availability; RO water from Reverse Osmosis (RO) treatment plant, groundwater from a deep tub well, tap water from the local municipality (Kolkata Municipality Corporation) water supply, treated water from the municipality treated water supply, purified water from commercial water filter machine (Eureka Forbes AGCCP model, https://www.eurekaforbes.com/business/water-purifiers/agccp), and rainwater collected during rainfall. Every water sample was accurately prepared for the measurement of Total Dissolved Solids (TDS), specific gravity, pH, electrical conductivity, and the weight of residual substances. The entire measurement process is detailed in Chapter 3. The results of the various measurement parameters are displayed in the table 6.3.

Table 6.3 Different measurement parameters of water samples

Water sample	**Mass of sample* (gm)**	**Density of sample (gm/ml)**	**TDS (ppm)**	**Conductivity (us/cm)**	**pH**	**Mass of residual substance (gm)**
RO Water	50.3810	1.00362	69	138	6.75	0.0011
Ground water	50.5618	1.01124	2387	4787	7.19	0.1387
Tap Water	50.2791	1.00858	273	468	7.48	0.0116
Treated Water	49.9294	1.00559	171	203	7.36	0.0188
Purified Water#	50.0785	1.00257	94	148	7.39	0.0131
Rain Water	49.9727	0.99945	7	22	6.92	0.0008

* Experiment used all sample volume 50 ml., # Without RO

The presence of high levels of impurities in the water employed for cleaning solar panels presents a potential risk of damaging the solar PV system. Hard water containing high levels of minerals like calcium and magnesium can leave behind deposits on the surface of solar panels after evaporation of water (Ahmed et al. 2023). These mineral deposits can reduce the transparency of the panels and decrease their efficiency over time. Water with a high salt content is used for cleaning, it can cause corrosion of the panel's surface or frame over time, leading to structural damage and reduced lifespan (Dewi et al.,2021). The water used for cleaning contains contaminants or residues from previous cleanings, it can leave behind streaks or spots on the surface of the panels, affecting their performance.

Based on the findings, rainwater and reverse osmosis (RO) water are deemed more suitable for cleaning solar PV panels. However, rainwater availability is seasonal, so cleaning purposes necessitate large storage reserves, though it proves costly for cleaning purposes. Conversely, RO water is comparatively expensive due to the reverse osmosis treatment process, making it less economical for smaller installations like rooftop solar PV systems but it's cost-effective for large solar PV power plants. Consequently, in our experiment, regular tap water was chosen for solar panel cleaning purposes in our experiment due to its easy availability in West Bengal.

6.6 Yearly Weighted Normalized Generation (YWNG) Calculation

The power generation of solar PV panels varies across seasons due to differences in radiation levels received by the panels. Consequently, to ensure consistent contribution throughout the year, it's necessary to apply a day-wise normalization factor to account for seasonal variations. The weighted average is a method of computation that considers the differing degrees of significance of numbers within a dataset across all seasons. This technique involves multiplying each number in the dataset by a predetermined weight before computing the final result. Compared to a simple average where all numbers carry equal weight, a weighted average has the potential to yield more precise outcomes. In this context, equation 6.1 is utilized to calculate the day-wise normalized generation. To ensure maximum power output throughout the year, it's crucial to maintain proper cleaning intervals. As the cleaning frequency of solar PV plants varies, it affects the calculation of the average normalized generation across different cleaning intervals, equation 6.2 is applied for this calculation. Equation 6.3 computed the weighted normalization generation value for each specific season. This equation further enabled determination of the weighted values of power generation during summer, monsoon, and winter seasons. Subsequently, applying equation 6.4 allows us to calculate the yearly weighted power generation value, and the value of different cleaning frequencies illustrated in Table 6.4.

$$\text{Normalized generation } (\mathrm{N_i}) = \frac{\text{Total Generation on } \mathrm{i^{th}} \text{ day}}{\text{Mean Radiation on } \mathrm{i^{th}} \text{ day}} \tag{6.1}$$

$$\text{Average Normalized generation for 'n' days cleaning interval } (N_{\mathrm{n}}) = \frac{\sum_{\mathrm{n}} \mathrm{N_i}}{\mathrm{n}} \tag{6.2}$$

$$\text{Weight of } \mathrm{N_i} \text{ for a particular season } (\mathrm{w_{season}}) = \frac{\text{Average } \mathrm{N_i} \text{ of season}}{\text{Total average } \mathrm{N_i} \text{ of all season}} \tag{6.3}$$

$$\text{Yearly weighted Normalized generation for 'n' cleaning interval} = (\mathrm{N_n^{su}} \times \mathrm{w_{su}}) + (\mathrm{N_n^{m}} \times \mathrm{w_m}) + (\mathrm{N_n^{w}} \times \mathrm{w_w}) \tag{6.4}$$

Where, $\mathrm{w_{su}}$ is weighted of summer season, $\mathrm{w_m}$ is weighted of monsoon season, $\mathrm{w_w}$ is weighted of the winter season, n is the cleaning interval time.

Table. 6.4 Yearly Weighted Normalized Generation value in different cleaning interval

∠0°	∠10°	∠22.5°	∠30°	∠40°	∠50°	∠60°	∠70°	∠80°	∠90°
Cleaning frequency- 7 Days									
0.0334	0.0363	0.0365	0.0358	0.0323	0.0266	0.0243	0.0205	0.0163	0.0130
Cleaning frequency- 14 Days									
0.0322	0.0352	0.0356	0.0348	0.0305	0.0249	0.0224	0.0187	0.0151	0.0120
Cleaning frequency- 21 Days									
0.0300	0.0325	0.0316	0.0321	0.0291	0.0242	0.0216	0.0178	0.0148	0.0111
Cleaning frequency- 28 Days									
0.0291	0.0316	0.0308	0.0317	0.0287	0.0239	0.0213	0.0179	0.0142	0.0108

6.7 Annual Energy Production of Solar Panels Accounting the Impact of Dust

Determination of the yearly total energy generation of solar panels was obtained from equation 6.5 by applying the yearly weighted normalized generation value.

$$\text{Annual Energy generation} = \frac{\text{Yearly Weighted Normalized Generation} \times 375 \times 365}{4.5} \tag{6.5}$$

In above equation annual average solar radiation of 375 W/m^2 per day (experimental) was considered and ten identical solar panels of 4.5 W_p rating ware utilized.

Table. 6.5 Total Annual Energy generation * in different cleaning interval

∠0°	∠10°	∠22.5°	∠30°	∠40°	∠50°	∠60°	∠70°	∠80°	∠90°
Cleaning frequency- 7 Days									
1016.2	1102.8	1111.0	1088.0	981.7	808.5	740.3	623.9	495.8	396.1
Cleaning frequency- 14 Days									
980.6	1071.6	1082.6	1058.0	928.1	757.1	682.0	568.5	459.6	364.6
Cleaning frequency- 21 Days									
911.7	988.1	961.2	975.6	886.2	737.3	657.1	541.4	449.2	337.7
Cleaning frequency- 28 Days									
885.7	961.4	937.3	964.7	872.8	726.9	648.8	543.8	431.1	327.1

* Unit - kWh/kW$_p$/year

6.8 Annual Energy Loss of Solar Panels Due to Dust Deposition

For the annual energy loss calculation, initially the day one yearly weighted sum of power generation values for each season was computed, taking into account their respective weights. This sum of day one represents the actual power generation of clean solar panels in typical environmental conditions over the course of the year. The Yearly Weighted Normalized Generation loss is obtained by subtracting the yearly weighted sum of power generation values from this initial value. This value is employed to calculate the annual energy loss using equation 6.6.

$$\text{Annual Energy loss} = \frac{\text{Yearly Weighted Normalized Generation loss} \times 375 \times 365}{4.5} \tag{6.6}$$

In the above equation, real time annual average solar radiation of 375 W/m² per day was applied for solar panel's rated at 4.5 W_p value for calculation. The annual energy loss corresponding to different tilt angles and cleaning interval is documented in Table 6.6.

Table. 6.6 Total Annual Energy loss * in different cleaning interval

∠0°	**∠10°**	**∠22.5°**	**∠30°**	**∠40°**	**∠50°**	**∠60°**	**∠70°**	**∠80°**	**∠90°**
Cleaning frequency- 7 Days									
51.90	80.37	80.65	75.05	56.25	47.76	43.78	43.49	39.03	37.25
Cleaning frequency- 14 Days									
87.59	111.64	109.04	105.04	109.83	99.16	102.07	98.93	75.22	68.72
Cleaning frequency- 21 Days									
156.48	195.06	230.48	187.45	151.71	118.91	126.93	125.97	85.63	95.67
Cleaning frequency- 28 Days									
182.44	221.79	254.40	198.36	165.17	129.38	135.25	123.60	103.73	106.21

* Unit - kWh/kW_p/year

6.9 Annual Revenue Loss of Solar PV Plants Due to Dust Deposition

The revenue loss of solar panels refers to the financial impact resulting from a decrease in their energy production or efficiency. To calculate the annual revenue loss, multiply the annual loss in energy production by the current electricity tariff. This provides an estimate of the financial impact of the decreased energy generation on revenue. According to the West Bengal State Electricity Distribution Company Limited (WBSEDCL), the average electricity tariff for consumers is 6.99 rupees per unit (WBSEDCL,2023). The annual revenue loss is calculated using Equation 6.7. The annual revenue loss corresponding to different tilt angles and cleaning frequencies is documented in Table 6.7.

$$\text{Annual revenue loss} = \text{Annual generation loss} \times \text{Tariff} \tag{6.7}$$

Table. 6.7 Annual revenue loss * in different cleaning interval

∠0°	∠10°	∠22.5°	∠30°	∠40°	∠50°	∠60°	∠70°	∠80°	∠90°
Cleaning frequency- 7 Days									
311.43	482.23	483.92	450.28	337.51	286.58	262.66	260.95	234.20	223.48
Cleaning frequency- 14 Days									
525.54	669.82	654.24	630.23	658.98	594.95	612.41	593.57	451.32	412.32
Cleaning frequency- 21 Days									
938.87	1170.4	1382.88	1124.7	910.24	713.44	761.58	755.81	513.78	574.04
Cleaning frequency- 28 Days									
1094.65	1330.77	1526.38	1190.2	991.02	776.30	811.50	741.61	622.40	637.25

*INR/kW_p

6.10 Cleaning Cost Analysis in Different Cleaning Intervals

Calculating the cleaning cost of a solar PV plant involves considering various factors such as labour cost, equipment cost, water cost, cleaning solutions cost, and interval of cleaning. The minimum wage per day for unskilled labourers in West Bengal is typically determined and regulated by the Labour Commissionerate, Government of West Bengal. However, wage rates can vary over time and may be subject to updates or revisions by the authorities (Labour Commissionerate, Govt. of WB,2024). According to an industrial survey, cleaning a 1 kW_p solar panel system requires approximately 30 minutes, it provides valuable insight into the labour time required for maintenance activities. This estimate can be utilized to factor in the labour cost component when calculating the overall cleaning cost of a solar PV plant. Tap water was used for cleaning the solar PV panels because of it is easy accessibility from the local municipality. Within the Kolkata Municipality Corporation area, the price for tap water used in domestic and partly commercial applications is rupees 15 per kiloliter (KMC, 2024). Additional expenses such as the cost of sprayer machines and glass wipers are also accounted for within miscellaneous costs.

$\text{Minimum wage rate for unskilled labourers in West Bengal} = 379\ \text{INR/Day}.$

$\text{Clean time for } 1\ \text{kW}_\text{p} \text{ panel } = 30 \text{ minutes}.$

Water cost in West Bengal (Tap water) $= 15$ INR/Kilo Liter.

$$\text{Water Consumption} = \frac{\text{Water requirement (L)} \times 365}{\text{Cleaning interval} \times \text{plant capacity}} \quad (6.8)$$

Table 6.2 outlines the water needed for cleaning solar panels at different cleaning frequencies. Equation 6.8 helps estimate water consumption for cleaning purposes. Table 6.8 presents an analysis of the final annual cleaning costs for a solar PV system for different cleaning intervals.

Table. 6.8 Yearly cleaning cost analysis for solar PV system

Cleaning frequency (Day)	**Labour cost INR/kW$_p$/Year**	**Water consumption L/kW$_p$/Year**	**Water cost INR/kW$_p$/Year**	**Miscell-aneous INR**	**Total cost INR**
7	1232.136	107.5707	1.613561	100	1333.749
14	616.0679	54.48929	0.817339	100	716.8852
21	410.7119	59.61667	0.89425	100	511.6062
28	308.0339	49.40536	0.74108	100	408.775

6.11 Dust Deposition Loss and Cleaning Cost Crossover of a Solar PV Plant

The cost crossover due to dust deposition loss and cleaning of a solar PV plant refers to the point beyond which the additional energy generated from cleaning the solar panels exceeds the cost of cleaning, resulting in a net financial benefit. Once the cost of cleaning is offset by the additional revenue generated from increased energy production, the solar PV plant reaches a cost crossover point where regular cleaning becomes financially beneficial. This underscores the importance of incorporating maintenance and cleaning costs into the overall financial analysis of solar PV projects. Fig. 6.6 (a) –(j) illustrates the crossover point for a specific cleaning day across various tilt angles of solar installation.

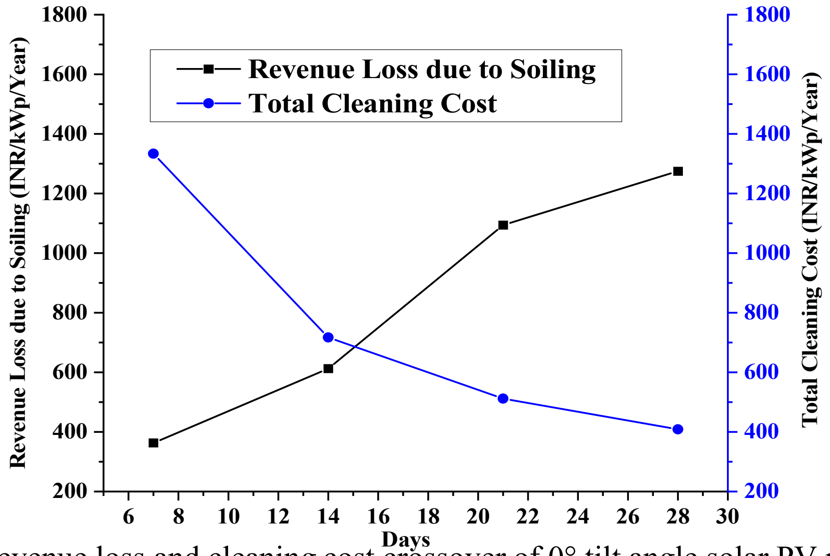

Fig. 6.6 (a) Revenue loss and cleaning cost crossover of 0° tilt angle solar PV panel

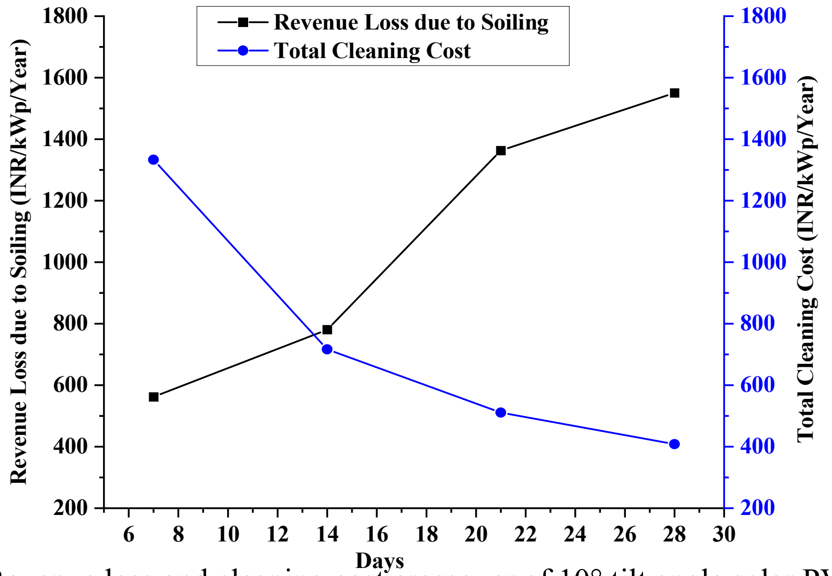

Fig. 6.6 (b) Revenue loss and cleaning cost crossover of 10° tilt angle solar PV panel

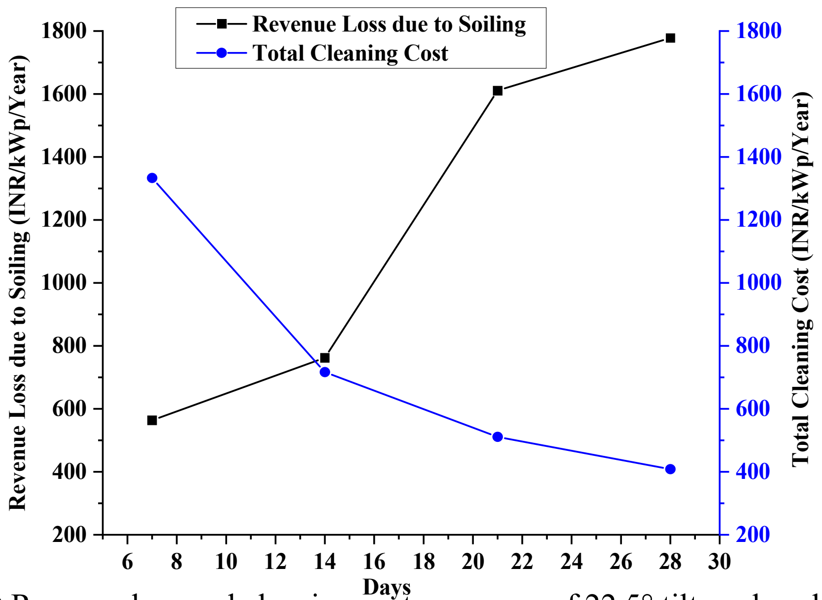

Fig. 6.6 (c) Revenue loss and cleaning cost crossover of 22.5° tilt angle solar PV panel

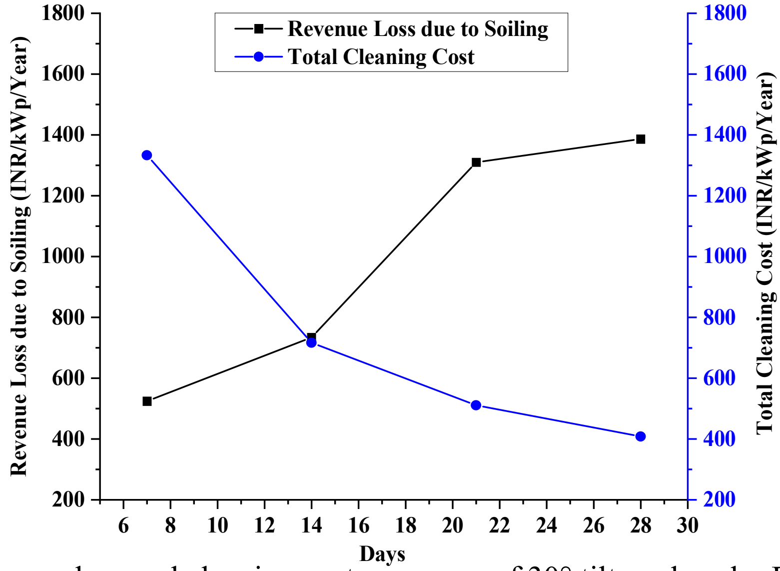

Fig. 6.6 (d) Revenue loss and cleaning cost crossover of 30° tilt angle solar PV panel

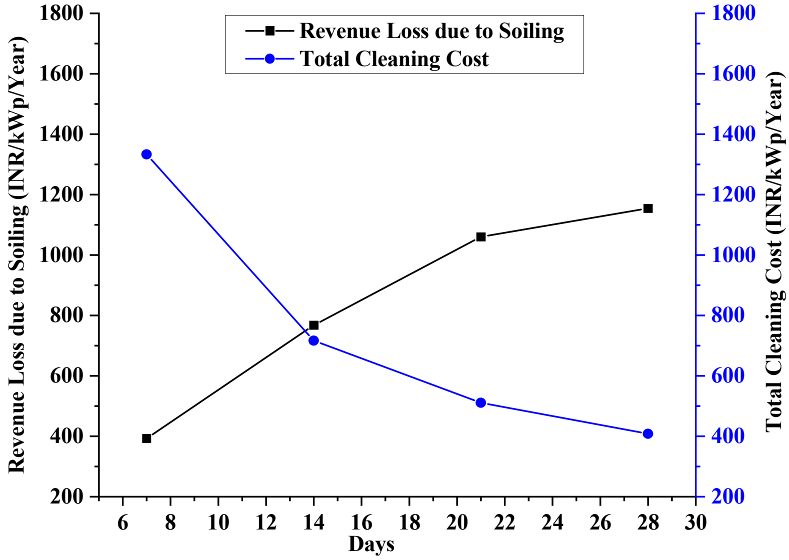

Fig. 6.6 (e) Revenue loss and cleaning cost crossover of 40° tilt angle solar PV panel

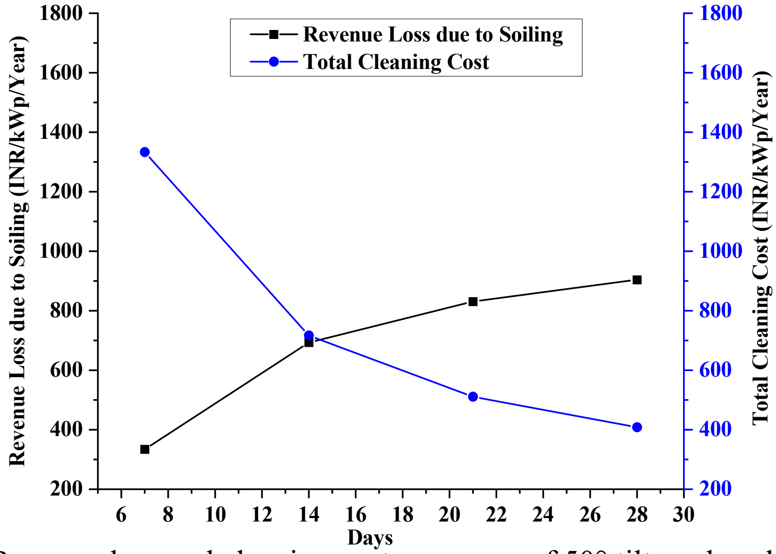

Fig. 6.6 (f) Revenue loss and cleaning cost crossover of 50° tilt angle solar PV panel

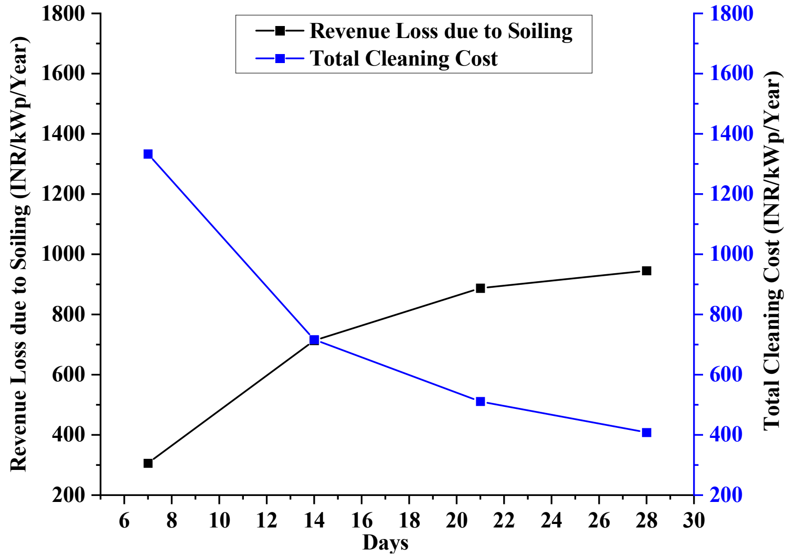

Fig. 6.6 (g) Revenue loss and cleaning cost crossover of 60° tilt angle solar PV panel

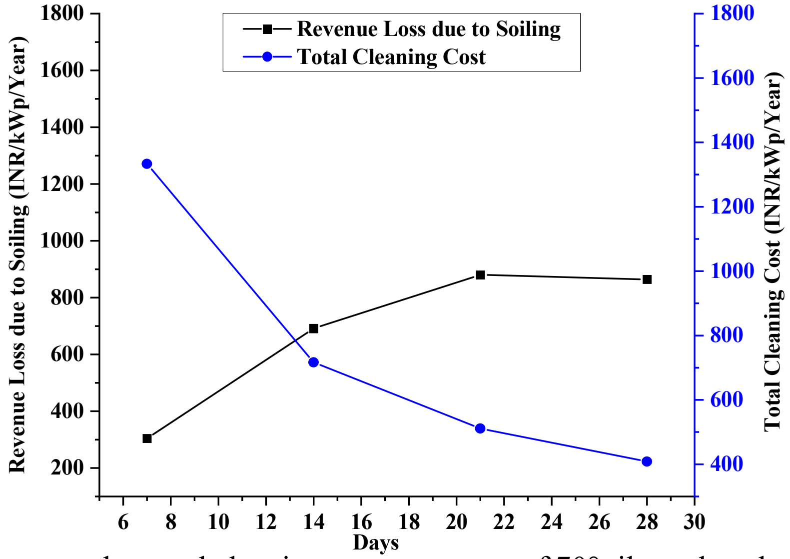

Fig. 6.6 (h) Revenue loss and cleaning cost crossover of 70° tilt angle solar PV panel

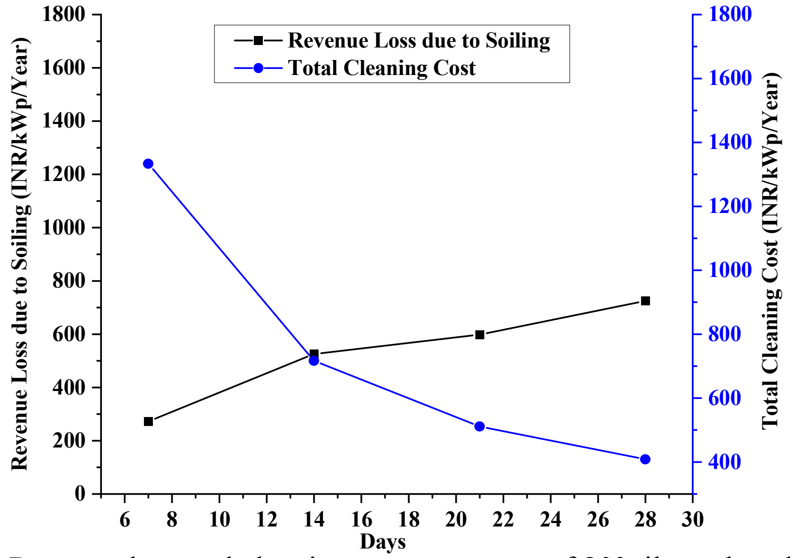

Fig. 6.6 (i) Revenue loss and cleaning cost crossover of 80° tilt angle solar PV panel

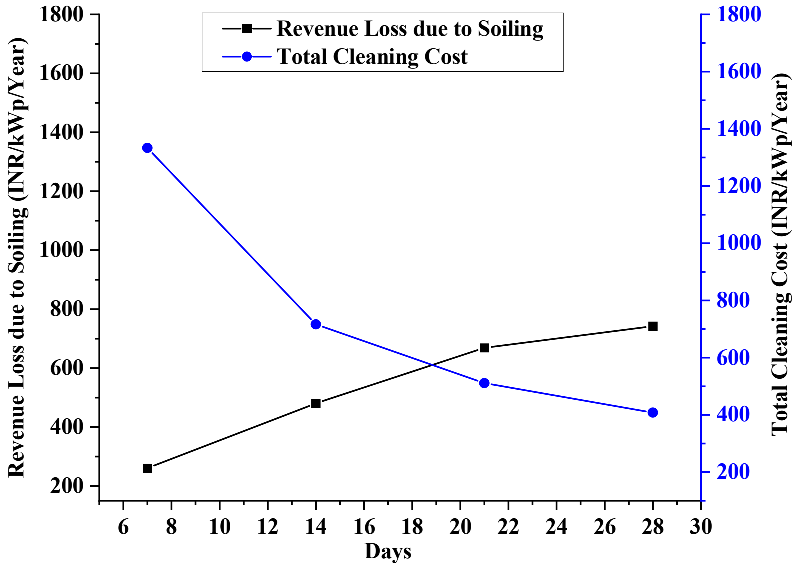

Fig. 6.6 (j) Revenue loss and cleaning cost crossover of 90° tilt angle solar PV panel

The figures above, Fig. 6.6 (a)-(j), clearly illustrate that the revenue loss resulting from dust deposition and the associated cleaning costs intersect within a 13 to 15 day interval, with the exception of the 90° tilt angle configuration. This data suggests that adhering to a cleaning schedule of every 14 days would result in financial benefits in the operation of a solar PV plant.

6.12 Cleaning Loss Factor (CLF) of Solar PV Plants Across Different Tilt Angles

The "Cleaning Loss Factor" refers to the reduction in performance of a photovoltaic (PV) system caused by dirt, dust, or other debris accumulating on the surface of the solar panels. Equation 6.9 was used to perform the calculation.

$$\text{Cleaning Loss Factor (CLF)} = \text{Revenue Loss} - \text{Cleaning Cost} \tag{6.9}$$

The revenue loss of a solar PV plant refers to the potential income reduction that a solar PV plant. Analyzing and addressing these factors are crucial for optimizing the financial performance of solar PV plants. The cleaning cost of a solar PV plant refers to the expenses associated with cleaning the solar panels to maintain their efficiency and ensure optimal energy production. By implementing cost-effective cleaning strategies, solar PV plant operators can manage cleaning expenses while ensuring optimal performance and maximizing the return on investment in solar energy generation.

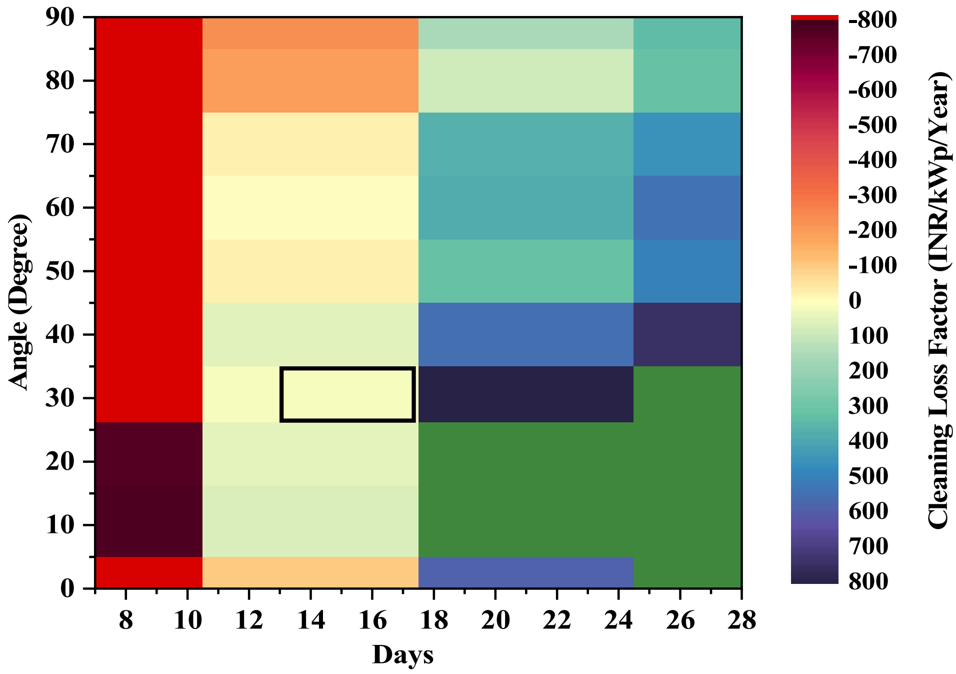

Fig. 6.7 Tilt angle versus Cleaning Loss Factor of solar PV plants

According to the above heat map in Fig. 6.7, when the Cleaning Loss Factor is zero, solar PV plants demonstrate their optimal performance. Conversely, as the value of the Cleaning Loss Factor shifts into positive or negative regions, it indicates an escalation in financial losses during the operation of the solar PV plant. Here the optimal performance observed within the tilt angle range of 26° to 35° over a period of up to 17 days.

6.13 Capacity Utilisation Factor (CUF) of Solar PV Plants Across Different Tilt Angles

The Capacity Utilization Factor (CUF) is the ratio of the actual annual energy produced by the PV system (annual energy output) to the energy that would be generated if the PV system operated continuously at full rated power for 24 hours per day throughout the year. It is typically denoted by equation 6.10.

$$\text{Capacity Utilization Factor (CUF)} = \frac{\text{Annual energy output}}{\text{Capacity} \times 24 \times 365} \tag{6.10}$$

When a system consistently delivers full-rated power, its CUF would be unity, equivalent to 100%. A higher CUF factor indicates the superior performance of the PV system.

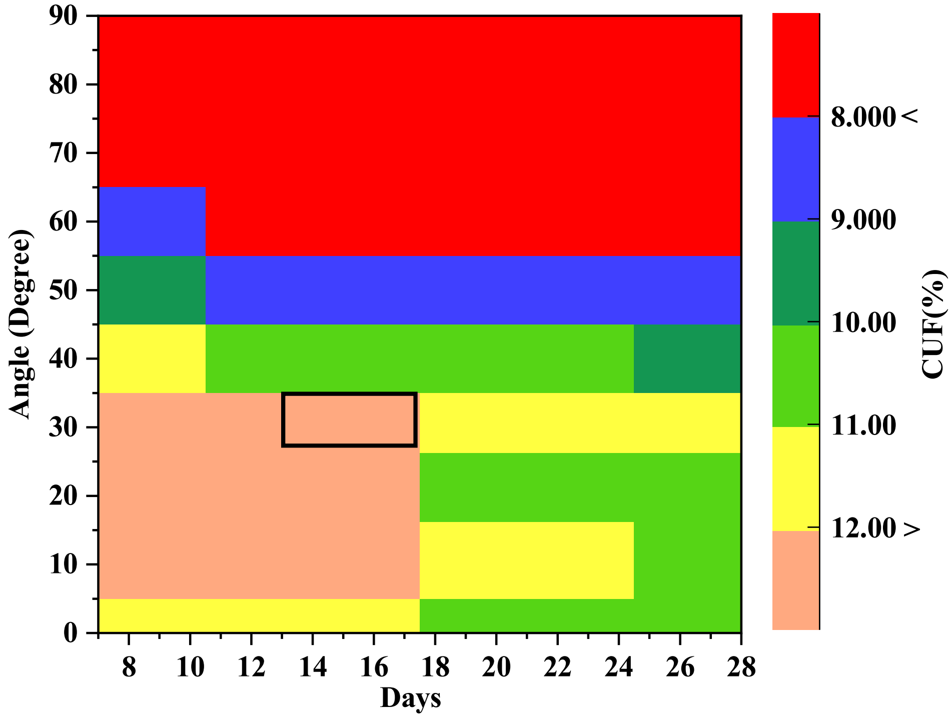

Fig. 6.8 Tilt angle versus CUF of solar PV plants

In Fig. 6.8, the heat map graph illustrates how the Capacity Utilization Factor (CUF) varies across different tilt angles, with optimal performance observed within the tilt angle range of 25° to 35° over a period of up to 17 days, the same conditions at which the CLF is at the optimum range, illustrated in the previous section (Fig. 6.7)

6.14 Performance Ratio (PR) of Solar PV Plants Across Different Tilt Angles

The Performance Ratio (PR) serves as an indicator of the overall impact of losses on the rated output attributed to different factors of solar PV plants. Typically, PR values tend to be higher during winter months compared to summer months due to losses stemming from PV module temperature. PR typically ranges from 60 to 80%, contingent on factors such as geographical location, solar irradiance levels, and prevailing climatic conditions (Sharma et al.,2017). However, it should be noted that PR does not directly reflect the amount of energy produced. For instance, a system with a lower PR in a region with high solar irradiation might generate more energy than a system with a higher PR in a location with lower solar irradiation (Marion et al., 2005). Performance Ratio (PR) is the ratio between the energy generated under typical outdoor conditions (final yield) and the energy that the system could potentially produce under laboratory conditions (reference yield). It is expressed as equation 6.11.

$$\text{Performance Ratio (PR)}\% = \frac{\text{final yield}}{\text{reference yield}} \times 100 \qquad (6.11)$$

The PR serves as an indicator of how closely a PV system achieves optimal performance in actual operation, enabling comparisons between PV systems independent of their location, tilt angle, orientation and nominal rated power capacity.

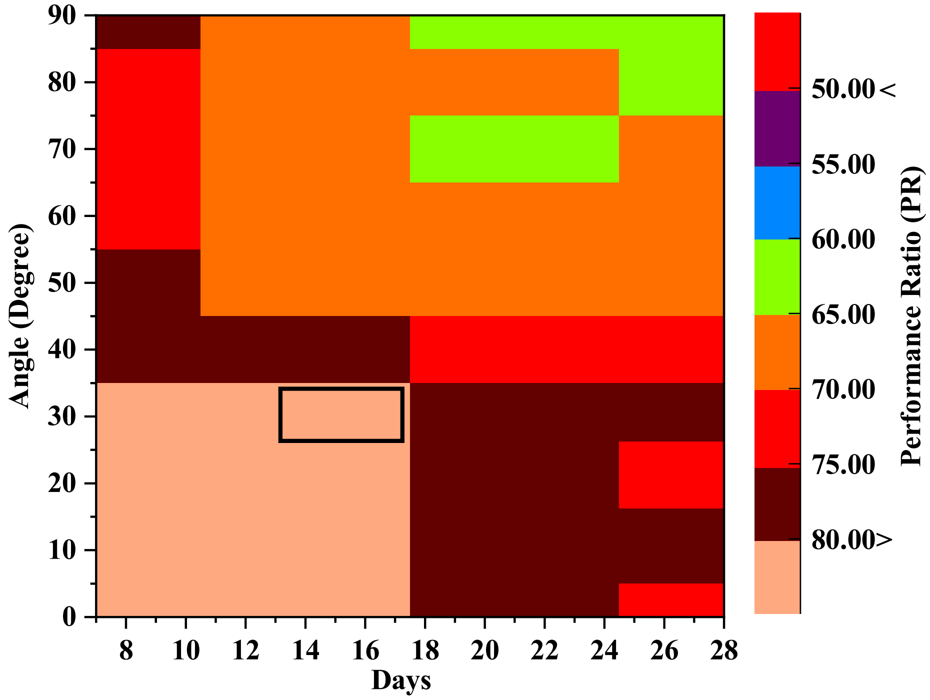

Fig. 6.9 Tilt angle versus PR of solar PV plants

In India, the Performance Ratio (PR) value of various solar power plants was observed to be 78% in Bhubaneswar (Sharma et al.,2017), 79% in Bhopal (Shukla et al.,2016), and 74% in Punjab (Sharma et al., 2013). Fig. 6.9, the heat map graph illustrates how the Performance Ratio (PR) varies across different tilt angles, with optimal performance observed within the tilt angle range of 26° to 35° over a period of up to 17 days, the similar conditions at which CLF and CUF of the PV system shared optimistic outcomes. All calculated data are described in Annexure IV.

6.15 Optimized Tilt Angle for Solar PV Installation in Kolkata

The Minitab statistical software was employed to optimize the tilt angle based on experimental data. Minitab stands out as a robust platform for statistical analysis and quality improvement endeavours (Minitab, 2021). With its extensive array of statistical tools and graphical analyses, Minitab aids users in data analysis, trend identification, and informed decision-making. Based on the analysis of the three aforementioned heat maps (Fig.6.6, Fig.6.7, Fig.6.8), a potential range of tilt angles for optimizing solar energy utilization has been identified. As discussed in the preceding section, the optimum cleaning frequency has already been determined. A 14-day interval as the optimal cleaning frequency was determined, using the "MINITAB" software, after which the tilt angle was optimized. In this optimization process, three parameters were considered: performance ratio (PR), cleaning loss factor (CLR), and capacity utilization factor (CUF).

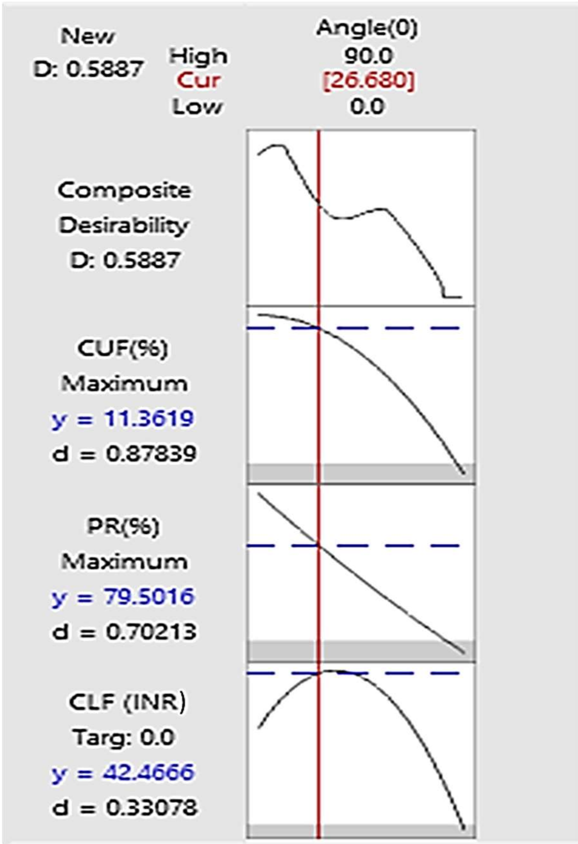

Fig. 6.10 Optimized tilt angle statistical analysis from Minitab software

The performance ratio and CUF were maintained at their maximum values, while the cleaning loss factor was set to zero. The statistical data output is shown in Fig. 6.10. Under these specified conditions, the optimized tilt angle was determined to be 26.680° ≈ 27 °.

6.16 Conclusion

In this chapter, various cleaning methods and their respective constraints ware examined. Based on this assessment, an appropriate cleaning technique for the solar PV plant in Kolkata was implemented during the experiment. Among the options, the most effective cleaning method for power plants in the Kolkata area is to cleaning by water equipped with manual pressurized spraying and glass wipers. This choice is favoured due to the suitability of water-based cleaning systems in the region, considering factors such as existing solar PV installations, water scarcity levels, and groundwater availability. A separate experimental study was conducted to determine the minimum water requirement for this cleaning process. Subsequently, annual energy generation, energy loss attributable to dust deposition, revenue loss, and cleaning costs were calculated at various time intervals. The scrutiny involved examining how the Cleaning Loss Factor (CLF), Capacity Utilization Factor (CUF), and Performance Ratio (PR) values fluctuated with different tilt angles of installation. It was ultimately determined that the tilt angle range of 26-35 degrees, coupled with a maximum cleaning interval of 14-17 days, is most conducive to the efficient operation of solar PV power plants in Kolkata, West Bengal. Moreover, the study suggests that the best performance for existing solar PV panels installed in West Bengal is achieved when the tilt angle ranges between 26 to 35 degrees, and the cleaning frequency is between 14 to 17 days. According to statistical analysis of experimental data, the optimum tilt angle for new installations is 27°, while a cleaning frequency of 14 days leads to the best performance.

Chapter 7

Design of North –South, Dual Orientation Fixed 90° Tilt Angle Tree Model

7.1 Introduction

Certainly, it is evident that the installation of renewable energy sources, encompassing solar, wind, geothermal heat, bioenergy, chemical, and various other sources, necessitates a considerable land area. Historically, solar photovoltaic (PV) power plants have been situated on unused land, which is now rare in urban areas. Rapid urbanization exacerbates the shortage of land, necessitating alternative solutions to maximize power generation within limited space. In such instances, employing a sustainable model, such as a combination of solar PV Trees and solar PV Artefact/tower structures along with energy storage, can demonstrate highly advantageous (Cao et al., 2014). Solar PV Tree structures offer a promising solution, ensuring access to reliable, sustainable, and modern energy sources, thereby contributing to the sustainable development goal. To meet the rising demand for power in urban areas with limited available land, suggest a sustainable solution by introducing solar PV Trees, each featuring unique designs to address the challenge. This chapter discussed the advantages of solar PV Tree models over traditional ground-mounted plants and highlighted groundwork for further research in integrating renewable energy into sustainability applications.

Solar panels installed on a solar tree complex are typically elevated above the ground. Solar panels mounted on traditional ground-level systems are more susceptible to debris blown by wind, including dirt, leaves, and other particles. Elevating the panels above ground level can mitigate this issue by reducing the likelihood of wind-blown debris reaching the panels. The vertical orientation of solar panels in a solar tree complex can also contribute to less surface area for dust accumulation compared to traditional horizontal arrays as has been already depicted in the previous chapter. This is because the vertical panels present a narrower profile to incoming dust particles, potentially reducing the overall amount of dust that settles on the panels. Overall, while vertical mounting configurations like solar PV tree models offer unique aesthetic and space-saving advantages, they may also experience decreased power generation compared to traditional horizontal or tilted panel installations. Careful design, orientation, and washing practices from dust deposition are crucial to diminish these losses and ensure optimal performance of vertical solar PV tree models.

7.2 Design of Solar Photovoltaic Tree Model

In this study a Dual orientation fixed 90° tilt Tree model has been conceptualized characterized by a central support pole structure branching into three arms, each branch capable of hosting eight PV modules, four in each of the back front sides in front side four and back side four. These panels are specifically chosen to be monocrystalline type with 120 cells, each rated at 335 W_p power (at STC).

Thus, a single Dual orientation fixed 90° tilt Tree accommodates 12 panels on each side yielding an effective 4.020 kW_p DC capacity at STC. The foundation footprint of this model occupies 10 m^2, resulting in a land usage ratio of 2.49 m^2/kW_p. With a ground clearance of approximately 2 m from the lowest edge of the solar PV module, the specific yield of this Solar Tree model is determined to be 5162 kWh/kW_p/year through simulation using PVSyst version 7.4 software. Within the simulation study, the dual orientation fixed 90° tilt solar PV Tree is positioned with an azimuth of 0° and a tilt angle of 90°, which is typically designed for all locations. The conceptual graphical layout of the solar PV Tree is depicted in Fig. 7.1, accompanied by a scale representation of an average human with a height of 1.67 m. To convert DC power to AC, a 4 kW inverter is employed separately for front and back side panels, which can be mounted either at the base of the Tree or on a separate stand. Flexible cable conduits are utilized to route the DC cables along the branches of the tree structure. The arrangement of the solar PV Trees can be adjusted to achieve optimal energy generation based on the desired azimuth and tilt angle for the specific installation location, but here only a due south 90° tilt angle installation was utilized. Fig. 7.1-7.4 illustrates the experimental setup for a 4 kW system, as part of the simulation study.

7.2.1 Dual Orientation: Fixed 90° Tilt Solar Tree (Panel on Front Side)

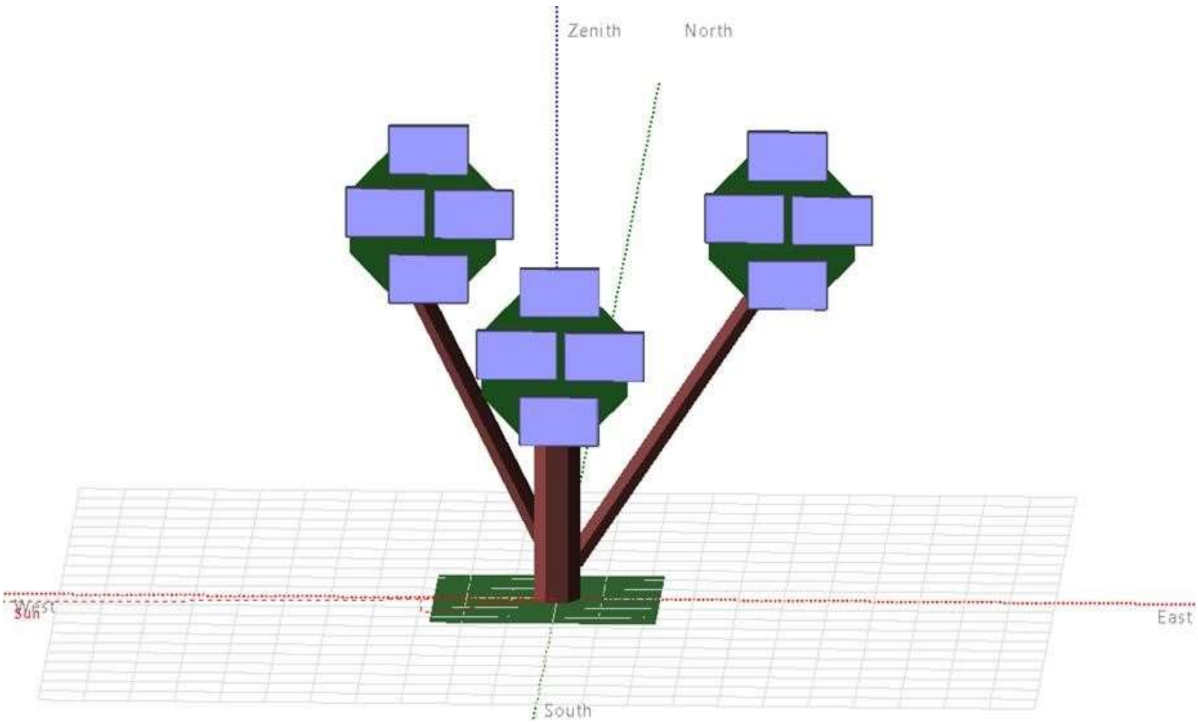

Fig. 7.1 Dual orientation fixed 90° tilt Tree model front side

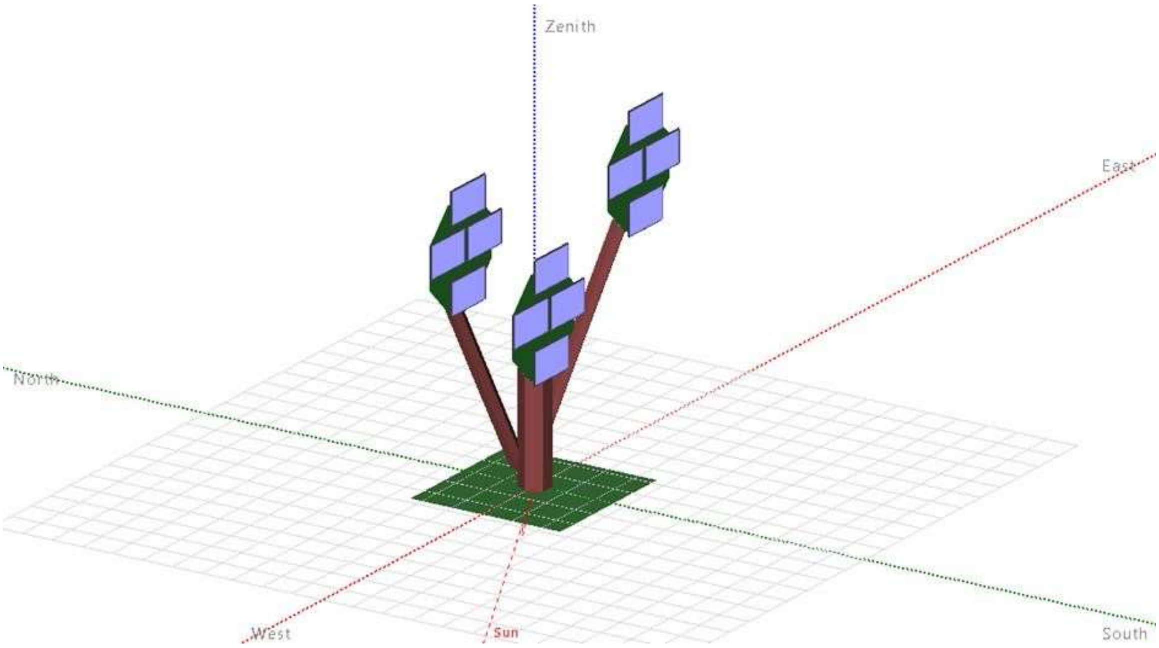

Fig. 7.2 Dual orientation fixed 90° tilt Tree Model Top view of front side

7.2.2 Dual Orientation: Fixed 90° Tilt Solar Tree (Panel on Back Side)

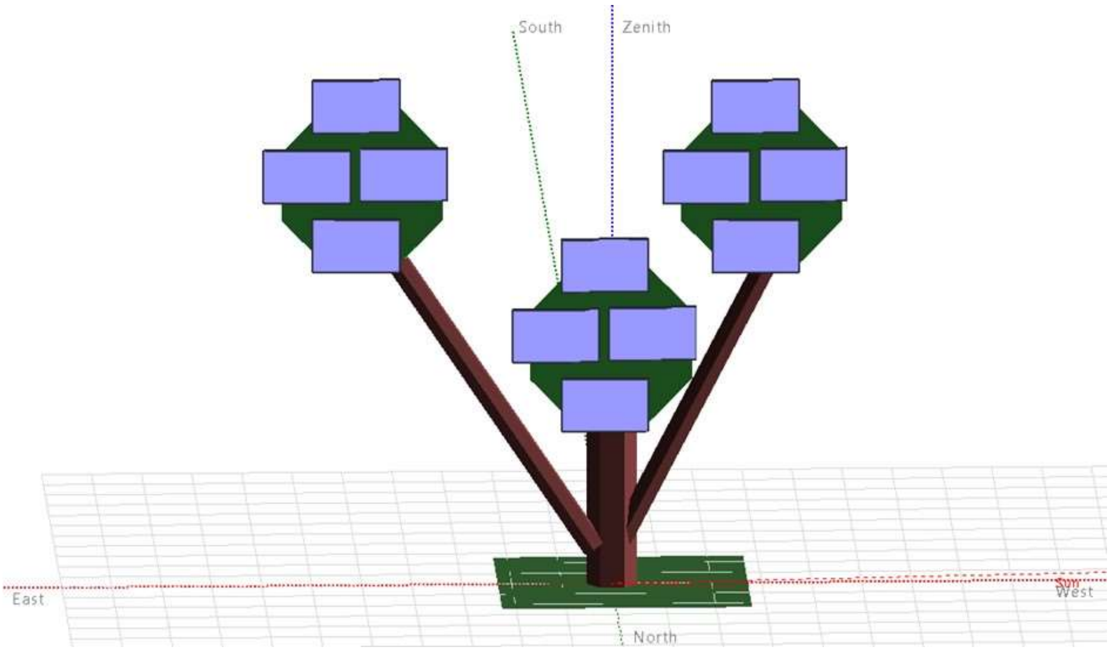

Fig. 7.3 Dual orientation fixed 90° tilt Tree model back side

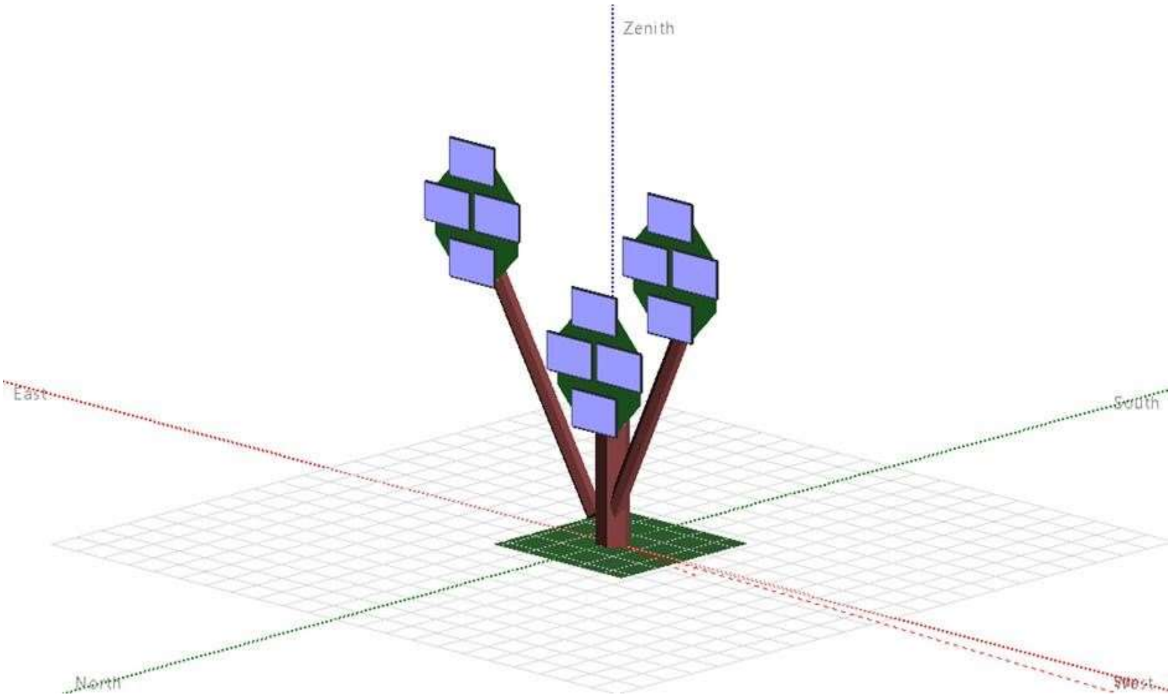

Fig. 7.4 Dual orientation fixed 90° tilt Tree Model Top view of back side

7.3 Normal Orientation: Ground Mounted Plant

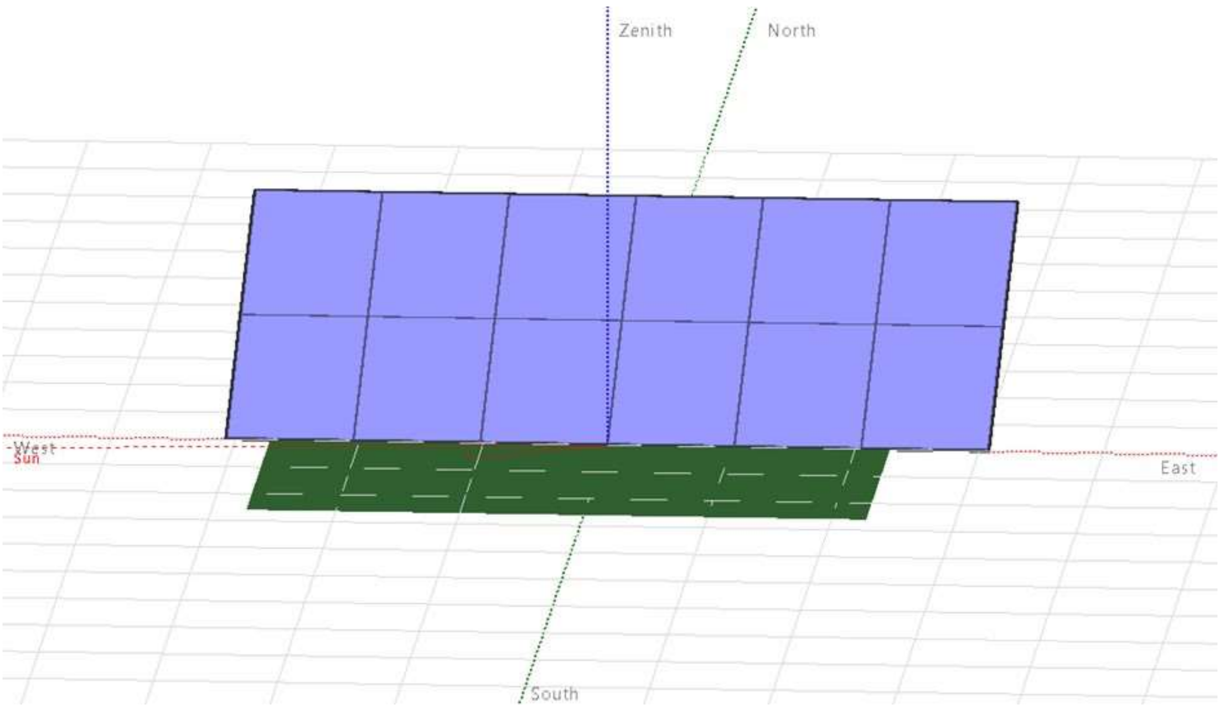

Fig. 7.5 Ground mounting fixed 22.5° tilt solar PV installation front view

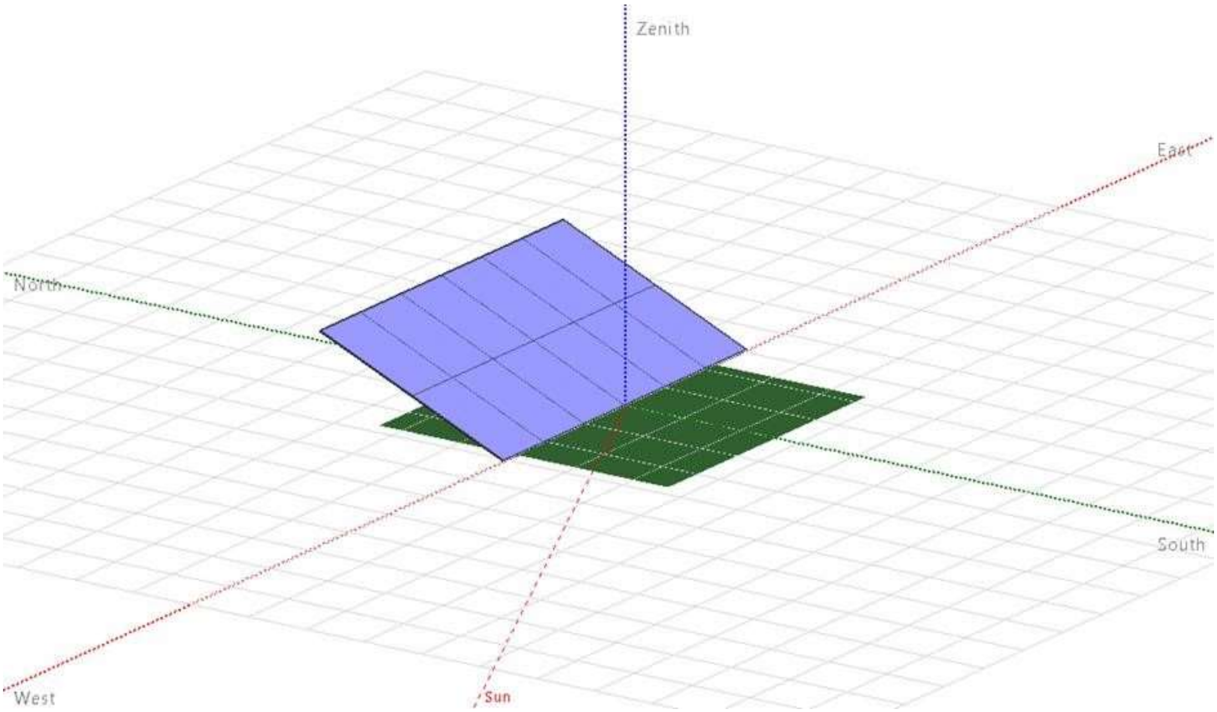

Fig. 7.6 Ground mounting fixed 22.5° tilt solar PV installation top view

According to the simulation shown in Fig. 7.1, the dual orientation tree model features a front side with a left branch installed at a 63° incline relative to its main middle branch, while the right side branch is installed at a 55° incline relative to its main branch (Dey and Pesala, 2020). While Fig. 7.3, panels were installed on the back side within the same branches., facing due north. Throughout the simulation process, this angled design ensures that the tree does not fall into any shading zones. Fig. 7.5 depicts a normal ground-mounted solar PV plant installed at a tilt angle of 22.5 degrees, while Fig. 7.6 provides a top view of the ground-mounted solar PV plant.

7.4 Details Comparison of Solar PV Tree v/s Ground-Mounted Solar PV Plant

To facilitate comparison, the solar PV Tree systems and the conventional ground-mounted system are maintained at the same levels, namely 4 kW_p. However, the number of structures in the simulated solar PV Tree model and the conventional ground-mounted plant model differs, as outlined in point in Table 7.1. While the tilt angle of the PV panel remains consistent across all panels, the mutual shading loss of zero due to differences in PV panel arrangement and optimal pitch of the tree branch has been established to ensure that the PV modules remain free from shading between sunrise to sunset. Consequently, this discrepancy results in variations in energy generation among the models during simulation. The correlations and detailed explanations of the parameters outlined in Table 7.1 are provided below.

Table 7.1 Electrical comparison of solar PV Tree v/s Ground-mounted Solar PV plant

Particulars	Ground Mounted Plant	Dual Orientation Fixed 90° Tilt Tree
Graphical Representation	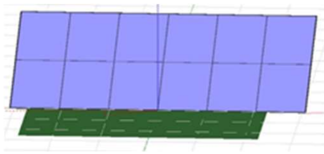	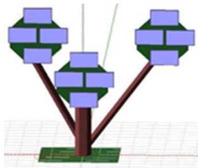
Each PV Panel's Rating (W_p)	335	335
Inverter Rating (kW)	4	4
Total DC Capacity (kW_p)	4	Front side – 4 Back side-4
GHI (kW/m^2/year)	1914	Front side – 1006 Back side-490
Annual Energy Output (kWh)	6420	Front side – 3481 Back side-1681
Ground Clearance (m)	0.5	2
Total Land Area required (m^2)	28	10
Land Area required per kW_p (m^2/kW_p)	7	2.5
Power to Land occupancy Ratio (PLR)	0.14:1	0.4:1
The land area occupied by base of the structures (m^2)	28	1
Land Coverage Ratio (LCR)	1:1	0.1:1

7.4.1 Ground Clearance

The Solar Tree design maintains a ground clearance on an average 2 meters, a height chosen to facilitate dual land usage beneath the solar PV Tree while avoiding excessive structural costs (Faizi et al., 2020). However, this clearance is flexible and can be adjusted to accommodate specific operational or situational requirements as necessary. Traditional ground-mounted structures are widely used due to their cost-effectiveness, but they render the land beneath them unusable due to their low ground clearance. Additionally, the increased ground clearance in solar PV Trees offers the advantage of better airflow beneath the PV modules, potentially enhancing their cooling and reducing temperature losses compared to conventional ground-mounted plants (Vyas et al., 2022).

7.4.2 Land Requirement

In this simulation, the land occupancy varies across respective structural designs. The Dual Orientation Fixed 90° Tilt Tree, for instance, occupies approximately 64.29% less land compared to a conventional ground-mounted solar plant, requiring only 2.5 m² of the area to generate 1 kW_p of power. Absolutely, considering the expensive nature of the land and the ongoing rise in land prices due to urbanization, solar PV Trees present themselves as a highly effective and sustainable solution. Particularly in areas with limited land availability and high electricity demands, such as densely populated regions or areas with many high-rise buildings, the proposed designs of SPV Trees offer a compelling advantage. They require significantly less land to produce the equivalent energy compared to traditional ground-mounted solar plants. Thus, solar PV Trees present a promising solution to address the challenges posed by land scarcity and increasing energy demands in urbanized areas.

7.4.3 Power to Land Occupancy Ratio (PLR)

A crucial aspect of this simulation study involves determining the total land area required for the installation of solar PV Trees.To comprehend this, simulations were conducted using a system with a 4 kW capacity. The land area requirement for the proposed and optimized solar PV Tree models was further compared with the standard industrial layout of ground-mounted 4 kW rated solar PV power plants. Analysis reveals that compared to the 28 m² land area needed for a ground-mounted plant, the land area values for solar PV Tree models are significantly lower, namely 10 m². Consequently, the land area required per kW_p is evaluated, yielding values of 2.5 m² compared to 7 m^2/kW_p for a ground-mounted PV plant (as illustrated in Table 7.1). This significant variance highlights the efficiency of solar PV Trees in terms of land area needed for large-scale renewable energy power plants, effectively addressing the needs of densely populated urban areas.

The most crucial factor highlighting the importance of implementing solar PV Trees in urban cities is the Power to Land Occupancy Ratio. PLR represents the maximum DC power generation achievable per unit of land space, which cannot be applied for any other purposes. It represents the ratio of DC power generated relative to the land area occupied by the structure of the installed Solar PV system, thereby making the land unsuitable for any alternative use. As indicated in Table 7.1, the PLR achieved for solar PV Trees is 0.4:1, in comparison for the considered ground-mounted solar PV Plant, the PLR is significantly lower at 0.14:1. Therefore, simulation studies clearly demonstrate that solar PV Trees can generate the equivalent amount of energy while utilizing only a small portion of the land area compared to conventional ground-mounted plants.

7.4.4 Land Coverage Ratio (LCR)

The Land Coverage Ratio (LCR) is another crucial factor in the proposed simulation study. The LCR represents the ratio of the land area taken up by the structures (incapable of being used for any alternative purposes) to the total land space available at the project site. This ratio can be observed in the graphical representation of the area occupied by the structure/foundation of the solar PV Tree and ground-mounted tree as depicted in Fig. 7.1 and Fig. 7.5. As indicated in Table 7.1, the LCR obtained for solar PV Trees 0.1:1, in comparison for the considered ground-mounted solar PV Plant, the LCR is 1:1. The conventional ground-mounted solar PV plant exhibits the highest Land Coverage Ratio (LCR) and the lowest Power to Land Occupancy Ratio (PLR). This signifies that for a traditional ground-mounted plant, the land area occupied by the plant becomes entirely incapable of being used for any other purpose. In contrast, the PLR increases in the case of solar PV Trees, as only the area covered by the foundation becomes unusable, while the rest of the land remains usable for other purposes.

7.4.5 Power Loss Due to Dust Accumulation on Solar PV Trees

The impact of dust accumulation on solar PV tree would be similar to that on standard solar panels. The degree of power loss would depend on factors such as the amount of dust accumulation, type of dust and the orientation of the solar panels within the "tree" structure. In Chapter 5, the patterns of dust accumulation on solar panels tilted angle at 90° are examined. By tilting the panels at this angle, it was aim is to minimize dust accumulation. To further investigate, an experiment was conducted under real environmental conditions comparing power generation patterns between ground-mounted panels tilted at 22.5° and two sets of panels tilted at 90° facing north and south, without any maintenance or cleaning. The detailed power generation graphs are depicted in Fig. 7.7. The graph clearly illustrates a decline in power generation for the 22.5° panels over time, attributed to dust deposition. As discussed in the previous Chapter 5, it was observed that the power generation of the 22.5° tilted panel decreased by an average of 20% under constant radiation after four weeks, whereas the power loss for the 90° panels was lower due to less dust deposition. As depicted in the graph, the power generation of the 22.5 ° tilted panel starts to decrease in comparison to the 90° tilt after approximately 25 to 26 days.

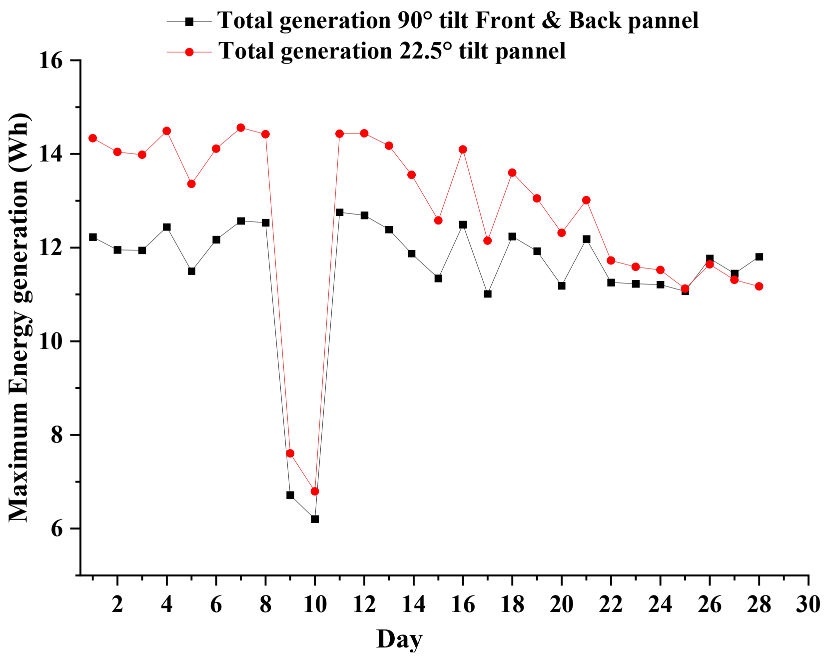

Fig. 7.7 Power generation pattern of 22.5° and two 90° tilted panels at facing north and south due to dust deposition

7.5 Conclusion

So far, the fundamental concept has been to utilize unused land for installing solar PV plants, aiming to transition most energy sources to renewables. However, in the context of smart city initiatives, deploying solar PV plants in urban areas poses challenges due to land scarcity and high occupancy. In response, the concept of the solar PV Tree emerges as an optimal solution, aiming to generate maximum electricity while occupying minimal land. The design of the solar PV Tree merges renewable energy technology with nature-inspired art, serving the main purpose of providing sustainable and eco-friendly energy to urban landscapes where land availability is limited and costs are soaring, significantly impacting investment returns. Extensive simulation studies and comparative analyses between solar PV Tree models and conventional ground-mounted PV plants have been conducted, the simulation studies reveal that the dual orientation 90° tilt solar PV Tree exhibits an LCR of 0.1 and a PLR of 0.4. The simulation studies carried out with the proposed solar PV Tree models demonstrate the ability to generate approximately the same amount of clean electricity, taking into account the impact of dust, while using minimal land compared to conventional ground-mounted PV plants. Under the condition of no cleaning for 26 days, the solar PV tree model generated more energy compared to conventional ground-mounted PV plants. Essentially, the renewable power plant designs achieve the lowest Land Coverage Ratio (LCR) and the highest Power Loss Ratio (PLR). Consequently, solar PV Trees emerge as an exceptionally effective solution, enabling the installation of large-capacity solar PV plants within significantly less land area compared to conventional ground-mounted plants.

Chapter 8

Conclusions & Future Scope of Work

8.1 Study Outcome

This study can be seen as a synthesis of three systematic phases, each focusing on analyzing the prediction and real-world performance of solar photovoltaic power plants. It delves into overcoming maintenance challenges to restore maximum power output through optimal design. The outcomes of this structured analytical approach are detailed in Table 8.1.

Table 8.1 Outcomes derived from the study

Phase 1	Phase 2	Phase 3
• Experimental data showed superior to simulation data in informing solar system design with greater accuracy. • Based on the experimental data, the derived fill factor (FF) model and power model reliably can predict FF and maximum power output for various environmental conditions. • The experimental-based simulation model's performance demonstrates the actual performance of solar panels.	• As increasing time interval, dust accumulation rises, leading to decreased energy output across all weather conditions. • In lower constant radiation and temperature, the energy loss due to dust accumulation is more pronounced compared to situations with higher constant radiation and temperatures. • Normalized energy generation data shows that dust deposition adversely affects energy production across all tilt angles.	• water-based manual cleaning method is considered optimal for cleaning solar panels in Kolkata. • A tilt angle of 27 degrees can be regarded as optimal for solar PV installations in Kolkata, especially considering the impact of dust accumulation. • A cleaning frequency of 14 days is estimated optimal to maximize energy generation from a solar PV plant in Kolkata.

The quest for accuracy and efficiency in solar PV system design, has led researchers to explore the reliability of experimental data over simulated models. Through meticulous experimentation, it has become evident that experimental data outperforms simulation data in informing the design of solar systems with superior precision. A robust framework for predicting the design fill factor (FF) and maximum power output across diverse environmental conditions has been observed to be offered by the power models derived from experimental data. These models serve as invaluable tools in optimizing the performance of solar installations, ensuring efficient energy generation in varying contexts. The present research has provided valuable insights into the influence of dust accumulation on the efficiency of solar panels over varying time intervals and under diverse weather conditions. A consistent pattern has emerged from observations: as the time interval increases, the accumulation of dust on solar panels intensifies, resulting in a notable reduction in energy output regardless of fluctuations. Based on the findings, the implementation of a water-based pressured manual cleaning method is suggested for mitigating the adverse effects of dust deposition and optimizing energy generation from solar PV panels in Kolkata. This approach has proven to be effective in removing dust build up and restoring panel efficiency. Additionally, the analysis suggests that a cleaning frequency of 14 days is optimal for maintaining peak energy generation efficiency from solar PV plants in the region. By adhering to this cleaning schedule, solar panel performance can be sustained at its highest level, ensuring reliable and sustainable energy production over time. The specific outcomes of this research are as follows:

- Studies from various literature indicate that solar PV performance is influenced by several environmental factors, with solar radiation and cell temperature being the most significant. Fluctuations in solar radiation lead to variations in cell temperature, consequently impacting PV generation. Moreover, changes in wind direction and speed can affect cell temperature. Similarly, alterations in humidity levels also contribute to fluctuations in PV cell temperature. Furthermore, the accumulation of dust on solar panels not only diminishes radiation levels but also affects the cell's temperature, leading to a gradual decline in PV performance. As cell temperature rises, efficiency tends to decrease, impacting overall performance.
- Accurate forecasting of PV panel power generation is crucial for effective planning and operational management. Several studies investigate estimating the I-V curve using equivalent circuit models. Leveraging manufacturer data, a PVsyst-based model was established and thoroughly validated across different conditions. Despite the valuable insights provided by PVsyst models, their practical applicability may be limited. Therefore, experimental models are developed to accurately evaluate real-world performance. These models encompass predicting fill factor (FF) for efficiency calculation, forecasting fill factor while considering dust accumulation, and estimating maximum power generation, independent of environmental factors. Future endeavours should focus on integrating experimental and outdoor data to enhance the precision of energy production calculations.
- During the summer season, the analysis of dust accumulation indicates a primarily increasing rate, followed by a slight decrease. In the monsoon season, dust accumulation on solar panels was erratic over time, due to rainfall washing away the dust. Winter dust effect was slightly higher compared to other seasons; however, during this period, lower ambient temperatures and radiation levels helped compensate for the generation loss.
- Under constant radiation and temperature conditions, the influence of dust deposition on energy production reveals that during periods of low radiation levels caused by dust accumulation, there is an increase in generation loss compared to periods of high radiation levels.

- The efficiency of the solar panel decreased over time at various tilt angles during both the summer and winter seasons due to dust deposition. Notably, during the summer, the highest efficiency was achieved with a 10° tilt angle panel, whereas in the winter season, the highest efficiency was achieved with a 30° tilt angle panel. However, during the monsoon season, the efficiency of the solar panel fluctuated in response to varying intensities of rainfall.
- After evaluating different cleaning methods, manual pressurized spraying and glass wiper cleaning method with water was consider as the most effective for solar PV plant in Kolkata. This decision is based on factors like water availability and existing installations. An experimental study determined the minimum water requirement for this process.
- Annual energy generation, energy loss from dust deposition, revenue loss, and cleaning expenses across different time frames were analyzed. The analysis incorporated Cleaning Loss Factor (CLF), Capacity Utilization Factor (CUF), and Performance Ratio (PR) values, which varied with installation tilt angles. The findings suggest that existing solar PV panels in Kolkata, West Bengal, achieve optimal performance within a tilt angle range of 26 to 35 degrees, coupled with cleaning frequencies between 14 to 17 days.
- Based on the statistical analysis of experimental data, it was found that the optimum tilt angle for new installations is 27 degrees. Additionally, it was determined that a cleaning frequency of 14 days' results in the best performance.
- Solar trees are often used in urban areas where space is limited or where traditional solar panel installations may not be feasible. The advantages of solar trees include their ability to maximize solar energy capture in a limited space, their potential to serve as charging stations for electric vehicles or mobile devices, and their contribution to sustainability and environmental awareness. The dual-orientation solar PV tree was designed to minimize the impact of dust deposition on power losses within the tree model.

8.2 Future Scope of Work

8.2.1 Optimal Tilt Angle and Cleaning Frequency Finding Base on Pollutant (PM_{10}) Data

In the previous chapter, the investigation was focused on addressing the issue of dust accumulation in solar photovoltaic (PV) systems in Kolkata, West Bengal. Through detailed analysis of dust deposition data gathered from this particular test site throughout the year. The emissions of aerosol particles from both anthropogenic and natural sources constitute pollution, and their consequential impact introduces an additional layer of complexity to the power generation of solar PV panels. Based on the data, expanding the analysis to establish a correlation between pollution and dust deposition on solar PV panels, and it's also presents an opportunity for optimization in solar PV installations, according to findings correlation. This level of specificity can lead to even more precise optimization of power generation output for solar installations across different regions of India. Leveraging existing PM_{10} data from government weather forecasting websites can provide a solid foundation for correlating dust accumulation patterns with energy generation for specific locations like Kolkata. By establishing a correlation between these variables, Predictive models will be developed to estimate the optimal tilt angle and cleaning frequency of solar modules for maximizing performance, not only in Kolkata but potentially for any location with similar environmental conditions. This approach has the potential to streamline solar PV setup and maintenance processes, making them more efficient and cost-effective. Additionally, it could contribute to the broader goal of expanding renewable energy adoption by enhancing the predictability and reliability of solar power generation systems across diverse geographical areas.

8.2.2 Design Centralize Maximum Power Point Tracking (MPPT) Devices for Power Plant

In this study experimental data has been utilized to design centralised maximum power point tracking devices (MPPT) for optimizing power generation in power plants. This optimization is achieved through a Maximum Power Point Tracking (MPPT) algorithm, which adjusts the resistance of the MPPT device to ensure that the PV panel operates at its maximum power output. In the single panel of the power plant, there's a measurement device that continuously monitors the solar radiation levels and the temperature of the panel. This data may be fed into a fill factor model equation, which likely takes into account factors such as temperature, irradiance, and other characteristics of the PV panel. The MPPT algorithm then uses the output of this equation to determine the optimal resistance for the MPPT device. By adjusting the resistance of the MPPT device based on real-time conditions, the system can maximize the power output of the PV panel, ensuring efficient energy generation from the available sunlight. This kind of optimization is crucial for maximizing the overall performance and efficiency of a solar power plant, especially in varying environmental conditions. This will serve as a foundation for future research endeavours in this field.

References

Ahmed, M. S., Karal, R., Das, B. K., & Das, A. (2023). Experimental investigation of cooling, wind velocity, and dust deposition effects on solar PV performance in a tropical climate in Bangladesh. *Case Studies in Thermal Engineering*, *50*, 103409. doi.org/10.1016/j.csite.2023.103 409.

Ahmed, R. R., Karaghool, H. A., Ismail, N. N., & Alabdraba, W. M. (2023, August). Removal of the Minerals Salts from Water Wells by Using the Solar Distillation. *In IOP Conference Series: Earth and Environmental Science* (Vol. 1222, No. 1, p. 012034). *IOP Publishing*, doi:10.1088/1755-1315/1222/1/012034.

Al Garni, H. Z. (2022). The impact of soiling on PV module performance in Saudi arabia. *Energies*, 15(21), 8033, doi.org/10.3390/en15218033.

Al Shehri, A., Parrott, B., Carrasco, P., Al Saiari, H., & Taie, I. (2017). Accelerated testbed for studying the wear, optical and electrical characteristics of dry cleaned PV solar panels. *Solar Energy*, 146, 8-19, dx.doi.org/10.1016/j.solener.2017.02.014.

Al-Hasan, A. Y., & Ghoneim, A. A. (2005). A new correlation between photovoltaic panel's efficiency and amount of sand dust accumulated on their surface. *International Journal of Sustainable Energy*, 24(4), 187-197, doi.org/10.1080/14786450500291834.

Almukhtar, H., Lie, T. T., & Al-Shohani, W. A. (2023). Comprehensive analysis of dust impact on photovoltaic module temperature: Experimental insights and mathematical modeling. *Solar Energy*, 265, 112125, doi.org/10.1016/j.solener.2023.112125.

Alshareef, M. J. (2023). A Comprehensive Review of the Soiling Effects on PV Module Performance. *IEEE Access*, 11, 134623-134651, doi 10.1109/ACCESS.2023.3337204.

Amiry, H., Benhmida, M., Bendaoud, R., Hajjaj, C., Bounouar, S., Yadir, S., ... & Sidki, M. (2018). Design and implementation of a photovoltaic IV curve tracer: Solar modules characterization under real operating conditions. *Energy Conversion and Management*, 169, 206-216, doi.org/10.1016/j.enconman.2018.05.046.

Asl-Soleimani, E., Farhangi, S., & Zabihi, M. S. (2001). The effect of tilt angle, air pollution on performance of photovoltaic systems in Tehran. *Renewable Energy*, 24(3-4), 459-468, doi.org/10.1016/S0960-1481(01)00029-5.

Assi, A., Hassan, A., Al-Shamisi, M., & Hejase, H. (2012, November). Removal of air blown dust from photovoltaic arrays using forced air flow of return air from air conditioning systems. *In 2012 International Conference on Renewable Energies for Developing Countries (REDEC)* (pp. 1-5). *IEEE*.

Ayompe, L. M., Duffy, A., McCormack, S. J., & Conlon, M. (2011). Measured performance of a 1.72 kW rooftop grid connected photovoltaic system in Ireland. *Energy conversion and management*, 52(2), 816-825, doi: 10.1016/j.enconman.2010.08.007.

Bagnold, R. A. (2012). The physics of blown sand and desert dunes. *Courier Corporation.*

Bergin, M. H., Ghoroi, C., Dixit, D., Schauer, J. J., & Shindell, D. T. (2017). Large reductions in solar energy production due to dust and particulate air pollution. *Environmental Science & Technology Letters*, *4*(8), 339-344. doi.org/10.1021/acs.estlett.7b00197.

Blott, S. J., & Pye, K. (2012). Particle size scales and classification of sediment types based on particle size distributions: *Review and recommended procedures. Sedimentology*, 59(7), 2071-2096, dx.doi.org/10.1111/j.1365-3091.2012.01335. x.

Boeing, A., Neda, M., Steinberg, S., & Batista, J. (2022). The impact of lower quality water on soiling removal from photovoltaic panels. *Renewable and Sustainable Energy Reviews*, 169, 112870, doi.org/10.1016/j.rser.2022.112870.

Boussaid, M., Belghachi, A., Agroui, K., Abdelaoui, M., & Otmani, M. (2016). Solar cell degradation under open circuit condition in out-doors-in desert region. *Results in physics*, 6, 837-842, dx.doi.org/10.1016/j.rinp.2016.09.013.

BRIDGE TO INDIA Energy Private Limited, 2018, Water use in solar power sector, https://bridgetoindia.com/report/water-use-in-solar-power-sector/ (Access on 31st March,2024)

Cao, W., Li, Z., Yang, Y., Zheng, Y., Yu, W., Afzal, R., & Xue, J. (2014). "Solar tree": Exploring new form factors of organic solar cells. *Renewable energy*, 72, 134-139, dx.doi.org/10.1016/j.renene.2014.06.045.

CGWB, Central Ground Water Board Department of Water Resources, *Government of India*, National Compilation on DYNAMIC GROUND WATER RESOURCES OF INDIA, 2023.

Chaibi, Y., Salhi, M., El-Jouni, A., & Essadki, A. (2018). A new method to extract the equivalent circuit parameters of a photovoltaic panel. *Solar Energy*, 163, 376-386.

Chander, S., Purohit, A., Sharma, A., Nehra, S. P., & Dhaka, M. S. (2015). A study on photovoltaic parameters of mono-crystalline silicon solar cell with cell temperature. *Energy Reports*, 1, 104-109, doi.org/10.1016/j.egyr.2015.03.004.

Chander, S., Purohit, A., Sharma, A., Nehra, S. P., & Dhaka, M. S. (2015). A study on photovoltaic parameters of mono-crystalline silicon solar cell with cell temperature. *Energy Reports*, *1*, 104-109. doi.org/10.1016/j.egyr.2015.03.004.

Chen, Y., Liu, Y., Tian, Z., Dong, Y., Zhou, Y., Wang, X., & Wang, D. (2019). Experimental study on the effect of dust deposition on photovoltaic modules. *Energy Procedia*, *158*, 483-489. doi:10.1016/j.egypro.2019.01.139.

Chiteka, K., Arora, R., Sridhara, S. N., & Enweremadu, C. C. (2020). A novel approach to Solar PV cleaning frequency optimization for soiling mitigation. *Scientific African*, 8, e00459, doi.org/10.1016/j.sciaf. 2020.e00459.

Cordero, R. R., Damiani, A., Seckmeyer, G., Jorquera, J., Caballero, M., Rowe, P., ... & Laroze, D. (2016). The solar spectrum in the Atacama Desert. *Scientific reports*, 6(1), 22457, doi: 10.1038/srep22457.

Dagher, M. M., & Kandil, H. A. (2023). Computational prediction of dust deposition on solar panels. *Environmental Science and Pollution Research*, 30(5), 12545-12557, doi.org/10.1007/s11356-022-22993-y.

Deb, D., & Brahmbhatt, N. L. (2018). Review of yield increase of solar panels through soiling prevention, and a proposed water-free automated cleaning solution. *Renewable and Sustainable Energy Reviews*, 82, 3306-3313, dx.doi.org/10.1016/j.rser.2017.10.014.

Dewi, T., Taqwa, A., Kusumanto, R. D., & Sitompul, C. R. (2021, February). The Investigation of Sea Salt Soiling on PV Panel. *In 4th Forum in Research, Science, and Technology* (FIRST-T1-T2-2020) (pp. 141-147). *Atlantis Press*.

Dey, S., & Pesala, B. (2020). Solar tree design framework for maximized power generation with minimized structural cost. *Renewable energy*, 162, 1747-1762, doi.org/10.1016/j. renene.2020.07.035.

Dieter, G. E. (1986). Mechanical Metallurgy, *McGraw-Hill Inc*.

Dong, T. T., & Lee, B. K. (2009). Characteristics, toxicity, and source apportionment of polycylic aromatic hydrocarbons (PAHs) in road dust of Ulsan, Korea. *Chemosphere*, 74(9), 1245-1253, doi: 10.1016/j.chemosphere.2008.11.035.

Dubey, S., Sarvaiya, J. N., & Seshadri, B. (2013). Temperature dependent photovoltaic (PV) efficiency and its effect on PV production in the world–a review. *Energy procedia*, 33, 311-321.

Duffie, J. A., & Beckman, W. A. (2013). Solar engineering of thermal processes. *John Wiley & Sons.*

Durisch, W., Urban, J., & Smestad, G. (1996). Characterisation of solar cells and modules under actual operating conditions. *Renewable Energy*, 8(1-4), 359-366.

ECBC, 2017 *https://beeindia.gov.in/sites/default/files/ECBC%20book%20final%20one%20%202017%20with%20Amendements.pdf*, accessed on 08.11.2023.

Eicke, L., Eicke, A., & Hafner, M. (2022). Solar Power Generation. In *The Palgrave Handbook of International Energy Economics* (pp. 157-169). *Cham: Springer International Publishing*. doi.org/10.1007/978-3-030-86884-0_9.

Eisa, K., Shenouda, R., Abd-Elhady, M. S., Kandil, H. A., & Khalil, T. (2023). Mitigation of dust on PV panels that operate light posts using a wind shield, mechanical vibrations and AN antistatic coating. *Ain Shams Engineering Journal*, 14(5), 101993, doi.org/10.1016/ j.asej.2022.101993.

Ember, "Global Electricity Review 2023", 11 April 2023, *https://ember-climate.org/insights/ research/global-electricityreview-2023*.

Faizi, M. A., Sandipkumar, V. M., Verma, A., Suman, & Jain, V. K. (2020). Design and optimization of solar photovoltaic power plant in case of agrivoltaics. *In Recent Trends in Materials and Devices: Proceedings of ICRTMD 2019* (pp. 59-69). *Springer Singapore*, doi.org/10.1007/978-981-15-8625-5_7.

First Solar,inc,2017, *https://www.firstsolar.com/-/media/First-Solar/Technical-Documents/ Series-4-Application-Note/Module-Cleaning-Guidelines.ashx?la=en* (Access on 31st March,2024).

Fuentes, M., Vivar, M., Burgos, J. M., Aguilera, J., & Vacas, J. A. (2014). Design of an accurate, low-cost autonomous data logger for PV system monitoring using Arduino™ that complies with IEC standards. *Solar Energy materials and solar cells*, 130, 529-543, dx.doi.org /10.1016/j.solmat.2014.08.008.

Gholami, A., Saboonchi, A., & Alemrajabi, A. A. (2017). Experimental study of factors affecting dust accumulation and their effects on the transmission coefficient of glass for solar applications. *Renewable energy*, 112, 466-473, doi.org/10.1016/j.renene.2017.05.050.

Green, M., Dunlop, E., Hohl-Ebinger, J., Yoshita, M., Kopidakis, N., & Hao, X. (2021). Solar cell efficiency tables (version 57). *Progress in photovoltaics: research and applications*, *29*(1), 3-15 doi.org/10.1002/pip.3371.

Green, M., Dunlop, E., Hohl-Ebinger, J., Yoshita, M., Kopidakis, N., & Hao, X. (2021). Solar cell efficiency tables (version 57). *Progress in photovoltaics: research and applications*, *29*(1), 3-15. doi.org/10.1002/pip.3371.

Gwandu, B. A. L., & Creasey, D. J. (1995). Humidity: a factor in the appropriate positioning of a photovoltaic power station. *Renewable Energy*, 6(3), 313-316, doi.org/10.1016/0960-1481 (95)00073-S.

Haghdadi, N., Copper, J., Bruce, A., & MacGill, I. (2017). A method to estimate the location and orientation of distributed photovoltaic systems from their generation output data. *Renewable Energy*, 108, 390-400, doi.org/10.1016/j.renene.2017.02.080.

Hassan, A. K. F., & Abdullah, O. A. (2015). New methodology for prestressing fiber composites. *Univers. J. Mech. Eng*, *3*, 252-261. doi: 10.13189/ujme.2015.030605.

He, B., Lu, H., Zheng, C., & Wang, Y. (2023). Characteristics and cleaning methods of dust deposition on solar photovoltaic modules-A review. *Energy*, 263, 126083, doi.org/10.1016/j.energy.2022.126083.

https://zeiss-campus.magnet.fsu.edu/print/lightsources/tungstenhalogen-print.html

Incropera, F. P., DeWitt, D. P., Bergman, T. L., & Lavine, A. S. (1996). *Fundamentals of heat and mass transfer* (Vol. 6, p. 116). New York: Wiley.

India Meteorological Department, Regional Meteorological Centre, Kolkata. Weekly Weather Report (WWR) for West Bengal, Sikkim and Bay of Bengal. *https://mausam.imd.gov.in/kolkata/*

India Meteorological Department. (2022). *IMD* Annual Report 2022. *chrome-extension://efaidnbmnnnibpcajpcglclefindmkaj/https://mausam.imd.gov.in/imd_latest/contents/ar2022.pdf.*

International Electrotechnical Commission. (2016). IEC 61215 Terrestrial photovoltaic (PV) modules-Design qualification and type approval. *International Electrotechnical Commission, International Standard.*

Irwan, Y. M., Leow, W. Z., Irwanto, M., Amelia, A. R., Gomesh, N., & Safwati, I. (2015). Indoor test performance of PV module through water cooling method. *Energy Procedia*, *79*, 604-611. doi.org/10.1016/j.egypro.2015.11.540.

Isaifan, R. J., Johnson, D., Ackermann, L., Figgis, B., & Ayoub, M. (2019). Evaluation of the adhesion forces between dust particles and photovoltaic module surfaces. *Solar Energy Materials and Solar Cells*, 191, 413-421, doi.org/10.1016/j.solmat.2018.11.031.

Ishaque, K., Salam, Z., & Taheri, H. (2011). Simple, fast and accurate two-diode model for photovoltaic modules. *Solar energy materials and solar cells*, *95*(2), 586-594. doi.org/10.1016/j.solmat.2010.09.023.

IWT 4.0, India water tool 4.0, 2023, *http://www.indiawatertool.in/*, (Access on 31st March,2023).

Jaiganesh, K., Reddy, K. B. S., Shobhitha, B. K. D., & Goud, B. D. (2022). Enhancing the efficiency of rooftop solar photovoltaic panel with simple cleaning mechanism. *Materials Today: Proceedings*, 51, 411-415, doi.org/10.1016/j.matpr.2021.05.565.

Jamil, B., Siddiqui, A. T., & Akhtar, N. (2016). Estimation of solar radiation and optimum tilt angles for south-facing surfaces in Humid Subtropical Climatic Region of India. *Engineering Science and Technology, an International Journal*, 19(4), 1826-1835, doi.org/10.1016/j.jestch.2016.10.004.

Jankovec, M., Galliano, F., Annigoni, E., Li, H. Y., Sculati-Meillaud, F., Perret-Aebi, L. E., ... & Topič, M. (2016). In-situ monitoring of moisture ingress in PV modules using digital humidity sensors. *IEEE journal of photovoltaics*, *6*(5), 1152-1159. doi:10.1109/ JPHOTOV.2016.2583779.

Jaszczur, M., Koshti, A., Nawrot, W., & Sędor, P. (2020). An investigation of the dust accumulation on photovoltaic panels. *Environmental Science and Pollution Research*, 27(2), 2001-2014, doi.org/10.1007/s11356-019-06742-2.

Jia, X., Klemeš, J. J., & Tan, R. R. (2021). Overview of Water Use in Renewable Electricity Generation. *Chemical Engineering Transactions*, 89, 403-408, doi: 10.3303/CET2189068.

Jin, Y., Behrens, P., Tukker, A., & Scherer, L. (2019). Water use of electricity technologies: A global meta-analysis. *Renewable and Sustainable Energy Reviews*, 115, 109391, doi.org/10.1016/j.rser.2019.109391.

Johnston, E., Szabo, P. S., & Bennett, N. S. (2021). Cooling silicon photovoltaic cells using finned heat sinks and the effect of inclination angle. *Thermal Science and Engineering Progress*, *23*, 100902. doi.org/10.1016/j.tsep.2021.100902.

Kazem, H. A., Chaichan, M. T., Al-Waeli, A. H., & Sopian, K. (2022). Effect of dust and cleaning methods on mono and polycrystalline solar photovoltaic performance: An indoor experimental study. *Solar Energy*, 236, 626-643, doi.org/10.1016/j.solener.2022.03.009.

Khalid, H. M., Rafique, Z., Muyeen, S. M., Raqeeb, A., Said, Z., Saidur, R., & Sopian, K. (2023). Dust accumulation and aggregation on PV panels: An integrated survey on impacts, mathematical models, cleaning mechanisms, and possible sustainable solution. *Solar Energy*, 251, 261-285, doi.org/10.1016/j.solener.2023.01.010.

Khan, F., Singh, S. N., & Husain, M. (2010). Effect of illumination intensity on cell parameters of a silicon solar cell. *Solar energy materials and solar cells*, 94(9), 1473-1476.

Khlifi, A., Khlifi, Y., & Elhafyani, M. L. (2023). Design and Realization of a Photovoltaic Tracer using DC/DC Converter. *Applied Solar Energy*, 59(6), 791-802, doi: 10.3103/S0003701X23601321.

Kinsey, G. S., & Edmondson, K. M. (2009). Spectral response and energy output of concentrator multijunction solar cells. *Progress in Photovoltaics: Research and Applications*, 17(5), 279-288, doi.org/10.1002/pip.875.

Kittel, C. (2005). *Introduction to solid state physics*. John Wiley & sons, inc.

KMC- *Kolkata Municipal Corporation, Government of West Bengal*, 2024, Fees and Charges for The Year of 2024- 2025, *https://www.kmcgov.in/KMCPortal/jsp/WaterSupplyFees.jsp.*

Kongtragool, B., & Wongwises, S. (2008). A four power-piston low-temperature differential Stirling engine using simulated solar energy as a heat source. *Solar Energy*, *82*(6), 493-500. doi.org/10.1016/j.solener.2007.12.005.

Konyu, M., Ketjoy, N., & Sirisamphanwong, C. (2020). Effect of dust on the solar spectrum and electricity generation of a photovoltaic module. *IET Renewable Power Generation*, 14(14), 2759-2764, doi.org/10.1049/iet-rpg.2020.0456.

Kumar, N. M., Reddy, P. R. K., & Praveen, K. (2017). Optimal energy performance and comparison of open rack and roof mount mono c-Si photovoltaic Systems. *Energy Procedia*, *117*, 136-144. doi.org/10.1016/j.egypro.2017.05.116 .

Kumar, N. M., Yadav, S. K., Chopra, S. S., Bajpai, U., Gupta, R. P., Padmanaban, S., & Blaabjerg, F. (2020). Operational performance of on-grid solar photovoltaic system integrated into pre-fabricated portable cabin buildings in warm and temperate climates. *Energy for Sustainable Development*, 57, 109-118, doi.org/10.1016/j.esd.2020.05.008.

Kumar, S., & P. B. L Chaurasia. (2014). Experimental Study on the Effect of Dust Deposition on Solar Photovoltaic Module in Jaipur (Rajasthan). *International Journal of Science and Research*, vol. 3, issue 6, pp.1690-1693.

Labour Commissionerate, Government of West Bengal, 2024, (Access on 31st March,2024). *https://wblc.gov.in/synopsys/January/2024,https://wblc.gov.in/sites/default/files/upload/min_wages/january-2024/6%20Circular%2031%20emp%202%20zones_0.pdf.*

Landrock, C., Omrane, B., Aristizabal, J., Kaminska, B., & Menon, C. (2011, May). An Improved light source using filtered tungsten lamps as an affordable solar simulator for testing of photovoltaic cells. In *2011 IEEE 17th International Mixed-Signals, Sensors and Systems Test Workshop* (pp. 153-158). *IEEE*. doi: 10.1109/IMS3TW.2011.25.

Lillo-Sánchez, L., López-Lara, G., Vera-Medina, J., Pérez-Aparicio, E., & Lillo-Bravo, I. (2021). Degradation analysis of photovoltaic modules after operating for 22 years. A case study with comparisons. *Solar Energy*, 222, 84-94, doi.org/10.1016/j.solener.2021.04.026.

Lisco, F., Bukhari, F., Uličná, S., Isbilir, K., Barth, K. L., Taylor, A., & Walls, J. M. (2020). Degradation of hydrophobic, anti-soiling coatings for solar module cover glass. *Energies*, 13(15), 3811, doi.org/10.3390/en13153811.

Maghami, M. R., Hizam, H., Gomes, C., Radzi, M. A., Rezadad, M. I., & Hajighorbani, S. (2016). Power loss due to soiling on solar module: A review. *Renewable and Sustainable Energy Reviews*, *59*, 1307-1316. doi.org/10.1016/j.rser.2016.01.044.

Mahato, M. K., & Singh, A. K. (2020). Evaluation of atmospheric dust deposition rates and their mineral characterization in copper and iron mining areas, Singhbhum, India. *Journal of the Air & Waste Management Association*, 70(12), 1378-1389, doi: 10.1080/10962247.2020.1818647.

Maka, A. O., & O'Donovan, T. S. (2019). Analysis of thermal response and electrical characterisation of triple-junction solar cells based on variable solar spectral irradiance and air mass. *Thermal Science and Engineering Progress*, 10, 269-279, doi.org/10.1016/j.tsep.2019.02.005.

Maka, A. O., & O'Donovan, T. S. (2022). Effect of thermal load on performance parameters of solar concentrating photovoltaic: high-efficiency solar cells. *Energy and Built Environment*, 3(2), 201-209, doi.org/10.1016/j.enbenv.2021.01.004.

Marion, B., Adelstein, J., Boyle, K. E., Hayden, H., Hammond, B., Fletcher, T., ... & Townsend, T. (2005, January). Performance parameters for grid-connected PV systems. *In Conference Record of the Thirty-first IEEE Photovoltaic Specialists Conference*, 2005. (pp. 1601-1606). *IEEE*, doi: 10.1109/PVSC.2005.1488451.

Martins, A. C., Chapuis, V., Virtuani, A., & Ballif, C. (2017, June). Ultra-lightweight PV module design for building integrated photovoltaics. *In 2017 IEEE 44th Photovoltaic Specialist Conference (PVSC)* (pp. 2104-2108). *IEEE*, doi: 10.1109/PVSC.2017.8366791.

Martins, A. C., Chapuis, V., Virtuani, A., Li, H. Y., Perret-Aebi, L. E., & Ballif, C. (2018). Thermo-mechanical stability of lightweight glass-free photovoltaic modules based on a composite substrate. *Solar Energy Materials and Solar Cells*, 187, 82-90, doi.org/10.1016/j.solmat.2018.07.015.

Mazumder, M., Horenstein, M. N., Stark, J. W., Girouard, P., Sumner, R., Henderson, B., ... & Sharma, R. (2013). Characterization of electrodynamic screen performance for dust removal from solar panels and solar hydrogen generators. *IEEE Transactions on industry applications*, 49(4), 1793-1800.

Mekhilef, S., Saidur, R., & Kamalisarvestani, M. (2012). Effect of dust, humidity and air velocity on efficiency of photovoltaic cells. *Renewable and sustainable energy reviews*, 16(5), 2920-2925, doi: 10.1016/j.rser.2012.02.012.

Mekhilef, S., Saidur, R., & Kamalisarvestani, M. (2012). Effect of dust, humidity and air velocity on efficiency of photovoltaic cells. *Renewable and sustainable energy reviews*, *16*(5), 2920-2925. doi.org/10.1016/j.rser.2012.02.012.

Minitab, LLC. (2021). Minitab. Retrieved from *https://www.minitab.com*

MNRE (2023). Ministry of New and Renewable Energy, Government of India, https://mnre.gov.in/year-wise-achievement/.

MNRE, 2023, *https://pib.gov.in/PressReleasePage.aspx?PRID=1992732*

MNRE, 2024, *https://mnre.gov.in/physical-progress/*

MOEF, 2022, Ministry of Environment, Forest and Climate Change, Annual Report 2023-24, *https://moef.gov.in/wp-content/uploads/2024/03/Annual-Report-English-2023-24.pdf*

Moharram, K. A., Abd-Elhady, M. S., Kandil, H. A., & El-Sherif, H. (2013). Influence of cleaning using water and surfactants on the performance of photovoltaic panels. *Energy Conversion and Management*, 68, 266-272, dx.doi.org/10.1016/j.enconman.2013.01.022.

Myyas, R. E. N., Al-Dabbasa, M., Tostado-Véliz, M., & Jurado, F. (2022). A novel solar panel cleaning mechanism to improve performance and harvesting rainwater. *Solar Energy*, 237, 19-28, doi.org/10.1016/j.solener.2022.03.068.

Najeeb, N. S., Soori, P. K., & Kumar, T. R. (2018, May). A low-cost and energy-efficient smart dust cleaning technique for solar panel system. *In 2018 International Conference on Smart Grid and Clean Energy Technologies (ICSGCE)* (pp. 125-129). *IEEE*.

Nakamoto, Y., & Eguchi, S. (2024). How do seasonal and technical factors affect generation efficiency of photovoltaic power plants? *Renewable and Sustainable Energy Reviews*, 199, 114441, doi.org/10.1016/j.rser.2024.114441.

Nasrin, R., Hasanuzzaman, M., & Rahim, N. A. (2018). Effect of high irradiation on photovoltaic power and energy. *International Journal of Energy Research*, 42(3), 1115-1131, doi: 10.1002/er.3907.

Nayan, M. F., & Ullah, S. S. (2015, September). Modelling of solar cell characteristics considering the effect of electrical and environmental parameters. In *2015 3rd International Conference on Green Energy and Technology (ICGET)* (pp. 1-6). *IEEE*.

Nguyen, T. P., Nguyen, H., Phan, V. H., & Ngo, H. Q. T. (2021). Modeling and practical implementation of motion controller for stable movement in a robotic solar panel dust-removal system. Energy Sources, *Part A: Recovery, Utilization, and Environmental Effects*, 1-23, doi.org/10.1080/15567036.2021.1934194.

Obiwulu, A. U., Chendo, M. A., Erusiafe, N., & Nwokolo, S. C. (2020). Implicit meteorological parameter-based empirical models for estimating back temperature solar modules under varying tilt-angles in Lagos, Nigeria. *Renewable Energy*, 145, 442-457, doi.org/10.1016/j.renene.2019.05.136.

Olorunfemi, B. O., Ogbolumani, O. A., & Nwulu, N. (2022). Solar panels dirt monitoring and cleaning for performance improvement: a systematic review on smart systems. *Sustainability*, 14(17), 10920, doi.org/10.3390/su141710920.

Paudyal, B. R., & Shakya, S. R. (2016). Dust accumulation effects on efficiency of solar PV modules for off grid purpose: A case study of Kathmandu. *Solar Energy*, 135, 103-110, dx.doi.org/10.1016/j.solener.2016.05.046.

Peng, J., Lu, L., & Wang, M. (2019). A new model to evaluate solar spectrum impacts on the short circuit current of solar photovoltaic modules. *Energy*, 169, 29-37, doi.org/10.1016/j.energy.2018.12.003.

Pouladian-Kari, A., Eslami, S., Tadjik, A., Kirchner, L., Pouladian-Kari, R., & Golshanfard, A. (2022). A novel solution for addressing the problem of soiling and improving performance of PV solar systems. *Solar Energy*, 241, 315-326.

Priyadarshini, S., Prakash, A., Gupta, S., Mishra, A., & Payal, H. (2023). Fabrication and characterization of epoxy solar glass. *Materials Today: Proceedings*, 80, 552-557, doi.org/10.1016/j.matpr.2022.11.046.

PVsyst (2023), Version 7.4, *https://www.pvsyst.com/.*

Qasem, H., Betts, T. R., Müllejans, H., AlBusairi, H., & Gottschalg, R. (2014). Dust-induced shading on photovoltaic modules. *Progress in Photovoltaics: Research and Applications*, *22*(2), 218-226. doi: 10.1002/pip.2230.

Qu, H., & Li, X. (2019). Temperature dependency of the fill factor in PV modules between 6 and 40 C. *Journal of Mechanical Science and Technology*, 33(4), 1981-1986, DOI 10.1007/s12206-019-0348-4.

Quan, Z., Lu, H., Zhao, W., Zheng, C., Zhu, Z., Qin, J., & Yue, M. (2022). A review of dust deposition mechanism and self-cleaning methods for solar photovoltaic modules. *Coatings*, 13(1), 49, doi.org/10.3390/coatings13010049.

Rahman, M. M., Hasanuzzaman, M., & Rahim, N. A. (2015). Effects of various parameters on PV-module power and efficiency. *Energy Conversion and Management*, *103*, 348-358. doi.org/10.1016/j.enconman.2015.06.067.

Ramkiran, B., Sundarabalan, C. K., & Sudhakar, K. (2020). Performance evaluation of solar PV module with filters in an outdoor environment. *Case Studies in Thermal Engineering*, *21*, 100700. doi.org/10.1016/j.csite.2020.100700.

Roberts, T., Mosbrucker, G., Petersen, J., & Osman, M. (2014, July). Flexible solar simulator for renewable energy instruction laboratory. In *2014 IEEE Conference on Technologies for Sustainability (SusTech)* (pp. 264-268). *IEEE*. doi: 10.1109/SusTech.2014.7046255.

Said, S. A., Hassan, G., Walwil, H. M., & Al-Aqeeli, N. (2018). The effect of environmental factors and dust accumulation on photovoltaic modules and dust-accumulation mitigation strategies. *Renewable and Sustainable Energy Reviews*, 82, 743-760, dx.doi.org/10.1016/j.rser.2017.09.042.

Sayyah, A., Horenstein, M. N., Mazumder, M. K., & Ahmadi, G. (2016). Electrostatic force distribution on an electrodynamic screen. *Journal of Electrostatics*, 81, 24-36, doi.org/10.1016/j.elstat.2016.02.004.

Sharma, R., & Goel, S. (2017). Performance analysis of a 11.2 kWp roof top grid-connected PV system in Eastern India. *Energy Reports*, 3, 76-84, dx.doi.org/10.1016/j.egyr.2017.05.001.

Sharma, S., Rishi, R., Tarun, Sahdev, R. K., & Tiwari, S. (2023). Impact of Temperature Variation from 300 to 400 K on the Performance of Silicon Solar Cell. *Applied Solar Energy*, 59(6), 803-810, doi: 10.3103/S0003701X23600935.

Sharma, V., & Chandel, S. S. (2013). Performance analysis of a 190 kWp grid interactive solar photovoltaic power plant in India. *Energy*, 55, 476-485, doi.org/10.1016/j. energy.2013.03.075.

Shukla, A. K., Sudhakar, K., & Baredar, P. (2016). Simulation and performance analysis of 110 kWp grid-connected photovoltaic system for residential building in India: A comparative analysis of various PV technology. *Energy Reports*, 2, 82-88, doi.org/10.1016/ j.egyr.2016.04.001.

Siddiqui, M. U., Arif, A. F. M., Bilton, A. M., Dubowsky, S., & Elshafei, M. (2013). An improved electric circuit model for photovoltaic modules based on sensitivity analysis. *Solar Energy*, 90, 29-42.

Siefer, G., & Bett, A. W. (2014). Analysis of temperature coefficients for III–V multi-junction concentrator cells. *Progress in Photovoltaics: Research and Applications*, 22(5), 515-524.

Sisodia, A. K., & Mathur, R. K. (2020). Performance analysis of photovoltaic module by dust deposition in Western Rajasthan. *Indian J Sci Technol*, 13(08), 921-933, doi: 10.17485/ijst/2020/v13i08/149928.

Skoplaki, E., & Palyvos, J. A. (2009). On the temperature dependence of photovoltaic module electrical performance: A review of efficiency/power correlations. *Solar energy*, *83*(5), 614-624. doi.org/10.1016/j.solener.2008.10.008.

Soulayman, S., & Hababa, M. A. (2017). The Solar Panel's Performance Dependence on Incident Radiation Intensity and its Surface Temperature. *Journal of Solar Energy Research Updates*, 4, 9-17.

Sugiartha, N., Ardana, I. G. N., Sugina, I. M., Widiantara, I. B. G., Suparta, I. N., & Adi, I. K. (2020, February). Preliminary design and test of a water spray solar panel cleaning system. *In Journal of Physics: Conference Series* (Vol. 1450, No. 1, p. 012108). *IOP Publishing*, doi:10.1088/1742-6596/1450/1/012108.

Sukhatme, S. P., J. K. Nayak. *SOLAR ENERGY*. United States: *Tata McGraw-Hill*, 2017.

Syafiq, A., Pandey, A. K., Adzman, N. N., & Abd Rahim, N. (2018). Advances in approaches and methods for self-cleaning of solar photovoltaic panels. *Solar Energy*, 162, 597-619, doi.org/10.1016/j.solener.2017.12.023.

Tina, G. M., & Scrofani, S. (2008, May). Electrical and thermal model for PV module temperature evaluation. In *MELECON 2008-The 14th IEEE Mediterranean Electrotechnical Conference* (pp. 585-590). IEEE. doi: 10.1109/MELCON.2008.4618498.

Tripathi, A. K., Ray, S., Aruna, M., & Prasad, S. (2021). Evaluation of solar PV panel performance under humid atmosphere. *Materials Today: Proceedings*, 45, 5916-5920, doi.org/10.1016/j.matpr. 2020.08.775.

Tyagi, V. V., Rahim, N. A., Rahim, N. A., Jeyraj, A., & Selvaraj, L. (2013). Progress in solar PV technology: Research and achievement. *Renewable and sustainable energy reviews*, *20*, 443-461. doi.org/10.1016/j.rser.2012.09.028.

Vasisht, M. S., Srinivasan, J., & Ramasesha, S. K. (2016). Performance of solar photovoltaic installations: Effect of seasonal variations. *Solar Energy*, 131, 39-46, dx.doi.org/10.1016/j.solener.2016.02.013.

Vyas, M., Chowdhury, S., Verma, A., & Jain, V. K. (2022). Solar Photovoltaic Tree: Urban PV power plants to increase power to land occupancy ratio. *Renewable Energy*, 190, 283-293, doi.org/10.1016/j.renene.2022.03.129.

Wakim, F. (1981). Introduction of PV power generation to Kuwait. *Kuwait Institute for Scientific Researchers*, Kuwait City, 204.

WBSEDCL-West Bengal State Electricity Distribution Company Limited, Government of West Bengal Enterprise, 2023, *https://www.wbsedcl.in/irj/go/km/docs/internet/new_website /pdf/Tariff _Volumn/Tariff_chart_dated_30.03.2023_for_the_year_2023-24_18_04.pdf.*

Wen, C., Fu, C., Tang, J., Liu, D., Hu, S., & Xing, Z. (2012). The influence of environment temperatures on single crystalline and polycrystalline silicon solar cell performance. *Science China Physics, Mechanics and Astronomy*, 55, 235-24, doi.org/10.1007/s11433-011-4619-z.

WRIS, Water Resources Information System, 2023, Ministry of Jal Shakti, Government of India, *https://wdo.indiawris.gov.in/.*

Yazdani, H., & Yaghoubi, M. (2022). Dust deposition effect on photovoltaic modules performance and optimization of cleaning period: A combined experimental–numerical study. *Sustainable Energy Technologies and Assessments*, 51, 101946, doi.org/10.1016/j.seta.2021.101946.

Younis, A., & Onsa, M. (2022). A brief summary of cleaning operations and their effect on the photovoltaic performance in Africa and the Middle East. *Energy Reports*, 8, 2334-2347, doi.org/10.1016/j.egyr.2022.01.155.

Zhao, W., Lv, Y., Wei, Z., Yan, W., & Zhou, Q. (2021). Review on dust deposition and cleaning methods for solar PV modules. *Journal of Renewable and Sustainable Energy*, 13(3), doi.org/10.1063/5.0053866.

ANNEXURE-I

Arduino Programme for Relay Module Operation

```
void setup ()
{
 // put your setup code here, to run once:

//digitalWrite (LED_BUILTIN, HIGH); pinMode (LED_BUILTIN, OUTPUT);

//for relay pin: 5, 3,4,1,2

pinMode (34, OUTPUT);
pinMode (36, OUTPUT);
pinMode (37, OUTPUT);
pinMode (38, OUTPUT);
pinMode (39, OUTPUT);

//for relay pin: 15, 16,13,14,12

pinMode (24, OUTPUT);
pinMode (25, OUTPUT);
pinMode (26, OUTPUT);
pinMode (27, OUTPUT);
pinMode (29, OUTPUT);

// for power supply pin:

pinMode (22, OUTPUT);
pinMode (40, OUTPUT);
digitalWrite (22, LOW);
digitalWrite (40, HIGH);

}

void loop()
 {
 // put your main code here, to run repeatedly:

digitalWrite(34, HIGH);
digitalWrite(36, HIGH);
digitalWrite(37, HIGH);
digitalWrite(38, HIGH);
digitalWrite(39, HIGH);
digitalWrite(24, HIGH);
digitalWrite(25, HIGH);
digitalWrite(26, HIGH);
digitalWrite(27, HIGH);
digitalWrite(29, HIGH);
```

```
 delay(1200000);

  int var=0;
while (var<2)
{

digitalWrite (34, LOW);
digitalWrite (36, LOW);
digitalWrite (37, LOW);
digitalWrite (38, LOW);
digitalWrite (39, LOW);
digitalWrite (24, LOW);
digitalWrite (25, LOW);
digitalWrite (26, LOW);
digitalWrite (27, LOW);
digitalWrite (29, LOW);

 delay (120000);

digitalWrite (34, HIGH);
digitalWrite (36, HIGH);
digitalWrite (37, HIGH);
digitalWrite (38, HIGH);
digitalWrite (39, HIGH);
digitalWrite (24, HIGH);
digitalWrite (25, HIGH);
digitalWrite (26, HIGH);
digitalWrite (27, HIGH);
digitalWrite (29, HIGH);

delay (120000);

var++;
}

//digitalWrite (LED_BUILTIN, LOW);
// turn the LED off by making the voltage LOW

}
```

ANNEXURE-II

Table: PVsyst model output data of different parameter of project used solar PV panel

Radiation (W/m^2)	Temperature (°C)	V_{OC} (V)	I_{SC} (A)	P_{max} (W)	FF	Efficiency (η%)
200	20	6.8245	0.1656	0.8959	0.7927	3.5218
	30	6.6181	0.1666	0.8654	0.7849	3.4020
	40	6.4137	0.1676	0.8344	0.7762	3.2800
	50	6.2111	0.1686	0.8035	0.7672	3.1585
	60	6.0104	0.1696	0.7726	0.7580	3.0374
400	20	7.0263	0.3311	1.8352	0.7888	7.2143
	30	6.8283	0.3331	1.7754	0.7805	6.9791
	40	6.6321	0.3351	1.7155	0.7719	6.7439
	50	6.438	0.3371	1.6556	0.7628	6.5082
	60	6.2458	0.3391	1.5954	0.7533	6.2719
600	20	7.1446	0.4966	2.7737	0.7818	10.9038
	30	6.9513	0.4995	2.6848	0.7732	10.5542
	40	6.7601	0.5025	2.5961	0.7642	10.2056
	50	6.5708	0.5055	2.5075	0.7549	9.8573
	60	6.3837	0.5085	2.4191	0.7452	9.5098
800	20	7.2287	0.662	3.7008	0.7733	14.5482
	30	7.0388	0.666	3.5838	0.7645	14.0884
	40	6.851	0.67	3.4668	0.7553	13.6286
	50	6.6653	0.674	3.3500	0.7457	13.1693
	60	6.4817	0.678	3.2334	0.7358	12.7109
1000	20	7.2959	0.8267	4.6119	0.7647	18.1298
	30	7.1238	0.8324	4.4658	0.7531	17.5557
	40	6.9264	0.8372	4.3206	0.7451	16.9846
	50	6.7384	0.8416	4.1760	0.7364	16.4163
	60	6.5504	0.8481	4.0320	0.7258	15.8502
1200	20	7.3471	0.993	5.5014	0.7541	21.6269
	30	7.162	0.999	5.3278	0.7446	20.9441
	40	6.9791	1.005	5.1543	0.7349	20.2622
	50	6.7983	1.011	4.9815	0.7248	19.5828
	60	6.6197	1.017	4.8100	0.7145	18.9087
1400	20	7.392	1.1585	6.3682	0.7436	25.0342
	30	7.2088	1.1655	6.1665	0.7339	24.2414
	40	7.0277	1.1725	5.9655	0.7240	23.4510
	50	6.8488	1.1795	5.7650	0.7137	22.6630
	60	6.6721	1.1865	5.5665	0.7032	21.8825
1600	20	7.4308	1.324	7.2107	0.7329	28.3462
	30	7.2492	1.332	6.9811	0.7230	27.4437
	40	7.0698	1.34	6.7526	0.7128	26.5453
	50	6.8925	1.348	6.5249	0.7023	25.6500
	60	6.7174	1.356	6.2992	0.6915	24.7628

PVsyst Simulation Model - 1

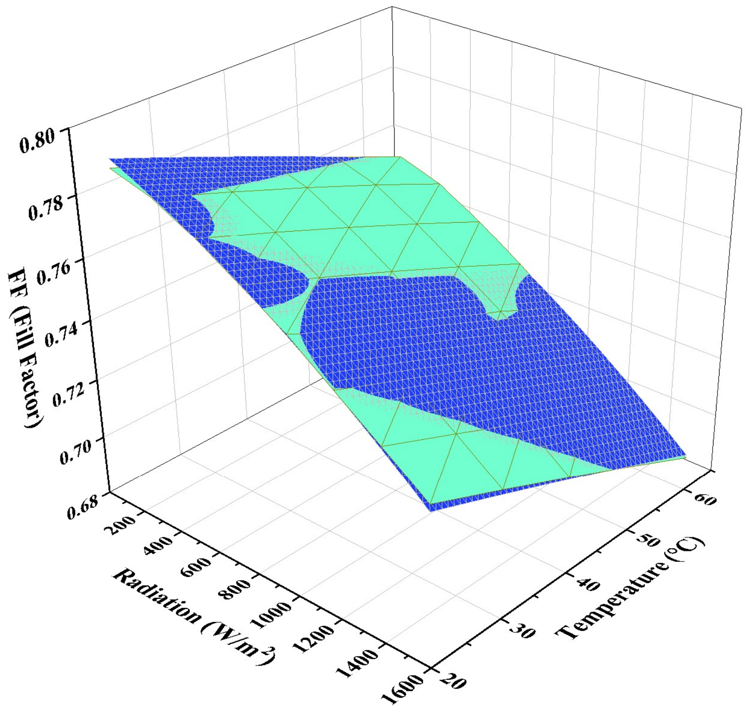

Fig.4.19 PVsyst simulation based FF model with respect to radiation and Temperature

$$Z = z0 + A \times exp^{\left(\left(-0.5\times\left(\frac{(x-xc)}{w1}\right)^2\right)-\left(0.5\times\left(\frac{(y-yc)}{w2}\right)^2\right)\right)} \qquad (1)$$

Table 2 Parameter value of nonlinear surface fit regression for FF model

Parameter	z0	A	xc	w1	yc	w2
Value	-30.66984	31.62167	-1005.17609	35903.16714	-289.42466	3301.74472

R-Square (COD) value of the simulation model is 0.99809 and Adj. R-Square value is 0.99781.

PVsyst Simulation Model - 2

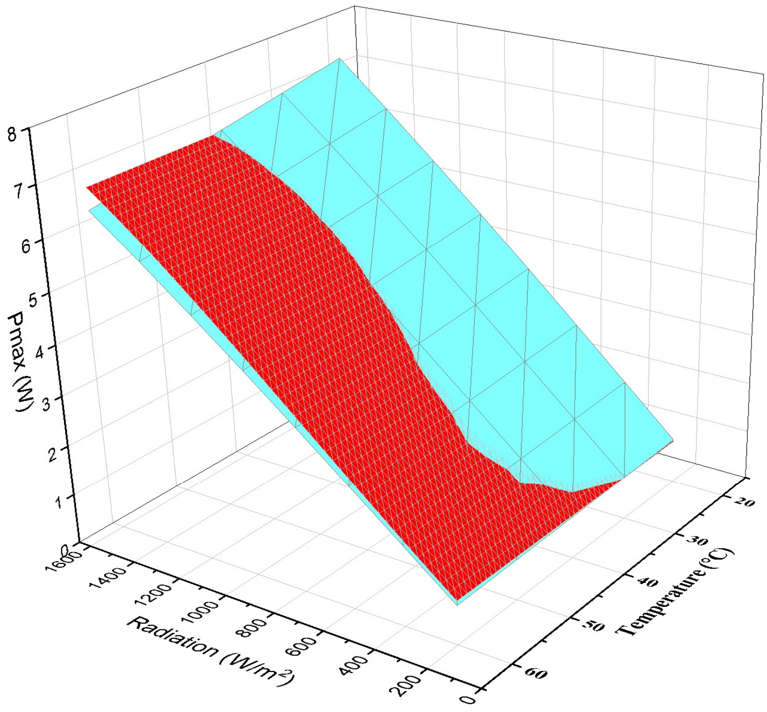

Fig.2 PVsyst simulation based maximum power (P_{max}) model with respect to radiation and Temperature

$$Z = z0 + A \times exp^{\left(\left(-0.5\times\left(\frac{(x-xc)}{w1}\right)^2\right)-\left(0.5\times\left(\frac{(y-yc)}{w2}\right)^2\right)\right)} \quad (2)$$

Table 4.3 Parameter value of nonlinear surface fit regression for PVsyst simulation P_{max} model

Parameter	z0	A	xc	w1	yc	w2
Value	-5.12357	13.84305	2659.23185	1899.51685	1.45624E148	4.7389E150

R-Square (COD) value of the simulation model is 0.98879 and Adj. R-Square value is 0.98714.

PVsyst Simulation Model - 3

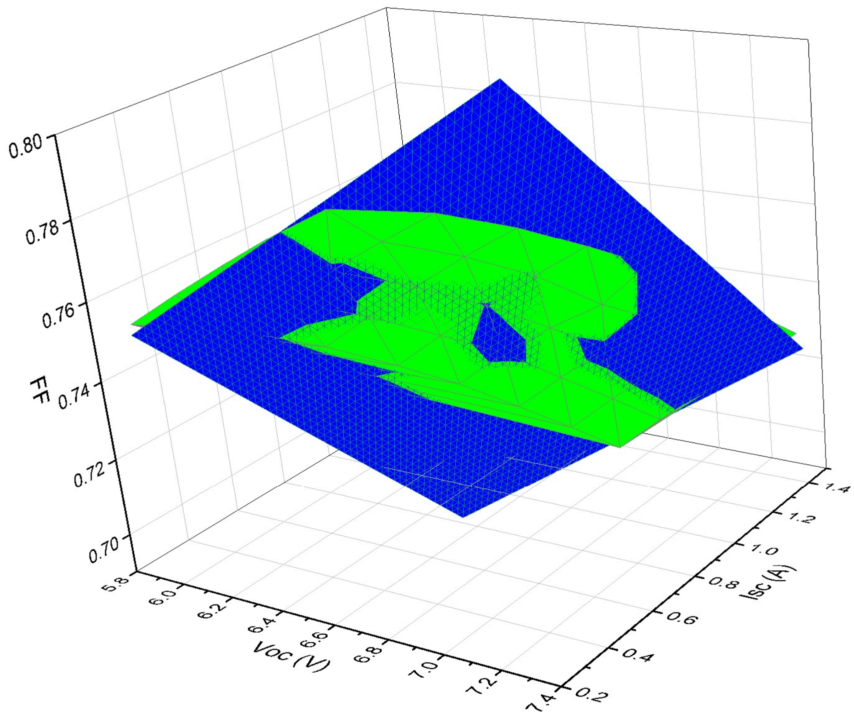

Fig. 3 PVsyst simulation based FF model with respect to open circuit voltage (Voc) and short circuit current(Isc)

$$Z = z0 + A \times exp^{\left(\left(-0.5 \times \left(\frac{(x-xc)}{w1}\right)^2\right) - \left(0.5 \times \left(\frac{(y-yc)}{w2}\right)^2\right)\right)} \quad (3)$$

Table 3 Parameter value of nonlinear surface fit regression for PVsyst simulation FF model

Parameter	z0	A	xc	w1	yc	w2
Value	-1554.2141	3617.7727	26134.8505	29093.6985	-17063.0923	18166.4438

R-Square (COD) value of the simulation model is 0.99745 and Adj. R-Square value is 0.99707.

ANNEXURE - III

Table 1. Total maximum power generation with cumulative dust deposition in summer season

Tilt angle of solar panels (∠)	Parameters	Day-1	Day-7	Day-14	Day-21	Day-28
0°	Dust deposition (gm/m^2)	0	7.4213	9.9095	11.0906	11.5079
	Total P_{max} generation (W-h)	17.6782	116.8370	215.2174	303.0763	385.5332
10°	Dust deposition (gm/m^2)	0	6.0197	8.2520	9.6417	10.4095
	Total P_{max} generation (W-h)	19.0158	124.632	228.2476	319.7635	406.4719
22.5°	Dust deposition (gm/m^2)	0	5.5079	8.1575	9.3543	9.6221
	Total P_{max} generation (W-h)	17.3212	116.9739	217.2066	306.7594	391.1363
30°	Dust deposition (gm/m^2)	0	4.6300	7.8898	9.1102	9.3110
	Total P_{max} generation (W-h)	16.4361	109.6515	201.4886	287.3676	368.1681
40°	Dust deposition (gm/m^2)	0	4.9173	7.4882	9.0394	9.6654
	Total P_{max} generation (W-h)	15.4265	104.9658	191.4419	272.6185	348.8843
50°	Dust deposition (gm/m^2)	0	4.4213	7.3937	8.4016	8.8819
	Total P_{max} generation (W-h)	14.1412	96.4586	174.8760	247.9624	317.6413
60°	Dust deposition (gm/m^2)	0	3.0315	6.5551	7.3740	7.9567
	Total P_{max} generation (W-h)	13.5116	89.2665	161.7822	230.4306	294.6548
70°	Dust deposition (gm/m^2)	0	3.8504	5.6575	6.4410	7.0827
	Total P_{max} generation (W-h)	10.9361	76.7745	140.5097	203.5142	262.8876
80°	Dust deposition (gm/m^2)	0	3.5079	5.4882	6.3661	6.2874
	Total P_{max} generation (W-h)	9.2704	67.1551	124.5201	181.9498	236.4862
90°	Dust deposition (gm/m^2)	0	3.2598	5.3543	6.8268	6.3465
	Total P_{max} generation (W-h)	7.6664	53.8035	103.0231	153.0945	201.2257

Table 2. Total maximum power generation with cumulative dust deposition in monsoon season

Tilt angle of solar panels (∠)	Parameters	Day-1	Day-7	Day-14	Day-21	Day-28
0°	Dust deposition (gm/m^2)	0	2.1102	1.1043	2.1752	0.9626
	Total P_{max} generation (W-h)	14.8049	67.6524	126.2407	185.4538	256.5094
10°	Dust deposition (gm/m^2)	0	2.0866	0.9350	2.0354	0.8346
	Total P_{max} generation (W-h)	15.3142	70.2255	130.5761	188.8343	261.9118
22.5°	Dust deposition (gm/m^2)	0	1.9685	1.0236	1.5807	0.9154
	Total P_{max} generation (W-h)	15.9151	66.9343	124.6065	182.7998	253.2228
30°	Dust deposition (gm/m^2)	0	1.9264	0.9311	0.5177	0.9488
	Total P_{max} generation (W-h)	14.0229	61.0745	116.6604	172.8315	239.8845
40°	Dust deposition (gm/m^2)	0	1.5736	1.1575	1.9154	0.6362
	Total P_{max} generation (W-h)	12.4419	54.2390	105.7161	158.3523	222.2518
50°	Dust deposition (gm/m^2)	0	1.1654	0.8327	3.1319	0.5531
	Total P_{max} generation (W-h)	9.8893	47.9476	96.8912	148.8874	210.4420
60°	Dust deposition (gm/m^2)	0	1.3701	0.7205	2.1437	0.5335
	Total P_{max} generation (W-h)	8.5603	41.3842	85.2654	131.7213	184.6777
70°	Dust deposition (gm/m^2)	0	1.2224	0.7559	1.8799	0.5906
	Total P_{max} generation (W-h)	7.0132	36.3958	74.4062	115.8391	163.7811
80°	Dust deposition (gm/m^2)	0	0.6882	0.6555	0.8346	0.4587
	Total P_{max} generation (W-h)	5.6786	34.5929	68.8676	104.7527	146.1106
90°	Dust deposition (gm/m^2)	0	0.4370	0.4705	0.7720	0.2047
	Total P_{max} generation (W-h)	4.9247	29.8105	59.7604	92.1362	125.7070

Table 3. Day wise power generation (W-h) in monsoon season

Day	**∠0°**	**∠10°**	**∠22.5°**	**∠30°**	**∠40°**	**∠50°**	**∠60°**	**∠70°**	**∠80°**	**∠90°**
Day-1	14.805	15.314	15.915	14.023	12.442	9.889	8.560	7.013	5.679	4.925
Day-2	6.945	7.159	6.557	5.989	5.198	4.506	3.946	3.588	3.528	3.052
Day-3	9.589	10.118	9.246	9.038	7.257	6.872	5.575	5.042	4.804	4.297
Day-4	11.432	12.025	10.852	10.010	8.534	8.030	6.465	5.378	5.837	4.735
Day-5	3.658	3.764	3.380	2.853	2.799	2.658	2.437	2.219	2.876	2.470
Day-6	11.490	11.890	11.342	9.658	8.843	7.122	6.421	6.018	5.965	4.695
Day-7	9.734	9.955	9.642	9.504	9.165	8.871	7.980	7.137	5.904	5.637
Day-8	10.333	10.395	10.122	10.004	9.865	9.471	8.580	7.232	5.914	5.537
Day-9	9.195	9.171	8.929	8.783	7.262	6.905	5.580	4.717	4.810	4.546
Day-10	9.432	9.516	9.152	9.028	8.321	8.034	7.117	6.165	5.378	4.837
Day-11	3.652	3.746	3.399	2.977	2.766	2.735	2.463	2.248	2.896	1.973
Day-12	6.212	6.863	6.570	6.285	5.582	5.310	4.189	3.655	3.446	2.968
Day-13	9.703	10.065	9.668	9.238	8.835	8.105	7.978	6.621	5.568	5.026
Day-14	10.061	10.594	9.832	9.271	8.844	8.384	7.974	7.373	6.263	5.063
Day-15	9.595	8.111	8.929	8.783	7.262	7.805	5.580	5.717	4.810	4.546
Day-16	9.524	9.943	9.899	9.088	8.586	8.641	7.878	8.005	6.819	4.899
Day-17	9.432	9.516	9.152	8.728	8.227	8.034	7.297	6.465	5.378	5.337
Day-18	5.312	4.906	4.389	4.957	4.806	4.705	4.443	4.228	3.886	3.473
Day-19	8.432	8.716	8.852	8.228	8.127	7.534	7.097	6.165	5.278	5.037
Day-20	7.184	7.111	6.929	6.583	5.862	5.805	5.580	3.717	3.810	3.546
Day-21	9.734	9.955	10.042	9.804	9.765	9.471	8.580	7.137	5.904	5.537
Day-22	9.734	9.955	10.142	10.004	9.865	9.471	8.580	7.037	5.904	5.537
Day-23	11.669	11.909	10.798	10.739	10.330	10.319	8.914	8.158	6.924	4.103
Day-24	12.835	14.048	13.879	12.881	12.337	11.693	8.958	8.591	7.610	4.832
Day-25	8.092	7.965	7.652	6.688	6.255	5.885	5.588	5.331	5.198	4.776
Day-26	9.132	9.166	8.852	8.528	8.127	7.534	7.197	6.445	5.388	5.847
Day-27	6.722	6.926	6.399	5.987	5.746	5.675	4.633	4.328	4.226	3.973
Day-28	12.871	13.109	12.701	12.226	11.238	10.978	9.087	8.053	6.109	4.503

Table 4. Day wise dust deposition (gm/m^2) in monsoon season

Day	∠0°	∠10°	∠22.5°	∠30°	∠40°	∠50°	∠60°	∠70°	∠80°	∠90°
Day-1	0	0	0	0	0	0	0	0	0	0
Day-2	0.187	0.088	0.068	0.029	0.088	0.049	0.088	0.068	0.068	0.068
Day-3	0.701	0.603	0.524	0.405	0.366	0.326	0.326	0.307	0.247	0.149
Day-4	0.829	0.750	0.651	0.572	0.513	0.493	0.572	0.553	0.434	0.375
Day-5	1.394	1.196	1.078	0.900	0.802	0.644	0.703	0.703	0.604	0.506
Day-6	0.495	0.455	0.376	0.317	0.278	0.238	0.258	0.219	0.080	0.120
Day-7	2.110	2.087	1.969	1.926	1.574	1.165	1.370	1.222	0.688	0.437
Day-8	1.595	1.457	1.418	1.299	1.201	1.063	0.924	0.885	0.747	0.628
Day-9	1.803	1.685	1.567	1.507	1.448	1.409	1.350	1.093	0.955	0.777
Day-10	2.025	1.926	1.808	1.690	1.611	1.512	1.413	1.275	1.137	1.078
Day-11	2.061	1.805	1.687	1.509	1.450	1.351	1.292	1.213	1.075	1.075
Day-12	1.306	1.385	1.029	0.792	1.385	1.128	1.148	0.950	0.812	0.713
Day-13	0.389	0.389	0.231	0.231	0.389	0.172	0.172	0.270	0.191	0.211
Day-14	1.104	0.935	1.024	0.931	1.157	0.833	0.720	0.756	0.656	0.470
Day-15	1.125	0.928	0.809	0.770	0.691	0.809	0.770	0.730	0.612	0.513
Day-16	1.548	1.448	1.310	1.152	1.290	1.211	1.113	1.034	0.955	0.856
Day-17	1.299	1.260	1.082	0.964	0.628	0.984	1.003	0.826	0.767	0.688
Day-18	0.556	0.398	0.319	0.200	0.102	0.220	0.200	0.398	0.378	0.279
Day-19	0.329	0.290	0.211	0.132	0.112	0.290	0.231	0.290	0.290	0.231
Day-20	0.759	0.522	0.443	0.404	0.305	0.522	0.443	0.522	0.502	0.502
Day-21	2.175	2.035	1.581	0.518	1.915	3.132	2.144	1.880	0.835	0.772
Day-22	1.416	1.239	1.041	0.883	0.528	1.002	0.824	0.923	0.726	0.568
Day-23	0.348	0.288	0.209	0.150	0.111	0.131	0.052	0.229	0.288	0.288
Day-24	0.430	0.370	0.272	0.213	0.193	0.272	0.272	0.331	0.370	0.370
Day-25	0.841	0.703	0.565	0.506	0.446	0.624	0.565	0.762	0.703	0.703
Day-26	1.208	1.050	0.912	0.774	0.676	0.873	0.833	0.794	0.735	0.597
Day-27	0.603	0.563	0.445	0.386	0.326	0.307	0.386	0.425	0.366	0.307
Day-28	1.190	1.013	0.836	0.712	0.577	0.474	0.395	0.413	0.301	0.205

Table 5. Total maximum power generation with cumulative dust deposition in winter season

Tilt angle of solar panels (∠)	Parameters	Day-1	Day-7	Day-14	Day-21	Day-28
0°	Dust deposition (gm/m^2)	0	7.1299	8.7815	10.2382	11.9823
	Total P_{max} generation (W-h)	12.8104	80.8950	143.9104	198.5222	253.1151
10°	Dust deposition (gm/m^2)	0	6.7717	8.0217	9.5177	11.3071
	Total P_{max} generation (W-h)	14.4322	86.7052	155.1020	215.4899	275.4320
22.5°	Dust deposition (gm/m^2)	0	5.9449	7.3209	8.2736	10.6004
	Total P_{max} generation (W-h)	15.3688	90.5396	163.0999	227.1167	292.4018
30°	Dust deposition (gm/m^2)	0	5.4697	6.8327	7.9980	9.2146
	Total P_{max} generation (W-h)	16.0258	98.6658	180.5160	251.9268	326.0078
40°	Dust deposition (gm/m^2)	0	4.7232	6.6693	7.8209	8.1165
	Total P_{max} generation (W-h)	15.4186	96.3909	176.6329	246.7793	317.9131
50°	Dust deposition (gm/m^2)	0	4.3150	5.1634	6.6752	7.5217
	Total P_{max} generation (W-h)	14.9486	92.7829	170.5093	238.2865	307.4062
60°	Dust deposition (gm/m^2)	0	4.1260	5.8386	6.0807	7.2264
	Total P_{max} generation (W-h)	13.9557	88.4586	163.4003	226.0592	292.6994
70°	Dust deposition (gm/m^2)	0	3.5472	5.0886	5.4232	5.7087
	Total P_{max} generation (W-h)	13.3198	84.9450	154.4622	213.0824	278.1120
80°	Dust deposition (gm/m^2)	0	3.4244	4.0807	4.9685	5.5768
	Total P_{max} generation (W-h)	12.7481	82.5621	146.8435	200.6828	256.0225
90°	Dust deposition (gm/m^2)	0	2.9961	3.6988	4.7091	5.3228
	Total P_{max} generation (W-h)	11.9821	74.4871	131.2657	181.5343	231.4896

ANNEXURE - IV

Table 1. Clean Loss Factor differential data in different tilt angle

Cleaning Freq.(Day) -	∠0°	∠10°	∠22.5°	∠30°	∠40°	∠50°	∠60°	∠70°	∠80°	∠90°
7	-971	-772	-770	-809	-941	-1000	-1028	-1030	-1061	-1073
14	-105	63	45	17	51	-24	-3	-25	-191	-237
21	582	852	1099	799	549	320	376	369	87	157
28	866	1142	1369	978	746	496	537	455	316	334

Table 2. Capacity Utilisation Factor (CUF) data in different tilt angle

Cleaning Freq.(Day) -	∠0°	∠10°	∠22.5°	∠30°	∠40°	∠50°	∠60°	∠70°	∠80°	∠90°
7	11.60	12.59	12.68	12.42	11.21	9.23	8.45	7.12	5.66	4.52
14	11.19	12.23	12.36	12.08	10.59	8.64	7.78	6.49	5.25	4.16
21	10.41	11.28	10.97	11.14	10.12	8.42	7.50	6.18	5.13	3.85
28	10.11	10.97	10.70	11.01	9.96	8.30	7.41	6.21	4.92	3.73

Table 3. Performance Ratio (PR) data in different tilt angle

Cleaning Freq.(Day) -	∠0°	∠10°	∠22.5°	∠30°	∠40°	∠50°	∠60°	∠70°	∠80°	∠90°
7	85.33	87.43	87.64	86.47	79.99	75.88	73.20	73.32	74.59	75.67
14	82.06	84.72	84.60	83.86	76.93	69.62	68.64	67.21	67.93	68.56
21	76.64	78.09	75.07	77.48	73.59	68.25	67.14	64.60	66.14	63.31
28	74.89	76.42	73.83	77.32	73.84	68.69	68.11	66.56	64.66	62.94

Paper Publications

A review of the change in performance of photovoltaic panels due to dust accumulation- Challenges and their solution

Tarak Nath Chell*, Ratan Mandal, Tushar Jash

School of Energy Studies, Jadavpur University, Kolkata, India

**Corresponding Author: Tel:(+91) 9732107019 Email: talk2tarak@gmail.com*

Abstract:

In India, growing energy demand has increased the interest in photovoltaic solar power, with an aspect of environmental concerns, as a promising renewable energy source. The national solar mission of India has enhanced the targets of 20 GW to 100 GW of solar power installation by 2022. The primary disadvantage of a photovoltaic(PV) system is restricted efficiency the range of which lies between 12%-20% and the amount of power generated is greatly influenced by different environmental conditions. Dust accumulation on solar photovoltaic panel is a major problem which hampers the conversion efficiency. A number of techniques has been used for reducing dust deposition like regular manual washing, increasing inclination angle, using anti reflecting coating, fluoropolymer coating, mechanical dust removal, ultrasonic driving etc., but some of these techniques are either expensive or are not feasible based on the location of installation. This study attempts to discuss some of the alleviation techniques to enhance the performance efficiency of photovoltaic panels.

Further this study attempts to propose the most feasible techniques suitable for the climatic condition for region of Kolkata.

Keywords: PV performance, Dust deposition, Dust removable techniques, Environmental factor.

Introduction

The modern era depicted rapid increase in the energy consumption due to population growth and modern lifestyle. Especially in India energy crisis is a vital problem and fossil fuel serves as the major component to meet this demand. However clean energy generation from solar photovoltaic is a favorable solution to meet the energy demand without hampering the ecosystem. Generally solar photovoltaic modules are installed in ground mounting structure or building rooftops, however due to outdoor environment mainly dust formation on panel surface is affect the performance of PV power generation. Dust deposition for long period harms the layer of the solar panel, bring about less yield and reducing longevity (Said *et al.*, 2014). The output power losses of the solar panels can be kept away from if modules are cleaned intermittently (Tylim, 2013).

The research works discussed in this paper reveals how the performance of photovoltaic modules are impacted by the deposition of dust and the techniques that can help to enhance the module efficacy for a particular geographical location and weather condition. However, it does not discuss or specify any technique that is more appropriate for the city conditions. This study aims at paving the way for further research in this

Indian J. of Environmental Protection, Paper No-20230914, 2023 (Accepted on 29th November 2023)

Techno-Economic and Environmental Performances of Mono- and Poly- Crystalline Silicon Solar Cell Based SPV Power Plants: A Case Study at Saboo, Ladakh in India

Tarak Nath Chell[1] ,Debanjan Bagui[1] ,Arnab Jyoti Mandal[1] ,Ratan Mandal[1] ,Tushar Jash[1]*

[1]Jadavpur University, School of Energy Studies, Kolkata, West Bengal, 700032 India

Abstract

The following study presents an analysis and comparison of monocrystalline (m-Si) and polycrystalline (p-Si) based grid-connected SPV systems based on the existing market cost of photovoltaic (PV) components including PV modules, inverters, and electrical and mechanical equipment along with necessary accessories for a 5 MW SPV power plant at Saboo village, Ladakh, India using PVSyst. The study revealed that the average yearly energy generation for m-Si is 11.34 GWh and 11.32 GWh for p-Si PV systems. The Levelized Cost of Electricity (LCOE), payback period, and Return on Investment (ROI) for m-Si and p-Si PV systems are (1.495 INR/kWh, 638%, 3.2 years) and (1.450 INR/kWh, 674%, 3.1 years) respectively. Throughout the lifetime of the proposed PV plant, a total emission of 203.3 ktCO$_2$ for m-Si and 202.8 ktCO$_2$ for p-Si can be averted. Performance results indicate that in terms of efficient energy generation and performance ratio (PR), the m-Si PV system has a slight edge over the p-Si PV system. However, due to the affordability of the p-Si module, the initial investment cost for the p-Si PV system can be lowered up to 5% compared to the m-Si PV system which makes it economically more viable.

KEYWORDS

Solar PV Power Plant, Performance Ratio, PVSyst Simulation, Techno-Economic Analysis, Performance Parameters

1. INTRODUCTION

Energy comprises a fundamental pillar of current society, catalyzing economic progress and social advancement with diverse energy production and consumption methods, nations worldwide seek to secure affordable, abundant, and eco-friendly energy sources. The International Energy Agency (IEA) projects that global energy demand will increase by an average of 1% per year to 2030 [1]. Globally out of the total consumed energy, around 85% comes from fossil fuels [2] as a result the reliance on coal, oil, and natural gas, has led to concerns about their finite nature and the associated environmental consequences. The world is currently facing a significant energy crisis concerning fossil fuels [3], and India, as one of the largest energy consumers and emerging economies, is not exempt from these challenges. Not only the escalating climate crisis but also rising temperatures and extreme weather events, have intensified the urgency to transition away from fossil fuels and towards cleaner, renewable energy sources. In the context of India, the challenges are even more due to its rapidly growing population, increasing energy demand, and heavy reliance on fossil fuels. India heavily imports fossil fuels (around 40%) [4], making it vulnerable to global price fluctuations and supply disruptions. This dependence poses a significant strain on the country's balance of payments and fiscal health. As per reports The global energy mix is expected to become less reliant on fossil fuels by 2050, with the share of fossil fuels falling from 80% to 60%. This will be accompanied by a decline in global CO$_2$ emissions, from 37 billion

IJEP 43 (5) : 440-451 (2023) (ISSN : 0253-7141)

Possibilities of Private Bus Operators Adopting Electric Buses in Passenger Transport: A Case Study in Kolkata, India

Atanu Dutta, Deepanjan Majumdar, Tarak Nath Chell and Tushar Jash*

Jadavpur University, School of Energy Studies, Kolkata, West Bengal - 700 032, India

**Corresponding author, Email: tusharjash@yahoo.co.uk; atanu.dutta07@gmail.com*

Passenger transit activities of a region are an appropriate reflection of the economic and technological aspects in-situ. Buses play an important role in mass transit activities in urban regions, however, in developing economies, the traffic scenario shows distinctive implications on its dynamic performance. In India, only 7.3% of the buses are operated by State Road Transport Undertakings, whereas private operators play a significant role. The present study discusses the electrification programme of buses in Indian scenario, based on the case study of Kolkata city. The possibility of involvement of private bus owners in the vehicle electrification programme has been illustrated, based on the conventional vehicle ownership model, exhibited in the bus sector. The study also illustrates the real-world operating scenarios for the presently deployed electric buses compared to their conventional counterparts. It was observed that electric buses exhibited a mean energy consumption rate of 0.97 kWh/km. Moreover, the benefit expenditure ratio for electric buses varied from -0.14 to 0.26 compared to 0.10 for diesel buses from the private owners' perspective.

KEYWORDS

Electric bus, Energy consumption, Traffic performance, Financial analysis

1. INTRODUCTION

Depleting energy resources and continuous increase in atmospheric pollution levels have been a major concern over the years, especially for the road transport sector, leading to plethora of research in similar fields. As already known, internal combustion engine vehicles (ICEVs) run on fossil fuels and their tailpipe emissions are a substantial contributor to atmospheric pollution. Ramachandra illustrated decentralized emission inventories for road transport sector and observed that the total emission of CO_2 for Indian transport sector was 258.10 teragram (Tg) for the year 2003-2004 [1]. Also, road transport sector accounted for 94.5% and 53.3% of CO_2 and CO emitted, respectively out of the total transport sector emissions. Emissions from the transport sector depend on various factors, such as types of fuel, condition of the vehicle, road conditions, congestion scenario, vehicle loading, driver behaviour, etc. Replacement of the ICEVs with electric vehicles (EVs) can be a way to address both energy consumption and emission issues to some extent. Faster adoption and manufacturing of hybrid and electric vehicles (FAME), a Government of India initiative, which is an integral part of National Electric Mobility Mission Plan (NEMMP) in India, was introduced to reduce the use of fossil fuel powered vehicles. However, it has to be understood that as long as EVs represent only a small portion of the total vehicle fleet, the tailpipe emissions of ICEVs on congested roads and slow moving traffic will nullify the benefits of the EVs. A congestion free road with smooth moving traffic can be achieved only when commuters choose mass transit over personalized vehicles. A more effective approach is for commuters to switch to electric mode of mass transit, such as electric buses (eBuses). In order to achieve this, there should be adequate availability of eBus services that can enable commuters to reach their destination within a reasonable time. Government has taken a sensible approach in introducing eBuses to address this scenario. The first phase of FAME was from 2015 to 2019 and the second phase was from 2019 to 2022, with a target of introducing 30% EVs by 2030 [2-4]. The scheme included subsidies for EVs meant for privately owned vehicles, alongside different policies and funding programmes for vehicles of mass transit. Around 220 eBuses under FAME I are operating in eight cities and 2450 eBuses have been procured as of November 2020 out of 5595 buses allotted under FAME II [5].

In India, where buses account for 75% of public transport trips, buses operated by State Road Transport

Solar RRL, Manuscript Number: solr.202400410 (Under Review)

Study on Efficiency Behaviour of Polycrystalline Silicon Solar Photovoltaic Module – An Experimental Approach

Tarak Nath Chell, Debanjan Bagui*, Arnab Jyoti Mandal, Deepanjan Majumdar, Ratan Mandal, Tushar Jash

Abstract

The study emphasizes on developing an empirical correlation between efficiency, solar radiation and module temperature for polycrystalline (p-Si) solar photovoltaic (SPV) modules with a three dimensional (3D) curve fitting technique, using experimental data. The proposed corelation allows to predict the efficiency of PV module by utilizing solar radiation and module temperature as input parameters. The correlation-equation is validated by comparing its predicted performance with experimental data along with statistical error assessment metrics, such as the coefficient of determination (R2), adjusted coefficient of determination (R2 adj), root mean square error (RMSE), and the sum of squared error (SSE). The results indicated a robust agreement between the predicted and measured data, with values of 1.407×10-3 for RMSE, an R2 of 0.9557, an R2 adj of 0.9335, and an SSE of 4.356×10-5. The performance of the proposed corelation further compared with existing solar module efficiency models and results show the proposed methodology offers an accurate and simplified alternative method to existing models for accurate prediction of PV modules efficiency.

Keywords

Polycrystalline Solar, Solar Module Efficiency, Statistical Analysis, Corelation

1. Introduction

Solar photovoltaic (SPV) systems contributed to 4.5% of the world's total electricity production [5] in 2022, with an investment of 298 billion USD out of the 500 billion USD allocated to renewable energy investment [6]. To sustain such a substantial investment in the renewable energy field, it is essential to assess and continuously monitor the power generation of an SPV plant and prioritize the efficient generation of energy. In the context of SPV systems, the efficiency of modules and thus the resulting power output is significantly influenced by ambient and module temperature, solar irradiance, etc. [7,8]. Solar radiation being a function of geographical location, the total irradiance received at a specific location fluctuates over time throughout the year. Alongside this, the energy conversion efficiency on the module decreases by approximately 0.4–0.5% for every Kelvin (K) [9,10] increase in temperature. As a result, power production will exhibit seasonal variance. Hence, to predict the efficienct output of solar modules under altering operational conditions and enable accurate estimations of energy generation aiding in the design, optimization, and feasibility analysis of SPV systems, the efficiency model stands out to be the rudimentary tool. Such models are beneficial in comparing different SPV technologies to determine which are the most suitable for a particular application based on their expected performance.

APSE Applied Solar Energy, Article Id: AppSolEn2460245Mandal (Under Review)

Development of TiO2-based Acrylic Color-Dye Sensitized Solar Cell: An Emerging Possibilities in Third-Gen Solar Cell Technology

Tarak Nath Chell, Debanjan Bagui*, Arnab Jyoti Mandal, Deepanjan Majumdar, Ratan Mandal,

Abstract

Dye-Sensitized Solar Cells are at the forefront of third-generation emerging solar cell technologies, representing a pivotal advancement. DSSCs primarily focus on low manufacturing costs, and the manufacturing process is relatively environmentally friendly compared to other solar cell technology. This study presents a comprehensive investigation into developing a dye-sensitized solar cell based on commercial Prussian blue (C18Fe7N18) acrylic color-dye as a new type of photo-sensitizer. The primary objective of the study is to explore the alternative dye for Dye Synthesized Solar Cell (DSSC) based on fill factor and power conversion efficiency under different natural intensities along with the band gap analysis of the photo-anode and the proposed dye. Additionally, the thicknesses of the photo-anode and back electrode are discussed. It is also dissected the absorption Ultraviolet-Visible (UV-Vis) spectrum of the dye and the dye loading on the surface of the photo-anode has analyzed. Through Ultraviolet-Visible (UV-Vis) absorption spectroscopy, it has been found that acrylic color dye can be diluted using distilled water, which exhibited a broader visible light spectrum range (400 to 800 nm) with a band gap of around 2.03eV. The results demonstrate promising photo-electrochemical parameters under different natural sunlight intensities, including an open-circuit voltage (V_{oc}) of 485 mV, a short-circuit current (I_{sc}) of 0.23 mA, and a Fill Factor (FF) of 0.36 and an Efficiency 0.24%.

Keywords

Dye-Sensitized Solar Cell, Acrylic colour-dye, Ultraviolet-Visible spectrum, Band Gap, Fill factor, Efficiency

Introduction

Over the years, technology has propelled us forward, and innovative advancements within the field have been instrumental in fostering the development of society, which holds especially true for the progression of the generations of solar cells. In contrast, silicon solar cells have been considered conventional, highly dependable, and currently own 90% of the market share [1]. Silicon-based solar cells, including mono and polycrystalline silicon, constituted the first photovoltaic sector. They are capitalized on the processing feedback and supply feedstock provided by the microelectronics industry [2]. The third generation of solar cells is an alternative approach to non-conventional solar cells, including perovskite, dye-sensitized, tandem, organic, and other emerging concepts. These cells represent a spectrum of possibilities, from inexpensive low-efficiency systems (such as dye-sensitized and organic solar cells) to costly

PhD Thesis_Study on the Impact of Variation in Design Parameters on the Performance of Solar Photovoltaic System

ORIGINALITY REPORT

7%
SIMILARITY INDEX

PRIMARY SOURCES

1	Maharshi Vyas, Sumit Chowdhury, Abhishek Verma, V.K. Jain. "Solar Photovoltaic Tree: Urban PV power plants to increase power to land occupancy ratio", Renewable Energy, 2022 Crossref	269 words — 1%
2	Letao Wan, Liqian Zhao, Wensheng Xu, Feihong Guo, Xiaoxiang Jiang. "Dust deposition on the photovoltaic panel: A comprehensive survey on mechanisms, effects, mathematical modeling, cleaning methods, and monitoring systems", Solar Energy, 2024 Crossref	231 words — 1%
3	www.scribd.com Internet	141 words — < 1%
4	Ali.O.M. Maka, Tadhg S O'Donovan. "Effect of thermal load on performance parameters of solar concentrating photovoltaic: High-efficiency solar cells", Energy and Built Environment, 2021 Crossref	71 words — < 1%
5	Subhash Chander, A. Purohit, Anshu Sharma, Arvind, S.P. Nehra, M.S. Dhaka. "A study on photovoltaic parameters of mono-crystalline silicon solar cell with cell temperature", Energy Reports, 2015	71 words — < 1%

Internet

10 words — < 1%

99	export.arxiv.org Internet	10 words — < 1%
100	iopscience.iop.org Internet	10 words — < 1%
101	lup.lub.lu.se Internet	10 words — < 1%
102	napier-repository.worktribe.com Internet	10 words — < 1%
103	patents.justia.com Internet	10 words — < 1%
104	ueaeprints.uea.ac.uk Internet	10 words — < 1%
105	www.eqmagpro.com Internet	10 words — < 1%
106	www.science.gov Internet	10 words — < 1%
107	www.ti.com.cn Internet	10 words — < 1%

EXCLUDE QUOTES	OFF	EXCLUDE SOURCES	OFF
EXCLUDE BIBLIOGRAPHY	ON	EXCLUDE MATCHES	< 10 WORDS

Tarak nath Chell 22/04/2024

Tarak Nath Chell

Study on the Impact of Variation in Design Parameters on the Performance of Solar Photovoltaic System

Reg. No. D-7/ISLM/91/18

Submitted By-Tarak Nath Chell

<u>"Response to Reviewer Comments"</u>

Reviewer 1

Comment 1:

Why haven't the dust characterizations been carried out?

Response to Comment 1:

I've completed the dust characterizations, but the testing data is delayed due to some issues with the measuring instruments. The SEM and EDX data aren't clear enough for analysis, so, I haven't included it in my thesis yet.

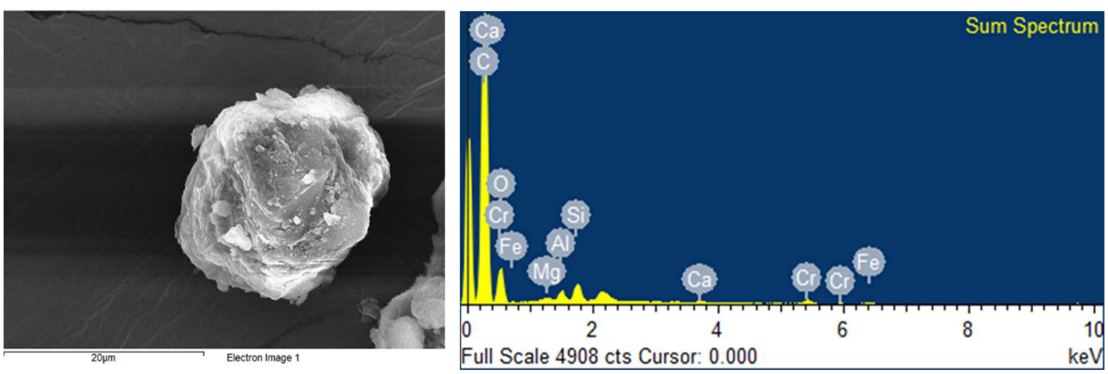

Elemental composition of dust sample (Kolkata)

Comment 2:

How many times the experiments were conducted (Table 4.2)? The standard deviation of these results could have been presented in Table 4.2.

Response to Comment 2:

The experiments were conducted three times to ensure reliability and to obtain a more robust set of data. Also the experiments involved a scanning time of 1 second for measuring temperature, and all data were presented as average values collected during this interval.

This averaging process enhances accuracy by smoothing out fluctuations and minimizing the impact of any outliers that might occur during the measurement.

Thank you for your suggestion regarding the presentation of standard deviation. I am produce some standard deviation data of the Table 4.2.

Radiation	Parameter	Temperature	Expt-1 SD	Expt-2 SD	Expt-3 SD	Final SD Data
1000	V_{oc}	20	0.00692	0.00890	0.00910	0.00741
		30	0.00676	0.00889	0.00687	0.00835
		40	0.00456	0.00270	0.00311	0.03382
		50	0.00435	0.00665	0.00456	0.00512
		60	0.00987	0.00810	0.00950	0.00946

Comment 3:

Explain in more detail the setup of the soiling test bed with glass slide alignment, as shown in Figure 3.23.

Response to Comment 3:

Transparent glass slides were utilized for the systematic collection of naturally accumulated dirt over a specified duration, allowing for accurate assessment of soiling effects. A glass holder base was meticulously designed and constructed, featuring a soiling test bed that accommodates multiple glass slides simultaneously. This setup ensures precise alignment with the installation angle of the photovoltaic modules. However, configuration of the soiling test bed, specifically addressing the alignment of the glass slides, is comprehensively outlined in Section 3.20 of Chapter 3.

Comment 4:

Will the trade-off between revenue loss due to dust deposition and cleaning costs be the same for other locations?

Response to Comment 4:

The trade-off between revenue loss from dust deposition and cleaning costs will vary significantly across locations due to multiple technical factors. Dust accumulation rates, influenced by local environmental conditions such as aridity and particulate matter in the air, directly affect the efficiency degradation of solar panels. Climates with higher rainfall may naturally reduce the need for cleaning, while regions with elevated solar irradiance levels can result in more pronounced revenue losses from soiling, thereby justifying more frequent cleaning interventions. Additionally, regional variations in labor costs, water availability, and cleaning methodologies further impact the economic assessment of cleaning practices. Collectively, these factors necessitate a location-specific analysis to optimize the balance between potential revenue losses and associated cleaning expenditures.

Comment 5:

What typical cleaning cycle is followed in large-capacity grid-connected solar power plants?

Response to Comment 5:

According to **BRIDGE TO INDIA Energy Private Limited, Water use in solar power sector (September 2018)** assessment was reported of water requirements in the solar sector, a typical operating assumption is two cleaning cycles per month in most cases. However, even brief periods of water scarcity can materially affect project returns due to decreased energy production and increased maintenance costs.

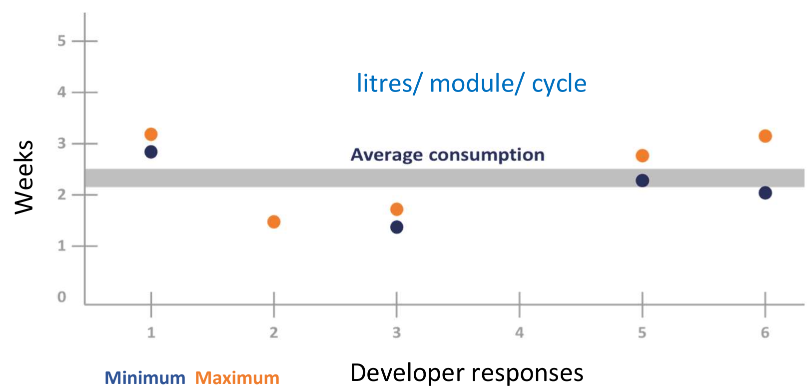

Source: Industry interviews (BRIDGE TO INDIA, Water use in solar power sector, 2018)

Comment 6:

What are the issues related to module cleaning in the case of residential rooftop solar power plants?

Response to Comment 6:

Module cleaning in residential rooftop solar power plants presents several challenges, including safety concerns related to accessing panels at heights, and the significant water usage required for cleaning, which is problematic in water-scarce areas. Accumulation of dust, bird droppings, and debris can reduce panel efficiency, but determining the optimal cleaning frequency is difficult. Additionally, selecting appropriate cleaning methods is crucial, as harsh chemicals or abrasive materials can damage the panels. The cost of professional cleaning services can be high, and require time and effort that may not be feasible for all homeowners. Ultimately, these factors can affect the efficiency and maintenance of residential solar systems.

Comment 7:

How the CUP maps are generated at different tilt angles? Were these results obtained from PVSyst simulation or experimental work?

Response to Comment 7:

To conduct the experiment for generating Capacity Utilization Factor (CUF) maps for solar panels at different tilt angles, I first set up adjustable solar panels on a sturdy frame, allowing for easy changes in tilt between 0°, 10°, 22.5° 30°, 40°, 50°, 60°, 70°, 80° and 90°. Each panel continuously monitor solar irradiance, temperature, and energy output over a year, ensuring that data logging occurred at regular intervals to capture variations throughout the day and seasons. After gathering the data, I calculated the CUF for each tilt angle by dividing the actual energy produced by the maximum potential output based on solar irradiance levels. With the CUF values in hand, I analyzed the results to identify the optimal tilt angle for maximum energy capture, and then I created visual maps to illustrate the performance at each angle.

The results were obtained from experimental work involving real-time data collection from different tilt angles installed solar panels.

Comment 8:

What will be the difference in energy generation between a solar tree and a ground- mounted plant with the same capacity?

Response to Comment 8:

The energy generation difference between a solar tree and a ground-mounted plant of the same capacity is influenced by several technical factors, including the orientation, tilt angle, and shading effects. Solar trees, often designed for aesthetic and space-efficient deployment, may have non-ideal orientations and suboptimal tilt angles, leading to reduced solar insolation capture compared to ground-mounted systems. Ground-mounted plants can utilize tracking systems that adjust the angle of solar panels throughout the day to maximize direct sunlight exposure, further enhancing energy output.

In Chapter 7 of the thesis was discussed that the solar tree design, which was based on reducing dust deposition effects, was found to generate lower energy output compared to a ground-mounted solar plant of equivalent capacity.

Comment 9:

In section 8.2.2, experimental data is mentioned as having been used to design centralized maximum point tracking devices (MPPT) for optimizing power generation in power plants. However, the thesis does not address the MPPT algorithm.

Response to Comment 9:

The thesis mentions the use of experimental data for designing centralized maximum power point tracking (MPPT) devices aimed at optimizing power generation in power plants. However, it does not delve into the details of the MPPT algorithm itself, as this topic is outlined as part of the future scope of work. This decision allows for a focused exploration of the current research while required in-depth discussion and analysis of the MPPT algorithm in subsequent studies.

Comment 10:

How is the MPPT algorithm used in large-scale grid-connected solar power plants?

Response to Comment 10:

The MPPT (Maximum Power Point Tracking) algorithm is vital in large-scale grid-connected solar power plants as it optimizes electricity generation from solar panels by continuously adjusting their operating points to maximize power output. It monitors voltage and current in real-time to identify the maximum power point, adapting quickly to changing conditions like sunlight intensity and temperature. Integrated with inverters, the algorithm ensures efficient conversion of the DC output from solar panels to AC for grid compatibility, ultimately enhancing the plant's energy yield and overall efficiency.

Reviewer 2

Comment 1:

The literature search on the target is found to be sufficient.

However, one table of comparison on the PV performance, available in different literature, with (i) panel tilt angles, (ii) the cleaning frequency, and (iii) cleaning techniques should be included in the final thesis.

Response to Comment 1:

References	Panel tilt angles	Cleaning frequency	Cleaning techniques
Kazem et al., 2022	Installed horizontally (Expt.)	15 days (Expt.)	Manual cleaning (sodium solution with rubber and cloth brushes)
Elshazly et al., 2021	∠0°-∠60° Best performance ∠30°	------	Self-cleaning coatings
Majeed, et al., 2020	∠15°-∠60°	Every day	Pressurized water, sprayed through a flat-fan nozzle to clean (Automatic)
Al-badra et al. (2020)	------	Twice a month	Passive (anti-soiling coating)
Simiyu (2020)	∠30°	Seven times per year	Machine-assisted
Chanchangi et al. (2020)	∠25°-∠45°	------	Rainfall (Manual)

Comment 2:

The experimental setup does not seem to be a developed one. Is it any customized setup, or is it available from vendors?

Response to Comment 2:

Yes, the setup was customized specifically for the experiment. It was tailored to meet unique requirements, allowing for more precise results. While modular components are procured from vendors, all details of the development of experimental setup are described in Chapter 3, Section 3.4.

Comment 3:

Running the experimental setup and taking many results are definitely appreciable. But the setup description with specifications may come in the annexure.

Response to Comment 3:

Thank you for your feedback. I wanted to mention that the detailed specifications of the laboratory experiment setup, outdoor experimental setup, and data collection system, as well as their component specifications, are already described in Chapter 3, Section 3.5 to 3.23.

Comment 4:

The experimental data presented in Tables 4-1 and 4-2 may have theoretical temperature coefficients also in a column for better understanding.

Response to Comment 4:

The theoretical temperature coefficients of solar cells—specifically the open circuit voltage (Voc), short circuit current (Isc), fill factor (FF), and maximum output power (Pmax) and its vary with temperature. These coefficients are expressed as the relative change in each parameter per degree Celsius. The relationships can be summarized as follows: (Chander et al., 2015):

Maximum Output Power (P_{max}):): $\frac{1}{P_{max}}\frac{dP_{max}}{dT} \approx -0.002$ per °C

Short Circuit Current (I_{sc}): $\frac{1}{I_{sc}}\frac{dI_{sc}}{dT} \approx 0.002$ per °C

Open Circuit Voltage (V_{oc}): $\frac{1}{V_{oc}}\frac{dV_{oc}}{dT} \approx -(0.0022$ to $0.0025)$ per °C

Fill Factor (FF): $\frac{1}{FF}\frac{d(FF)}{dT} \approx -0.0013$ per °C

Comment 5:

The equation to produce figures 6.6(a) to 6.6(j) is to be established with proper reference and has to be mentioned beforehand.

Response to Comment 5:

Figures 6.6(a) to 6.6(j) show the Revenue loss due to soiling and Total cleaning cost also mentioned in the Chapter 6, Table 6.7 and 6.8 respectively. However

Revenue loss was calculated as follows:

Revenue loss = Generation loss (at ɳth cleaning frequency) × Tariff

Total cleaning cost was calculated as:

Total cleaning cost= (Labour cost + Water consumption + Water cost) at ɳth cleaning frequency + Miscellaneous

Where ɳ represents the number of days.

Comment 6:

The paper presented in page number xiv does not have any citation link.

Response to Comment 6:

A review of the change in performance of photovoltaic panels due to dust Accumulation-Challenges and their solution, International Conference On Sustainable Water Resources Management under Changed Climate, ISBN number: 978-81-941009-3-5,2020,301-309.

References:

BRIDGE TO INDIA Energy Private Limited, Water use in solar power sector (September 2018)

Chander, S., Purohit, A., Sharma, A., Nehra, S. P., & Dhaka, M. S. (2015). A study on photovoltaic parameters of mono-crystalline silicon solar cell with cell temperature. Energy Reports, 1, 104-109.

Elshazly, E., Abdel-Rehim, A. A., ABDEL KADER, A. M. R., & El-Mahallawi, I. (2021). Effect of dust and high temperature on photovoltaics performance in the new capital area.

Majeed, R., Waqas, A., Sami, H., Ali, M., & Shahzad, N. (2020). Experimental investigation of soiling losses and a novel cost-effective cleaning system for PV modules. Solar Energy, 201, 298-306.

Chanchangi, Y. N., Ghosh, A., Sundaram, S., & Mallick, T. K. (2020). Dust and PV Performance in Nigeria: A review. Renewable and Sustainable Energy Reviews, 121, 109704.

Al-Badra, M. Z., Abd-Elhady, M. S., & Kandil, H. A. (2020). A novel technique for cleaning PV panels using antistatic coating with a mechanical vibrator. Energy Reports, 6, 1633-1637.

Semaoui, S., Arab, A. H., Boudjelthia, E. K., Bacha, S., & Zeraia, H. (2015). Dust effect on optical transmittance of photovoltaic module glazing in a desert region. Energy Procedia, 74, 1347-1357.

PhD Thesis_Study on the Impact of Variation in Design Parameters on the Performance of Solar Photovoltaic System

ORIGINALITY REPORT

7%

SIMILARITY INDEX

PRIMARY SOURCES

1	Maharshi Vyas, Sumit Chowdhury, Abhishek Verma, V.K. Jain. "Solar Photovoltaic Tree: Urban PV power plants to increase power to land occupancy ratio", Renewable Energy, 2022 Crossref	269 words — 1%
2	Letao Wan, Liqian Zhao, Wensheng Xu, Feihong Guo, Xiaoxiang Jiang. "Dust deposition on the photovoltaic panel: A comprehensive survey on mechanisms, effects, mathematical modeling, cleaning methods, and monitoring systems", Solar Energy, 2024 Crossref	231 words — 1%
3	www.scribd.com Internet	141 words — < 1%
4	Ali.O.M. Maka, Tadhg S O'Donovan. "Effect of thermal load on performance parameters of solar concentrating photovoltaic: High-efficiency solar cells", Energy and Built Environment, 2021 Crossref	71 words — < 1%
5	Subhash Chander, A. Purohit, Anshu Sharma, Arvind, S.P. Nehra, M.S. Dhaka. "A study on photovoltaic parameters of mono-crystalline silicon solar cell with cell temperature", Energy Reports, 2015	71 words — < 1%

Crossref

6 sist.sathyabama.ac.in
Internet
56 words — < 1%

7 Renu Sharma, Sonali Goel. "Performance analysis of a 11.2 kWp roof top grid-connected PV system in Eastern India", Energy Reports, 2017
Crossref
51 words — < 1%

8 Hussein A. Kazem, Miqdam T. Chaichan, Ali H.A. Al-Waeli, K. Sopian. "Effect of dust and cleaning methods on mono and polycrystalline solar photovoltaic performance: An indoor experimental study", Solar Energy, 2022
Crossref
45 words — < 1%

9 downacademia.com
Internet
45 words — < 1%

10 "Advances in Smart Grid and Renewable Energy", Springer Science and Business Media LLC, 2018
Crossref
40 words — < 1%

11 Amrita Ghosh, Subhasis Neogi. "Effect of fenestration geometrical factors on building energy consumption and performance evaluation of a new external solar shading device in warm and humid climatic condition", Solar Energy, 2018
Crossref
38 words — < 1%

12 Ashutosh Sharma, Mehmet Ali Kallioğlu, Anchal Awasthi, Ranchan Chauhan, Gusztáv Fekete, Tej Singh. "Correlation formulation for optimum tilt angle for maximizing the solar radiation on solar collector in the Western Himalayan region", Case Studies in Thermal Engineering, 2021
Crossref
38 words — < 1%

13 www.researchgate.net
Internet
37 words — < 1%

14 noexperiencenecessarybook.com
Internet
36 words — < 1%

15 Akshaya Tripathi, Jasmeen Snadhu, Kartik Arunachalam, Saurabh Biswas. "A step forward in précising building roof top areas for Solar PV installations", 2015 International Conference on Smart Technologies and Management for Computing, Communication, Controls, Energy and Materials (ICSTM), 2015
Crossref
34 words — < 1%

16 Pereira, Ricardo Jorga da Silva. "Design and Optimization of Building Integration Pv/T Systems (Bipv/T)", Universidade de Evora (Portugal), 2021
ProQuest
34 words — < 1%

17 c.coek.info
Internet
33 words — < 1%

18 www.mdpi.com
Internet
33 words — < 1%

19 www.slideshare.net
Internet
33 words — < 1%

20 Hussam Almukhtar, Tek Tjing Lie, Wisam A.M. Al-Shohani. "Comprehensive analysis of dust impact on photovoltaic module temperature: Experimental insights and mathematical modeling", Solar Energy, 2023
Crossref
32 words — < 1%

21 arduino-due-pdf-datasheet-8893.peatix.com
Internet
30 words — < 1%

22	research.jcu.edu.au Internet	28 words —	< 1%
23	patents.google.com Internet	27 words —	< 1%
24	www.adb.org Internet	27 words —	< 1%
25	khazna.ku.ac.ae Internet	26 words —	< 1%
26	ore.exeter.ac.uk Internet	26 words —	< 1%
27	Chaitanya B. Pande, Johnbosco C. Egbueri, Romulus Costache, Lariyah Mohd Sidek et al. "Predictive modeling of land surface temperature (LST) based on Landsat-8 satellite data and machine learning models for sustainable development", Journal of Cleaner Production, 2024 Crossref	24 words —	< 1%
28	arrow.tudublin.ie Internet	23 words —	< 1%
29	dokumen.pub Internet	23 words —	< 1%
30	moam.info Internet	23 words —	< 1%
31	umexpert.um.edu.my Internet	23 words —	< 1%
32	E. Pinheiro, F. Bandeiras, M. Gomes, P. Coelho, J. Fernandes. "Performance analysis of wind	22 words —	< 1%

generators and PV systems in industrial small-scale applications", Renewable and Sustainable Energy Reviews, 2019
Crossref

33 Hamed Yazdani, Mahmood Yaghoubi. "Dust deposition effect on photovoltaic modules performance and optimization of cleaning period: A combined experimental–numerical study", Sustainable Energy Technologies and Assessments, 2022 — 22 words — < 1%
Crossref

34 Md Shakil Ahmed, Raihan Karal, Barun K. Das, Arnob Das. "Experimental investigation of cooling, wind velocity, and dust deposition effects on solar PV performance in a tropical climate in Bangladesh", Case Studies in Thermal Engineering, 2023 — 22 words — < 1%
Crossref

35 d.docksci.com — 22 words — < 1%
Internet

36 Lalia Miloudi, Dalila Acheli. "Prediction global solar radiation and modeling photovoltaic module based on artificial neural networks", 2015 3rd International Conference on Control, Engineering & Information Technology (CEIT), 2015 — 21 words — < 1%
Crossref

37 Muhannad J. Alshareef. "A comprehensive review of the soiling effects on PV Module Performance", IEEE Access, 2023 — 21 words — < 1%
Crossref

38 Shaima A. Alnaqbi, Abdul Hai Alami. "Sustainability and Renewable Energy in the UAE: A Case Study of Sharjah", Energies, 2023 — 21 words — < 1%
Crossref

39	s3.amazonaws.com Internet	21 words — < 1%
40	repository.up.ac.za Internet	20 words — < 1%
41	Parveen Bhola, Saurabh Bhardwaj. "Clustering-based computation of degradation rate for photovoltaic systems", Journal of Renewable and Sustainable Energy, 2019 Crossref	19 words — < 1%
42	Saigeeta Priyadarshini, Aman Prakash, Sanya Gupta, Akanksha Mishra, Himanshu Payal. "Fabrication and characterization of epoxy solar glass", Materials Today: Proceedings, 2022 Crossref	19 words — < 1%
43	T. Ikegami, T. Maezono, F. Nakanishi, Y. Yamagata, K. Ebihara. "Estimation of equivalent circuit parameters of PV module and its application to optimal operation of PV system", Solar Energy Materials and Solar Cells, 2001 Crossref	19 words — < 1%
44	eprints.kfupm.edu.sa Internet	19 words — < 1%
45	scholar.dgist.ac.kr Internet	19 words — < 1%
46	www.dline.info Internet	19 words — < 1%
47	tel.archives-ouvertes.fr Internet	18 words — < 1%

48	Mohamed Benghanem, Abdullah Almohammedi, Mohammed Taukeer Khan, Ahmad Al-Masraqi. "Effect of dust accumulation on the performance of photovoltaic panels in desert countries: A case study for Madinah, Saudi Arabia", International Journal of Power Electronics and Drive Systems (IJPEDS), 2018 Crossref	17 words — < 1%
49	desert-technologies.com Internet	17 words — < 1%
50	krishijagran.com Internet	17 words — < 1%
51	www.scirp.org Internet	17 words — < 1%
52	www.yumpu.com Internet	17 words — < 1%
53	fastercapital.com Internet	16 words — < 1%
54	meral.edu.mm Internet	16 words — < 1%
55	malque.pub Internet	15 words — < 1%
56	D. Paul, S.N. Mandal, D. Mukherjee, S.R. Bhadra Chaudhuri. "Optimization of significant insolation distribution parameters – A new approach towards BIPV system design", Renewable Energy, 2010 Crossref	14 words — < 1%
57	Kumari Namrata, R. P. Saini, D. P. Kothari. "Wind and Solar Energy Systems", Springer Science and	13 words — < 1%

Business Media LLC, 2024
Crossref

58 Pallavee Bhatnagar, R. K. Nema. "A maximum power point tracking algorithm for photovoltaic systems using bang-bang controller", Journal of Renewable and Sustainable Energy, 2014 — 13 words — < 1%
Crossref

59 cyberleninka.org — 13 words — < 1%
Internet

60 slideplayer.com — 13 words — < 1%
Internet

61 www.ee.cityu.edu.hk — 13 words — < 1%
Internet

62 www.giiresearch.com — 13 words — < 1%
Internet

63 Halim Eddahbi, Loubna Benaaouinate, Mohamed Khafallah, Aziz El Afia. "Performance Assessment and Analysis of a 1 MW Three-Phase Photovoltaic Power Station Connected to a Factory's Electrical Grid in Morocco", Energies, 2023 — 12 words — < 1%
Crossref

64 Luciana Marques, Hendrigo Batista da Silva, Jagruti Thakur, Wadaed Uturbey, Pragya Thakur. "Categorizing shared photovoltaic business models in renewable markets: An approach based on CANVAS and transaction costs", Energy Reports, 2023 — 12 words — < 1%
Crossref

65 Yong-Kwon Kang, Jaewon Joung, Seheon Kim, Junseok Park, Jae-Weon Jeong. "Design of a — 12 words — < 1%

thermoelectric generator-assisted photovoltaic panel hybrid harvester using microencapsulate phase change material", Journal of Building Engineering, 2024
Crossref

66	hess.copernicus.org Internet	12 words — < 1%
67	ir.lib.uth.gr Internet	12 words — < 1%
68	www.ics.ee.nctu.edu.tw Internet	12 words — < 1%
69	www.ijeat.org Internet	12 words — < 1%
70	www.wjoud.com Internet	12 words — < 1%
71	Ahed Hameed Jaaz, Kamaruzzaman Sopian, Tayser Sumer Gaaz. "Study of the electrical and thermal performances of photovoltaic thermal Collector-Compound parabolic concentrated", Results in Physics, 2018 Crossref	11 words — < 1%
72	I. R. Ganesh Kumar, S. Vijay Kumar, Jagannath Reddy, G. Rajendra, Yoga Sainath Reddy, Sai Ranjith Reddy, Biplab Das. "Chapter 7 Optimisation of Energy and Exergy Analysis of 100W Solar Photovoltaic Module Using ANN Method", Springer Science and Business Media LLC, 2023 Crossref	11 words — < 1%
73	Josephson, Lilian Lam. "Microrheology for Protein Therapeutics Development.", University of Delaware, 2020 ProQuest	11 words — < 1%

74 Magdi M. El-Saadawi, Ahmed E. Hassan, Khaled M. Abo-Al-Ez, Mahmoud S. Kandil. "A proposed framework for dynamic modelling of photovoltaic systems for DG applications", International Journal of Ambient Energy, 2011 — 11 words — < 1%
Crossref

75 Yusuf N. Chanchangi, Aritra Ghosh, Senthilarasu Sundaram, Tapas K. Mallick. "Dust and PV Performance in Nigeria: A review", Renewable and Sustainable Energy Reviews, 2020 — 11 words — < 1%
Crossref

76 ebin.pub — 11 words — < 1%
Internet

77 en.openei.org — 11 words — < 1%
Internet

78 energiasolarfotovoltaica.org — 11 words — < 1%
Internet

79 krishikosh.egranth.ac.in — 11 words — < 1%
Internet

80 m.canelink.miami.edu — 11 words — < 1%
Internet

81 semaphore.uqar.ca — 11 words — < 1%
Internet

82 www.frontiersin.org — 11 words — < 1%
Internet

83 www.hindawi.com — 11 words — < 1%
Internet

84 İlhami Yıldız. "1.15 Solar Energy", Elsevier BV, 2018
Crossref

11 words — < 1%

85 1library.net
Internet
10 words — < 1%

86 Athar Hussain, Ankit Batra, Rupendra Pachauri. "An experimental study on effect of dust on power loss in solar photovoltaic module", Renewables: Wind, Water, and Solar, 2017
Crossref
10 words — < 1%

87 Brian Parrott, Pablo Carrasco Zanini, Ali Shehri, Konstantinos Kotsovos, Issam Gereige. "Automated, robotic dry-cleaning of solar panels in Thuwal, Saudi Arabia using a silicone rubber brush", Solar Energy, 2018
Crossref
10 words — < 1%

88 Joji Johnson, S. Manikandan. "Resource potential mapping of bifacial photovoltaic systems in India", iScience, 2023
Crossref
10 words — < 1%

89 Karimov, Kh.S.. "Temperature-dependent properties of organic-on-inorganic Ag/p-CuPc/n-GaAs/Ag photoelectric cell", Solar Energy Materials and Solar Cells, 200505
Crossref
10 words — < 1%

90 Muhammad Shoaib Hanif, Irfan Qasim, Muhammad Imran Malik, Muhammad Farooq Nasir, Owais Ahmad, Asim Rashid. "Development of low-cost and high-efficiency solar modules based on perovskite solar cells for large-scale applications", Heliyon, 2024
Crossref
10 words — < 1%

91	Muhammad Shoaib, Sheher Yar Khan, Naveed Ahmed, Mariam Mahmood, Adeel Waqas, Mumtaz A. Qaisrani, Nadia Shehzad. "Thermal management of solar photovoltaic module by using drilled cylindrical rods integrated with phase change materials", Journal of Energy Storage, 2022 Crossref	10 words — < 1%
92	R. Nasrin, M. Hasanuzzaman, N.A. Rahim. "Effect of high irradiation on photovoltaic power and energy", International Journal of Energy Research, 2018 Crossref	10 words — < 1%
93	S. Sumathi, L. Ashok Kumar, P. Surekha. "Solar PV and Wind Energy Conversion Systems", Springer Science and Business Media LLC, 2015 Crossref	10 words — < 1%
94	Suneel Kumar Joshi, Sanjeev Gupta, Rajiv Sinha, Alexander Logan Densmore et al. "Strongly heterogeneous patterns of groundwater depletion in Northwestern India", Journal of Hydrology, 2021 Crossref	10 words — < 1%
95	Thomas E. Murphy, Halil Berberoglu. "Flux balancing of light and nutrients in a biofilm photobioreactor for maximizing photosynthetic productivity", Biotechnology Progress, 2014 Crossref	10 words — < 1%
96	baadalsg.inflibnet.ac.in Internet	10 words — < 1%
97	dspace.dtu.ac.in:8080 Internet	10 words — < 1%
98	epdf.tips	

Internet

10 words — < 1%

99 export.arxiv.org
Internet

10 words — < 1%

100 iopscience.iop.org
Internet

10 words — < 1%

101 lup.lub.lu.se
Internet

10 words — < 1%

102 napier-repository.worktribe.com
Internet

10 words — < 1%

103 patents.justia.com
Internet

10 words — < 1%

104 ueaeprints.uea.ac.uk
Internet

10 words — < 1%

105 www.eqmagpro.com
Internet

10 words — < 1%

106 www.science.gov
Internet

10 words — < 1%

107 www.ti.com.cn
Internet

10 words — < 1%

EXCLUDE QUOTES	OFF	EXCLUDE SOURCES	OFF
EXCLUDE BIBLIOGRAPHY	ON	EXCLUDE MATCHES	< 10 WORDS